Study and evaluation of a frequential multiplexing based on OFDM/OQAM

Mohamed Gharba

CONSERVATOIRE NATIONAL DES ARTS ET MÉTIERS

École Doctorale Technologique et Professionnelle

Conservatoire National des Arts et Métiers

Lasers, Métrologie, Communications

THÈSE DE DOCTORAT

présentée par : **Mohamed GHARBA**

soutenue le : **13 Juillet 2012**

pour obtenir le grade de : **Docteur du Conservatoire National des Arts et Métiers**

Spécialité : **Radiocommunication**

Equipe d'accueil : **France Télécom, Orange Labs (RESA/WASA/CREM) à Rennes**

Etude et évaluation d'un multiplexage fréquentiel basé sur l'OFDM/OQAM

THÈSE DIRIGÉE PAR

M. SIOHAN Pierre	*PhD, HDR, France Télécom, Orange Labs, Rennes*
M. TERRE Michel	*Professeur, CNAM, Paris*

RAPPORTEURS

Mme BOUCHERET Marie-Laure	*Professeur, ENSEEIHT, Toulouse*
M. PALICOT Jacques	*Professeur, SUPELEC, Rennes*

EXAMINATEURS

M. HELARD Jean-François	*Professeur, INSA, Rennes*
M. LIN Hao	*PhD, France Télécom, Orange Labs, Rennes*

CONSERVATOIRE NATIONAL DES ARTS ET MÉTIERS

École Doctorale Technologique et Professionnelle

Conservatoire National des Arts et Métiers

Lasers, Métrologie, Communications

Ph.D. Thesis

presented by : **Mohamed GHARBA**

defended on : **July 13, 2012**

in partial fulfillement of the requirements for the Degree of : **Doctor of Philosophy from the Conservatoire National des Arts et Métiers**

Specialization : **Radiocommunication**

This thesis takes place at : **France Telecom, Orange Labs (RESA/WASA/CREM), Rennes**

Study and evaluation of a frequential multiplexing based on OFDM/OQAM

THESIS DIRECTED BY

M. SIOHAN Pierre	*PhD, HDR, France Télécom, Orange Labs, Rennes*
M. TERRE Michel	*Professor, CNAM, Paris*

REPORTERS

Mme BOUCHERET Marie-Laure	*Professor, ENSEEIHT, Toulouse*
M. PALICOT Jacques	*Professor, SUPELEC, Rennes*

EXAMINATORS

M. HELARD Jean-François	*Professor, INSA, Rennes*
M. LIN Hao	*PhD., France Télécom, Orange Labs, Rennes*

"This PhD thesis is dedicated to my mother Mona GHARBA to whom I owe everything in my life."
Mohamed GHARBA

Acknowledgements

This research work has been one of the most significant challenges I have ever had to face and without the support, guidance and patience of the people who I want to acknowledge this work wouldn't be accomplished.

I want to thank France Telecom Orange Labs (CREM team) and CNAM for giving me this opportunity of doing this thesis in the first instance.

I am heartily thankful to my supervisors Dr. Pierre SIOHAN, Dr. Hao LIN, Prof. Michel TERRE and my former supervisor Dr. Rodolphe LEGOUABLE whose encouragement from beginning to the end helped me to understand, develop and achieve my work.

My colleagues from the CREM team of Orange Labs supported me in my research work. I want to thank them for all their help, support, interest and valuable hints.

I also want to thank my former team leader Mr. Pierre GELPI, my current team leader Mr. Jean-Chrisyophe Rault and our secretary Mrs. Gislaine LE GOUALLEC for their great helps in difficult times.

Their help and support are deeply appreciated. Lastly, I offer my regards and blessings to all of those who supported me in any respect during the completion of the project.

July 13, 2012.
Rennes, France
Mohamed GHARBA.

Résumé

Cette thèse est consacrée à l'étude de la modulation OFDM/OQAM en tant qu'alternative à la modulation OFDM. Nous traitons plus particulièrement le contexte multiusagers. De ce point de vue, les aspects de synchronisation sont déterminants. Les différentes options plus le choix de la forme d'onde sont donc examinés de ce point de vue. Un autre objectif est de montrer de manière précise comment la modulation OFDM/OQAM peut s'adapter à une transmission de type cellulaire, en prenant comme référence le système 3GPP/LTE. Les principales contributions que nous avons apportées sont : 1) Une analyse des phénomènes de désynchronisation : nous analysons l'effet de la désynchronisation, suivant les axes temporel et fréquentiel, sur les performances de l'OFDM/OQAM au récepteur. 2) Méthode de synchronisation : nous analysons une méthode de synchronisation temporelle définie dans un contexte de transmission OFDM/OQAM mono-usager et nous l'adaptons à un scénario de type multi-usagers. 3) Proposition d'un schéma d'accès multiple : nous proposons un schéma d'accès multiple basé sur la modulation OFDM/OQAM, alternatif aux techniques connues OFDMA et SC-FDMA, pour la transmission en liaison montante dans un contexte de type 3GPP/LTE.

Mots clés : OFDM, OFDM/OQAM, synchronisation, OFDMA, SC-FDMA, OQAMA, DFT-OQAMA, 3GPP/LTE

Abstract

This thesis is dedicated to the study of the OFDM/OQAM modulation as an alternative to the OFDM modulation. We treat more especially the multiuser environment. In this respect, synchronization aspects are crucial. The different options plus the choice of the waveform are examined in this point of view. Another objective is to precisely show how the OFDM/OQAM can be adapted to a cellular transmission type, taking as reference the 3GPP/LTE system. The main contributions we have made are : 1) Analysis of the desynchronization phenomena : we analyze the effect of desynchronization, according to the time and frequency axes, on the performance of OFDM/OQAM at the receiver side. 2) Synchronization method : we analyze a method of temporal synchronization defined in a single user OFDM/OQAM transmission and we adapt it to a multiuser scenario type. 3) Proposing for a multiple access scheme : we propose a multiple access scheme based on the OFDM/OQAM modulation, alternative to the known techniques OFDMA and SC-FDMA, for the UL transmission in a 3GPP/LTE context.

Keywords : OFDM, OFDM/OQAM, synchronization, OFDMA, SC-FDMA, OQAMA, DFT-OQAMA, 3GPP/LTE

Table of Contents

List of Tables

List of Figures

Introduction

During the last two decades we have witnessed a tremendous development of new telecommunications applications, for example, mobile phones or the Internet. If these applications are now well established, they are based on techniques that have not reached their limits. However they have created more new requirements with, in particular, expectations for new services with high bit rates. Consequently, it seems essential to continue improving the various elementary links in the transmission chain. Thus, the choice of an appropriate modulation scheme and its optimization are crucial to increase the transmission rate of future wired and wireless communication, for the Internet and mobile phones. Therefore, the physical layer and all the subsequent concepts that enable the end to end transmission is of paramount importance in this lifestyle mode. Thus, increasing the data rate at the physical layer has become an up-to-date task of digital communication research and is important for economic growth and for social connectivity. In that respect, one of the most challenging issues in wireless communications today is the high demand for reliable multimedia services accessed by many simultaneous users.

Currently, the fourth mobile generation (LTE-based) is on the verge to be commercially available, soon providing worldwide a very high quality mobile radio system including different types of services with different data rates and high performance. Beyond this last technological step, further improvements are still to be expected concerning modulation and multiple access schemes. Indeed, the role of modulation, which is to generate a signal being sufficiently effective against the disturbances caused by the transmission channel, and the one of the multiple access, which is to cleverly share the radio resource between different users/services, are still of great importance. Each mobile radio generation has brought new modulation features and there are always new projects, e.g. PHYDYAS [81],

to introduce new modulation and multiple access concepts.

The early digital communication systems were single carrier-based. Generally, if we want to increase the bit rate of this single carrier system, we have to reduce the symbol duration time. However, the presence of a multipath channel introduces Inter Symbol Interference (ISI) which then requires complex equalization process. In this respect, multicarrier modulations have appeared as a more attractive solution, and as a good alternative in order to have a good trade-off between complexity and higher bit rate. Indeed, the fact of using several carriers in parallel allows making the transmission robust against the frequency selective channels because it is then carried out on reduced frequency bands [54].

Nowadays, the main multicarrier modulation is CP-OFDM (Cyclic Prefix- Orthogonal Frequency Division Multiplex(ing)). The large popularity of CP-OFDM, mainly comes from its two most attractive features. Firstly, CP-OFDM corresponds to a block transform that can be easily implemented using fast algorithms. Secondly, the equalization problem is simply solved with OFDM thanks to the addition of the CP [78]. For all these reasons the OFDM has been adopted in various standardized air interfaces, as in DAB, DVB-T, IEEE 802.11, 802.16 [21] and in downlink 3GPP/LTE transmission [2]. However, CP-OFDM has also some drawbacks including a loss of spectral efficiency due to the CP and a bad frequency localization. These weaknesses have shifted researchers to other multicarrier systems.

To cope with these shortcomings, a possible solution called OFDM/OQAM (OFDM with Offset Quadrature Amplitude Modulation) [32] could be used instead. This modulation has the same spectral efficiency as OFDM without CP, while having the possibility of using pulse shapes other than the rectangular one. For this, we change the data transmission scheme in order to transmit real symbols only. The orthogonality is not verified in the complex field as in conventional OFDM, but in the real field. Since, when using a proper waveform, the OFDM/OQAM modulation does not require the use of a CP during the transmission, it inherently exhibits a higher spectral efficiency compared to CP-OFDM.

The appearance of the first multicarrier modulation systems using pulse shaping filters other than the rectangular one dates back to the 60's [15], [88]. Subsequently, an approach involving Fourier transforms was introduced in 1981 by B. Hirosaki in [46]. The

acronym OFDM/OQAM only appeared in 1995 in [32]. Other names have been used to designate identical or equivalent systems : Orthogonally multiplexed QAM or O-QAM in [45], OQAM-OFDM in [99] for continuous time systems ; OMC (for Orthogonal Multiple Carrier) in [31] for discrete time systems. However, the OFDM/OQAM system, that can also be presented using a filter bank approach [92] and is therefore also named FBMC/OQAM (Filter Bank Multi Carrier with OQAM) [87], has its own shortcomings. As FBMC/OQAM cannot take advantage of a CP, its sensitivity to time offset remains questionable.

Beyond the theoretical description of the analog and digital versions of OFDM/OQAM signals, many challenging problems had still to be solved concerning practical communication aspects.

When this thesis was launched several problems related to OFDM/OQAM were still opened, e.g. :

- Time and frequency domains synchronization analysis.
- Synchronization methods.
- The combination of OFDM/OQAM with a multiple access technique for the multiuser transmission in the 3GPP/LTE context.

This PhD thesis brings contributions on all these hot topics for the OFDM/OQAM modulation. Our argumentations are presented into 3 chapters. The content of these chapters are given below.

The chapter 2 is dedicated to the description of the OFDM and OFDM/OQAM modulation techniques including the corresponding implementation architectures.

We illustrate the advantages of the OFDM/OQAM system over the OFDM one and present the prototype filters to be used in the following chapters, each one having different time/frequency localization and interference features.

The chapter 3 is concerned with the study of the OFDM/OQAM system. An analytical performance is derived under a desynchronized condition. We analyze the OFDM/OQAM in time and frequency domains and present a method for synchronization.

The OFDM/OQAM's sensitivity to time offset makes interference analysis [87] due to desynchronization be a very important topic in the physical layer design. The results presented in [32] are interesting but they are not fully analyzed. On another hand, the more detailed analysis provided in [87] only leads to approximations of the SIR (Signal to Interference Ratio). In this chapter, we focus on the interference caused by timing and carrier frequency offsets for OFDM/OQAM. Reusing the analysis provided in [58] concerning the transmission of an OFDM/OQAM signal through a multipath channel, we derive two very simple ISI and ICI expressions as well as an exact SIR expression. Then, we illustrate the effect of the pulse shape on this interference term. Then we compare our exact SIR model with the simulated SIR numerically using different prototype filters. These results are also compared with the ones obtained for OFDM. In our study, through a detailed demonstration for the case of orthogonal prototype filters, we highlight a link between our analysis and the one in [32]. And finally, we present a synchronization method for the multi user uplink (UL) transmission.

The chapter 4 proposes an alternative multiple access scheme based on the OFDM/OQAM modulation for the UL 3GPP/LTE context :

For the downlink, 3GPP/LTE standard has unanimously considered OFDMA as the most appropriate technique for achieving high spectral efficiency. For the UL, 3GPP/LTE has selected the SC-FDMA [2] instead of OFDMA, since it leads to a lower Peak to Average Power Ratio (PAPR). SC-FDMA can be viewed as a new hybrid modulation scheme that provides quasi-similar PAPR as single-carrier systems. SC-FDMA has already proved its ability to fight against frequency selective channels, thanks to the use of the CP-OFDM modulation and its flexibility in multiple access, thanks to the FDMA component. The OFDMA and SC-FDMA, being both based on the OFDM modulation with cyclic prefix, give rise to 2 drawbacks, loss of spectral efficiency and sensitivity to frequency dispersion, e.g. Doppler spread. Both of them can be counteracted using OFDM/OQAM. Thus, as shown in [32], it is an efficient means to get in the meantime spectral efficiency and robustness to the Doppler spread. In this chapter, we discuss the suitability of using OQAMA (OFDM/OQAM for multiple Access) and DFT-OQAMA (Discrete Fourier Trans-

form OQAMA) instead of OFDMA and SC-FDMA for the UL 3GPP/LTE scenario, regardless to the PAPR considering perfect time and frequency synchronizations.

Finally, we conclude our thesis by highlighting its most significant results and some new perspectives in the field.

Part I

Part1

Chapter 1

Résumé Français

Pendant les deux dernières décennies nous avons assisté à un énorme développement dans les nouvelles applications de télécommunications, par exemple, les téléphones portables ou l'internet. Si ces applications sont maintenant bien établies, elles sont basées sur des techniques qui n'ont pas encore atteint leurs limites. Cependant, elles ont créé en plus de nouvelles exigences avec, en particulier, des attentes pour de nouveaux services avec des débits élevés. En conséquence, il semble essentiel de continuer d'améliorer les divers liens élémentaires dans la chaîne de transmission. Ainsi, le choix d'un schéma de modulation approprié et son optimisation sont essentiels pour augmenter le débit de transmission des communications filaires et sans fil du futur. Par conséquent, la couche physique et tous les concepts suivants qui permettent la transmission de bout en bout est d'importance primordiale pour notre mode de vie actuelle. Ainsi, l'augmentation du débit à la couche physique demeure un enjeu capital pour la recherche en communication numérique et est aussi importante pour la croissance économique et pour la connectivité sociale. À cet égard, un des challenges les plus critiques dans les communications sans fil est aujourd'hui lié à la forte demande pour des services multimédias fiables accédés par beaucoup d'utilisateurs simultanés.

Actuellement, la quatrième génération mobile (basée sur le LTE) est sur le point d'être commercialement disponible, fournissant bientôt dans le monde entier une très haute qualité de système radio mobile incluant différents types de services avec différents débits et haute performance. Au-delà de cette dernière étape technologique, d'autres améliorations

sont encore à prévoir concernant la modulation et les schémas d'accès multiple. En effet, la modulation, qui consiste à générer un signal suffisamment efficace contre les perturbations provoquées par le canal de transmission, et l'accès multiples, qui a pour rôle de partager intelligemment la ressource radio entre différents utilisateurs/services, sont toujours d'une grande importance. Chaque génération de téléphonie mobile a apporté de nouvelles fonctionnalités de modulation et il y a toujours de nouveaux projets, e.g. PHYDYAS [81], pour introduire une nouvelle modulation et des concepts d'accès multiples.

Les premiers systèmes de communication numérique étaient basés sur des systèmes monoporteuse. Généralement, si on veut augmenter le débit de ce système monoporteuse, nous devons réduire le temps de durée du symbole. Toutefois, la présence d'un canal multi-trajets introduit de l'interférence entre symboles (ISI) qui nécessite alors un processus d'égalisation complexe. À cet égard, les modulations multiporteuses sont apparues comme une solution plus attractive, et comme une bonne alternative pour avoir un bon compromis entre la complexité et le débit binaire plus élevé. En effet, le fait d'utiliser plusieurs porteuses en parallèle permet de réaliser une transmission robuste contre les canaux sélectifs en fréquence car il est alors effectué sur des bandes de fréquences réduites [54].

Aujourd'hui, la principale modulation multiporteuse est le CP-OFDM (Cyclic Prefix-Orthogonal Frequency Division Multiplex(ing)). La grande popularité du CP-OFDM, provient principalement de ses deux caractéristiques les plus attractives. Premièrement, le CP-OFDM correspond à une transformée en blocs qui peut être facilement mise en oeuvre en utilisant des algorithmes rapides. Deuxièmement, le problème de l'égalisation est tout simplement résolu avec l'OFDM grâce à l'ajout du CP [78]. Pour toutes ces raisons l'OFDM a été adopté dans diverses interfaces radio standardisées, comme dans DAB, DVB-T, IEEE 802.11, 802.16 [21] et en lien descendant de la transmission 3GPP/LTE [2]. Cependant, le CP-OFDM a aussi quelques inconvénients, notamment une perte d'efficacité spectrale en raison de l'ajout du CP et une mauvaise localisation en fréquence du fait de sa forme d'onde rectangulaire. Ces faiblesses ont poussé les chercheurs à examiner d'autres systèmes multiporteuses.

Pour faire face à ces lacunes, une solution possible appelée OFDM/OQAM (OFDM with Offset Quadrature Amplitude Modulation) [32] pourrait être utilisée à la place de l'OFDM.

Cette modulation a la même efficacité spectrale que l'OFDM sans CP, tout en ayant la possibilité d'utiliser des formes d'onde autres que la forme rectangulaire. Pour cela, on change le schéma de transmission de données pour transmettre des symboles réels seulement. L'orthogonalité n'est pas vérifiée dans le domaine complexe comme dans l'OFDM classique, mais dans le domaine réel. Ainsi, grâce à l'utilisation de formes d'onde appropriées, la modulation OFDM/OQAM ne nécessite pas l'utilisation d'un CP lors de la transmission, et présente de fait une efficacité spectrale théorique supérieure par rapport à CP-OFDM.

L'apparition des premiers systèmes de modulation multiporteuse en utilisant des filtres de forme d'onde autres que la forme rectangulaire remonte aux années 60 [15], [88]. Par la suite, une approche impliquant la transformée de Fourier discrète a été introduite en 1981 par B. Hirosaki dans [46]. L'acronyme OFDM/OQAM n'est apparu qu'en 1995 dans [32]. D'autres noms ont été utilisés pour désigner des systèmes identiques ou équivalents : Orthogonally multiplexed QAM ou O-QAM dans [45], OQAM-OFDM dans [99] pour les systèmes en temps continu ; OMC (for Orthogonal Multiple Carrier) dans [31] pour des systèmes en temps discret. Cependant, le système OFDM/OQAM, qui peut également être présenté en utilisant une approche de banc de filtres [92] et est donc également nommé FBMC/OQAM (Filter Bank Multi Carrier with OQAM) [87], a ses propres défauts. Comme le FBMC/OQAM ne peut pas profiter d'un CP, sa sensibilité au décalage temporel reste problématique.

Au-delà de la description théorique des versions analogiques et numériques des signaux OFDM/OQAM, de nombreux problèmes difficiles devaient encore être résolus concernant les aspects pratiques de communication.

Lorsque cette thèse a été lancée plusieurs problèmes liés à l'OFDM/OQAM étaient encore ouverts, par exemple :

- L'analyse de la synchronisation dans le domaine temporel et fréquentiel.
- Méthodes de synchronisation.
- La combinaison de l'OFDM/OQAM avec une technique d'accès multiple pour la transmission multi-utilisateurs dans le contexte 3GPP/LTE.

Cette thèse apporte des contributions sur tous ces sujets d'actualité pour la modula-

tion OFDM/OQAM. Nos argumentations sont présentées en 3 chapitres. Le contenu de ces chapitres est donné à suivre.

1.1 Chapitre 2

Le Chapitre 2 est consacré à la description des techniques de modulation OFDM et OFDM/OQAM, y compris la mise en oeuvre des architectures correspondantes.

Nous illustrons les avantages du système OFDM/OQAM en comparaison de celles de l'OFDM et on présente les filtres prototypes qui seront utilisés dans les chapitres suivants, chacun ayant différentes caractéristiques de localisation temporelle/fréquentielle et d'interférence.

L'objectif de cette thèse est d'étudier une classe de systèmes de modulation multiporteuse (MCM) différente de l'OFDM et offrant un certain nombre d'avantages en termes de robustesse au décalage fréquentiel (CFO) et temporel (TO). Pour le système MCM que nous présentons, nous remplaçons la fenêtre rectangulaire par une forme d'onde avec des propriétés améliorées. Dans le même temps, nous cherchons à préserver les caractéristiques de l'OFDM, à savoir l'orthogonalité et une bonne efficacité spectrale (idéalement la même que dans l'OFDM sans intervalle de garde).

Dans un cadre mathématique le signal OFDM peut être considéré comme un membre de la famille des fonctions de Gabor, où une fonction prototype est modulée exponentiellement. Pour l'OFDM la fonction prototype est une fenêtre rectangulaire de durée T_0, qui est également la durée des symboles de données complexes qui sont transmis sur chaque sous-porteuse. L'orthogonalité complexe est assurée, pour la reconstruction à la réception de ces symboles complexes, si la modulation exponentielle est juste un décalage de fréquence par F_0 ($F_0 = 1/T_0$), entre 2 sous-porteuses consécutives. Basé sur le théorème de Balian-Low [30], on sait que si on veut trouver une alternative à l'OFDM qui appartient aussi à une famille de fonction de Gabor, on doit :

- *i)* Soit relâcher la contrainte d'orthogonalité complexe de l'OFDM ;
- *ii)* Ou diminuer la densité $\rho = \frac{1}{F_0 T_0}$, (qui est une mesure de l'efficacité spectrale avec

$\rho = 1$ la valeur maximale théorique).

L'hypothèse *i)* a conduit à la modulation OFDM/OQAM (OFDM/Offset Quadrature Amplitude Modulation), tandis que *ii)* a conduit à l'OFDM suréchantillonné, voir par exemple [93] pour un aperçu récent, ou de manière équivalente à la modulation Filtered Multi Tone (FMT) [16]. Dans cette thèse, on se concentre uniquement sur la modulation OFDM/OQAM comme une alternative au CP-OFDM. Le schéma de modulation OFDM/OQAM n'utilise pas le CP et il peut utiliser différents types de filtres prototypes.

La modulation OFDM/OQAM vise à proposer une solution orthogonale avec une efficacité spectrale identique à l'OFDM sans CP, tout en conservant la possibilité d'utiliser une forme d'onde non rectangulaire. L'idée est d'échapper à la portée stricte de la théorie de Gabor et du théorème de Balian-Low en proposant un schéma différent de transmission de données. Ainsi, au lieu de transmettre un symbole complexe $c_{m,n} = c^{\mathcal{R}}_{m,n} + jc^{\mathcal{I}}_{m,n}$ de durée T_0 à l'indice de fréquence m, i.e. mF_0, et à l'indice de temps n, i.e. nT_0, comme en OFDM, il est proposé de transmettre avec un décalage temporel égal à $T_0/2$ soit la partie réelle ou imaginaire du symbole $c_{m,n}$, tout en imposant que deux symboles adjacents en temps et en fréquence aient une différence de phase égale à $\pi/2$. Se référant à la possibilité (non unique) de l'utilisation d'une constellation QAM pour chaque sous-porteuse, ce schéma de transmission est appelé OQAM (pour Offset QAM) en raison du décalage introduit entre la partie imaginaire et réelle du symbole à valeur complexe à transmettre comme le montre la table 1.1.

TAB. 1.1 – Schéma de transmission des symboles.

	$nT_0 - T_0/2$	nT_0	$nT_0 + T_0/2$
$(2m+1)F_0$	$c^{\mathcal{R}}_{2m+1,n-1}$	$jc^{\mathcal{I}}_{2m+1,n}$	$c^{\mathcal{R}}_{2m+1,n}$
$2mF_0$	$jc^{\mathcal{I}}_{2m,n-1}$	$c^{\mathcal{R}}_{2m,n}$	$jc^{\mathcal{I}}_{2m,n}$
$(2m-1)F_0$	$c^{\mathcal{R}}_{2m-1,n-1}$	$jc^{\mathcal{I}}_{2m-1,n}$	$c^{\mathcal{R}}_{2m-1,n}$

Ainsi, en supposant que g est une fonction prototype continue à valeur réelle ou même à valeur complexe de $\mathcal{L}_2(\mathbf{R})$, on peut écrire le signal en bande de base associé à ce schéma

de transmission, en supposant que M est pair ($M = 2N$), de la manière suivante :

$$s(t) = \sum_{m=0}^{N-1} \sum_{n} \left(c^{\mathcal{R}}_{2m,n} g(t - nT_0) + j c^{\mathcal{I}}_{2m,n} g(t - nT_0 - \frac{T_0}{2}) \right) e^{j2\pi(2m)F_0 t} + \left(c^{\mathcal{R}}_{2m+1,n} g(t - nT_0 - \frac{T_0}{2}) + j c^{\mathcal{I}}_{2m+1,n} g(t - nT_0) \right) e^{j2\pi(2m+1)F_0 t}, \quad (1.1)$$

avec T_0 le temps symbole et F_0 l'espacement inter-symbole. Comme on cherche un système à efficacité spectrale identique à celle de l'OFDM, on met $T_0 F_0 = 1$.

On peut écrire le signal (1.1) d'une manière plus compacte

$$s(t) = \sum_{n=-\infty}^{+\infty} \sum_{m=0}^{2N-1} a_{m,n} g_{m,n}(t), \quad (1.2)$$

avec la base de modulation $g_{m,n}(t)$ comme suit :

$$g_{m,n}(t) = g(t - n\tau_0) e^{j2\pi m F_0 t} e^{j\phi_{m,n}}, \quad (1.3)$$

où le terme de phase $\phi_{m,n}$

$$\phi_{m,n} = \begin{cases} 0, & \text{si } m \text{ et } n \text{ ont la même parité,} \\ \frac{\pi}{2}, & \text{si } m \text{ et } n \text{ n'ont pas la même parité.} \end{cases} \quad (1.4)$$

Cette expression indique que cette modulation transmet effectivement des symboles de données à valeurs réelles, i.e. $a_{m,n}$, et non des symboles à valeurs complexes comme dans l'OFDM. Les symboles $a_{m,n}$ sont obtenus en prenant les parties réelles et imaginaires des alphabets de constellation à valeurs complexes.

Ainsi, comme la modulation l'OFDM/OQAM transmet des réels, les équations de démodulation sont écrits en utilisant le produit scalaire réel. Ensuite :

$$\hat{a}_{m,n} = \langle g_{m,n}, s \rangle_{\mathbf{R}} = \Re\{ \int_{-\infty}^{+\infty} g^*_{m,n}(t) s(t) dt \}. \quad (1.5)$$

L'émetteur OFDM/OQAM peut être écrit sous la forme d'un banc de filtre de synthèse et le récepteur peut être écrit sous la forme d'un banc de filtre d'analyse [92]. A partir de ces bancs de filtres, des structures plus efficaces de modems OFDM/OQAM peuvent être obtenues en combinant une transformée rapide, en utilisant soit la FFT ou l'IFFT [89], avec un filtre polyphase, comme représenté dans la figure Figure 1.1.

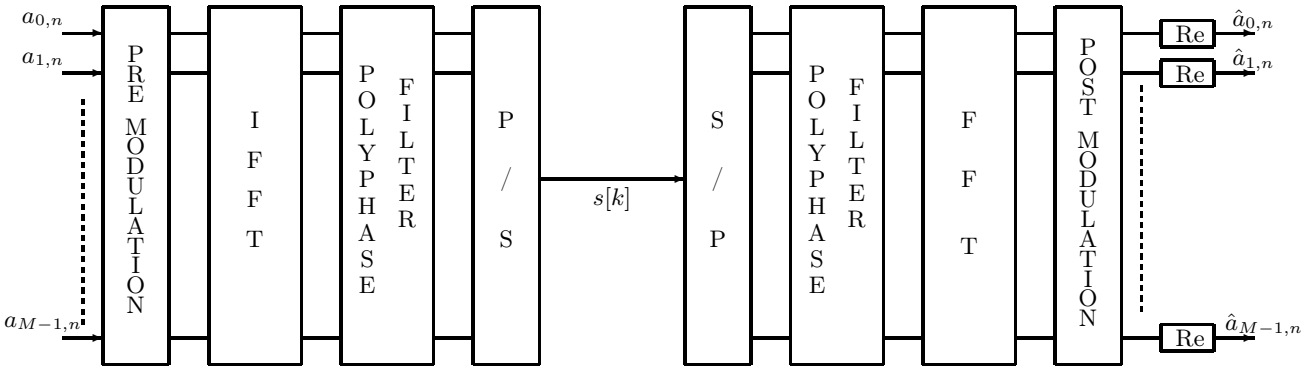

FIG. 1.1 – Structure générale du modem de l'OFDM/OQAM avec "Fast Fourier Transforms".

Par rapport à l'OFDM, avec l'OFDM/OQAM la fonction prototype g, ou le filtre prototype, ne sont pas nécessairement rectangulaire.

Par conséquent, l'étude de fonctions prototypes et des filtres prototypes est d'un intérêt particulier pour l'OFDM/OQAM, car il représente un degré important de liberté par rapport à ce qui est possible avec l'OFDM. Un prototype OFDM/OQAM doit répondre à des contraintes d'orthogonalité qui peuvent être dérivées en temps continu pour la fonction prototype, ou en temps discret pour le filtre prototype. De plus, ces prototypes peuvent être construits pour satisfaire certains objectifs clés, par exemple, la sélectivité fréquentielle ou la localisation temporelle-fréquentielle.

Comme exemple on peut considérer trois fonctions prototypes particulièrement importantes, nous avons la fonction fenêtre rectangulaire, le Square Root Raised Cosine Function (SRRC) et l'Isotropic Orthogonal Transform Algorithm (IOTA).

Tout d'abord, la fonction rectangulaire est définie dans le domaine temporel par :

$$\Pi(t) = \begin{cases} 1 & \text{pour } \mid t \mid \leq \frac{T_0}{2} \\ \\ 0 & \text{pour } \mid t \mid > \frac{T_0}{2}. \end{cases} \tag{1.6}$$

$\Pi(t)$ répond à la contrainte d'orthogonalité réelle. C'est la même fonction que celle utilisée dans l'OFDM. Nous allons l'utiliser comme une référence pour comparer avec des prototypes plus couramment utilisés en OFDM/OQAM.

SRRC est une fonction prototype très connue, dans les systèmes de communication numérique, car la combinaison des filtres SRRC de l'émission et de réception satisfait à la condition de Nyquist. L'expression du filtre SRRC dans le domaine fréquentiel est comme ci-dessous

$$R_c(\nu) = \begin{cases} \frac{1}{\sqrt{F_0}}, |\nu \leq (1-r)\frac{F_0}{2}| \\ \frac{1}{\sqrt{F_0}} \cos(\frac{\pi}{2}(\frac{|\nu|}{F_0} - \frac{1-r}{2})), (1-r)\frac{F_0}{2} < |\nu| \leq (1+r)\frac{F_0}{2} \\ 0, (1+r)\frac{F_0}{2} < |\nu| \end{cases} .$$

où $0 \leq r \leq 1$ est le facteur roll-off.

La réponse temporelle du filtre SRRC en temps continu s'écrit

$$r_c(t) = \sqrt{F_0} \frac{4rF_0t\cos(\pi(1+r)F_0t) + \sin(\pi(1-r)F_0t)}{(1-(4rF_0t)^2)\pi F_0t}$$

Extended Gaussian Function (EGF) est une fonction prototype qui résulte d'une procédure d'orthogonalisation de la fonction gaussienne [32]. Comme la fonction gaussienne ne répond pas à la propriété d'orthogonalité dans [4],[32] il a été proposé de l'orthogonaliser par une procédure en deux étapes. La fonction prototype résultante est appelée IOTA. En utilisant le même algorithme, un calcul direct conduit à l'EGF. EGF est définie dans le temps par :

$$Z_{\lambda,\mu_0,\tau_0}(t) = \frac{1}{2}\sum_{k=0}^{+\infty} d_{\lambda,\mu_0,\tau_0}[g_\lambda(t+\frac{k}{\mu_0}) + g_\lambda(t-\frac{k}{\mu_0})] \sum_{l=0}^{\infty} d_{l,1/\lambda,\mu_0,\tau_0}\cos(2\pi l\frac{t}{\tau_0}), \qquad (1.7)$$

avec λ un paramètre réel, d_{λ,μ_0,τ_0} des coefficients réels et $g_\lambda(t)$ la fonction Gaussienne donnée par :

$$g_\lambda(t) = (2\lambda)^{1/4} e^{-\pi\lambda t^2},$$

$\mu_0 = F_0 = \frac{1}{2\tau_0}$.

En posant $\mu_0 = \tau_0$ et $\lambda = 1$, on retrouve la fonction prototype IOTA.

Parmi les autres exemples bien connus de la classe des fonctions prototypes, on peut citer, outre le SRRC, l'Optimal Finite Duration Pulse (OFDP) [99], qui toutes deux peuvent offrir une bonne sélectivité fréquentielle, ou l'impulsion Hermite [41], [42] qui conduit à une bonne localisation temporelle-fréquentielle.

Dans la classe des filtres prototypes nous nous intéresserons aux trois types suivants : Mirabbasi, Martin, Bellanger (MMB) [65], [11], [67], Frequency Selective (FS) [80], [79] et Time Frequency Localization (TFL) [92], [79]. Les avantages du filtre prototype MMB sont les suivants : Tout d'abord, il est très simple d'obtenir les coefficients de ce filtre, le deuxième, le filtre obtenu peut avoir une décroissance rapide en fréquence, c'est-à-dire une pente raide des lobes secondaires dite fall-off rate. En outre, n'importe quel fall-off rate peut être librement atteint par le filtre prototype MMB mais au prix de l'augmentation de la longueur du filtre. Le filtre prototype MMB s'écrit sous la forme suivante :

$$g[n] = \begin{cases} \frac{1}{bM}(k_0 + 2\sum_{l=1}^{b-1} k_l \cos(\frac{2\pi ln}{bM})), & 0 \leq n \leq L_f \\ 0, & sinon \end{cases}. \tag{1.8}$$

où $L_f = bM + 1$ avec un nombre entier positif b signifiant le facteur de recouvrement, et k_l $(0 \leq l \leq b)$ des coefficients réels qui sont donnés dans [67] pour b jusqu'à 8.

Pour le filtre prototype FS [80], [79], le problème de conception correspondant est indiqué comme un problème d'optimisation sans contrainte, qui s'écrit comme

$$\underset{\{paramètres\}}{min} \quad \frac{E(f_c)}{E(0)} \qquad avec \qquad E(f_c) = \int_{f_c}^{\frac{1}{2}} |P(e^{j2\pi n\nu})|^2 d\nu, \tag{1.9}$$

où f_c est la fréquence de coupure et a l'expression $f_c = (1+\rho)\frac{1}{2M}$. Nous notons que le facteur ρ peut également être considéré comme un facteur "roll-off" entre [0, 1].

Pour le filtre prototype TFL, le critère de TFL vise à maximiser une mesure TFL $\xi_d(p)$ pour un filtre prototype p. Notons que dans les algorithmes de conception [92], [79] le critère utilisé est adapté pour les signaux à temps-discret et est donné par :

$$\xi_d(p) = \frac{1}{4\pi\sqrt{m_2(p)M_2(p)}}, \tag{1.10}$$

où $m_2(p)$ et $M_2(p)$ sont les moments de localisation temporelle et fréquentielle définis par Doroslovački dans [27]. Avec cette définition, il est possible d'obtenir une mesure bornée $0 \leq \xi_d(p) \leq 1$. Une caractéristique particulièrement intéressante de l'optimisation TFL, c'est que l'on peut obtenir d'excellentes mesures TFL, i.e. $\xi_d \simeq 0.91$, avec des filtres prototypes de courte longueur $(L = M)$. Ce n'est pas possible avec des prototypes IOTA tronqués [92]. Cela donne un solide avantage pour TFL par rapport à la complexité de la mise en

oeuvre et aussi dans la perspective d'une transmission exigeant des préambules courts (cf. Part 3) et/ou utilisant des trames courtes (cf. Part 4).

1.2 Chapitre 3

Le Chapitre 3 concerne l'étude du système OFDM/OQAM. Une analyse de performance est obtenue sous une condition de désynchronisation. Nous analysons l'OFDM/OQAM en temps et en fréquence et on présente une méthode pour la synchronisation.

La sensibilité de l'OFDM/OQAM au décalage temporel rend l'analyse de l'interférence [87] due à la désynchronisation un sujet très important dans la conception de la couche physique. Les résultats présentés dans [32] sont intéressants, mais ils ne sont pas complètement analysés. D'autre part, l'analyse plus détaillée dans [87] ne conduit qu'à des approximations du SIR (Signal to Interference Ratio).

Dans ce chapitre, on se concentre sur l'interférence causée par les décalages temporel et fréquentiel pour l'OFDM/OQAM. Réutilisant l'analyse présentée dans [58] concernant la transmission d'un signal OFDM/OQAM à travers un canal multi-trajets, on dérive deux expressions très simples de l'ISI et de l'interférence entre porteuses (ICI) ainsi que l'expression exacte du SIR. Ensuite, nous illustrons l'effet de la forme de d'onde sur ce terme d'interférence. Puis on compare notre modèle SIR exact avec le SIR simulé numériquement en utilisant différents filtres prototypes. Ces résultats sont également comparés à ceux obtenus pour l'OFDM. Dans notre étude, à travers une démonstration détaillée dans le cas des filtres prototypes orthogonaux, on met en évidence un lien entre notre analyse et celle dans [32]. Et enfin, on présente une méthode de synchronisation pour la transmission multi-utilisateurs en lien montant.

Quand on considère un environnement général avec le temps et la sélectivité fréquentielle, l'expression du modèle de canal multi-trajets équivalent s'écrit :

$$h(t,\tau) = \sum_{i=0}^{P-1} c_i e^{j2\pi f_d^i t} \delta(\tau - d_i), \tag{1.11}$$

où P est le nombre de trajets (le premier trajet étant le trajet de référence avec délai $d_0 = 0$) et c_i est le gain du canal variable avec le temps pour le i^{ime} trajet qui pourra être

exprimé comme $c_i = \rho_i e^{j\theta_i}$ avec ρ_i l'atténuation du i^{ime} trajet et θ_i la rotation de phase due au délai d_i ; f_d^i est la fréquence de Doppler du i^{ime} trajet ; $\delta(\cdot)$ est la fonction Dirac delta.

Alors on obtient la version "Z-transform" du modèle de canal à temps discret

$$H(k,z) = \sum_{l=0}^{L_h-1} c_l e^{j2\pi f_d^l k T_s} z^{-l}, \tag{1.12}$$

avec $T_s = \frac{1}{F_s}$ le temps d'échantillonnage, où F_s est la fréquence d'échantillonage.

En OFDM/OQAM, chaque sous-porteuse porte un symbole de valeur réelle $a_{m,n}$ qui correspond à la partie soit réelle ou imaginaire du symbole de donnée complexe QAM $c_{m,n}$. Dans ce qui suit, on note $\tau_0 = \frac{T_0}{2}$ la durée du symbole OFDM/OQAM de donnée réel $a_{m,n}$.

Comme rappelé dans le chapitre 2, le signal bande de base OFDM/OQAM est exprimé comme suit [92] :

$$s(t) = \sum_{m=0}^{M-1} \sum_{n\in\mathbf{Z}} a_{m,n} \underbrace{g(t-n\tau_0) e^{j2\pi m F_0 t} e^{j\phi_{m,n}}}_{g_{m,n}(t)}, \tag{1.13}$$

avec F_0 l'espacement inter-porteuses et $\phi_{m,n} = \frac{\pi}{2}(m+n)$ et $g(t)$ une fonction prototype paire à valeur réelle normalisée ($\|g\| = 1$).

Lorsqu'on néglige l'effet du bruit, le signal reçu en bande de base s'écrit

$$\begin{aligned} y(t) &= \sum_{i=0}^{P-1} h(t,d_i) s(t-d_i) \\ &= \sum_{i=0}^{P-1} c_i e^{j2\pi f_d^i t} \sum_{n\in\mathbf{Z}} \sum_{m=0}^{M-1} a_{m,n} g(t-d_i-n\tau_0) e^{j2\pi m F_0 (t-d_i)} e^{j\phi_{m,n}} \end{aligned} \tag{1.14}$$

Ensuite, le signal OFDM/OQAM démodulé s'écrit

$$\begin{aligned} y_{m_0,n_0} &= \int y(t) g^*_{m_0,n_0}(t) dt \\ &= \sum_{n\in\mathbf{Z}} \sum_{m=0}^{M-1} a_{m,n} e^{j\Delta\phi} \sum_{i=0}^{P-1} c_i e^{-j2\pi m F_0 d_i} \\ &\times \int_{-\infty}^{+\infty} g(t-d_i-n\tau_0) g(t-n_0\tau_0) e^{j2\pi((m-m_0)F_0+f_d^i)t} dt \\ &= \sum_{n\in\mathbf{Z}} \sum_{m=0}^{M-1} a_{m,n} e^{j\Delta\phi} \sum_{i=0}^{P-1} c_i e^{-j2\pi m F_0 d_i} e^{j2\pi((m-m_0)F_0+f_d^i)(\frac{n_0+n}{2}\tau_0+\frac{d_i}{2})} \\ &\times A_g((n_0-n)\tau_0 - d_i, (m_0-m)F_0 - f_d^i), \end{aligned} \tag{1.15}$$

où A_g est la fonction d'ambiguité de $g(t)$, $\Delta\phi = \phi_{m,n} - \phi_{m_0,n_0}$, avec $\phi_{m,n} = \frac{\pi}{2}(m+n)$, et $*$ représente la conjugaison complexe.

Le signal OFDM/OQAM démodulé en temps discret s'écrit

$$\begin{aligned} y_{m_0,n_0} &= \sum_{(p,q)} a_{m_0+p,n_0+q} e^{j\frac{\pi}{2}(p+q+pq)} e^{j\pi p n_0} \sum_{l=0}^{L_h-1} c_l e^{j\pi[\frac{(2n_0+q)}{2}+\frac{l}{M}]\frac{1}{r}} \\ &\times A_g[-qN-l, -(p+\frac{1}{r})] e^{-j\frac{\pi(2m_0+p)l}{M}} \\ &= \underbrace{\sum_{l=0}^{L_h-1} c_l e^{j\pi[n_0+\frac{l}{M}]\frac{1}{r}} A_g[-l, -\frac{1}{r}] e^{-j\frac{2\pi m_0 l}{M}}}_{distortion:\alpha_{m_0,n_0}} a_{m_0,n_0} \\ &+ \underbrace{\sum_{(p,q)\neq(0,0)} a_{m_0+p,n_0+q} e^{j\frac{\pi}{2}(p+q+pq)} e^{j\pi p n_0} \sum_{l=0}^{L_h-1} c_l e^{j\pi[\frac{(2n_0+q)}{2}+\frac{l}{M}]\frac{1}{r}} A_g[-qN-l, -(p+\frac{1}{r})] e^{-j\frac{\pi(2m_0+p)l}{M}}}_{ISI+ICI:J_{m_0,n_0}} \end{aligned} \tag{1.16}$$

En se basant sur l'équation (1.16), on analyse l'interférence causée par le décalage temporel (considérant la synchronisation fréquentielle parfaite), le décalage fréquentiel (considérant la synchronisation temporelle parfaite) et le décalage temporel-fréquentiel pour l'OFDM/OQAM et on dérive l'expression exacte du SIR basée sur l'expression de l'interférence dérivée dans notre analyse qu'on compare avec celle dans [32].

Toute cette analyse est réalisée en utilisant les formes d'ondes TFL1, IOTA4, FS4 et MMB4 et également comparée à l'OFDM, illustrant leur effet sur le terme d'interférence et montrant les bonnes performances des formes d'ondes en cas de décalage temporel et/ou fréquentiel par rapport aux autres.

De plus, pour vérifier l'utilité de notre propre expression pour les filtres prototypes nonorthogonaux, on a également considéré un filtre prototype SRRC de courte longueur, $L = M$ nommé SRRC1, avec un roll-of égal à 0.5 pour le comparer avec l'un de nos filtres prototypes orthogonaux (TFL1). Notre propre expression et celle de Alard [32], en utilisant le filtre prototype TFL1, aboutissent exactement au même résultat, et d'autre part, on voit que lorsque on utilise le filtre prototype SRRC1 les calculs ne conduisent pas exactement au même résultat. Pour confirmer ces résultats analytiques, on effectue aussi des simulations

avec ces filtres prototypes TFL1 et SRRC1. Elles montrent que notre expression donne les mêmes résultats que les courbes simulées pour TFL1 et SRRC1, mais par contre si l'expression [32, eq.35] donne les même résultats pour la courbe TFL1 ceux-ci différent pour la courbe SRRC1 simulée.

En raison des meilleures performances dans le domaine fréquentiel, le problème de synchronisation fréquentielle est moins critique pour l'OFDM/OQAM que pour l'OFDM. Au contraire dans le domaine temporel, à la différence du CP-OFDM, l'OFDM/OQAM ne peut pas profiter des propriétés de corrélation liées au CP. Ainsi, comme la synchronisation temporelle peut-être le point le plus critique de cette modulation, on va se concentrer uniquement sur elle dans la deuxième partie de ce chapitre, tout en considérant les cas mono et multi-utilisateurs.

Il existe plusieurs méthodes utilisées pour la synchronisation temporelle pour l'OFDM/OQAM. En général, ces méthodes utilisent la corrélation dans le domaine temporel du signal reçu. Cette corrélation peut, par exemple, être créée en utilisant les pilotes déterministes groupés sous la forme de préambules [34] ou, alternativement, à partir de pilotes répartis basés sur des séquences pseudo-aléatoires [50]. La synchronisation utilisée dans [50] souffre d'une grande complexité en raison de l'utilisation de plusieurs corrélations successives. Une autre technique utilisée dans [95] réalise la synchronisation, dans le domaine fréquentiel. Mais alors de longs préambules sont nécessaires. Dans cette thèse, en relation avec l'application cible décrite au chapitre 4, on préfére se concentrer sur les méthodes de synchronisation qui sont appropriées pour la transmission par paquets. Comme ces préambules doivent être courts, on peut prendre [34] comme référence. Conformément à [34], une relation entre des échantillons du signal peut être obtenue par un préambule spécifique (les porteuses impaires sont mises à zéro) et ces relations peuvent être maintenues après filtrage en utilisant un filtre prototype de longueur impaire. Un inconvénient est que la longueur du préambule [34] augmente avec la longueur du filtre prototype.

Plus récemment la thèse de Y. Dandach [22] a montré la possibilité de limiter la durée du préambule égal à un symbole multiporteuse (M). En plus, le choix d'un préambule déterministe permet la création de pics à la sortie IFFT, qui peut être utile pour réduire la complexité de l'estimateur.

On rappelle ici les principes de base de la méthode proposée et on va montrer comment elle peut être étendue à la synchronisation temporelle pour le multi-utilisateurs.

Comme dans [34], l'idée est d'exploiter les propriétés de conjugaison qui sont exactement remplies à la sortie du modulateur. Ensuite, il est attendu que, après transmission à travers un canal multi-trajets et un ajout de bruit, elles seront toujours approximativement satisfaites. Ensuite, une mesure moindres carrés (Least Squares) peut être utilisée pour décider quelle estimation conduit à la meilleure approximation.

On désigne par $v_{k,n}$ la sortie de l'IFFT d'indice k à l'instant n du système OFDM/OQAM représenté à la Figure 1.1. Considérant un filtre prototype de longueur $L = qM$, avec q un entier, il a été montré dans [23] que les $v_{k,n}$ satisfont les relations suivantes

$$\begin{cases} v_{k,n} &= (-1)^n v^*_{\frac{M}{2}-k-1,n} \\ v_{\frac{M}{2}+k,n} &= (-1)^n v^*_{M-k-1,n}. \end{cases} \tag{1.17}$$

Ces relations générales s'appliquent pour toute entrée IFFT et sont donc également valables pour tout type de préambule, déterministe ou aléatoire.

Une autre propriété de conjugaison apparaît si nous choisissons, comme dans [34], un préambule où une sous-porteuse sur 2 est mise à zéro. Ensuite, il peut être démontré [22] que, en plus de (1.17), on a aussi

$$v_{k,n} = (-1)^n v^*_{M-k-1,n} \qquad \text{pour} \qquad 0 \le k \le \frac{M}{2} - 1. \tag{1.18}$$

Posant $L = M$, on peut utiliser le préambule suivant

$$\begin{cases} p_{2m,0} = (-1)^m \frac{\sqrt{2}}{2} \\ \\ p_{2m+1,0} = 0 \end{cases} \qquad \text{pour} \qquad 0 \le m \le \tfrac{M}{2} - 1, \tag{1.19}$$

et

$$p_{m,1} = 0, \qquad \text{pour} \qquad 0 \le m \le M - 1. \tag{1.20}$$

La durée du préambule est limitée à deux symboles pilotes successifs, ici $n = 0$ et 1. Le symbole nul est introduit pour séparer les symboles pilotes et les données.

On peut noter que le préambule donné dans (1.19) mène à 4 pics aux sorties de l'IFFT d'indices 0, $\frac{M}{2} - 1$, $\frac{M}{2}$ et $M - 1$ comme le montre l'exemple avec $M = 64$ donné dans la

Figure 1.2. Ces valeurs de pics sont le moins affecté en présence du bruit ou d'un canal multi-trajets. Ainsi, on peut obtenir des estimateurs plus robustes et moins complexe en négligeant au côté récepteur les calculs qui ne correspondent pas aux valeurs de crête.

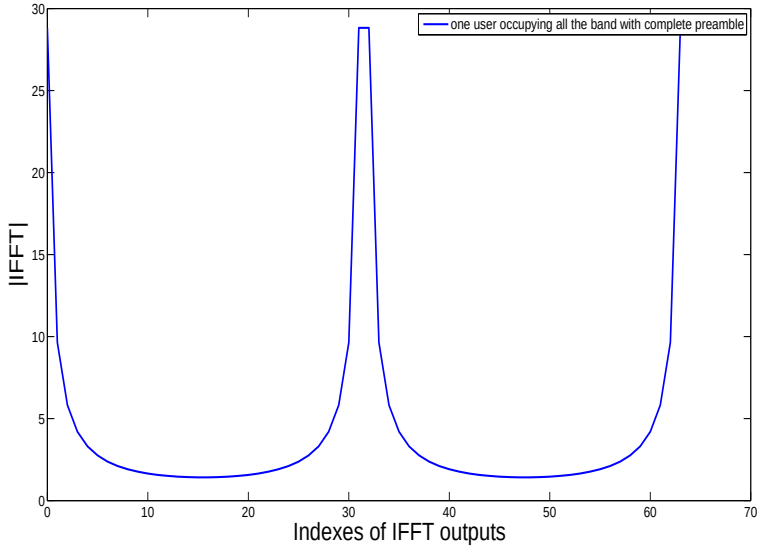

FIG. 1.2 – Valeur d'amplitude de la sortie de l'IFFT pour le préambule utilisé dans le système de transmission mono-utilisateur en lien descendant.

L'estimateur dérivé dans [34] s'écrit :

$$\hat{\tau}_{LS} = \arg\max_{\hat{\tau}} |\sum_{k=0}^{\frac{M}{2}-1} r[k+\hat{\tau}]r[M-1-k+\hat{\tau}]|. \tag{1.21}$$

L'estimateur utilisé dans la présente section, et proposé dans [22], peut s'écrire comme suit :

$$\hat{\tau}_{LS} = \arg\max_{\hat{\tau}} |r[\hat{\tau}]r[M-1+\hat{\tau}] + r[\frac{M}{2}-1+\hat{\tau}]r[\frac{M}{2}+\hat{\tau}]|. \tag{1.22}$$

Cet estimateur peut être réduit à :

$$\hat{\tau}_{LS} = \arg\max_{\hat{\tau}} |r[\frac{M}{2}-1+\hat{\tau}]r[\frac{M}{2}+\hat{\tau}]|. \tag{1.23}$$

Par conséquent, il est clair que l'estimateur (1.23) est beaucoup moins complexe à mettre en oeuvre que celui de (1.21).

La synchronisation multi-utilisateurs en lien montant est, en général, une tâche difficile qui présente une vision radicalement différente de la situation de lien descendant correspondante [36], [35]. La raison principale est que les signaux en lien montant transmis par des utilisateurs distincts sont caractérisés par différents décalages temporel et fréquentiel et, par conséquent, le récepteur doit estimer beaucoup plus de paramètres que dans le lien descendant.

En conséquence, les méthodes utilisées dans le lien descendant ne s'appliquent pas à un scénario de lien montant car les signaux sont affectés par des erreurs de synchronisation différentes et la correction du décalage temporel et fréquentiel d'un utilisateur causera un désalignement entre les autres utilisateurs initialement alignés.

Dans notre étude, on considère un système de transmission en lien montant multi-utilisateurs, avec une situation dans laquelle les sous-canaux différents sont attribués à des utilisateurs distincts, même si dans la pratique plusieurs sous-canaux peuvent être attribués à un seul utilisateur donné en fonction de son débit de données requis. Les sous-porteuses sont réparties entre les utilisateurs actifs, elles sont attribuées par blocs, chaque utilisateur dispose de ses propres porteuses adjacentes [70]. L'attribution d'un groupe de sous-porteuses contiguës à chaque utilisateur actif rend la tâche de synchronisation simple. Chacun de ces utilisateurs est affecté de différents décalages temporels, le système multi-utilisateurs représentant nos simulations pour évaluer l'estimateur de chaque utilisateur [70] est présenté à la Figure 1.3, dans la pratique la correction est effectuée à l'émission.

Pour séparer les signaux des utilisateurs au niveau du récepteur, nous utilisons un banc de filtres [70], qui peut sélectionner la bande appropriée aux utilisateurs. Cette opération de filtrage permet au récepteur d'effectuer l'estimation de synchronisation indépendamment pour chaque utilisateur actif, comme on le voit dans les équations suivantes, où (1.24) est l'entrée du banc de filtres et (1.25) est la sortie du banc de filtres (l'entrée d'estimateur de chaque utilisateur).

$$r(t) = \sum_{u=0}^{U-1} r_u^{\tau_u}(t) = \sum_{u=0}^{U-1} r_u(t - \tau_u), \tag{1.24}$$

$$u \in \{u_0, u_1, u_2, ..., U-1\},$$

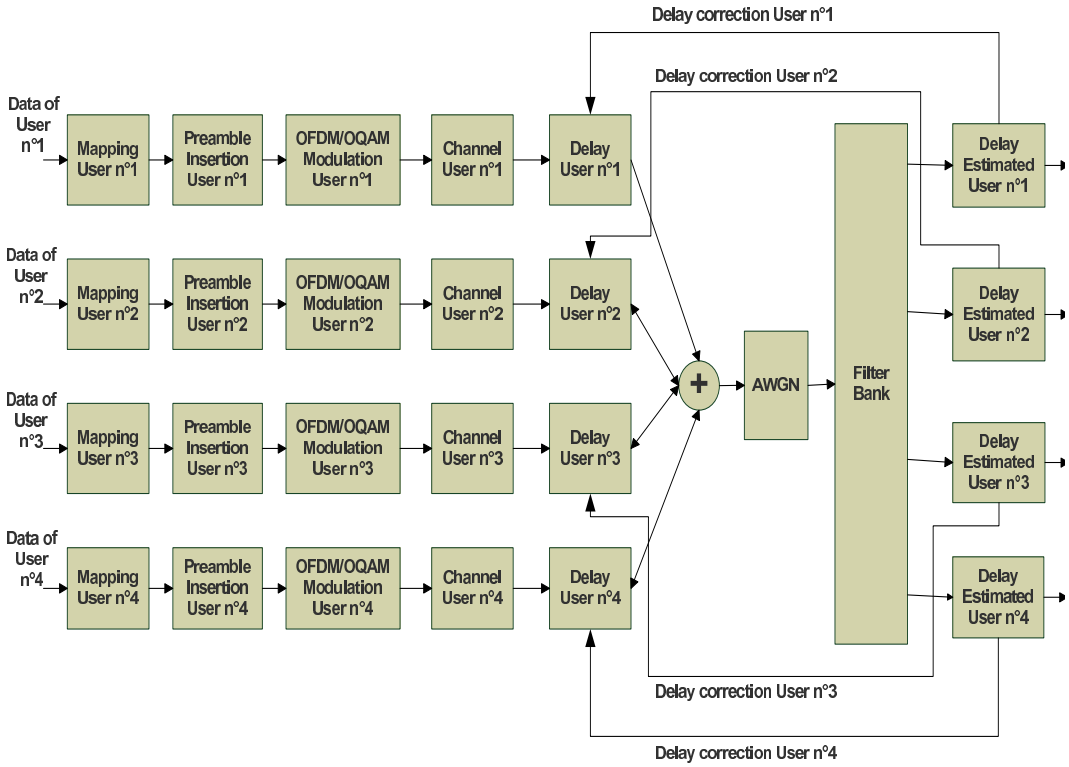

FIG. 1.3 – Le système de transmission multi-utilisateurs en lien montant utilisé dans nos simulations.

$$r_u(t-\tau_u) = r(t) \otimes P^u_{FB}(t), \tag{1.25}$$

où $\otimes$ est l'opération de convolution et P^u_{FB} est le banc de filtres utilisé pour séparer les signaux des utilisateurs $s_u(t)$ de délai τ_u.

La méthode dans [22] a été proposée pour la transmission mono-utilisateur en lien descendant, en utilisant un seul préambule de la taille de la FFT comme indiqué dans la Figure 1.4. Pour adapter le préambule pour la transmission multi-utilisateurs en lien montant, les Figures 1.5-1.8 montrent que chaque utilisateur a son propre préambule. Donc, ce préambule pourrait être défini comme suit

$$p^u_{2m,0} = \begin{cases} (-1)^m \frac{\sqrt{2}}{2} & \text{pour} \quad m^b_u \leq m \leq m^s_u \\ 0 & \text{autrement} \end{cases} \tag{1.26}$$

avec $u = 0, 1, ..., U-1$, $\bigcup_u [m^b_u, m^s_u] = [0, M-1]$ et $\bigcap_u [m^b_u, m^s_u] = \phi$.

Dans notre configuration de simulation on considère 4 utilisateurs ($U = 4$) partageant

également une bande passante constituée de $M = 16$ sous-porteuses. Puis, comme le montre la Figure 1.9, même si la sortie de l' IFFT est légèrement différente de celle représentée à la Figure 1.2 pour le cas mono-utlisateur, les quatre pics sont toujours présents.

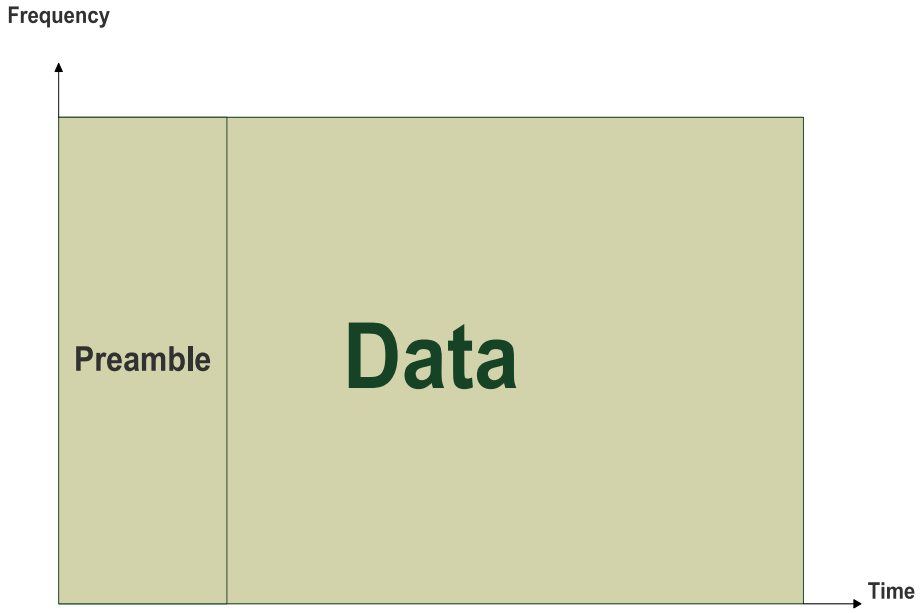

FIG. 1.4 – Le préambule utilisé dans le système de transmission mono-utilisateur en lien descendant.

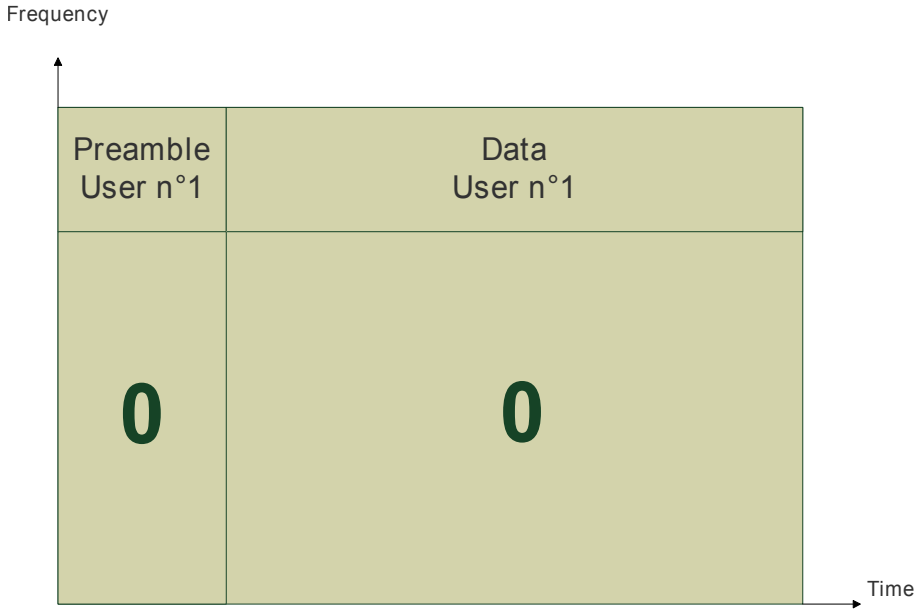

FIG. 1.5 – Le préambule modifié utilisé par l'utilisateur n.1 dans le système de transmission multi-utilisateurs en lien montant.

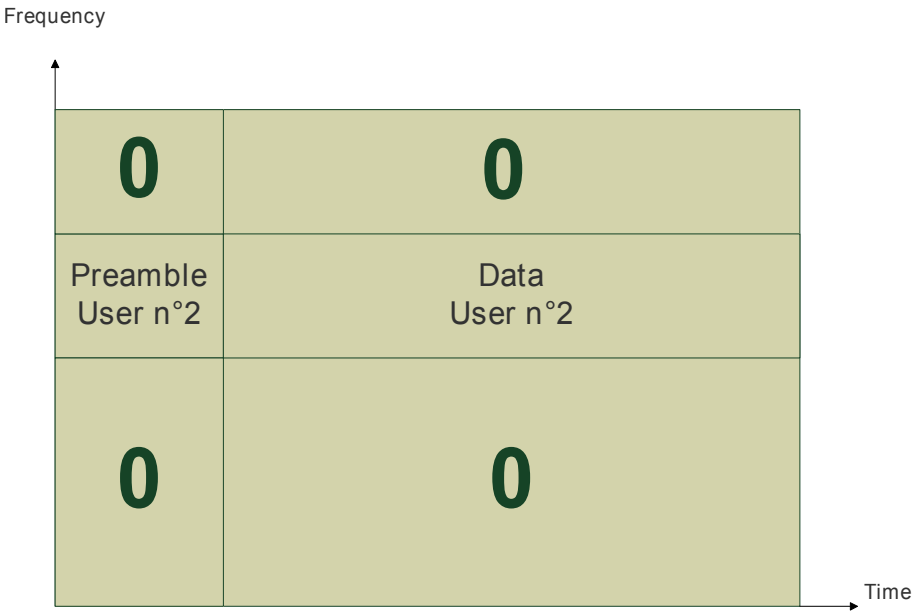

FIG. 1.6 – Le préambule modifié utilisé par l'utilisateur n.2 dans le système de transmission multi-utilisateurs en lien montant.

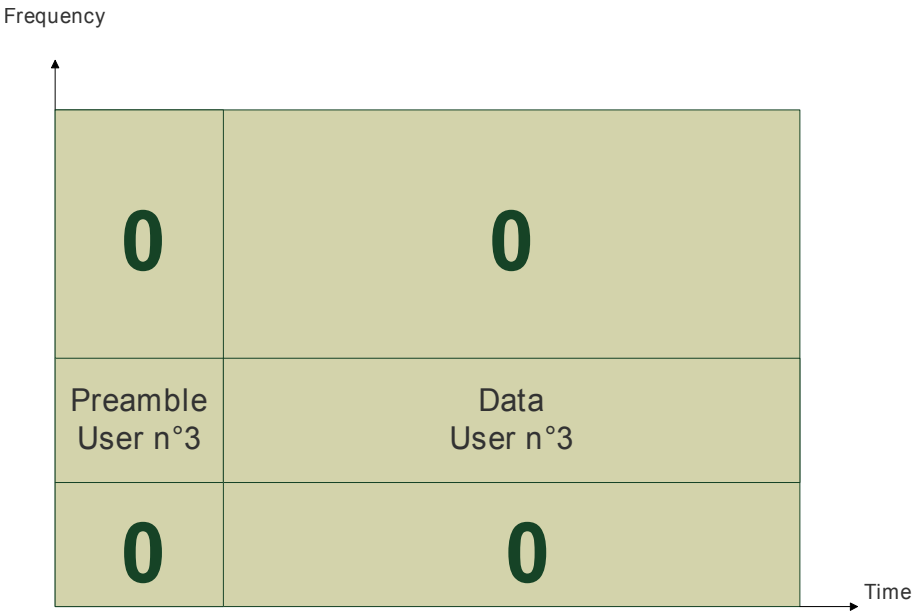

FIG. 1.7 – Le préambule modifié utilisé par l'utilisateur n.3 dans le système de transmission multi-utilisateurs en lien montant.

Dans ce cas, basé sur (1.23), l'estimateur de temps de chaque utilisateur est :

$$\hat{\tau}^u_{LS} = \arg\max_{\hat{\tau}^u} |r[\frac{M}{2} - 1 - \hat{\tau}^u] r[\frac{M}{2} - \hat{\tau}^u]|. \tag{1.27}$$

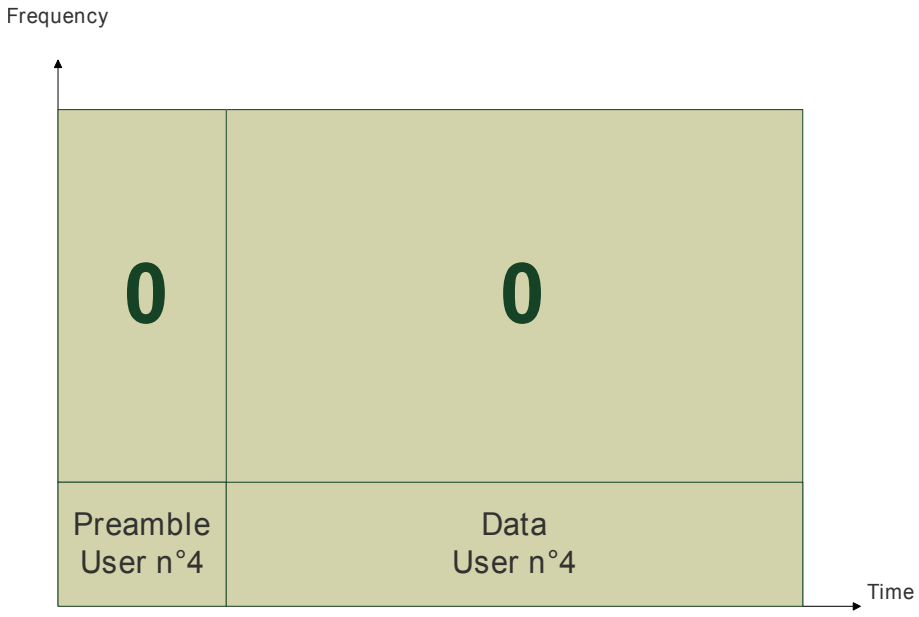

FIG. 1.8 – Le préambule modifié utilisé par l'utilisateur n.4 dans le système de transmission multi-utilisateurs en lien montant.

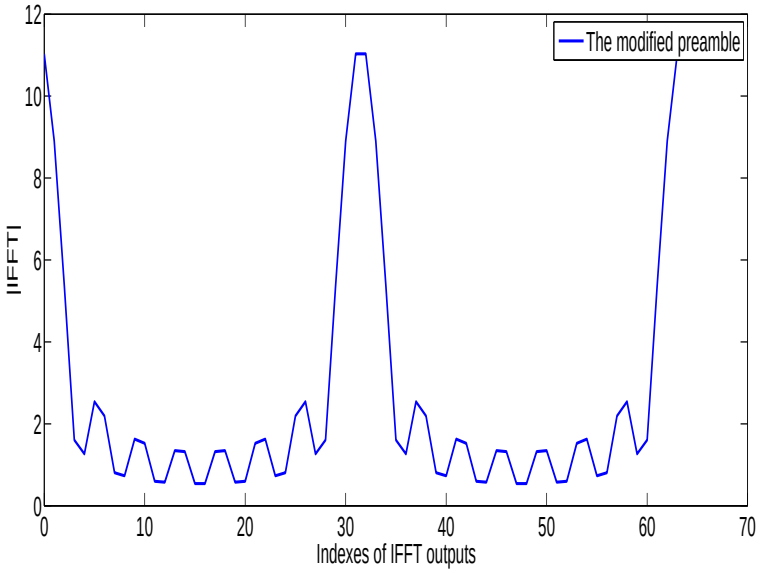

FIG. 1.9 – Valeur d'amplitude de la sortie de l'IFFT pour le préambule de chaque utilisateur dans le système de transmission multi-utilisateurs en lien montant.

Pour évaluer les performances de la nouvelle méthode de synchronisation pour la transmission multi-utilisateurs en lien montant, on évalue les performances de l'estimateur en présence d'un canal AWGN et multi-trajet, en considérant différents valeurs de délai, on

examine chaque utilisateur individuellement, on montre la bonne performance des estimateurs utilisés, montrant son efficacité à détecter et à estimer le décalage temporel de chaque utilisateur et que les délais n'ont pas d'impact sur la performance de l'estimateur en présence du canal multi-trajet.

Enfin, on évalue l'exactitude de l'estimateur en simulant le BER d'un tel utilisateur après avoir corrigé le délai estimé par l'estimateur, contre le SNR pour chaque utilisateur et avec des délais différents, on le compare avec le cas de synchronisation parfaite. On montre que les performances des utilisateurs avec les délais corrigés dans les différents cas sont les mêmes, ce qui prouve l'efficacité et la stabilité de la performance de l'estimateur avec différents délais.

1.3 Chapitre 4

Le Chapitre 4 propose un schéma d'accès multiple alternatif basé sur la modulation OFDM/OQAM pour le contexte 3GPP/LTE UL.

Pour le lien descendant, la norme 3GPP/LTE a unanimement considéré l'OFDMA comme la technique la plus appropriée pour atteindre une grande efficacité spectrale. Pour le lien montant, le 3GPP/LTE a choisi le SC-FDMA [2] au lieu de l'OFDMA, car il conduit à un PAPR (Peak to Average Power Ratio) inférieur. Le SC-FDMA peut être considéré comme un nouveau schéma de modulation hybride qui offre un PAPR quasi-similaire comme les systèmes mono-porteuses. Le SC-FDMA a déjà prouvé sa capacité à lutter contre les canaux sélectifs en fréquence, grâce à l'utilisation de la modulation CP-OFDM et sa flexibilité en matière d'accès multiples, grâce à la composante FDMA. L'OFDMA et le SC-FDMA, étant à la fois basés sur la modulation OFDM avec préfixe cyclique, donnent lieu à 2 inconvénients, la perte d'efficacité spectrale et la sensibilité à la dispersion de fréquence, par exemple, l'étalement Doppler. Tous les deux peuvent être contrecarrés en utilisant l'OFDM/OQAM qui, comme indiqué dans [32], est un moyen efficace pour obtenir de l'efficacité spectrale et de la robustesse à l'étalement Doppler. Dans ce chapitre, on discute de la possibilité d'utiliser l'OQAMA (OFDM/OQAM for multiple Access) et le DFT-OQAMA (Discrete Fourier Transform OQAMA) à la place de l'OFDMA et du

SC-FDMA pour le scénario de 3GPP/LTE en lien montant, indépendamment du problème de PAPR et tout en considérant les synchronisations temporelle et fréquentielle parfaites.

On présente brièvement les quatre différentes modulations et schémas d'accès, OFDMA, SC-FDMA, OQAMA and DFT-OQAMA, considérés dans ce chapitre et présentés dans la Fig. 1.10. Dans cette description schématique les blocs non-colorés correspondent aux fonctionnalités communes, tandis que les blocs en bleu sont pour l'OFDMA et aussi pour le SC-FDMA en ajoutant les blocs rouge, enfin, les blocs verts sont pour l'OQAMA et aussi pour le DFT-OQAMA en ajoutant les blocs en rouge.

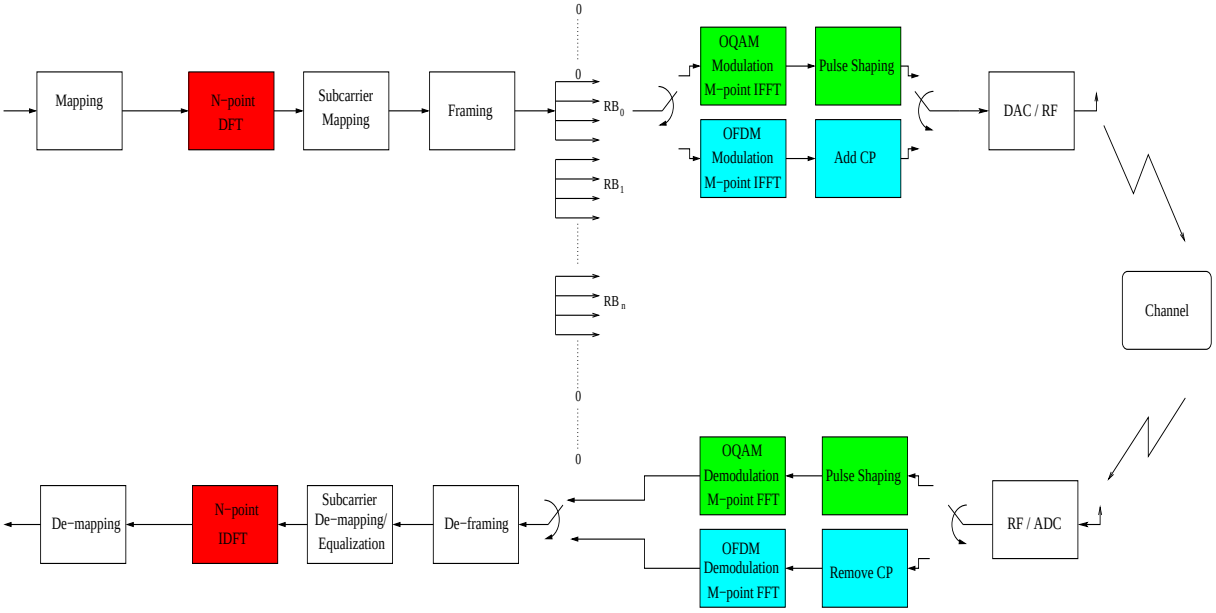

FIG. 1.10 – Configurations des systèmes OFDMA, SC-FDMA, OQAMA et DFT-OQAMA en lien montant.

En cours de transmission, le signal est perturbé par la présence d'échos et, éventuellement, par la présence de Doppler. Les conséquences des perturbations liées au canal peuvent être mesurées en partie par le BER, qui indique la quantité de bits de données mal transmises sur un canal considéré. Ainsi, pour les canaux sévères, avec de nombreux différents types de perturbations, il devient nécessaire de compenser les effets du canal au niveau du récepteur.

Actuellement dans les systèmes de télécommunications les plus pratiques, comme pour le 3GPP/LTE par exemple, une partie de la trame est dédiée à l'insertion des pilotes pour

l'estimation de canal. L'objectif de l'estimation de canal est de trouver une approximation de la fonction de transfert du canal qui va ensuite servir à son égalisation.

Dans le cas de systèmes de modulation multi-porteuses, lorsqu'ils sont correctement dimensionnés, l'estimation de canal revient à déterminer un coefficient de canal par porteuse, ce qui simplifie le problème. Ainsi, que ce soit un critère de type Zero Forcing (ZF) ou un critère de type de minimisation de l'erreur quadratique moyenne (MMSE), on peut effectivement limiter les effets du canal et du bruit. Dans le cas de modulations multi-porteuses, l'estimation de canal doit être effectuée à n'importe quel moment et pour n'importe quelle fréquence. Pour réaliser une telle estimation, des symboles appelés symboles pilotes sont généralement insérés dans la trame de transmission. Ces symboles pilotes sont connus par le récepteur. Dans ce chapitre, on se concentre sur les méthodes d'estimation de canal et d'égalisation qui peuvent être utilisées pour l'OFDM/OQAM et le DFT-OQAM. On présente la méthode d'estimation de canal présentée par C. Lélé et al. [62] IAM (Interference Approximation Method) et la méthode d'égalisation Complex FIR Subcarrier Equalizer (CFIR-SCE) [56] qui sont utilisées dans nos évaluations de performances fournis en section 4.5.

On simule la modulation OFDM/OQAM en accès multiple (OQAMA) pour voir l'impact de l'interférence produite par les utilisateurs adjacents. On montre que les performances pour l'utilisateur ciblé ne dépend que du canal et de la fonction prototype utilisés et non pas des ordres de modulation utilisés par les utilisateurs voisins.

On précise les paramètres du système et on propose d'adapter la structure de la trame de transmission de l'OQAMA dans le context LTE.

Dans notre travail, on compare OQAMA et DFT-OQAMA aux techniques OFDMA et SC-FDMA bien connues, dans un contexte 3GPP/LTE en lien montant, tout en considérant les synchronisations temporelle et fréquentielle parfaites et indépendamment du PAPR.

On a simulé des utilisateurs occupant soit 20 Ressource Block (RBs) ou 1 RB à vitesses de 3 Km/h et 120 Km/h, avec l'estimation de canal parfaite et réelle. Pour l'OFDMA et le SC-FDMA, on utilise les séquences de pilotes complexes de Zadoff Chu [2], et pour l'OQAMA et le DFT-OQAMA on utilise la méthode IAM-I pour l'estimation de canal

réelle.

Par conséquent on voit que pour le même BER et PER cible pour l'estimation de canal réelle, dans la plupart des cas, selon les configurations l'OQAMA a un gain SNR supérieur de 0.14 à 1.4 dB par rapport à l'OFDMA et au SC-FDMA et donc surpasse ces deux schémas de transmission, et cela est vrai aussi pour le DFT-OQAMA comparé au SC-FDMA. En effet, par un choix judicieux du préambule la méthode IAM-I augmente en réception la puissance des pilotes transmis qui devient supérieure à la puissance des pilotes du CP-OFDM, et nous avons ainsi une meilleure estimation de canal. Ainsi, l'utilisation de symboles pilotes en préambule dans le cadre de la 3GPP/LTE est favorable à l'OQAMA et au DFT-OQAMA par rapport à l'OFDMA et au SC-FDMA montrant que l'OQAMA et DFT-OQAMA sont robustes pour la transmission 3GPP/LTE en lien montant.

Jusqu'à présent on a considéré que côté modulation les distorsions étaient seulement dues à la distorsion du canal et du bruit additif. Cela est vrai pour les schémas de l'OFDMA et du SC-FDMA qui n'introduisent pas de chevauchement entre les symboles successifs. Au contraire, avec l'OFDM/OQAM les symboles multiporteuses successifs se chevauchent et par conséquent la durée pour transmettre une séquence de symboles de données doit être étendue en proportion de la longueur du filtre prototype. Un travail précédent a analysé ce problème, dans [10], où les auteurs tentent de réduire les effets des bords par l'introduction d'une fonction de pondération. Si la méthode est utilisable pour des filtres prototypes longs, toutefois, elle ne permet pas, comme [24], une récupération parfaite des symboles tronqués même dans des situations de transmission idéales.

Dans [22], la transmission en mode paquet est seulement analysée dans une configuration théorique : pas de canal, pas de bruit. Dans ce chapitre, on étudie l'effet de deux stratégies de transmission par préambule pour construire le cadre 3GPP/LTE et nous les évaluons dans des conditions réelles de transmission.

Dans la section 4.5, on a présenté les résultats que nous avons déjà obtenus dans [37] où, afin d'éviter les chevauchements entre les trames successives, c'est à dire entre les utilisateurs, on a introduit un intervalle de garde de longueur τ_0. Ensuite, dans la section suivante, on compare les deux options pour le tramage de l'OFDM/OQAM en 3GPP/LTE.

Utilisant la première solution, dans la section 4.5, on a pu éviter l'interférence, mais elle a entraîné une perte d'efficacité spectrale, qui est de $\frac{30}{31}$ (ou 0.14 dB). Pour éviter cette perte, on a appliqué, dans le contexte de transmission 3GPP/LTE en lien montant, la méthode rappelée à la section 4.6. En l'utilisant, on peut récupérer un symbole complet, avec seulement la transmission d'une version tronquée de la forme d'onde associée. En utilisant cette méthode, on a pu envoyer 31 symboles réelles de données au lieu de 30, et on peut obtenir les mêmes performances que celles présentées dans [37] évitant la perte de 0.14 dB due à l'intervalle de garde de τ_0.

Pour vérifier cela plus précisément, on a évalué les performances du mode d'OFDM/OQAM par paquet et on a comparé avec celles des simulations du système OFDM/OQAM dans [37], en utilisant 20 RBs et en supposant l'estimation de canal parfaite. Les simulations ont été effectuées avec les mêmes valeurs de paramètres que dans [37] utilisant le même canal à 6 trajets et un canal à un trajet. On montre que la transmission de l'OQAMA par paquets conduit aux mêmes résultats que ceux de l'OQAMA avec une bande de garde à zéro ajoutée entre les trames. Cela prouve l'efficacité de cette méthode de transmission par paquets dans le contexte 3GPP/LTE en lien montant.

Finalement, on conclut notre thèse en mettant en évidence ses résultats les plus significatifs et quelques nouvelles perspectives dans le domaine.

Part II

Part 2

Chapter 2

Overview of the OFDM/OQAM modulation

To fight against frequency selectivity of the transmission channels, one of the possible solutions is to use the Multi-Carrier Modulation (MCM). Indeed, it is now recognized that MCM presents strong advantages.

In this chapter, we first give some mathematical tools that can help to better understand OFDM/OQAM scheme from a Gabor theory point of view. Then, we pay more attention on the presentation of OFDM/OQAM including the basic idea, its implementation and the initial set of prototype filters used in this thesis.

2.1 OFDM modulation scheme

2.1.1 Historical overview

The idea of transmitting modulated data in parallel, over multiple carriers frequencies can be aged back to 50's. Nevertheless, due to the complexity issue over a long period Frequency Division Multiplex (FDM) was not considered in any of the real system implementation. This type of solution could only become competitive if the subcarriers were orthogonal to each other. Which allows the optimization of the the spectral occupation of the signal. In the late 50's a solution appeared using an orthogonal frequency multiplex [26], [71]. Since then, over the 60's, these systems began to be more and more advanced [15], [88] and better understood. In the 80's, one of these MCM variants started to be

known under the acronym OFDM [18], [52].

Since that time, with the development of methods and algorithms for digital signal processing and applications that require high throughput, OFDM has become increasingly popular [107]. In addition, this modulation is now integrated into many existing telecommunication standards, such as ADSL, DAB, DVB-T, IEEE 802.11 and IEEE 802.16 standards [21].

2.1.2 The OFDM signal

The OFDM modulation consists of transmitting complex data $c_{m,n}$ with $m \in \{0, \ldots, M-1\}$ and $n \in \mathbf{Z}$ by means of M sub-carriers using the following baseband signal $s(t)$:

$$s(t) = \sqrt{\frac{1}{T_0}} \sum_{m=0}^{M-1} \sum_{n \in \mathbf{Z}} c_{m,n} \Pi(t - nT_0) e^{j2\pi m F_0 t}, \tag{2.1}$$

where $j^2 = -1$ and Π represents the rectangular function, given by :

$$\Pi(t) = \begin{cases} 1, & \text{if } -\frac{T_0}{2} \leq t < \frac{T_0}{2}, \\ 0, & \text{otherwise.} \end{cases} \tag{2.2}$$

$F_0 = 1/T_0$ is the inter-carrier spacing. T_0 is the OFDM symbol duration. The complex data $c_{m,n}$ are, in most practical cases, issued from a complex constellation of type Phase Shift Keying (PSK) or Quadrature Amplitude Modulation (QAM). We can talk about orthogonal frequency multiplex because we easily show that the family of functions :

$$\Pi_{m,n}(t) = \sqrt{\frac{1}{T_0}} \Pi(t - nT_0) e^{j2\pi m F_0 t} \tag{2.3}$$

forms an orthonormal basis with all the squared integrable functions, i.e. in $\mathcal{L}_2(\mathbf{R})$, for the complex scalar product :

$$\langle f, g \rangle = \int_{\mathbf{R}} f(t) g^*(t) dt, \tag{2.4}$$

where $*$ represents the conjugate operation. Indeed, we get :

$$\langle \Pi_{m,n}, \Pi_{p,q} \rangle = \delta_{m,p} \delta_{n,q}, \tag{2.5}$$

δ being the Kronecker symbol. The demodulation of the signal simply comes by realizing a scalar product :

$$\hat{c}_{p,q} = \langle \Pi_{p,q}, s \rangle . \tag{2.6}$$

In order to realize the transmission systems in digital form, which is the most common case, it is necessary first to study the behavior of discrete time signals and systems to implement. With a sampling rate of $T_s = T_0/M$, the OFDM modulation can be simply driven by an Inverse Discrete Fourier Transform (IDFT) of the sent data :

$$[s(nMT_s), \ldots, s((nM + M - 1)T_s)] = \text{IDFT}\{c_{0,n}, \ldots, c_{M-1,n}\}, \tag{2.7}$$

while the demodulation conducts to a Discrete Fourier Transform (DFT) of the signal samples :

$$[\hat{c}_{0,n}, \ldots, \hat{c}_{M-1,n}] = \text{DFT}\{s(nMT_s), \ldots, s((nM + M - 1)T_s)\}. \tag{2.8}$$

The practical interest of such processing based on IDFT and DFT is related to the possibility, as shown in Figure 2.1, of using fast algorithms of Inverse Fast Fourier Transform (IFFT) or Fast Fourier Transform (FFT) type. The OFDM modem structure in discrete time is conceptually simple because it is equivalent to putting an IFFT and a FFT back to back, and use a parallel-to-serial (P/S) conversion at the transmitter and a serial-to-parallel (S/P) conversion at the receiver side.

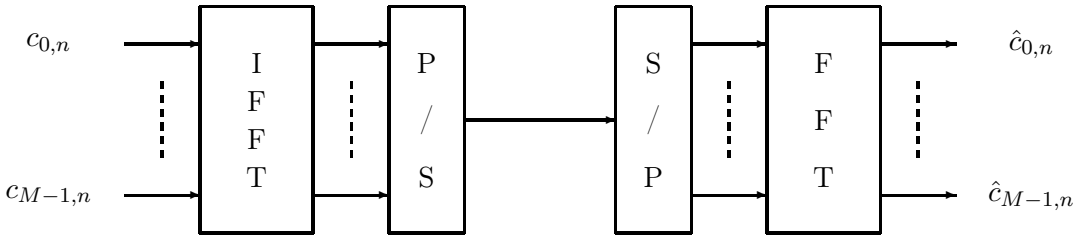

FIG. 2.1 – Digital OFDM Modem.

2.1.3 Robustness to frequency selective channels

When a single-carrier signal is sent in a wide bandwidth channel, this signal is likely to be affected by deep fading due to the channel propagation. This perturbation gets severer while the frequency band (B) gets larger. However, using a signal with M sub-carriers, this is equivalent to transmitting data on narrower frequency bands as $\frac{B}{M}$. Thus, given B, the

higher M is, the more we can consider that the transmission is performed on frequency bands where the channel transfer function can be considered as constant. This limits the effect of strong frequency selectivity and thus inter-symbol interference. The equalization of the system then returns to perform channel compensation in a much simpler way.

On the other hand, when the number of carriers increases, then the duration of the OFDM symbol time increases. In addition to the problems of complexity, the system still remains sensitive to intersymbol interference (ISI). To fight against this phenomenon, Peled and Ruiz in [78], introduced a modified version of OFDM systems consisting of extending the duration of the symbol, going from T_0 to $T_0' = T_0 + \Delta$, by duplicating a part of the OFDM symbol, and therefore it has been named cyclic prefix (CP). The addition of this time interval of duration Δ helps to absorb the echoes due to the channel, and it can also be used for synchronization at the receiver side. This technique was then massively applied to the OFDM modulation. The baseband CP-OFDM signal can be written as :

$$s(t) = \frac{1}{\sqrt{T_0}} \sum_{m=0}^{M-1} \sum_{n \in \mathbf{Z}} c_{m,n}\, \Pi_\Delta(t - nT_1) e^{j2\pi m F_0 t}, \tag{2.9}$$

with $T_1 = T_0 + \Delta > T_0$ and

$$\Pi_\Delta(t) = \begin{cases} 1 & \text{if } -\Delta - \frac{T_0}{2} \leq t < \frac{T_0}{2}, \\ 0 & \text{otherwise.} \end{cases} \tag{2.10}$$

If we take a guard interval of length at least equal to the maximum delay introduced by a multipath channel, we are able to fully eliminate the ISI.

For the CP-OFDM scheme, the modulated signal writes as :

$$[s(nNT_s), \ldots, s((nN + M - 1)T_s)] = \text{IDFT}\left\{c_{0,n}, \ldots, c_{M-1,n}\right\}, \tag{2.11}$$

with $N > M$ and (see Figure 2.2)

$$[s((nN + M - N)T_s), \ldots, s((nN - 1)T_s)] = [s(nN + 2M - NT_s), \ldots, s((nN + M - 1)T_s)]\,.$$

The discrete time expression is then given by :

$$s[k] = \sum_n \sum_{m=0}^{M-1} c_{m,n} \Pi_N[k - nN] e^{j\frac{2\pi}{M}mk}, \tag{2.12}$$

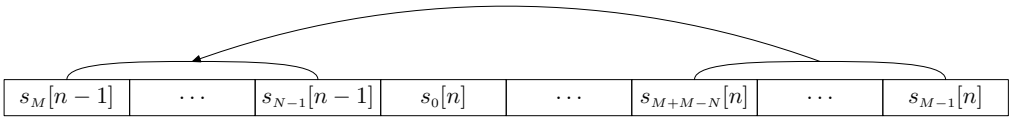

FIG. 2.2 – Cyclic Prefix for the n^{th} OFDM symbole time.

with

$$\Pi_N[k] = \begin{cases} 1 & \text{if } k \in \{0, ..., N-1\}, \\ 0 & \text{otherwise.} \end{cases} \tag{2.13}$$

.

In discrete time, the equalization method is simple, it only amounts to remove the CP at the receiver to avoid interference between the blocks.

2.1.4 The OFDM limits

We have seen that OFDM can be an appropriate modulation for transmission towards a multipath channel. However, OFDM avoids ISI by using a CP longer than the maximum delay spread of the channel. The CP carries redundant information and thus reduces the bandwidth efficiency of the system. Moreover, the OFDM modulation uses a rectangular pulse shape, which results in a sinc characterization in frequency domain. A direct consequence of such a pulse shape is to lead to a bad power spectrum localization. This causes large intercarrier interference (ICI) in the presence of any carrier frequency offset (CFO). In addition, if OFDM is used for the uplink of a multiple access network, i.e. OFDMA network, any mismatch between the carrier frequencies of the different nodes in the network will result in a loss of orthogonality between subcarriers, leading to a significant performance loss [70]. The above mentioned weaknesses have shifted researchers to alternative MCMs which are predicted to provide certain improvements. The idea for the new MCM schemes is, firstly, to replace the OFDM rectangular waveform with a waveform having better properties in terms of localization and having, in particular, a frequency response with a higher attenuation, and, secondly, to avoid using any CP in order to improve the spectral efficiency.

2.2 Advanced multicarrier modulation

The goal of this thesis is to study a class of MCM systems being different from OFDM and offering a number of advantages in terms of robustness to CFO and multiple access effects. For the MCM scheme we present, we replace the rectangular window by a waveform with improved properties. At the same time, we seek to preserve the characteristics of OFDM, namely the orthogonality and good spectral efficiency (ideally the same as in OFDM without guard interval). Also, as for conventional OFDM and differently from [96] who consider hexagonal configurations, in this thesis we only focus on the case of rectangular time-frequency lattices. At first, let us recall some definitions from part of the book [30].

2.2.1 Time-Frequency analysis

Let g be a function of $\mathcal{L}_2(\mathbf{R})$. We denote $G(\nu)$ as its Fourier transform. We denote $||.||$ as the norm associated with the scalar product defined in (2.4). We define the moments of order 1 and 2 in time and frequency as follows :

– moment of order 1 in time :

$$m^{(1)}(g) = \frac{1}{\|g\|^2} \int_{-\infty}^{+\infty} t|g(t)|^2 dt \,; \tag{2.14}$$

– moment of order 2 in time :

$$m^{(2)}(g) = \frac{1}{\|g\|^2} \int_{-\infty}^{+\infty} \left(t - m^{(1)}(g)\right)^2 |g(t)|^2 dt \,; \tag{2.15}$$

– moment of order 1 in frequency :

$$M^{(1)}(g) = \frac{1}{\|g\|^2} \int_{-\infty}^{+\infty} \nu|G(\nu)|^2 d\nu \,; \tag{2.16}$$

– moment of order 2 in frequency :

$$M^{(2)}(g) = \frac{1}{\|g\|^2} \int_{-\infty}^{+\infty} \left(\nu - M^{(1)}(g)\right)^2 |G(\nu)|^2 d\nu. \tag{2.17}$$

Similarly to [32], we define the time-frequency localization as follows :

Definition 1 (Time-Frequency Localization) *We call the time-frequency localization of a function g of $\mathcal{L}_2(\mathbf{R})$ the quantity $\xi(g)$ defined by :*

$$\xi(g) = \frac{1}{4\pi\sqrt{m^{(2)}(g)M^{(2)}(g)}}. \tag{2.18}$$

We have also the following result :

Theorem 2.2.1 (Heisenberg-Gabor Inequality) *When $g \in \mathcal{L}_2(\mathbf{R})$, then :*

$$0 \leq \xi(g) \leq 1 \tag{2.19}$$

and the equality $\xi(g) = 1$ is reached if and only if $g(t) = Ce^{-st^2}$ with $C \in \mathbb{C}$ and $s > 0$ (Gaussian function).

Let us introduce now some definitions and results concerning the Weyl-Heisenberg (or Gabor) families.

Definition 2 (Weyl-Heisenberg Family) *When $g \in \mathcal{L}_2(\boldsymbol{R})$, $F_0 \in \boldsymbol{R}$ and $T_0 \in \boldsymbol{R}$, we call* Weyl-Heisenberg family *(or Gabor's) of $\mathcal{L}_2(\boldsymbol{R})$ all $(g_{m,n})_{(m,n)\in\boldsymbol{Z}^2}$ family of functions of $\mathcal{L}_2(\boldsymbol{R})$ verifying :*

$$\forall t \in \mathbb{R},\ g_{m,n}(t) = g(t - nT_0)e^{j2\pi mF_0 t}. \tag{2.20}$$

The function g is called prototype function. The $g_{m,n}$ functions are the translated in time and frequency of the prototype function. Moreover, we call the magnitude $\rho = \frac{1}{T_0F_0}$ the density of the Weyl-Heisenberg family.

It is then proved in [25] that a Weyl-Heisenberg (W-H) family forms an orthogonal basis of $\mathcal{L}_2(\mathbf{R})$ if $\rho = 1$. Finally, it should be noted, by observing (2.3), that the familly of $(\Pi_{m,n})$ functions forms a family of Weyl-Heisenberg of density 1.

2.2.2 Balian-Low Theorem and its consequences

Theorem 2.2.2 (Balian-Low Theorem) *When $(g_{m,n})_{(m,n)\in\mathbb{Z}^2}$ is a W-H family of density 1 of $\mathcal{L}_2(\boldsymbol{R})$, forming an orthogonal basis [1], then,*

$$m^{(2)}(g)M^{(2)}(g) = +\infty.$$

[1] To be more precise, the Balian-Low theorem concerns the concept of frames [30], [89], but in this thesis we only focus on the particularly case of orthogonal bases.

This theorem explains that for such families of functions, it is not possible to have a prototype function g that possesses both orthogonality and excellent localization at the same time. According to the Balian-Low theorem and the definition of time-frequency localization (definition 1), in the case of OFDM we obtain a localization measure that tends to 0. Based on this theorem we can also deduce the following property :

property 1 *For W-H family, we can have only two of these three characteristics simultaneously :*

1. $\rho = 1$ *;*
2. *an orthogonal system ;*
3. *a waveform well localized in time and frequency.*

2.2.3 Escaping to Balian-Low theorem

In a mathematical framework the OFDM signal can be seen as a member in the family of Gabor functions, where a prototype function is exponentially modulated. For OFDM the prototype function is a rectangular window of duration T_0, which is also the duration of the complex data symbols that are transmitted on each subcarrier. The complex orthogonality is insured, for the reconstruction at reception of these complex symbols, if the exponential modulation is just a frequency shift by F_0 ($F_0 = 1/T_0$), between 2 consecutive sub-carriers. Based on Balian-Low's theorem [30], we know that if we want to find an alternative to OFDM that also belongs to a family of Gabor function, we must :

- *i)* Either relax the complex orthogonality constraint of OFDM ;
- *ii)* Or decrease the density $\rho = \frac{1}{F_0 T_0}$, (which is a measure of the spectral efficiency with $\rho = 1$ the maximum theoretical value).

The hypothesis *i)* has led to the OFDM/OQAM (OFDM/Offset Quadrature Amplitude Modulation) modulation, whereas *ii)* has led to oversampled OFDM, see e.g. [93] for a recent overview, or, equivalently, to the Filtered Multi Tone (FMT) modulation [16]. In this thesis, we only focus on the OFDM/OQAM modulation as an alternative to CP-OFDM. The OFDM/OQAM modulation scheme does not use CP and it can use various types of prototype filters.

2.3 The OFDM/OQAM modulation scheme

2.3.1 Principle of the OFDM/OQAM

It is important to recall at first a brief historical evolution of OFDM/OQAM. The pioneering works containing the basic ingredients of what will be called later on OFDM/OQAM date back to the sixties. Indeed in [15], [88], the authors show how a multi-carrier modulation (MCM) system can work if an appropriate time-offset is introduced on each sub-carrier to transmit PAM (Pulse Amplitude Modulation) and QAM constellations, respectively, with for QAM a time shift between the real and imaginary components. In 1981 a digital implementation of these analog schemes, including the Discrete Fourier Transform (DFT), was proposed in [46]. The OFDM/OQAM denomination only appeared 14 years later [32]. This publication, together with Haas' PhD thesis [41], highlighted the interest of using OFDM/OQAM. Indeed, these publications were the first ones to illustrate the importance of time-frequency localization for the OFDM/OQAM waveforms in the case of a transmission through time-frequency dispersive channels, proposing in the meantime some optimized prototype functions. Moreover, from the signal processing perspective, the link with the filter bank theory, initiated in [31] with the so-called Orthogonal Multiple Carrier (OMC), was fully assessed later on in [90], [89], [92], where the authors also tackle the design problem for discrete-time prototype filters.

In general, since the mid-90s, the interest of using OFDM/OQAM has been well emphasized not only in continuous time formulations, but also in discrete time formulations, then illustrating the link between the OFDM/OQAM and the theory of filter banks. This resulted into a few Ph.D. theses conducted in France [41], [47], [82], [59], [89], [22] and abroad [12], [55]. In the following sections, we rely primarily on the work carried out in France Telecom by C. Siclet [89], A. Skrzypczak [93] and H. Lin [56] to study the OFDM and OFDM/OQAM modulation techniques including the corresponding implementation architectures. We illustrate the advantages of the OFDM/OQAM system over the OFDM one, and present the prototype filters to be used in the future chapters, each one having different time/frequency localization features.

2.3.2 The OFDM/OQAM system

The OFDM/OQAM aims to propose an orthogonal solution with spectral efficiency being identical to the OFDM without CP while retaining the ability of using a non rectangular waveform. The idea is to escape to the strict scope of Gabor theory and Balian-Low theorem by proposing a different scheme of data transmission. Thus, instead of transmitting a complex symbol $c_{m,n} = c^{\mathcal{R}}_{m,n} + jc^{\mathcal{I}}_{m,n}$ of duration T_0 at frequency index m, i.e. mF_0, and time index instant n, i.e. nT_0, like in OFDM, it is proposed to transmit with an offset time equal to $T_0/2$ either the real or imaginary part of the $c_{m,n}$ symbol, while requiring that two adjacent symbols in time and frequency have a phase difference equal to $\pi/2$. Referring to the possibility (not unique) of using a QAM constellation for each subcarrier, this transmission scheme is called OQAM (for Offset QAM) because of the offset introduced between the real and the imaginary part of the complex-valued symbol to be transmitted. Table 2.1 shows more clearly such a staggered structure.

TAB. 2.1 – Symbols transmission scheme.

	$nT_0 - T_0/2$	nT_0	$nT_0 + T_0/2$
$(2m+1)F_0$	$c^{\mathcal{R}}_{2m+1,n-1}$	$jc^{\mathcal{I}}_{2m+1,n}$	$c^{\mathcal{R}}_{2m+1,n}$
$2mF_0$	$jc^{\mathcal{I}}_{2m,n-1}$	$c^{\mathcal{R}}_{2m,n}$	$jc^{\mathcal{I}}_{2m,n}$
$(2m-1)F_0$	$c^{\mathcal{R}}_{2m-1,n-1}$	$jc^{\mathcal{I}}_{2m-1,n}$	$c^{\mathcal{R}}_{2m-1,n}$

Thus, assuming g is a continuous, real-valued, or even complex-valued function of $\mathcal{L}_2(\mathbf{R})$, we can write the baseband signal associated with this transmission scheme, assuming that M is even ($M = 2N$), in the following way :

$$s(t) = \sum_{m=0}^{N-1} \sum_{n} \left(c^{\mathcal{R}}_{2m,n} g(t - nT_0) + jc^{\mathcal{I}}_{2m,n} g(t - nT_0 - \frac{T_0}{2}) \right) e^{j2\pi(2m)F_0 t} + \left(c^{\mathcal{R}}_{2m+1,n} g(t - nT_0 - \frac{T_0}{2}) + jc^{\mathcal{I}}_{2m+1,n} g(t - nT_0) \right) e^{j2\pi(2m+1)F_0 t}, \quad (2.21)$$

with T_0 and F_0 being the symbol time and the inter-carrier spacing, respectively. As we seek a system with spectral efficiency identical to OFDM, we set $T_0 F_0 = 1$. From the

viewpoint of the demodulation, the equations are written as follows :

$$\hat{c}^{\mathcal{R}}_{2m,n} = \Re\{\int_{-\infty}^{+\infty} \check{g}^*(t - nT_0)e^{-j2\pi(2m)F_0 t}s(t)dt\} \tag{2.22}$$

$$\hat{c}^{\mathcal{I}}_{2m,n} = \Im\{\int_{-\infty}^{+\infty} \check{g}^*(t - nT_0 - T_0/2)e^{-j2\pi(2m)F_0 t}s(t)dt\} \tag{2.23}$$

$$\hat{c}^{\mathcal{I}}_{2m+1,n} = \Im\{\int_{-\infty}^{+\infty} \check{g}^*(t - nT_0)e^{-j2\pi(2m+1)F_0 t}s(t)dt\} \tag{2.24}$$

$$\hat{c}^{\mathcal{R}}_{2m+1,n} = \Re\{\int_{-\infty}^{+\infty} \check{g}^*(t - nT_0 - T_0/2)e^{-j2\pi(2m+1)F_0 t}s(t)dt\}. \tag{2.25}$$

$\check{g}$ being an analog function of demodulation (a function of $\mathcal{L}_2(\mathbf{R})$ with real or complex values). By setting :

$$a_{2m,2n} = c^{\mathcal{R}}_{2m,n} \qquad g_{2m,2n}(t) = g(t - nT_0)e^{j2\pi(2m)F_0 t} \tag{2.26}$$

$$a_{2m,2n+1} = c^{\mathcal{I}}_{2m,n} \qquad g_{2m,2n+1}(t) = jg(t - nT_0 - T_0/2)e^{j2\pi(2m)F_0 t} \tag{2.27}$$

$$a_{2m+1,2n} = c^{\mathcal{R}}_{2m+1,n} \qquad g_{2m+1,2n}(t) = jg(t - nT_0)e^{j2\pi(2m+1)F_0 t} \tag{2.28}$$

$$a_{2m+1,2n+1} = c^{\mathcal{R}}_{2m+1,n} \qquad g_{2m+1,2n+1}(t) = g(t - nT_0 - T_0/2)e^{j2\pi(2m+1)F_0 t}, \tag{2.29}$$

we can rewrite the signal $s(t)$ in (2.21) in a more compact way :

$$s(t) = \sum_{n=-\infty}^{+\infty} \sum_{m=0}^{2N-1} a_{m,n}g_{m,n}(t). \tag{2.30}$$

This expression shows that this modulation actually transmits real-valued data symbols, i.e. $a_{m,n}$, and not complex-valued symbols as in OFDM. The symbols $a_{m,n}$ are obtained by taking the real and imaginary parts of the complex-valued constellation alphabets according to (2.26 - 2.29). Also, to establish a link with OFDM and the Gabor family, we can set $\tau_0 = \frac{T_0}{2} = \frac{1}{2F_0}$ and define the phase term $\phi_{m,n}$ as :

$$\phi_{m,n} = \begin{cases} 0, & \text{if } m \text{ and } n \text{ have the same parity,} \\ \frac{\pi}{2}, & \text{if } m \text{ and } n \text{ are of different parities.} \end{cases} \tag{2.31}$$

It appears that the base of modulation $g_{m,n}$ forms a family of Gabor with density 2 :

$$g_{m,n}(t) = g(t - n\tau_0)e^{j2\pi mF_0 t}e^{j\phi_{m,n}}. \tag{2.32}$$

For this scheme, considering the transmission of real numbers, the rectangular time-frequency lattice has a density $\rho = \frac{1}{T_0F_0} = 1$. But, here as we only transmit real-valued symbols, and

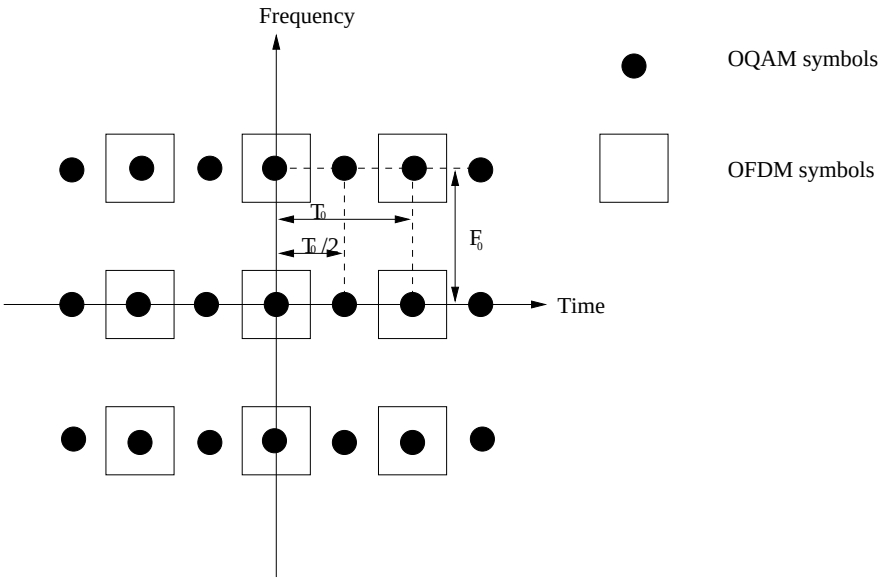

FIG. 2.3 – OFDM and OQAM symbol representation in the rectangular time-frequency plane.

not complex ones, the Balian-Low theorem does not apply. Indeed, for OFDM/OQAM orthogonality constraints only hold in the real field, and thus, it is actually possible, as it will be illustrated later on, to build a system that is both orthogonal and having a waveform with good time-frequency localization. Regarding the spectral efficiency, we see that in OFDM/OQAM, we send a real data symbol per frequency and on a duration of τ_0. We will then send the equivalent of a complex data symbol per frequency and per multicarrier symbol time (T_0) as shown in Figure 2.3. We can therefore conclude that the spectral efficiencies of an OFDM without CP system and of OFDM/OQAM are identical.

For the equations of demodulation, we define the base of demodulation as follows :

$$\check{g}_{m,n}(t) = \check{g}(t - n\tau_0)e^{j2\pi mF_0 t}e^{j\phi_{m,n}}. \tag{2.33}$$

Thus, as the OFDM/OQAM modulation transmits reals, the equations of demodulation are written by using the real scalar product. Then :

$$\hat{a}_{m,n} = \langle \check{g}_{m,n}, s \rangle_{\mathbf{R}} = \Re\{\int_{-\infty}^{+\infty} \check{g}^*_{m,n}(t)s(t)dt\}. \tag{2.34}$$

The real orthogonality, or biorthogonality condition, leading to $\hat{a}_{m,n} = a_{m,n}$, $\forall$ (m,n), is

satisfied if :

$$\Re\{\int_{-\infty}^{+\infty} g_{m,n}^*(t)\check{g}_{p,q}(t)dt\} = \delta_{m,p}\delta_{n,q}. \tag{2.35}$$

If the waveform $\check{g}$ at the receiver satisfies (2.35) and that :

- $\check{g} = g$, we talk about orthogonal systems (or OFDM/OQAM).
- $\check{g} \neq g$, we talk about biorthogonal systems (or BFDM/OQAM) [89], [90], [13], [68].

In the remainder of this thesis, we will only consider the orthogonal case with g an even real-valued function which is the most frequent case.

Finally, there are explicit expressions of the additive phase $\phi_{m,n}$ given in (2.31). Thus, in [32], this phase is defined by :

$$\phi_{m,n} = \frac{\pi}{2}(m+n). \tag{2.36}$$

On the other hand, in [89], [92], this phase is defined by :

$$\phi_{m,n} = \frac{\pi}{2}(m+n) - \pi mn. \tag{2.37}$$

Similarly, in the remainder of this thesis, we will only use the first $\phi_{m,n}$ definition (2.36).

A formulation in continuous-time does not usually generate systems directly usable in practice. This is why the study in discrete-time makes more sense, especially since most systems are implemented digitally. In another hand, a continuous filter g may have infinite support also yielding non-causality. It is then necessary to look for a Finite Impulse Response (FIR) digital prototype filter. Initially, we note that the band occupied by the OFDM/OQAM signal is approximately $B = MF_0$. Thus, we deduce from the theorem of Shannon the critical sampling frequency $F_s = MF_0$ as well as the sampling time $T_s = T_0/M$. Now suppose that the energy of the waveform g is focused on a time interval of finite length L_gT_s equal to $\left[-\frac{D+1}{2}T_s, \left(L_g - \frac{D}{2}\right)T_s\right]$ with L_g and D strictly positive integers. In the orthogonal case, we have $D = L_g - 1$. To obtain causal FIR filters of length L_g after sampling, we introduce a time shift of $DT_s/2$ to g. This gives [92], [89] :

$$s[k] = \sqrt{T_s}s\left((k - D/2)T_s\right) = \sum_{n=-\infty}^{+\infty}\sum_{m=0}^{2N-1} a_{m,n}\sqrt{T_s}g_{m,n}\left((k - D/2)T_s\right). \tag{2.38}$$

Denoting $g_{m,n}[k] = \sqrt{T_s} g_{m,n}\left((k - D/2)T_s\right)$, we then get the expression of a discrete-time Gabor family :

$$\begin{aligned} g_{m,n}[k] &= \sqrt{T_s} g_{m,n}\left((k - D/2)T_s\right), \\ &= \sqrt{T_s} g\left((k - D/2)T_s - n\tau_0\right) e^{j2\pi m F_0((k-D/2)T_s)} e^{j\phi_{m,n}}, \\ &= \sqrt{T_s} g\left(T_s(k - nN - D/2)\right) e^{j\frac{2\pi}{2N}m(k-D/2)} e^{j\phi_{m,n}}, \\ &= g[k - nN] e^{j\frac{2\pi}{2N}m(k-D/2)} e^{j\phi_{m,n}}. \end{aligned} \tag{2.39}$$

and then :

$$s[k] = \sum_{n=-\infty}^{+\infty} \sum_{m=0}^{2N-1} a_{m,n} g_{m,n}[k] = \sum_{n=-\infty}^{+\infty} \sum_{m=0}^{2N-1} a_{m,n} g[k - nN] e^{j\frac{2\pi}{2N}m(k-D/2)} e^{j\phi_{m,n}}. \tag{2.40}$$

Then, at the demodulation step, an estimation $\hat{a}_{m,n}$ of the transmitted symbols $a_{m,n}$ is obtained after discretization of (2.34). The projection of the transmitted signal $s[k]$ over the resulting discrete-time Gabor family, $g_{m,n}$, leads to :

$$\hat{a}_{m,n} = \Re\{ \sum_{k=-\infty}^{+\infty} g^*_{m,n}[k] s[k] \}. \tag{2.41}$$

For this discrete-time system the orthogonality condition is satisfied, leading to $\hat{a}_{m,n} = a_{m,n}$, $\forall$ (m,n), if :

$$\Re\{ \sum_{k=-\infty}^{+\infty} g^*_{m,n}[k] g_{p,q}[k] \} = \delta_{m,p}\delta_{n,q}. \tag{2.42}$$

Otherwise said $< g_{m,n}, g_{p,q} >$ is a pure imaginary if $(p,q) \neq (m,n)$.

2.3.3 The OFDM/OQAM modem implementation

In this section, we only consider discrete-time structures of the modem. By observing (2.40) and (2.41), we can show that the OFDM/OQAM transmitter can be written in the form of a synthesis filter bank (SFB) and the receiver can be written in the form of an analysis filter bank (AFB) [92].

The simplest OFDM/OQAM modem may be achieved using a transmultiplexer (TMUX) whose structure is illustrated in figure 2.4, α and β are such that : $D = \alpha N - \beta$, and where $G_m(z) = \sum_k g_m[k] z^{-k}$ with :

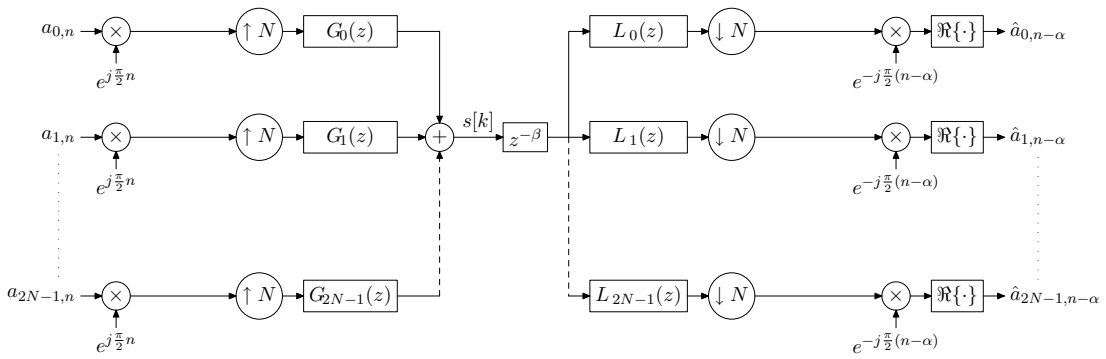

FIG. 2.4 – Transmultiplexer associated with the OFDM/OQAM modulation.

$$g_m[k] = g[k]e^{j\frac{2\pi}{2N}m\left(k-\frac{D-N}{2}\right)}. \tag{2.43}$$

Likewise, $L_m(z) = \sum_k l_m[k]z^{-k}$ with :

$$l_m[k] = g^*[D-k]e^{j\frac{2\pi}{2N}m\left(k-\frac{D+N}{2}\right)}. \tag{2.44}$$

From these filter banks, more effective structures of OFDM/OQAM modems can be obtained by combining a fast transform, using either FFT or IFFT [89], with a polyphase filter, as shown in Figure 2.5. The OFDM/OQAM modulator is performed using an IFFT and polyphase components of the prototype filter $g[k]$, with $K_l(z)$ for $0 \leq l \leq M-1$ the M polyphase components of the filter $G(z)$ defined by :

$$K_l(z) = \sum_n g[l+nM]z^{-n} \tag{2.45}$$

This means that the filter $G(z)$ can be expressed in terms of its M polyphase components as follows :

$$G(z) = \sum_{l=0}^{M-1} z^{-l}K_l(z^M) \tag{2.46}$$

The demodulator can be done similarly by using also an IFFT and $G_l(z)$ the polyphase components of $L(z)$.

Compared to OFDM, here the IFFT/FFT has to run twice faster. Some studies have been carried out on the computational complexity, analysis and optimization. Either, they consider acausal systems [14], [102], or, based on [92], causal systems [23]. In this latter

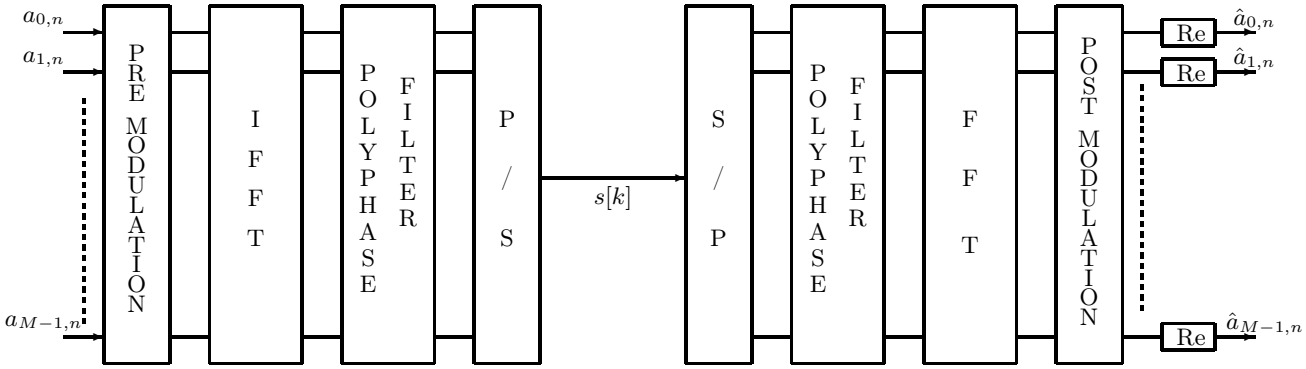

FIG. 2.5 – General structure of the OFDM/OQAM modem with Fast Fourier Transforms.

case, a causal modulator structure is proposed leading, under certain conditions, to a computational complexity which is roughly equivalent to the one of the OFDM modulator.

2.4 Prototype functions and prototype filters

Compared to OFDM, with OFDM/OQAM the prototype function g, see (2.32), or the prototype filter, see (2.39) are not necessarily rectangular.

Thus, the study of prototype functions and prototype filters is of a particular interest for OFDM/OQAM because it represents an important degree of freedom with respect to what is possible with OFDM. An OFDM/OQAM prototype has to meet orthogonality constraints that may be derived in continuous-time for the prototype function, from (2.35) or in discrete-time for the prototype filter from (2.42). Furthermore, these prototypes can be built to satisfy some key objectives, e.g. frequency selectivity or time-frequency localization.

2.4.1 Examples of prototype functions

As a matter of example we can consider three particularly important prototype functions. First of all, we have the rectangular window function.

2.4.1.1 Rectangular window function

The Rectangular Window (RW) function is defined in the time domain by :

$$\Pi(t) = \begin{cases} 1 & \text{for } \mid t \mid \leq \frac{T_0}{2} \\ \\ 0 & \text{for } \mid t \mid > \frac{T_0}{2}. \end{cases} \tag{2.47}$$

$\Pi(t)$ meets the real-orthogonality constraint. It is the same function as the one used in OFDM. We will use it as a reference to compare with more commonly used prototypes used in OFDM/OQAM.

2.4.1.2 The Square Root Raised Cosine Function (SRRC)

It is well known, in digital communication systems, that the combination of the transmit and receiver SRRC filters satisfies the Nyquist condition. Although the perfect Nyquist condition satisfaction requires SRRC filter to be continuous-time and with infinite length, the truncated discrete-time SRRC is still widely applied in digital communications. The frequency domain expression of SRRC filter is as below

$$R_c(\nu) = \begin{cases} \frac{1}{\sqrt{F_0}}, |\nu \leq (1-r)\frac{F_0}{2}| \\ \frac{1}{\sqrt{F_0}} \cos(\frac{\pi}{2}(\frac{|\nu|}{F_0} - \frac{1-r}{2})), (1-r)\frac{F_0}{2} < |\nu| \leq (1+r)\frac{F_0}{2} \\ 0, (1+r)\frac{F_0}{2} < |\nu| \end{cases} .$$

where $0 \leq r \leq 1$ is the roll-off factor.

Temporal response SRRC filter in continuous time reads

$$r_c(t) = \sqrt{F_0} \frac{4rF_0t\cos(\pi(1+r)F_0t) + \sin(\pi(1-r)F_0t)}{(1-(4rF_0t)^2)\pi F_0t}$$

Compared with rectangular filter, SRRC has better frequency localization feature but with a cost of time localization loss. Figs. 2.6 and 2.7 depict the comparison between SRRC vs. rectangular in time and frequency domain, with SRRC filter length M (M = 2048 the number of carriers) and r = 0.5.

2.4.1.3 The Extended Gaussian Function (EGF)

This class of prototype function results from an orthogonalization procedure of the Gaussian function [32]. Since the Gaussian function does not meet the orthogonality pro-

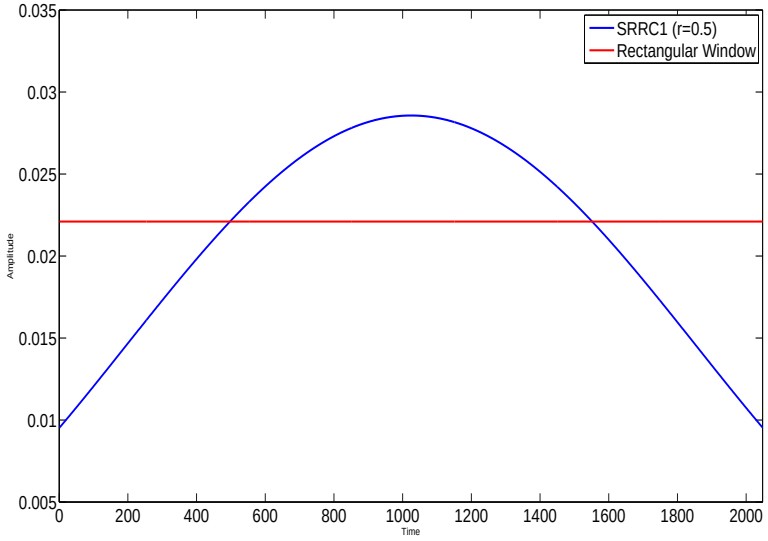

FIG. 2.6 – Time representation of the SRRC1 ($L = M = 2048$) prototype filter (in linear scale) Vs time.

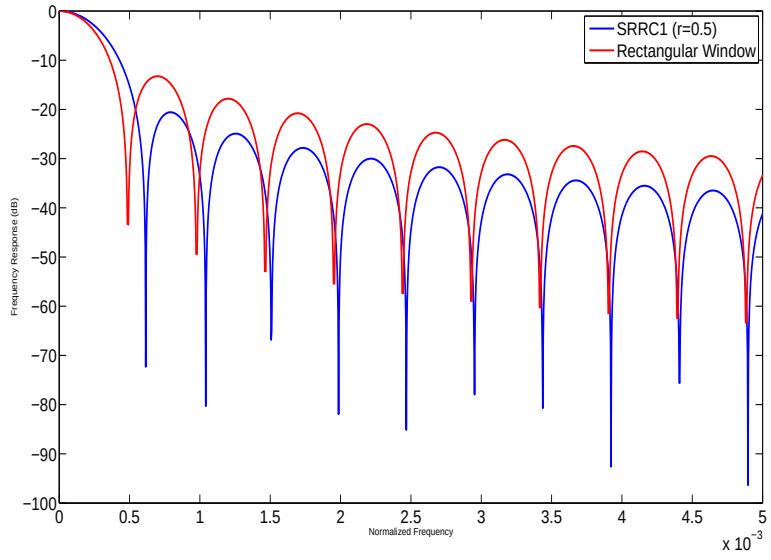

FIG. 2.7 – Frequency representation of the SRRC1 ($L = M = 2048$) prototype filter (in dB scale) Vs normalized frequency($\frac{\omega}{2\pi}$).

perty in [4],[32] it has been proposed to orthogonalize it in a two-step procedure. The resulting prototype function is named Isotropic Orthogonal Transform Algorithm (IOTA). Using the same algorithm, a direct computation leads to the EGF. The EGF is defined in time by [91] :

$$Z_{\lambda,\mu_0,\tau_0}(t) = \frac{1}{2}\sum_{k=0}^{+\infty} d_{\lambda,\mu_0,\tau_0}[g_\lambda(t+\frac{k}{\mu_0}) + g_\lambda(t-\frac{k}{\mu_0})]\sum_{l=0}^{\infty} d_{l,1/\lambda,\mu_0,\tau_0}\cos(2\pi l\frac{t}{\tau_0}), \qquad (2.48)$$

with λ a real parameter, d_{λ,μ_0,τ_0} real coefficients and $g_\lambda(t)$ is the Gaussian function given by :

$$g_\lambda(t) = (2\lambda)^{1/4}e^{-\pi\lambda t^2},$$

$\mu_0 = F_0 = \frac{1}{2\tau_0}$.

Setting $\mu_0 = \tau_0$ and $\lambda = 1$, we recover the IOTA prototype filter.

2.4.2 From continuous to discrete-time

In practice the filter implementations are not directly based on (2.47) or (2.48) but use instead causal discrete-time versions of these expressions.

But the truncation and discretization of a continuous-time prototype function introduce a distortion ϵ, which can be defined by :

$$\Re\{\langle g_{m,n}, g_{p,q}\rangle\} = \delta_{m,p}\delta_{n,q} + \epsilon_{m,n}^{p,q}.$$

As analyzed in [92], under certain conditions, for Square Root Raised Cosine (SRRC) and Extended Gaussian Function (EGF) prototype filters of sufficient length, $|\epsilon_{m,n}^{p,q}|$ can be considered as negligible when compared to the channel noise. In terms of filter banks that means SRRC and EGF prototype filters can lead to Nearly Perfect Reconstruction (NPR) filter banks. There is a vast literature concerning the way to use filter banks to obtain by duality a transmultiplexer [9]. The principle has been described at first in [103] and it has been used afterwards to get some modulated transmultiplexers. For instance, as shown in [89], [92], OFDM/OQAM can be seen as the dual of the Modified Discrete Fourier Transform (MDFT) filter bank [51]. Another example is the Exponentially Modulated

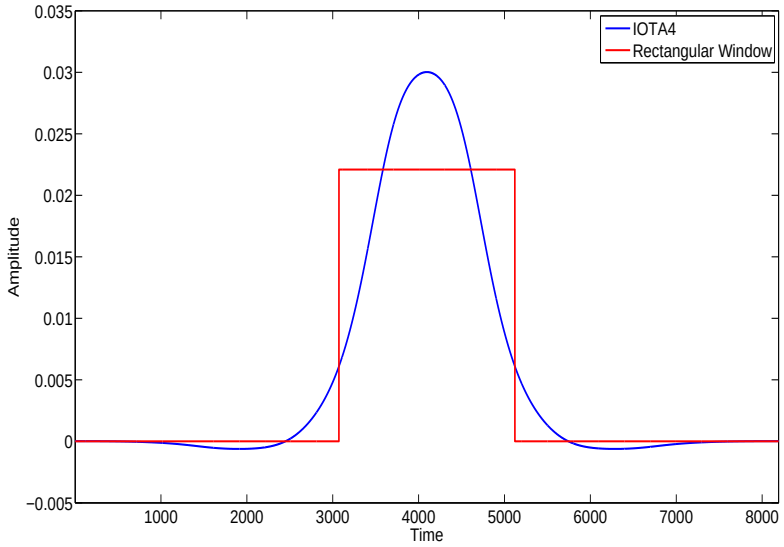

FIG. 2.8 – Time representation of the IOTA4 ($L = 4M = 8192$) prototype function (in linear scale) Vs time.

Filter Bank (EMFB) that can be used as a filter bank or a transmultiplexer [6], [7], [104]. In this context the prototype filter, associated to the modulated filter bank, is directly designed in discrete-time including NPR or PR constraints. Let us look at some examples of prototype filters.

For their graphical displays, these various prototype filters will be depicted using their causal representation in time-domain and a normalized scale ($f_{max} = \frac{1}{2}$) in frequency domain.

2.4.3 Different families of prototype filters

2.4.3.1 Prototypes based on continuous-time functions

A truncation, when necessary, and a discretization allow us to get a prototype filter from a continuous-time function. For instance starting from the rectangular window and the EGF we get the prototype filters depicted in time and frequency in Figures 2.8 and 2.9 respectively.

Note that for the rectangular window the length is limited to the number of subcarriers ($= M$) while for the EGF the length is equal to $4M$, with here $M = 2048$. Thus, we denote

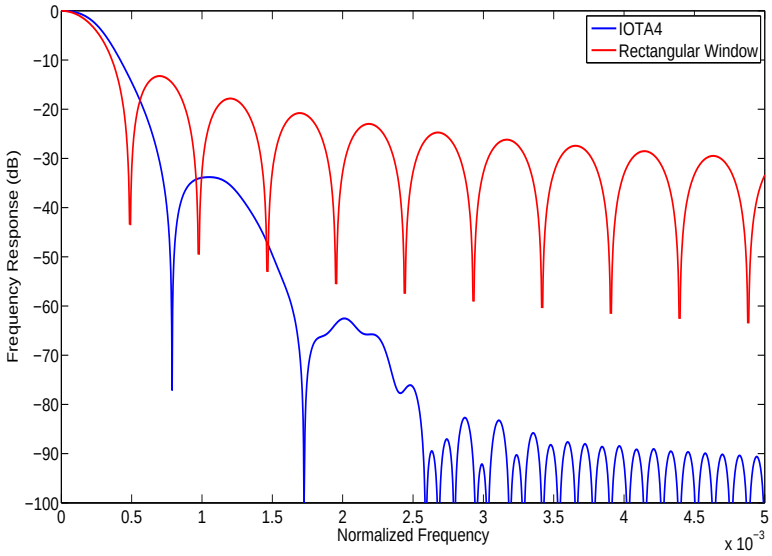

FIG. 2.9 – Frequency representation of the IOTA4 ($L = 4M = 8192$) prototype function (in dB scale) Vs normalized frequency($\frac{\omega}{2\pi}$).

it IOTA4, meaning that its length is four times the number of subcarriers. The graphical displays in Figures 2.8 and 2.9 show that for IOTA4 the energy is concentrated around the center in time and frequency domain which is a typical feature for prototype filters having good time-frequency localization with here a measure, according to (2.18), given by $\xi = 0.977$. As, it can be also seen in Figure 2.8, this nice property is obtained at the price of a wider main lobe.

Among the other well-known examples of this class of prototype filters, one can mention the SRRC and the Optimal Finite Duration Pulse (OFDP) [99], that can provide good frequency selectivity, or the Hermite pulse [41], [42] that leads to good time-frequency localization. As explained in subsection 2.4.2, these prototype filters can only lead to NPR solutions.

2.4.3.2 Prototypes based on analytical expressions

The link of OFDM/OQAM systems with Cosine Modulated Filter Banks (CMFB) can be efficiently exploited for the design of NPR and PR prototype filters of particular interest are the closed-form expressions provided by Malvar in [64], [63] that can be directly reused

to build OFDM/OQAM systems with PR prototype filters of length $L_g = M$ and $L_g = 2M$, respectively. However, a limit of these solutions is to not satisfy a given optimization criterion. So, here we prefer to focus on another analytical expression that instead obey to appropriate rules for transmission systems. These rules have been presented in three successive papers [65], [11] and [67]. In [65] Martin using specific combinations of AFB outputs derived a method leading to closed-form expressions of NPR prototype filters with good stopband attenuations. Thus initial description was further developed in a paper by Mirabbasi and Martin [67] to explicitly cover the case of MDFT transmultiplexer, also proposing an extended set of solutions. In the meantime, in [11], M. Bellanger showed that Martin's method could be viewed as a frequency sampling design method. As these three authors have contributed to the design of a prototype filter, that recently served as a reference in an FP7 European research project named PHYDYAS (PHysical Layer for Dynamic Spectrum Access and Cognitive Radio) [105], we will name it MMB.

The advantages of this MMB prototype filter are that : First, it is very simple to obtain the filter coefficients ; Second, the obtained filter can have a fast decrease in frequency, i.e. a steep slope of the sidelobes termed fall-off rate. Furthermore, any fall-off rate can be freely reached by MMB prototype but at a price of filter length augmentation. The disadvantages of this method are : Firstly, a fast fall-off rate requires a high filter order which leads to a complexity increase ; Secondly, the faster fall-off rate does not mean that the filter has surely a small stopband energy ; Thirdly, the transition band of the designed filter is fixed. The closed-form of MMB prototype filter is as follows

$$g[n] = \begin{cases} \frac{1}{bM}(k_0 + 2\sum_{l=1}^{b-1} k_l \cos(\frac{2\pi l n}{bM})), & 0 \leq n \leq L_f \\ 0, & otherwise \end{cases} . \tag{2.49}$$

where $L_f = bM + 1$ with a positive integer b meaning the overlap factor, and k_l $(0 \leq l \leq b)$ are real coefficients which are given in [67] for b up to 8.

To get an even length for a MMB prototype filter by removing a zero [65], [67], [11], then we have a length equal to $4M$ (with $M = 2048$), Figures 2.10 and 2.11 give the MMB4 representation having an even length in the time and the frequency domain, respectively.

The frequency representation in Figure 2.11 shows the obvious superiority of MMB4

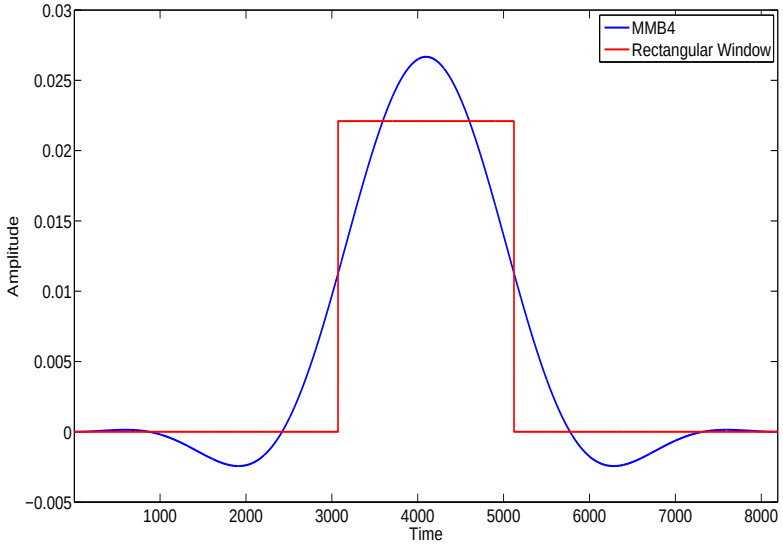

FIG. 2.10 – Time representation of the MMB4 ($L = 4M = 8192$) prototype filter (in linear scale) Vs time.

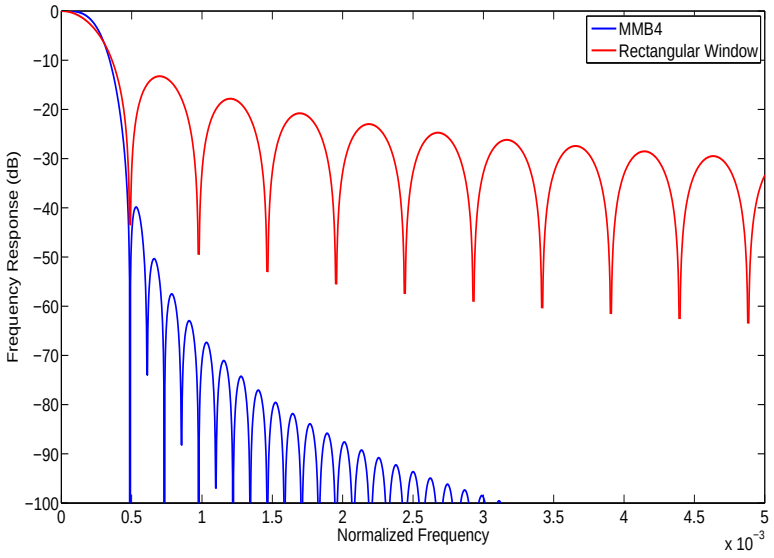

FIG. 2.11 – Frequency representation of the MMB4 ($L = 4M = 8192$) prototype filter (in dB scale) Vs normalized frequency($\frac{\omega}{2\pi}$).

over the rectangular window but also over IOTA4, cf. Figure 2.9. On the contrary a look at the time representation of MMB4 (see Figure 2.10) and IOTA4 (see Figure 2.8) also clearly shows that MMB4, differently from IOTA4, can hardly be truncated more severely.

2.4.3.3 Prototype filters obtained by optimization

The design of discrete-time prototype filters for OFDM/OQAM systems being directly related to the design of prototype filters for various types of modulated filter banks [92], a vast literature exists on this topic [100]. When these prototype filters have to satisfy given optimization criteria, differently from what has been presented in subsection 2.4.3.2, numerical optimization becomes mandatory.

These optimizations can either correspond to a direct search of the prototype filter coefficients under (near) orthogonality constraints, i.e. NPR or PR conditions, or they can take advantage of some lattice representations that structurally insure the PR property. Then, the aim is to optimize a set of angular parameters. Design examples using these two types of approaches are proposed in [100]. Two usual criteria for these different types of optimization are the minimization of the out-of-band energy and the maximization of the time-frequency localization.

– **Frequency Selective criterion**

  There are different, but nearly equivalent, formulations for the frequency selectivity criterion. In [80], [79] the corresponding design problem is stated as an unconstrained optimization problem which is written as

$$\min_{\{parameters\}} \quad \frac{E(f_c)}{E(0)} \qquad with \qquad E(f_c) = \int_{f_c}^{\frac{1}{2}} |P(e^{j2\pi n\nu})|^2 d\nu, \tag{2.50}$$

  where f_c is the cutoff frequency and has the expression as $f_c = (1+\rho)\frac{1}{2M}$. We note that the factor ρ can be also seen as a "roll-off" factor between [0, 1].

  The parameters in (2.50) correspond to the compact representation introduced in [80], [79]. Indeed, in these references it has been shown that when optimizing (2.50) using the usual set of angular parameters, the best solution had some particular features. Based on these observations, it is possible to derive a new set of parameters to optimize which leads, in general, to an optimization problem with a significantly

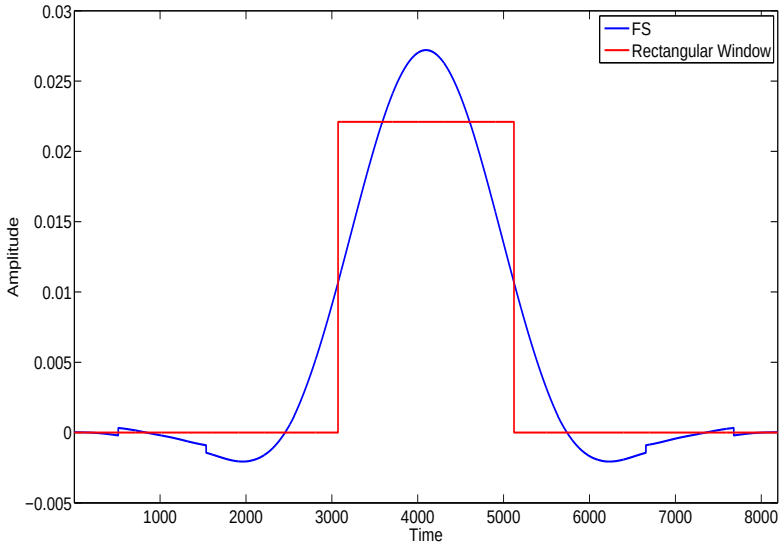

FIG. 2.12 – Time representation of the FS4 ($L = 4M = 8192$) prototype filter (in linear scale) Vs time.

smaller number of variables. Minimizing the above objective function using this compact representation leads to a so-called Frequency Selective (FS) prototype filter. The filter length can be chosen to be bM with positive integer b.

For a FS prototype filter of length equal to $4M$ (with M=2048) Figures 2.12 and 2.13 show the comparison between the FS4 ($b = 4$) with $\rho = 1$ against the rectangular window.

However, a more interesting comparison is the one in frequency with MMB4 (cf. figure 2.13 versus figure 2.11). If FS4 leads to slightly stronger attenuation for the first sidelobe, the attenuation slope remains nearly constant for the following ones. Indeed, based on (2.50), the attenuation is not optimized to decrease with frequency. Further, FS4 is concentrated to be PR while MMB4 is only NPR.

Based on the comparison in terms of Bit Error Rate (BER) provided in [56] by H. Lin in the case of a given static multipath channel, it appears that MMB4 leads to very slightly better performances than FS4 and Rossi4, another prototype filter ensuring a NPR property [85]. These all three prototype filters being also superior to SRRC4.

– **Time Frequency Localization (TFL)**

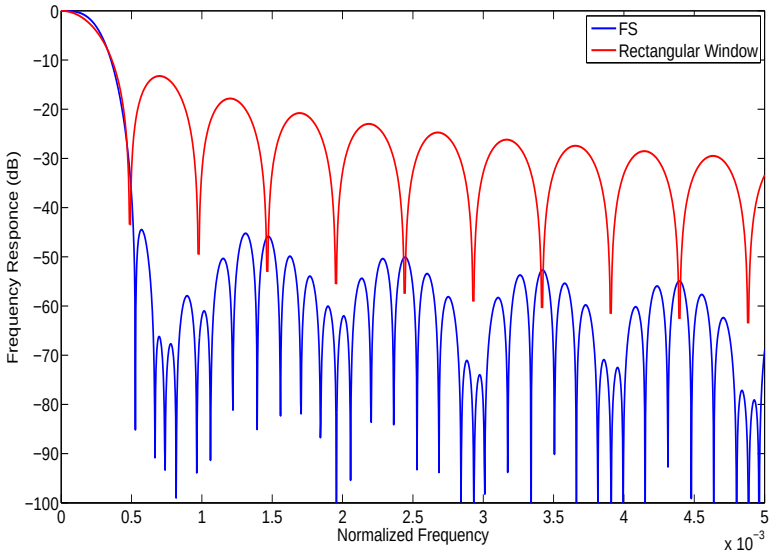

FIG. 2.13 – Frequency representation of the FS4 ($L = 4M = 8192$) prototype filter (in dB scale) Vs normalized frequency($\frac{\omega}{2\pi}$).

The counterpart to the IOTA prototype in discrete-time is naturally a prototype filter which also has an excellent Time Frequency Localization (TFL) property. So we designate by TFL the PR discrete-time prototypes which are optimized with respect to this criterion. The TFL criterion targets to maximize a TFL measure $\xi_d(p)$ for a prototype filter p. Note that in the design algorithms [92], [79] the used criterion is adapted to discrete-time signals and given by :

$$\xi_d(p) = \frac{1}{4\pi\sqrt{m_2(p)M_2(p)}}, \tag{2.51}$$

where $m_2(p)$ and $M_2(p)$ are the time and frequency localization moments defined by Doroslovački in [27]. With this definition, similarly to (2.19), it is still possible to get a bounded measure $0 \leq \xi_d(p) \leq 1$. For a TFL prototype filter of length equal to $M = 2048$, Figures 2.14 and 2.15 give the representations in the time and frequency domain, respectively. A particularly interesting feature with the TFL optimization is that one can get excellent TFL measures, i.e. $\xi_d \simeq 0.91$ with short length ($L = M$) PR prototype filters. That is not possible with truncated IOTA prototypes [92]. This gives a strong advantage to TFL with respect to the complexity implementation and

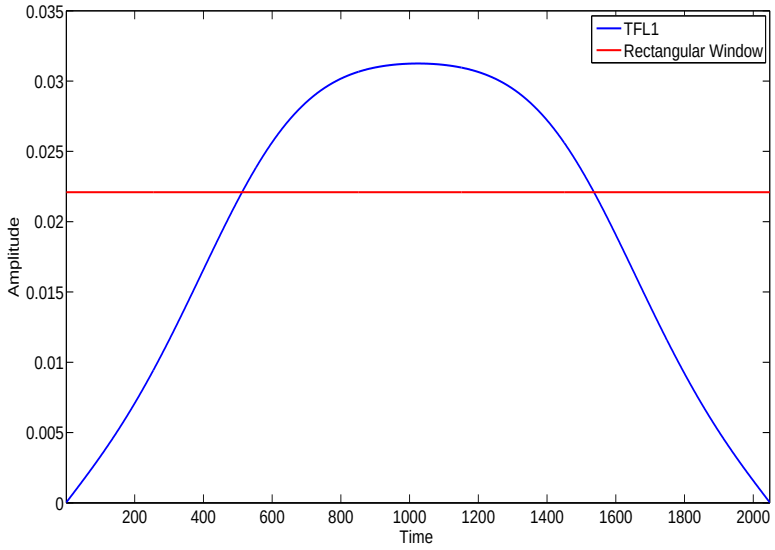

FIG. 2.14 – Time representation of the TFL1 ($L = M = 2048$) prototype filter (in linear scale) Vs time.

also in the perspective of a transmission requiring short preambles (cf. Part 3) and or using short frames (cf. Part 4).

2.5 3-D time-frequency localization and interference analysis with the Ambiguity function

2.5.1 Ambiguity function definition

The localization feature of a pulse shape over a phase space can also be analyzed by its ambiguity function [32], [42]. Let us define a sampled version of the ambiguity function of $g(t)$ as $A_g[l,k] = A_g(lT_0, kF_0)$ where $A_g(\tau,\nu)$ is given by

$$A_g(\tau,\nu) = \int_{-\infty}^{+\infty} g(t+\frac{\tau}{2})g^*(t-\frac{\tau}{2})e^{-j2\pi\nu t}dt.$$

This function gives an insight of the energy leakage of a given pulse shape over time and frequency axes. As explained in [32], the ambiguity function can also be used to check the orthogonality of the prototype functions, which is then expressed as

$$A_g(2n\tau_0, 2m\nu_0) = \begin{cases} 1, if \quad m = n = 0 \\ 0, \text{otherwise} \end{cases}. \tag{2.52}$$

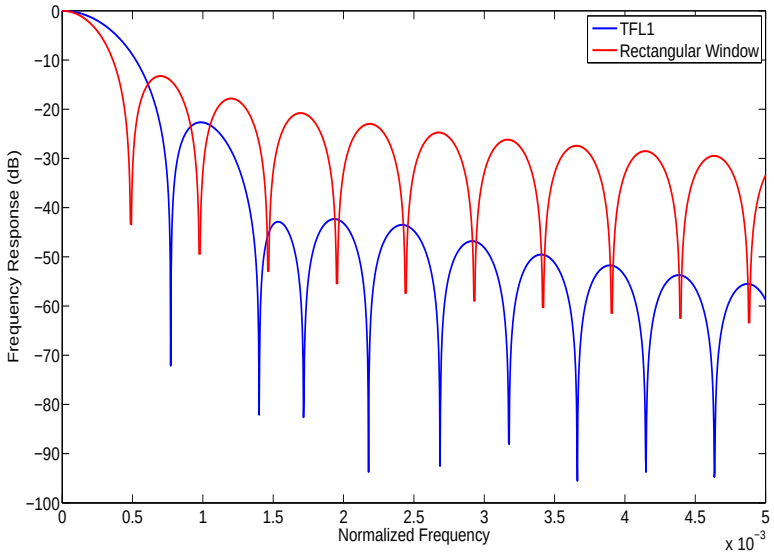

FIG. 2.15 – Frequency representation of the TFL1 ($L = M = 2048$) prototype filter (in dB scale) Vs normalized frequency($\frac{\omega}{2\pi}$).

Furthermore, the interference coefficients can be obtained via numerical computation of the ambiguity function. They are presented in Tables 2.3-2.6, with index p for frequency position pF_0 and index q for time position qT_0 with respect to the considered symbol which is at position $q = 0$ and $p = 0$.

When representing the interference coefficients in Tables 2.3 to 2.6, we can remark

- the symmetry of the interference coefficients with respect to the time/frequency axes (p and q indexes) around the considered symbol (p=0,q=0), this is due to the symmetry of the prototype filters which leads to : $A_g(\tau,\nu) = A_g(-\tau,\nu) = A_g(\tau,-\nu) = A_g(-\tau,-\nu)$;
- the extra symmetry of the IOTA prototype filter over the diagonals, i.e. $A_g(\tau,\nu) = A_g(\nu,\tau)$.

2.5.2 Rectangular window function

In Figure 2.16, we depict, the ambiguity function of the rectangular pulse with length T_0=M=2048. The graphical display shows that the energy is spreading more over frequency than time domain. This is not desirable in the case of transmission over channels with

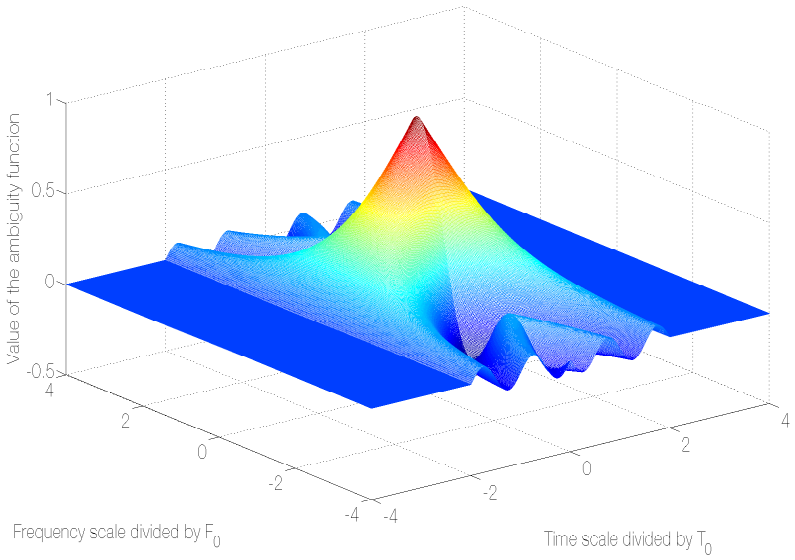

FIG. 2.16 – 3D Ambiguity function representation for the rectangular window.

narrowband noise nor in the case of a frequency selective channel, since it then leads to Inter-Carrier-Interference (ICI).

Indeed, we know that a good time localization results in a controlled ISI and good frequency localization leads to ICI immunity. To supplement our analysis, we can also draw the isocontours of the ambiguity function as shown in Figure 2.17. This helps to have a better vision when choosing the most suitable prototype filter for the OFDM/OQAM when it is affected by a delay spread and/or a frequency offset.

2.5.3 Our set of prototype filters

The ambiguity function representations for SRRC1, IOTA4, TFL1, MMB4 and FS4 are shown in figures 2.18, 2.19, 2.20, 2.22 and 2.21, respectively. As its name indicates, the energy of IOTA prototype filter has an isotropic spreading over time and frequency axes. IOTA filter is a particular case in EGF family, its spreading factor (in case of λ=1) leads to an EGF filter with similar spreading over time and frequency. For the TFL1 filter, we find that it has better localization in time than in frequency. And contrarily, we see that the FS4 filter has better frequency localization than time localization, and we can remark that the MMB4 filter has nearly the same localization features as FS4.

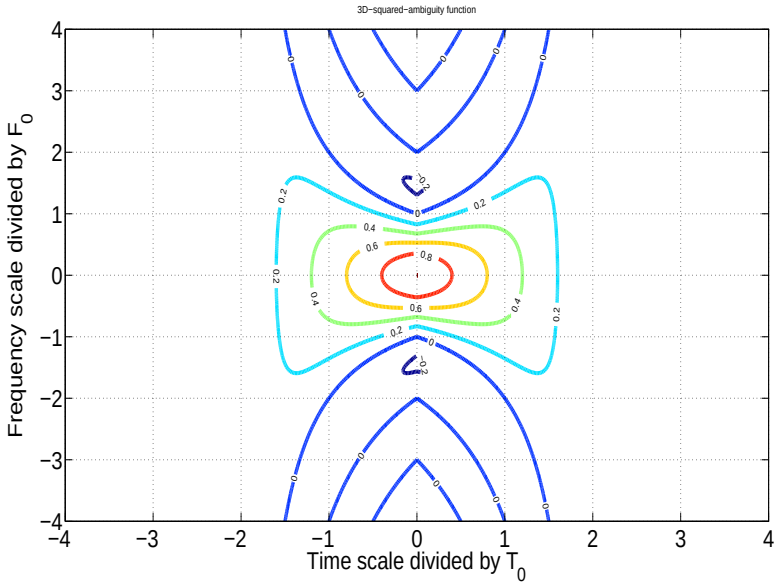

FIG. 2.17 – 2D Ambiguity function contour representation for the rectangular window.

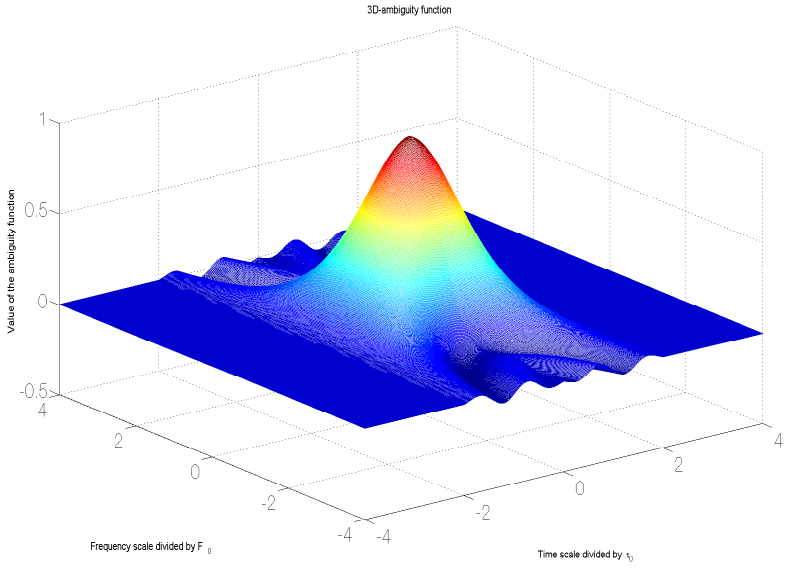

FIG. 2.18 – 3D Ambiguity function representation for SRRC1 ($L = M = 2048$).

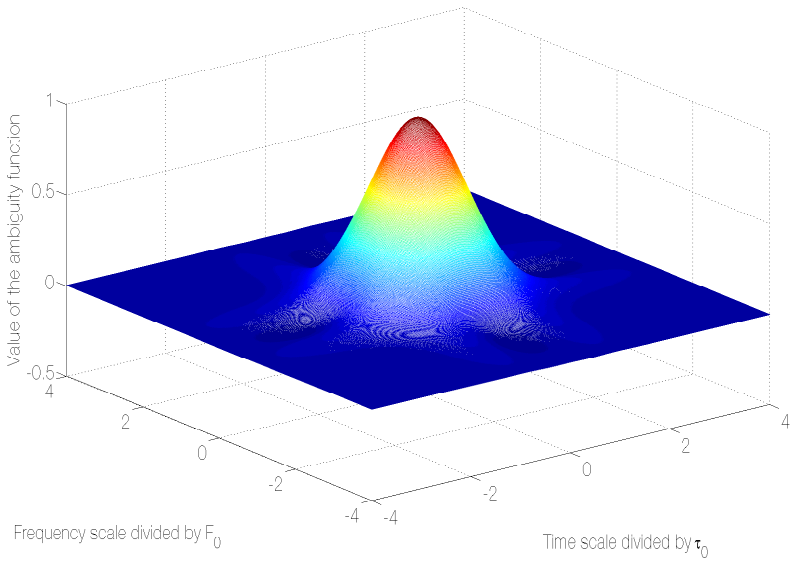

FIG. 2.19 – 3D Ambiguity function representation for IOTA4 ($L = 4M = 8192$).

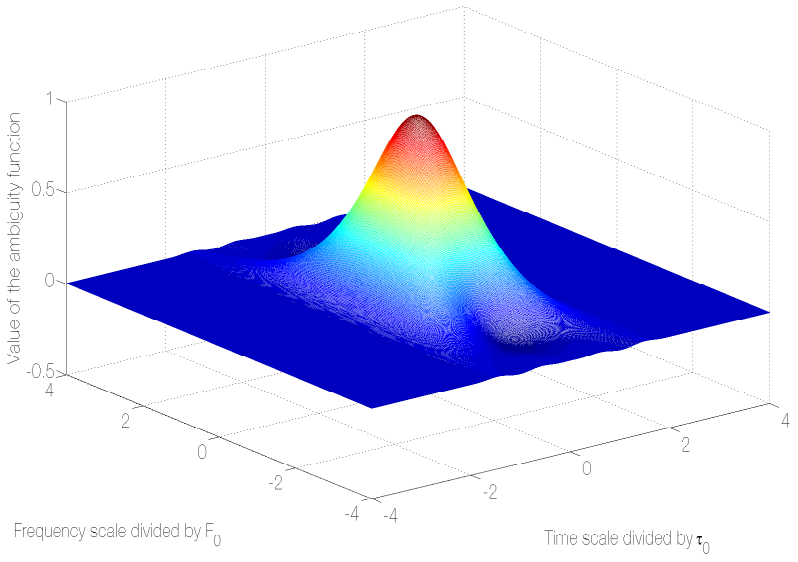

FIG. 2.20 – 3D Ambiguity function representation for TFL1 ($L = M = 2048$).

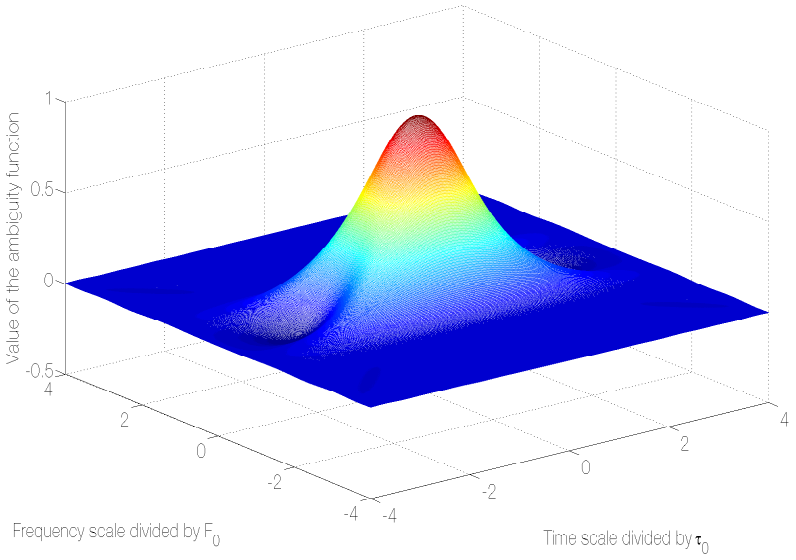

FIG. 2.21 – 3D Ambiguity function representation for FS4 ($L = 4M = 8192$).

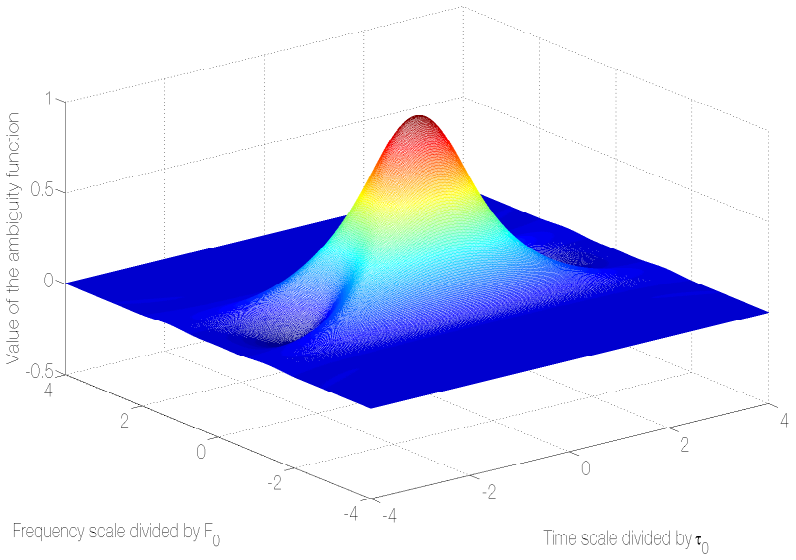

FIG. 2.22 – 3D Ambiguity function representation for MMB4 ($L = 4M = 8192$).

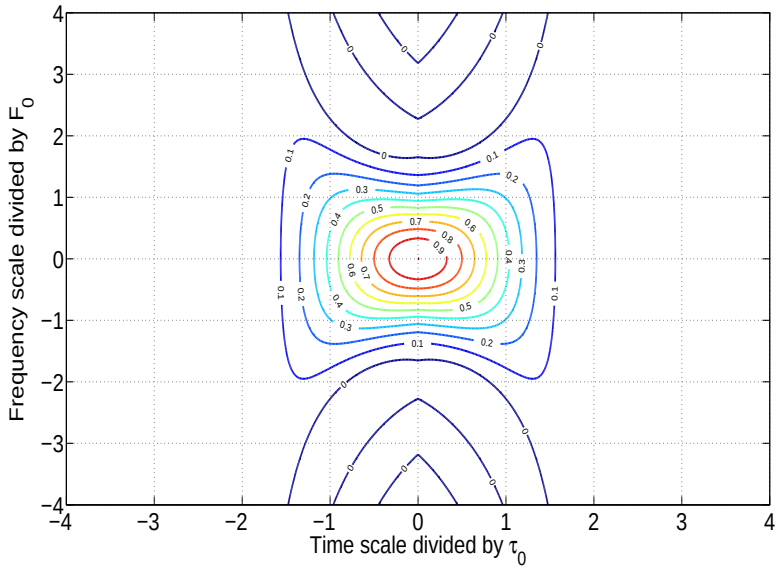

FIG. 2.23 – 2D Ambiguity function contour representation for SRRC1 ($L = M = 2048$).

The isocontour representations of the energy spreading of the ambiguity function for the SRRC1, IOTA4, TFL1, FS4 and MMB4 prototype filters are displayed in Figures 2.23, 2.24, 2.25, 2.26 and 2.27, respectively.

In addition, we can check the time-frequency features of the SRRC1, IOTA4, TFL1, FS4 and MMB4 filters in Tables 2.2, 2.3, 2.4, 2.5 and 2.6, respectively, which show the interference coefficients obtained via computational calculations of the ambiguity function using the prototype filters. Note also that for perfectly orthogonal prototype filters the orthogonality condition is only satisfied up to the accuracy of our numerical computation.

p \ q	0	1	2	3	4	5
5	0.0040	0.0355	0	0	0	0
4	−0.0062	−0.01	0	0	0	0
3	0.0107	−0.059	0	0	0	0
2	−0.0198	0.0503	0	0	0	0
1	0.3484	0.2956	0	0	0	0
0	0	0.4291	0	0	0	0

TAB. 2.2 – Interference coefficients for SRRC1.

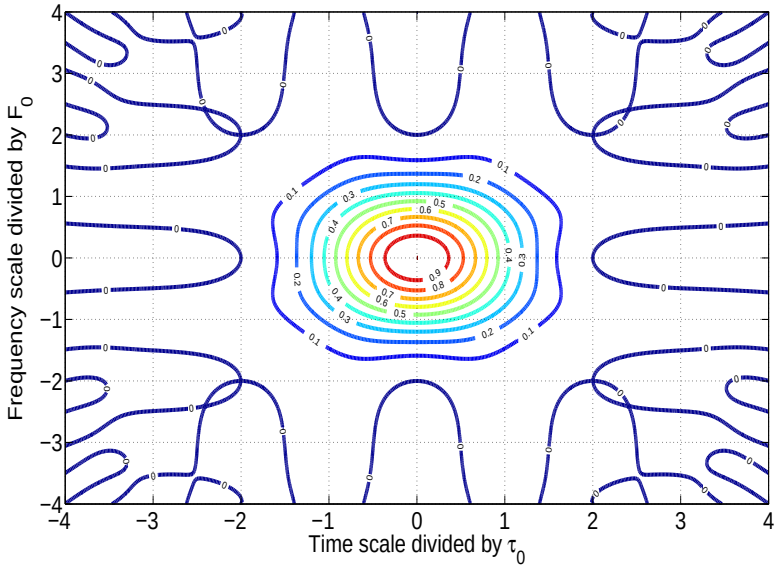

FIG. 2.24 – 2D Ambiguity function contour representation for IOTA4 ($L = 4M = 8192$).

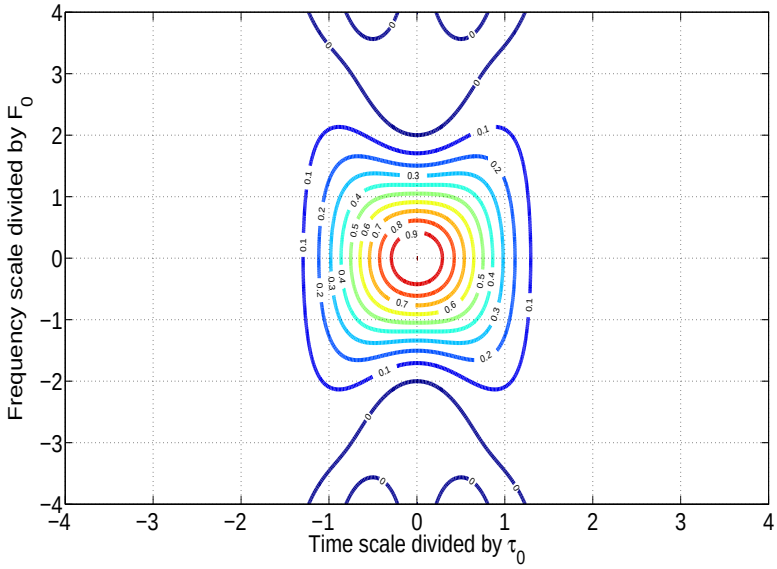

FIG. 2.25 – 2D Ambiguity function contour representation for TFL1 ($L = M = 2048$).

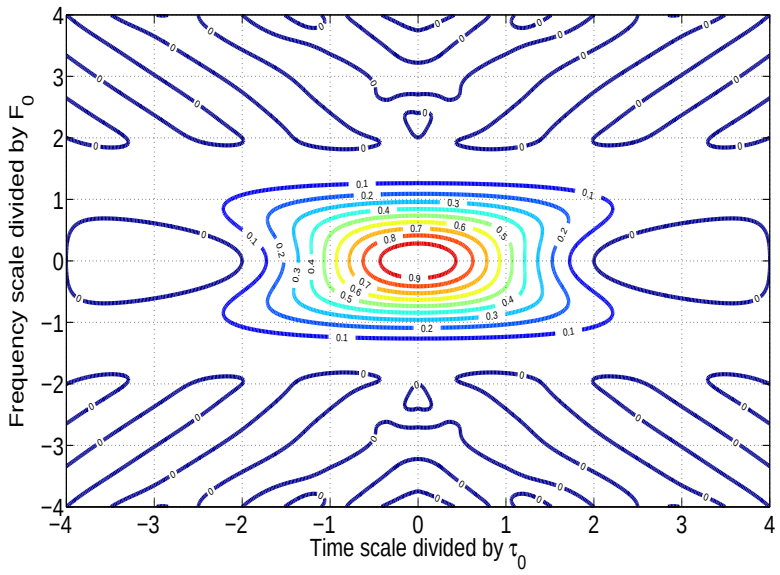

FIG. 2.26 – 2D Ambiguity function contour representation for FS4 ($L = 4M = 8192$).

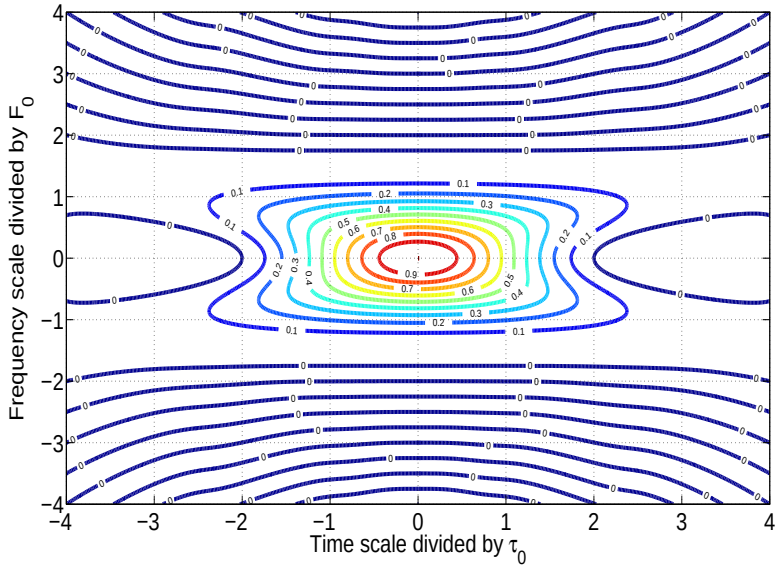

FIG. 2.27 – 2D Ambiguity function contour representation for MMB4 ($L = 4M = 8192$).

p\q	0	1	2	3	4	5
5	7.8812×10^{-4}	4.4453×10^{-4}	6.8062×10^{-5}	3.5557×10^{-5}	4.0652×10^{-6}	-1.5064×10^{-5}
4	3.3137×10^{-9}	0.0016	-1.2678×10^{-7}	-7.2717×10^{-5}	2.4487×10^{-6}	6.1435×10^{-6}
3	-0.0182	0.0103	-0.0016	4.3763×10^{-4}	-5.1471×10^{-5}	3.0340×10^{-5}
2	8.5636×10^{-9}	0.0381	-3.2856×10^{-7}	-0.0016	6.2412×10^{-6}	-8.6324×10^{-6}
1	0.4411	0.2280	0.0380	0.0103	0.0013	9.7054×10^{-5}
0	0	0.4411	1.4597×10^{-5}	-0.0183	-6.9007×10^{-4}	2.3540×10^{-4}

TAB. 2.3 – Interference coefficients for IOTA4.

p \ q	0	1	2	3	4	5
5	0.0020	9.7029×10^{-4}	0	0	0	0
4	-9.6759×10^{-17}	-0.0070	0	0	0	0
3	-0.0398	0.0213	0	0	0	0
2	-1.0419×10^{-16}	0.1126	0	0	0	0
1	0.5378	0.2277	0	0	0	0
0	0	0.2811	0	0	0	0

TAB. 2.4 – Interference coefficients for TFL1.

p \ q	0	1	2	3	4	5
5	3.5397×10^{-5}	2.2871×10^{-4}	0.0015	-2.8488×10^{-4}	-0.0017	-1.0679×10^{-4}
4	8.6727×10^{-17}	-1.6008×10^{-4}	7.6157×10^{-18}	-7.6388×10^{-5}	-1.6241×10^{-18}	9.0685×10^{-5}
3	-3.0695×10^{-4}	8.5822×10^{-4}	-0.0026	-5.6939×10^{-4}	0.0027	-3.5536×10^{-5}
2	-7.2269×10^{-17}	-0.0013	-9.4382×10^{-18}	0.0019	1.0996×10^{-18}	5.7579×10^{-6}
1	0.2664	0.2194	0.1138	0.0297	0.0031	8.3698×10^{-4}
0	0	0.5498	-1.8975×10^{-17}	-0.0519	-1.0302×10^{-19}	0.0010

TAB. 2.5 – Interference coefficients for FS4.

p \ q	0	1	2	3	4	5
5	2.3830×10^{-18}	-6.3621×10^{-8}	-3.7604×10^{-7}	-1.1301×10^{-5}	-7.4796×10^{-19}	1.1301×10^{-5}
4	1.0193×10^{-17}	-1.0873×10^{-6}	7.9452×10^{-7}	1.3044×10^{-5}	-8.7815×10^{-19}	-1.3044×10^{-5}
3	-1.1277×10^{-17}	-2.8273×10^{-6}	-7.4902×10^{-7}	5.7395×10^{-5}	-1.2209×10^{-18}	-5.7395×10^{-5}
2	-1.7625×10^{-17}	-4.7527×10^{-6}	-1.3043×10^{-4}	-5.8986×10^{-4}	-1.2683×10^{-18}	5.8986×10^{-4}
1	0.2393	0.2058	0.1250	0.0429	0.0054	0.0013
0	0	0.5644	2.0349×10^{-4}	-0.0668	-2.2649×10^{-10}	0.0023

TAB. 2.6 – Interference coefficients for MMB4.

2.6 Conclusion

In this chapter, we have presented the main framework of the OFDM and OFDM/OQAM systems. Thanks to the introduction of a CP in CP-OFDM, inter-block interference is avoided and a simple one tap equalization per subcarrier can be performed. However, this leads to a waste of useful information, and the use of a sinc shaped frequency response makes the transmission spectrum very poorly localized in frequency. The OFDM/OQAM is a MCM system presented to be an alternative to CP-OFDM. This alternative allows us to increase the spectral efficiency of the system since CP is not inserted. In addition, we have seen that different sorts of prototype filters can be used in OFDM/OQAM. Moreover, we can physically suppose that the different presented filters will differently impact the system regarding to their time and/or frequency localization(s) measures towards the propagation channel characteristics (timing offset, carrier frequency offest...). These both aspects seem to be advantageous when implementing OFDM/OQAM instead of CP-OFDM.

In the next chapter, we analyze the interference caused by delay spread and frequency offset for the OFDM/OQAM system using the 5 prototype filters presented previously (SRRC1, IOTA4, TFL1, FS4 and MMB4).

Part III

Part3

Chapter 3

OFDM/OQAM synchronization analysis

In this chapter we provide a theoretical analysis of the latest results in the field of non-perfect time and frequency synchronizations for Filter Bank Multi Carrier (FBMC) systems using an Offset Quadrature Amplitude Modulation (OQAM). In our work, we analyze the interference caused by timing offsets (TO) and carrier frequency offsets (CFO) for the FBMC/OQAM transmission model. We derive the interference power in a simple expression containing both inter-symbol interference (ISI) and inter-carrier interference (ICI), with which an exact signal to interference ratio (SIR) expression is presented. The numerical simulations are further carried out using different prototype filters for OFDM/OQAM to confirm the correctness of our analysis. In the case of an orthogonal prototype filter, we show that we exactly recover a previously published result [4], [32] that, up to now, seems to have not been noticed.

3.1 Channel model

When we consider a general environment with both time and frequency selectivity, the baseband equivalent time-varying multipath channel model in its continuous-time expression writes :

$$h(t,\tau) = \sum_{i=0}^{P-1} c_i e^{j2\pi f_d^i t} \delta(\tau - d_i), \tag{3.1}$$

where P is the number of resolvable path (the first path being the reference path with delay

$d_0 = 0$) and c_i is the time-varying channel gain to the i-th path which can be expressed as $c_i = \rho_i e^{j\theta_i}$ with ρ_i the attenuation of the i-th path and θ_i the phase rotation due to the delay d_i ; f_d^i is the Doppler frequency of the i-th path ; $\delta(\cdot)$ is the Dirac delta function.

Then we get the Z-transform version of the discrete-time channel model

$$H(k,z) = \sum_{l=0}^{L_h-1} c_l e^{j2\pi f_d^l k T_s} z^{-l}, \tag{3.2}$$

with $T_s = \frac{1}{F_s}$ the sampling time interval, where f_s is the sampling frequency, and we define that

$$c_l = \begin{cases} c_i, l = \ulcorner d_i f_s \urcorner \\ 0, \text{otherwise} \end{cases}. \tag{3.3}$$

and we have

$$L_h = \ulcorner d_{P-1} f_s \urcorner \tag{3.4}$$

with $\lceil a \rceil$ the smallest integer that is larger than a.

3.2 Multipath transmission of FBMC/OQAM with time and frequency offsets

In OFDM/OQAM, each subcarrier carries a real-valued symbol $a_{m,n}$ which corresponds to either the real or the imaginary parts of a complex QAM data symbol $c_{m,n}$. In the following, we note $\tau_0 = \frac{T_0}{2}$ the duration of the real OFDM/OQAM data symbol $a_{m,n}$.

As recalled in chapter 2, the baseband OFDM/OQAM signal is expressed as follows [92] :

$$s(t) = \sum_{m=0}^{M-1} \sum_{n \in \mathbf{Z}} a_{m,n} \underbrace{g(t - n\tau_0) e^{j2\pi m F_0 t} e^{j\phi_{m,n}}}_{g_{m,n}(t)}, \tag{3.5}$$

with F_0 the inter-carrier spacing and $\phi_{m,n} = \frac{\pi}{2}(m+n)$ and $g(t)$ a real-valued normalized even prototype function ($\|g\| = 1$).

Note that for OFDM/OQAM, as the orthogonality only holds in the real field, at the receiver side the real data symbols, $a_{m,n}$, are estimated taking the real part of the demodulated signals.

Similarly to [56], [58], we analyze the transmission of a continuous-time OFDM/OQAM modulated signal (3.5) considering the time-frequency dispersive channel described in subsection 3.1. When neglecting the noise effect, the baseband received signal writes

$$\begin{aligned} y(t) &= \sum_{i=0}^{P-1} h(t,d_i)s(t-d_i) \\ &= \sum_{i=0}^{P-1} c_i e^{j2\pi f_d^i t} \sum_{n\in\mathbf{Z}} \sum_{m=0}^{M-1} a_{m,n} g(t-d_i-n\tau_0) e^{j2\pi m F_0 (t-d_i)} e^{j\phi_{m,n}} \end{aligned} \tag{3.6}$$

Then, the demodulated OFDM/OQAM signal yields

$$\begin{aligned} y_{m_0,n_0} &= \int y(t) g^*_{m_0,n_0}(t) dt \\ &= \sum_{n\in\mathbf{Z}} \sum_{m=0}^{M-1} a_{m,n} e^{j\Delta\phi} \sum_{i=0}^{P-1} c_i e^{-j2\pi m F_0 d_i} \\ &\times \int_{-\infty}^{+\infty} g(t-d_i-n\tau_0) g(t-n_0\tau_0) e^{j2\pi((m-m_0)F_0+f_d^i)t} dt \end{aligned} \tag{3.7}$$

where $\Delta\phi = \phi_{m,n} - \phi_{m_0,n_0}$, with $\phi_{m,n} = \frac{\pi}{2}(m+n)$, and $*$ denoting complex conjugation.

We can compactly write the demodulated signal in an ambiguity function based expression by putting $t - d_i - n\tau_0 = \mu + \frac{\tau'}{2}$ and $t - n_0\tau_0 = \mu - \frac{\tau'}{2}$.

Then, we have

$$\begin{aligned} y_{m_0,n_0} &= \sum_{n\in\mathbf{Z}} \sum_{m=0}^{M-1} a_{m,n} e^{j\Delta\phi} \sum_{i=0}^{P-1} c_i e^{-j2\pi m F_0 d_i} \\ &\times \int_{-\infty}^{+\infty} g(\mu + \frac{\tau'}{2}) g(\mu - \frac{\tau'}{2}) e^{j2\pi((m-m_0)F_0+f_d^i)(\mu+\frac{n_0+n}{2}\tau_0+\frac{d_i}{2})} d\mu \\ &= \sum_{n\in\mathbf{Z}} \sum_{m=0}^{M-1} a_{m,n} e^{j\Delta\phi} \sum_{i=0}^{P-1} c_i e^{-j2\pi m F_0 d_i} e^{j2\pi((m-m_0)F_0+f_d^i)(\frac{n_0+n}{2}\tau_0+\frac{d_i}{2})} \\ &\times \int_{-\infty}^{+\infty} g(\mu + \frac{n_0-n}{2}\tau_0 - \frac{d_i}{2}) g(\mu - \frac{n_0-n}{2}\tau_0 + \frac{d_i}{2}) e^{-j2\pi[(m_0-m)F_0-f_d^i]\mu} d\mu \\ &= \sum_{n\in\mathbf{Z}} \sum_{m=0}^{M-1} a_{m,n} e^{j\Delta\phi} \sum_{i=0}^{P-1} c_i e^{-j2\pi m F_0 d_i} e^{j2\pi((m-m_0)F_0+f_d^i)(\frac{n_0+n}{2}\tau_0+\frac{d_i}{2})} \\ &\times A_g((n_0-n)\tau_0 - d_i, (m_0-m)F_0 - f_d^i) \end{aligned} \tag{3.8}$$

where A_g is the ambiguity function of $g(t)$ defined as

$$A_g(\tau,\nu) = \int_{-\infty}^{+\infty} g(t+\frac{\tau}{2}) g^*(t-\frac{\tau}{2}) e^{-j2\pi\nu t} dt.$$

Differently from [56], [58],that, at the end, uniquely consider a time-dispersive multipath channel, we now introduce a discretization step taking into account its impact in time but also in frequency.

To get the discrete-time expression, we introduce the following notations :

$$m = m_0 + p; n = n_0 + q, \quad F_0 = \frac{1}{MT_s}, \quad \tau_0 = NT_s, \quad \Delta\phi = \frac{\pi}{2}(p+q),$$

$$A_g[q,p] = A_g(qT_s, pF_0), \quad d_i = lT_s, \quad f_d^i = \frac{1}{rMT_s},$$

Here we introduce the parameter r to mean that the Doppler shift is a fraction of the frequency spacing F_0. In practice, it does not go beyond $\frac{F_0}{2}$, i.e. $|f_d| \leq \frac{F_0}{2}$, and $|r| \geq 2$. Note also that, as $f_d T_0 = \frac{1}{r}$, $\frac{1}{r}$ is the percentage of Doppler shift.

Hence the following terms can be digitized as

$$e^{j\pi((m-m_0)F_0)((n_0+n)\tau_0+d_i)} = e^{j\pi p(\frac{(2n_0+q)}{2}+\frac{l}{M})},$$

$$e^{j\pi f_d^i((n+n_0)\tau_0+d_i)} = e^{j\pi\frac{1}{r}(\frac{(2n_0+q)}{2}+\frac{l}{M})},$$

$$e^{-j2\pi m F_0 d_i} = e^{-j2\pi(m_0+p)\frac{l}{M}},$$

$$A_g((n_0-n)\tau_0-d_i,(m_0-m)F_0-f_d^i) = A_g(-qNT_s-lT_s,-(\frac{p}{MT_s}+\frac{1}{rMT_s})) = A_g[-qN-l,-(p+\frac{1}{r})],$$

with M the number of subcarriers, $N = \frac{M}{2}$, and p, q being both integers.

Then

$$\begin{aligned} y_{m_0,n_0} &= \sum_{(p,q)} a_{m_0+p,n_0+q} e^{j\frac{\pi}{2}(p+q+pq)} e^{j\pi p n_0} \sum_{l=0}^{L_h-1} c_l e^{j\pi[\frac{(2n_0+q)}{2}+\frac{l}{M}]\frac{1}{r}} \\ &\times A_g[-qN-l,-(p+\frac{1}{r})] e^{-j\frac{\pi(2m_0+p)l}{M}} \end{aligned} \tag{3.9}$$

We can alternately separate the previous expression into signal and interference parts,

$$\begin{aligned} y_{m_0,n_0} = &\underbrace{\sum_{l=0}^{L_h-1} c_l e^{j\pi[n_0+\frac{l}{M}]\frac{1}{r}} A_g[-l,-\frac{1}{r}] e^{-j\frac{2\pi m_0 l}{M}}}_{distortion:\alpha_{m_0,n_0}} a_{m_0,n_0} \\ &+ \underbrace{\sum_{(p,q)\neq(0,0)} a_{m_0+p,n_0+q} e^{j\frac{\pi}{2}(p+q+pq)} e^{j\pi p n_0} \sum_{l=0}^{L_h-1} c_l e^{j\pi[\frac{(2n_0+q)}{2}+\frac{l}{M}]\frac{1}{r}} A_g[-qN-l,-(p+\frac{1}{r})] e^{-j\frac{\pi(2m_0+p)l}{M}}}_{ISI+ICI:J_{m_0,n_0}} \end{aligned} \tag{3.10}$$

This equality shows that the demodulated OFDM/OQAM signal, at the phase-space point (m_0, n_0), is composed of a distorted transmitted symbol a_{m_0,n_0} plus an ISI + ICI term given by :

$$\begin{aligned} J_{m_0,n_0} &= \sum_{(p^0,q^0)} a_{m_0+p,n_0+q} e^{j\frac{\pi}{2}(p+q+pq)} e^{j\pi p n_0} \\ &\times \underbrace{\sum_{l=0}^{L_h-1} c_l e^{j\pi[\frac{(2n_0+q)}{2}+\frac{l_d}{M}]\frac{1}{r}} A_g[-qN-l_d, -(p+\frac{1}{r})] e^{-j\frac{\pi(2m_0+p)l_d}{M}}}_{H_{m_0,n_0}^{(p,q)}} \end{aligned} \tag{3.11}$$

where $\sum_{(p^0,q^0)}$ is the compact expression denoting $\sum_{(p,q)\neq(0,0)}$.

The integers (p,q) decide the interference neighboring zone size. It is worth noting that if the designed prototype is well-localized in time and frequency, the major interference can be limited into a very small zone. For example $|p| = |q| \leq 3$ for IOTA4.

3.3 Timing offset interference analysis for the FBMC/OQAM system

3.3.1 General formulation

In our analysis [38], we start with a time-invariant channel reduced to a simple delay. As there is no mobility during transmission, our channel model (3.1) is such that $P = 1$ and $c_0 = 1$, so we can write

$$h(\tau) = \delta(\tau - d), \tag{3.12}$$

then, based on (3.10), which for the discrete-time model (cf. 3.3), leads to $c_l = \delta(l - l_d)$, and again ignoring the noise, the demodulated OFDM/OQAM signal at the phase-space position (m_0, n_0) is re-written as

$$\begin{aligned} y_{m_0,n_0} &= \underbrace{A_g[-l_d, 0] e^{-j\frac{\pi 2 m_0 l_d}{M}}}_{\alpha_{m_0}} a_{m_0,n_0} \\ &+ \underbrace{\sum_{(p,q)\neq(0,0)} a_{m_0+p,n_0+q} e^{j\frac{\pi}{2}(p+q+pq)} e^{j\pi p n_0} \underbrace{A_g[-qN-l_d, -p] e^{-j\frac{\pi(2m_0+p)l_d}{M}}}_{H_{m_0}^{(p,q)}}}_{ISI+ICI: J_{m_0,n_0}} \\ &= \alpha_{m_0} a_{m_0,n_0} + \underbrace{J_{m_0,n_0}|_{(p=0,q\neq 0)}}_{ISI} + \underbrace{J_{m_0,n_0}|_{(p\neq 0)}}_{ICI} \end{aligned} \tag{3.13}$$

with $l_d = \lceil dF_s \rceil$ and

$$\alpha_{m_0} = A_g[-l_d, 0]e^{-j\frac{\pi 2m_0 l_d}{M}} \tag{3.14}$$

where we can note that, since the channel is now time-invariant, the distortion weight α_{m_0} and $H_{m_0}^{(p,q)}$ are no longer time dependent.

To compensate the distortion, we shall use an equalizer at the output of the demodulator. We can assume the equalizer to be a simple one-tap zero-forcing (ZF) equalizer, which eventually leads to the equalized signal after real-part-taken operation as

$$\hat{a}_{m_0,n_0} = \mathbf{Re}\left\{\frac{\alpha_{m_0}}{H'_{m_0}}\right\}a_{m_0,n_0} + \mathbf{Re}\left\{\frac{J_{m_0,n_0}}{H'_{m_0}}\right\}, \tag{3.15}$$

where H'_{m_0} is the ZF equalizer coefficient at m_0-th subcarrier.

We can write $H'_{m_0} = \alpha_{m_0}$ or $H'_{m_0} = e^{-j\frac{2\pi m_0 l_d}{M}}$, in both cases we obtain the same SIR at the end. In our study we chose to work with the second one to compare our results with the ones in [32].

Hence, the interference is written as

$$J_{m_0,n_0}^{\{ZF\}} = \frac{\sum_{p^0,q^0} a_{m_0+p,n_0+q}e^{j\frac{\pi}{2}(p+q+pq)}e^{j\pi pn_0}A_g[-qN - l_d, -p]e^{-j\pi(2m_0+p)\frac{l_d}{M}}}{e^{-j\frac{2\pi}{M}m_0 l_d}}$$

$$= \sum_{p^0,q^0} a_{m_0+p,n_0+q}e^{j\frac{\pi}{2}(p+q+pq)}e^{j\pi pn_0}e^{-j\pi p\frac{l_d}{M}}A_g[-qN - l_d, -p]$$

$$= \sum_{p^0,q^0} a_{m_0+p,n_0+q}e^{j(\frac{\pi}{2}(p+q+pq)+\pi(pn_0-p\frac{l_d}{M}))}A_g[-qN - l_d, -p] \tag{3.16}$$

Then, by taking into account the equalizer, the interference power can be written as

$$\begin{aligned} P_{ISI+ICI}^{\{demod\}\{ZF\}}(l_d) &= \mathbf{E}[|J_{m_0,n_0}^{\{ZF\}}|^2] \\ &= \sigma_a^2 \sum_{(p^0,q^0)} |\frac{e^{j\frac{\pi}{2}(p+q+pq)} H_{m_0}^{(p,q)}}{H'_{m_0}}|^2 \\ &= \sigma_a^2 \sum_{(p^0,q^0)} |\frac{e^{j\frac{\pi}{2}(p+q+pq)} A_g[-qN-l_d,-p] e^{-j\frac{\pi(2m_0+p)l_d}{M}}}{e^{-j\frac{\pi 2m_0 l_d}{M}}}|^2 \\ &= \sigma_a^2 \sum_{(p^0,q^0)} |e^{j\frac{\pi}{2}(p+q+pq)} A_g[-qN-l_d,-p] e^{-j\frac{\pi p l_d}{M}}|^2 \\ &= \sigma_a^2 \sum_{(p^0,q^0)} |e^{j(\frac{\pi}{2}(p+q+pq)-\pi p\frac{l_d}{M})} A_g[-qN-l_d,-p]|^2 \end{aligned} \tag{3.17}$$

and after the real-part-taken operation we get

$$P_{ISI+ICI}^{\mathbf{Re}\{demod\}\{ZF\}}(l_d) = \sigma_a^2 \sum_{(p^0,q^0)} |\mathbf{Re}\{e^{j(\frac{\pi}{2}(p+q+pq)-\pi p\frac{l_d}{M})} A_g[-qN-l_d,-p]\}|^2, \tag{3.18}$$

the prototype function being an even real-valued function, A_g is also real and even. Therefore, we have $\mathbf{Re}\{A_g\} = A_g$, and $\mathbf{Re}\{e^{j(\frac{\pi}{2}(p+q+pq)-\pi p\frac{l_d}{M})}\} = \cos(\frac{\pi}{2}(p+q+pq) - \pi p\frac{l_d}{M})$, then, we get

$$P_{ISI+ICI}^{\mathbf{Re}\{demod\}\{ZF\}}(l_d) = \sigma_a^2 \sum_{(p^0,q^0)} \cos^2(\frac{\pi}{2}(p+q+pq) - \pi p\frac{l_d}{M}) A_g^2[-qN-l_d,-p] \tag{3.19}$$

Then, the SIR for a delay equal to l_d writes

$$SIR_{l_d}^{\mathbf{Re}\{demod\}\{ZF\}} = \frac{|\mathbf{Re}\{\alpha_{m_0}^{\{ZF\}}\}|^2}{P_{ISI+ICI}^{\mathbf{Re}\{demod\}\{ZF\}}(l_d)} \sigma_a^2 \tag{3.20}$$

3.3.2 Case of an orthogonal prototype filter

Based on (3.17), and before real-part-taken operation, the power P_y of the total received signal y_{m_0,n_0} is given by

$$P_y = \sigma_a^2 \sum_{(p,q)} |H_{m_0}^{(p,q)}|^2 = \sigma_a^2 \sum_{(p,q)} A_g^2[-qN-l_d,-p] = \sigma_a^2 P_{l_d}. \tag{3.21}$$

This power remains constant after ZF equalization with $e^{-j\frac{2\pi m_0 l_d}{M}}$, i.e., $P_y^{ZF} = P_y$. Furthermore, as shown in appendix A.1, for an orthogonal prototype filter since $P_{l_d} = \sum_{p,q} A_g^2[-qN-$

$l_d, -p] = 2$, we have $P_y^{ZF} = 2\sigma_a^2$. On another hand, based on (3.13, 3.14), the demodulated signal after equalization writes

$$y_{m_0,n_0}^{ZF} = \frac{y_{m_0,n_0}}{e^{-j\frac{2\pi m_0 l_d}{M}}} = \underbrace{A_g[-l_d,0]a_{m_0,n_0}}_{u} + \underbrace{\frac{J_{m_0,n_0}}{e^{-j\frac{2\pi m_0 l_d}{M}}}}_{J^{ZF}}. \tag{3.22}$$

Since the real $\mathbf{Re}\{y_{m_0,n_0}^{ZF}\}$ and imaginary parts $\mathbf{Im}\{y_{m_0,n_0}^{ZF}\}$ of y_{m_0,n_0}^{ZF} are mutually independent and the variance of y^{ZF} is constant, equal to $2\sigma_a^2$, the power of the real part received signal is halved, i.e. $P_y^{\mathbf{Re},ZF} = \sigma_a^2$. Moreover $P_y^{\mathbf{Re},ZF} = P_u(l_d) + P_J^{\mathbf{Re},ZF}(l_d)$, which, means that the interference is given by

$$P_J^{\mathbf{Re},ZF}(l_d) = \sigma_a^2 - P_u(l_d) = \sigma_a^2(1 - A_g^2[-l_d,0]). \tag{3.23}$$

Then, multiplying by 2 both sides of this equality, we recover in a particular instance, no Doppler, the result provided without any proof in [32, eq.35]. However, a proof a bit different from the one proposed here can be found in Appendix of the IOTA patent hold by M. Alard [4]. Note that, compared to (3.19), it is easier to compute the interference with (3.23), but then the expression is only valid for orthogonal FBMC/OQAM systems.

In Figure 3.1, we present SIR curves in dB as a function of the normalized delay $(\frac{d}{T_0})$ %. They have been obtained with an orthogonal prototype filter named TFL1, meaning that its M (with here $M = 2048$) taps have been optimized for the Time Frequency Localization criterion using the design method described in [79]. Furthermore, to check the usefulness of our own expression for nonorthogonal prototype filters, we have also considered a short length $L = M$, SRRC filter, named SRRC1, with a roll-of equal to 0.5 [92]. It can be seen that the two alternative calculations using TFL1 prototype filter lead exactly to the same result, and on the other hand, we see that when using SRRC1 prototype filter the calculations do not lead exactly to the same result. To confirm these analytical results, we also run simulations with these TFL1 and SRRC1 prototype filters. We can see (cf. Figure 3.1) that our expression gives the same results as the simulated curves for TFL1 and SRRC1, but for Alard expression it gives the same results as the simulated TFL1 curve and gives a curve with a small difference at small delays for simulated SRRC1 curve.

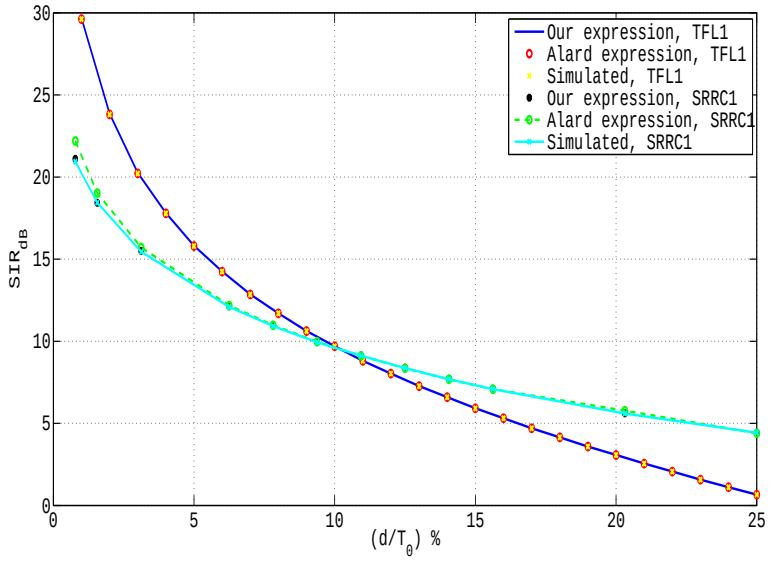

FIG. 3.1 – SIR_{dB} versus $(\frac{d}{T_0})$ % for the TFL1 and SRRC1 prototype filters ($L = M$ =2048).

3.3.3 Interference for OFDM

The ISI and ICI distortions have been already evaluated for OFDM systems with insufficient CP [44]. However this analysis does not provide the result corresponding to the problem of interest here where the channel is reduced to a simple time-offset corresponding to a transmission channel with a single tap given by $c_l = \delta(l - l_d)$.

The considered transmission system is based on the conventional OFDM with a simple one-tap ZF equalizer on receiver. The interference to be analyzed is positioned at the output of the equalizer. We also assume that the delay is less than one OFDM symbol duration.

The OFDM symbol at time index n can be written as

$$s_n[k] = \frac{1}{M} \sum_{m=0}^{M-1} c_{m,n} e^{j\frac{2\pi mk}{M}}, \tag{3.24}$$

The received signal after being filtered by the delayed channel is given by

$$r[k] = \sum_{l=0}^{l_d} c_l s_n[k-l] = s_n[k-l_d]. \tag{3.25}$$

Then the demodulated signal at m_0-th carrier yields

$$\begin{aligned} y_{m_0} &= \sum_{k=0}^{M-1} r[k] e^{-j\frac{2\pi m_0 k}{M}} \\ &= \sum_{k=0}^{l_d-1} s_{n-1}[M-l_d+k] e^{-j\frac{2\pi m_0 k}{M}} + \sum_{k=l_d}^{M-1} s_n[k-l_d] e^{-j\frac{2\pi m_0 k}{M}}, \end{aligned} \tag{3.26}$$

After some computations, reported in Appendix A.5, it is found that the total power of the interference is given by

$$P^I = \sigma_c^2 \frac{l_d(2M-l_d)}{(M-l_d)^2}, \tag{3.27}$$

where σ_c^2 represents the variance of the QAM symbols.

Then, focusing, as in [87], on the SIR which is the relevant ratio to analyze the interference impact, we get

$$SIR(l_d) = \frac{(M-l_d)^2}{l_d(2M-l_d)}. \tag{3.28}$$

If, as assumed, the delay is a fraction of M denoted by $1/P$, it can be seen that the SIR only depends on P.

3.3.4 Numerical results

For all our simulations, the transmission parameters used are the ones of the 3GPP/LTE standard [2], the transmission is carried out through a 30.72 MHz channel using $M = 2048$ subcarriers, yielding to a subcarrier spacing $\frac{30.72MHz}{2048}$=15 kHz, and a symbol spacing $\frac{1}{15kHz} = 66.66667\mu s$. We have compared the theoretical SIR derived in our work with the simulated SIR obtained numerically [38], using 4 different prototype filters : TFL1, IOTA4 [32], FS4 (frequency selectivity with length 4 T_0) [79] and MMB4 (Martin-Mirabbasi-Bellanger with length 4 T_0) [67], [11]. Among these four prototype filters, two of them TFL1, FS4 are perfectly orthogonal, while the two other ones, IOTA4, MMB4 are nearly orthogonal.

Figure 3.2 illustrates the SIR comparison between the simulation and the analytical expression (3.20) for different prototype filters. We also include the OFDM without CP with the expression provided in (3.28) in this comparison. The results are given as a function of the normalized delay ($\frac{d}{T_0}$) %.

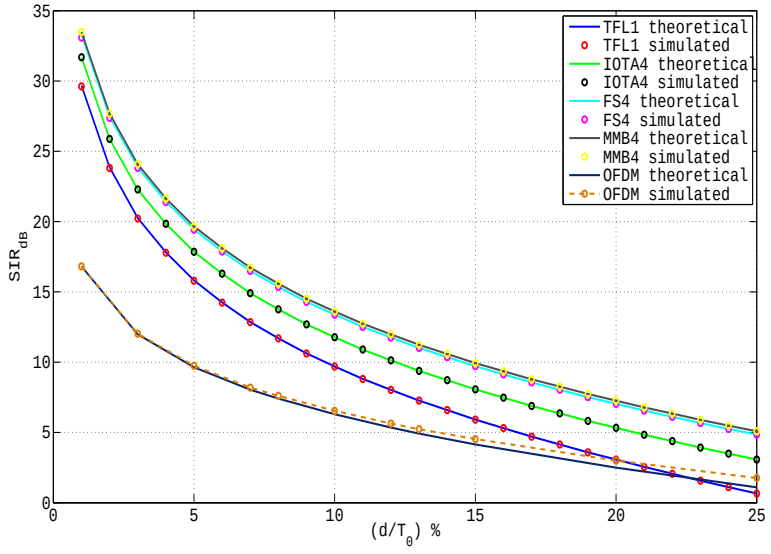

FIG. 3.2 – SIR_{dB} versus $(\frac{d}{T_0})$ %.

We can see that for each delay and each prototype filter, the theoretical expression (3.20), and simulation are matched with regards to the SIR, which proves the accuracy of our derived model.

Note also that, when using the interference expression given in (3.23), even for IOTA4 and MMB4, which are nonorthogonal but very close to orthogonal, we, exactly, recover the curves obtained with (3.20). So this last comparison is not reported in Figure 3.2.

We also can see that all the prototype filters have better performances against timing offset, compared to OFDM without CP. At TO=5%, we can see that TFL1 outperforms OFDM by 6.4 dB, and it is shown that MMB4 and FS4 are better, by 10.4 dB, than OFDM. At TO=10%, TFL1 outperforms OFDM by 3.6 dB, and we see that MMB4 and FS4 have better performance by 7.6 dB compared to OFDM. At TO> 20%, we can see that OFDM outperforms TFL1. When comparing among the prototype filters, we see that MMB4 and FS4, which are the more frequency selective filters, perform similarly and have the best performances. These curves illustrate a well known fact in practice. If a transmission channel introduces a significant delay, say $d \geq \frac{T_0}{10}$, then the FBMC/OQAM interference may become too high to insure acceptable performances if using a simple 1-

tap ZF equalizer. On the other hand, for OFDM a CP is imperatively required, which will remove the interference but at the cost of a bit rate reduction beyond 10%.

3.4 Carrier frequency offset interference analysis for the FBMC/OQAM system

3.4.1 General formulation

In our analysis we now consider another simple scenario including a static CFO without timing-offset, having one path and a unity gain, so the channel model writes :

$$h(t,\tau) = e^{j2\pi f_d t}\delta(\tau - d_0) \qquad \text{with} \qquad d_0 = 0.$$

To get the discrete-time model, remember that, as stated previously, the Doppler shift ($\frac{1}{r}$) is expressed as a percentage, denoting $f_d T_0 = \frac{1}{r}$. Then, based on (3.9-3.11), the demodulated OFDM/OQAM signal at the phase-space position (m_0, n_0) is re-written as

$$\begin{aligned} y_{m_0,n_0} &= \underbrace{e^{j\pi n_0 \frac{1}{r}} A_g[0, -\frac{1}{r}]}_{distortion:\alpha_{n_0}} a_{m_0,n_0} \\ &+ \underbrace{\sum_{(p,q)\neq(0,0)} a_{m_0+p,n_0+q} e^{j\frac{\pi}{2}(p+q+pq)} e^{j\pi p n_0} e^{j\frac{\pi}{2}[(2n_0+q)]\frac{1}{r}} A_g[-qN, -(p+\frac{1}{r})]}_{ISI+ICI:J_{m_0,n_0}} \end{aligned} \tag{3.29}$$

Let us examine more precisely the interference term

$$J_{m_0,n_0} = \sum_{(p^0,q^0)} a_{m_0+p,n_0+q} e^{j\frac{\pi}{2}(p+q+pq)} e^{j\pi p n_0} \underbrace{e^{j\frac{\pi}{2}[(2n_0+q)]\frac{1}{r}} A_g[-qN, -(p+\frac{1}{r})]}_{H_{n_0}^{(p,q)}}. \tag{3.30}$$

We note that the distortion weight α_{n_0} and $H_{n_0}^{(p,q)}$ are no longer frequency dependent. Then, by taking into account the equalizer $H'_{n_0} = e^{j\pi n_0 \frac{1}{r}}$, the interference power can

be written as

$$\begin{aligned} P_{ISI+ICI}^{\{demod\}\{ZF\}}(\frac{1}{r}) &= \mathbf{E}[|\frac{J_{m_0,n_0}}{H'_{n_0}}|^2] \\ &= \sigma_a^2 \sum_{(p^0,q^0)} |\frac{e^{j\frac{\pi}{2}(p+q+pq)} H_{n_0}^{(p,q)}}{H'_{n_0}}|^2 \\ &= \sigma_a^2 \sum_{(p^0,q^0)} |\frac{e^{j\frac{\pi}{2}(p+q+pq)} e^{j\frac{\pi}{2}[(2n_0+q)]\frac{1}{r}} A_g[-qN,-(p+\frac{1}{r})]}{e^{j\pi n_0 \frac{1}{r}}}|^2 \\ &= \sigma_a^2 \sum_{(p^0,q^0)} |e^{j\frac{\pi}{2}(p+q+pq)} e^{j\frac{\pi}{2}\frac{q}{r}} A_g[-qN,-(p+\frac{1}{r})]|^2 \\ &= \sigma_a^2 \sum_{(p^0,q^0)} |e^{j\frac{\pi}{2}((p+q+pq)+\frac{q}{r})} A_g[-qN,-(p+\frac{1}{r})]|^2 \end{aligned} \tag{3.31}$$

and after the real-part-taken operation, we get

$$P_{ISI+ICI}^{\mathbf{Re}\{demod\}\{ZF\}}(\frac{1}{r}) = \sigma_a^2 \sum_{(p^0,q^0)} \cos^2 \frac{\pi}{2}((p+q+pq)+\frac{q}{r}) A_g^2[-qN,-(p+\frac{1}{r})] \tag{3.32}$$

Finally, the signal-to-interference ratio (SIR) at CFO ($\frac{1}{r}$) writes

$$SIR^{\mathbf{Re}\{demod\}\{ZF\}}(\frac{1}{r}) = \frac{|\mathbf{Re}\{\alpha_{n_0}\}|^2 \cdot \sigma_a^2}{P_{ISI+ICI}^{\mathbf{Re}\{ZF\}}(\frac{1}{r})} \tag{3.33}$$

3.4.2 Case of an orthogonal prototype filter

As we discussed in section 3.3.2, the interference analysis for an orthogonal prototype filter caused by a TO, here in this section we analyze the interference due to CFO. Based on (3.31), the power of the total received signal y_{m_0,n_0} is given by

$$P_y = \sigma_a^2 \sum_{(p,q)} |H_{n_0}^{(p,q)}|^2 = \sigma_a^2 \sum_{(p,q)} A_g^2[-qN,-(p+\frac{1}{r})] = \sigma_a^2 P_{\frac{1}{r}}. \tag{3.34}$$

This power remains constant after ZF equalization with $e^{j\pi n_0 \frac{1}{r}}$, i.e., $P_y^{ZF} = P_y$. Furthermore, as shown in appendix (see A.3), for an orthogonal prototype filter since $P_{\frac{1}{r}} = \sum_{p,q} A_g^2[-qN,-(p+\frac{1}{r})] = 2$, we have $P_y^{ZF} = 2\sigma_a^2$. On another hand, based on (3.29), the demodulated signal after equalization writes

$$y_{m_0,n_0}^{ZF} = \frac{y_{m_0,n_0}}{e^{j\frac{\pi n_0}{r}}} = \underbrace{A_g[0,-\frac{1}{r}] a_{m_0,n_0}}_{u} + \underbrace{\frac{J_{m_0,n_0}}{e^{j\frac{\pi n_0}{r}}}}_{J^{ZF}}. \tag{3.35}$$

Since the real $\mathbf{Re}\{y^{ZF}_{m_0,n_0}\}$ and imaginary parts $\mathbf{Im}\{y^{ZF}_{m_0,n_0}\}$ of $y^{ZF}_{m_0,n_0}$ are mutually independent and the variance of y^{ZF} is constant, equal to $2\sigma_a^2$, the power of the real part received signal is halved, i.e. $P_y^{\mathbf{Re},ZF} = \sigma_a^2$. Moreover $P_y^{\mathbf{Re},ZF} = P_u(\frac{1}{r}) + P_J^{\mathbf{Re},ZF}(l_d)$, which, means that the interference is given by

$$P_J^{\mathbf{Re},ZF}(\frac{1}{r}) = \sigma_a^2 - P_u(\frac{1}{r}) = \sigma_a^2(1 - A_g^2[0, -\frac{1}{r}]). \tag{3.36}$$

Again multiplying by 2 both sides of this equality we recover in a particular setting, i.e. no time dispersion, the result provided in [32, eq.35] and proved in [4, Appendix 2]. Note that, compared to (3.31), it is easier to compute the interference with (3.36), but then the expression is only valid for orthogonal systems.

In Fig. 3.3, we present SIR curves in dB as a function of the normalized CFO $(\frac{1}{r}\times 100)\%$. They have been obtained with TFL1 and SRRC1 prototype filters. It can be seen that the two alternative calculations lead exactly to the same result for TFL1 only. To confirm our analytical results, we also run simulations with these TFL1 and SRRC1 prototype filters. We can see (cf. Figure 3.3) that our expression gives the same results as the simulated curves for TFL1 and SRRC1, but for Alard's expression it only gives the same results for the TFL1 prototype filter, while for SRRC1 there is a net difference between simulation and a theory that only holds for orthogonal prototype filter.

3.4.3 Interference analysis for the OFDM system

Since OFDM is the most widely adopted multicarrier technique, it is of interest to compare the above results with their counterpart in OFDM. A sensitivity analysis of OFDM to a CFO, has been reported by Moose in [69]. The following expression has been developed for interference (here interference is only due to ICI) power

$$P_I(\frac{1}{r}) = \sigma_s^2 \frac{\sin^2(\frac{\pi}{r})}{M^2} \sum_{p=1}^{M-1} \frac{1}{\sin^2\big(\frac{\pi(p+\frac{1}{r})}{N}\big)} \tag{3.37}$$

3.4.4 Simulation results

In this section, we present the numerical results that show the level of accuracy of the expression used in the previous section to arrive at the theoretical results of this chapter.

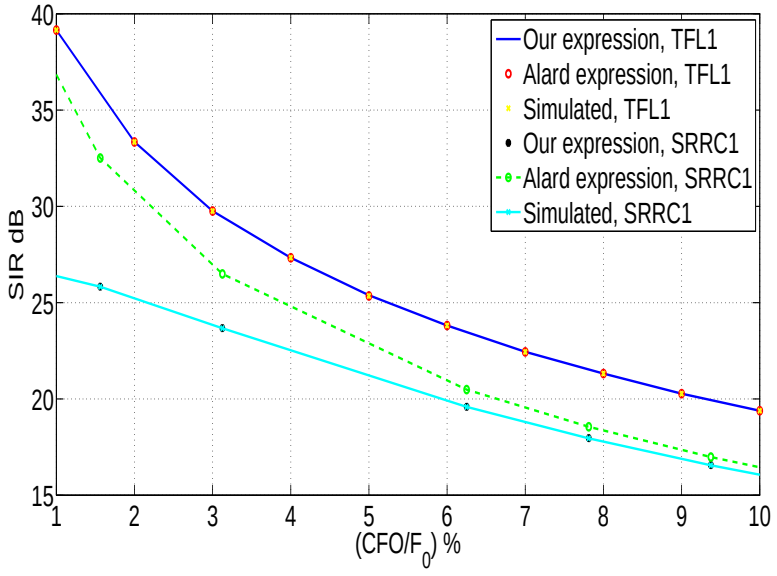

FIG. 3.3 – The theoretical SIR for TFL1 and SRRC1 Alard expression as a function of normalized CFO without timing offset.

For all the results, the transmission parameters used are the same as in section 3.3.4. In our work, we compare the theoretical SIR derived in our chapter with the simulated SIR obtained numerically, using 4 different prototype filters : TFL1, IOTA4, FS4 and MMB4.

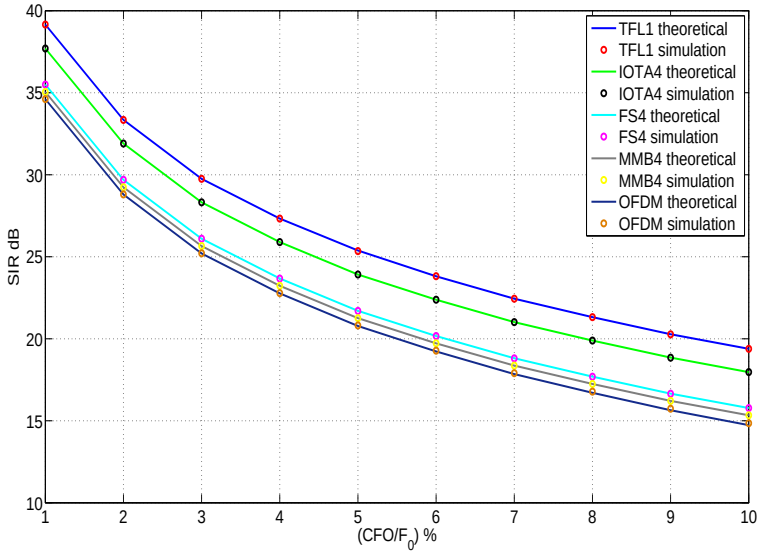

FIG. 3.4 – The theoretical and simulated SIR for TFL1, IOTA4, FS4 and MMB4 against OFDM as a function of the normalized CFO without timing offset.

Figure 3.4 illustrates the SIR comparison between the simulation and the analytical expression (3.33) for different prototype filters. We also include the OFDM without CP with the expression provided in [87] (borrowed from [69]) in this comparison. The results are given as a function of the normalized CFO $(\frac{1}{r} \times 100)\%$.

We can see that for each delay and each prototype filter, the theoretical expression (3.33), and simulation are perfectly matched with regards to SIR, which proves the accuracy of our derived model.

We can also see that all prototype filters have better performances against CFO, compared to OFDM without CP. At CF0=5%, we can see that IOTA4 is better than OFDM by 3.1 dB, and TFL1 has the best SIR by 4.7 dB difference compared to OFDM. At CFO=10%, IOTA4 has better SIR than OFDM by 3.1 dB, and TFL1 remains better by a difference of 4.7 dB compared to OFDM. When comparing among the prototype filters, we see that TFL1 has the best performance, matching with the results obtained in [89], [84], i.e. short prototype filters are the best.

3.5 Timing offset-Carrier frequency offset interference analysis for the FBMC/OQAM system

3.5.1 General formulation

In this section, we analyze the interference caused by both TO and CFO considering a simple scenario. In this analysis we combine the effect of a simple delay with the one of a static CFO which we presented previously. Starting with the channel model, we obtain,

$$h(t, \tau) = e^{j2\pi f_d t} \delta(\tau - d). \tag{3.38}$$

In this particular setting, the demodulated OFDM/OQAM signal can be written as a

particular case of (3.10), considering a single path delay (l_d) :

$$y_{m_0,n_0} = \underbrace{e^{j\pi n_0 \frac{1}{r}} A_g[-l_d, -\frac{1}{r}] e^{-j\frac{\pi 2 m_0 l_d}{M}}}_{distortion:\alpha_{m_0,n_0}} a_{m_0,n_0} + \underbrace{\sum_{(p,q)\neq(0,0)} a_{m_0+p,n_0+q} e^{j\frac{\pi}{2}(p+q+pq)} e^{j\pi p n_0} e^{j\frac{\pi}{2}[(2n_0+q)]\frac{1}{r}} A_g[-qN-l_d, -(p+\frac{1}{r})] e^{-j\frac{\pi(2m_0+p)l_d}{M}}}_{ISI+ICI:J_{m_0,n_0}} \tag{3.39}$$

The interference can be rewritten as follows

$$J_{m_0,n_0} = \sum_{(p^0,q^0)} a_{m_0+p,n_0+q} e^{j\frac{\pi}{2}(p+q+pq)} e^{j\pi p n_0} \underbrace{e^{j\frac{\pi}{2}[(2n_0+q)]\frac{1}{r}} A_g[-qN-l_d, -(p+\frac{1}{r})] e^{-j\frac{\pi(2m_0+p)l_d}{M}}}_{H^{(p,q)}_{m_0,n_0}} \tag{3.40}$$

Then, by taking into account the equalizer $H'_{m_0,n_0} = e^{j\pi n_0 \frac{1}{r}} e^{-j\frac{\pi 2 m_0 l_d}{M}}$, the interference power can be written as

$$\begin{aligned}
P^{\{demod\}\{ZF\}}_{ISI+ICI}(l_d, \frac{1}{r}) &= \mathbf{E}[|\frac{I_{m_0,n_0}}{H'_{m_0,n_0}}|^2] \\
&= \sigma_a^2 \sum_{(p^0,q^0)} |\frac{e^{j\frac{\pi}{2}(p+q+pq)} H^{(p,q)}_{m_0,n_0}}{H'_{m_0,n_0}}|^2 \\
&= \sigma_a^2 \sum_{(p^0,q^0)} |\frac{e^{j\frac{\pi}{2}(p+q+pq)} e^{j\frac{\pi}{2}[(2n_0+q)]\frac{1}{r}} A_g[-qN-l_d, -(p+\frac{1}{r})] e^{-j\frac{\pi(2m_0+p)l_d}{M}}}{e^{j\pi n_0 \frac{1}{r}} e^{-j\frac{\pi 2 m_0 l_d}{M}}}|^2 \\
&= \sigma_a^2 \sum_{(p^0,q^0)} |e^{j\frac{\pi}{2}(p+q+pq)} e^{j\frac{\pi}{2}\frac{q}{r}} A_g[-qN-l_d, -(p+\frac{1}{r})] e^{-j\frac{\pi p l_d}{M}}|^2 \\
&= \sigma_a^2 \sum_{(p^0,q^0)} |e^{j(\frac{\pi}{2}((p+q+pq)+\frac{q}{r})-\frac{\pi p l_d}{M})} A_g[-qN-l_d, -(p+\frac{1}{r})]|^2
\end{aligned} \tag{3.41}$$

and after the real-part-taken operation, we get

$$P^{\mathbf{Re}\{demod\}\{ZF\}}_{ISI+ICI}(l_d, \frac{1}{r}) = \sigma_a^2 \sum_{(p^0,q^0)} \cos^2(\frac{\pi}{2}((p+q+pq)+\frac{q}{r}) - \frac{\pi p l_d}{M}) A_g^2[-qN-l_d, -(p+\frac{1}{r})] \tag{3.42}$$

Finally, the signal-to-interference ratio (SIR) at TO(l_d) and CFO ($\frac{1}{r}$) writes

$$SIR^{\mathbf{Re}\{demod\}\{ZF\}}(l_d, \frac{1}{r}) = \frac{|\mathbf{Re}\{\alpha_{m_0,n_0}\}|^2 \cdot \sigma_a^2}{P^{\mathbf{Re}\{ZF\}}_{ISI+ICI}(l_d, \frac{1}{r})} \tag{3.43}$$

3.5.2 Case of an orthogonal prototype filter

As in [32], [4] and differently from sections 3.3.2 and 3.4.2, we now investigate the case of a static channel introducing simultaneously TO and CFO. Based on (3.41), the power of the total received signal y_{m_0,n_0} is given by

$$P_y = \sigma_a^2 \sum_{(p,q)} |H_{n_0}^{(p,q)}|^2 = \sigma_a^2 \sum_{(p,q)} A_g^2[-qN - l_d, -(p + \frac{1}{r})] = \sigma_a^2 P_{l_d,\frac{1}{r}}. \tag{3.44}$$

This power remains constant after ZF equalization with $(e^{j\pi n_0 \frac{1}{r}}.e^{-j\frac{2\pi m_0 l_d}{M}})$, i.e., $P_y^{ZF} = P_y$. Furthermore, for an orthogonal prototype filter since $P_{l_d,\frac{1}{r}} = \sum_{p,q} A_g^2[-qN - l_d, -(p+\frac{1}{r})] = 2$, based on Appendix A.4, we have $P_y^{ZF} = 2\sigma_a^2$. On another hand, based on (3.8), the demodulated signal after equalization writes

$$y_{m_0,n_0}^{ZF} = \frac{y_{m_0,n_0}}{e^{j\pi n_0 \frac{1}{r}}.e^{-j\frac{2\pi m_0 l_d}{M}}} = \underbrace{A_g[-l_d, -\frac{1}{r}]a_{m_0,n_0}}_{u} + \underbrace{\frac{J_{m_0,n_0}}{e^{j\frac{\pi n_0}{r}}.e^{-j\frac{2\pi m_0 l_d}{M}}}}_{J^{ZF}}. \tag{3.45}$$

Since the real $\mathbf{Re}\{y_{m_0,n_0}^{ZF}\}$ and imaginary parts $\mathbf{Im}\{y_{m_0,n_0}^{ZF}\}$ of y_{m_0,n_0}^{ZF} are mutually independent and the variance of y^{ZF} is constant, equal to $2\sigma_a^2$, the power of the real part received signal is halved, i.e. $P_y^{\mathbf{Re},ZF} = \sigma_a^2$. Moreover $P_y^{\mathbf{Re},ZF} = P_u(l_d, \frac{1}{r}) + P_J^{\mathbf{Re},ZF}(l_d, \frac{1}{r})$, which, means that the interference is given by

$$P_J^{\mathbf{Re},ZF}(l_d, \frac{1}{r}) = \sigma_a^2 - P_u(l_d, \frac{1}{r}) = \sigma_a^2(1 - A_g^2[-l_d, -\frac{1}{r}]). \tag{3.46}$$

After a multiplication by 2, we recover the result presented in [32, eq.35], [4], as a particular case of the more general result we have derived in subsection 3.5.1.

In Figure 3.5, we present SIR curves in dB as a function of equal normalized delay d and CFO $(\frac{d}{T_0}=\frac{1}{r}\times 100)\%$. They have been obtained with TFL1 and SRRC1 prototype filters. It can be seen that the two alternative calculations lead exactly to the same result for TFL1 only. To confirm our analytical results, we run simulations with these TFL1 and SRRC1 prototype filters. We can see (cf. Figure 3.5) that our expression gives the same results as the simulated curves for TFL1 and SRRC1, but for Alard's expression it only gives the same results for the TFL1 prototype filter, while for SRRC1 there is a net difference (for small delays) between simulation and a theory that only holds for orthogonal prototype filter. Note that in all our comparisons, with SRRC1, between theory and simulation as Alard's expression neglects part of the interference terms, it always overestimate the SIRs.

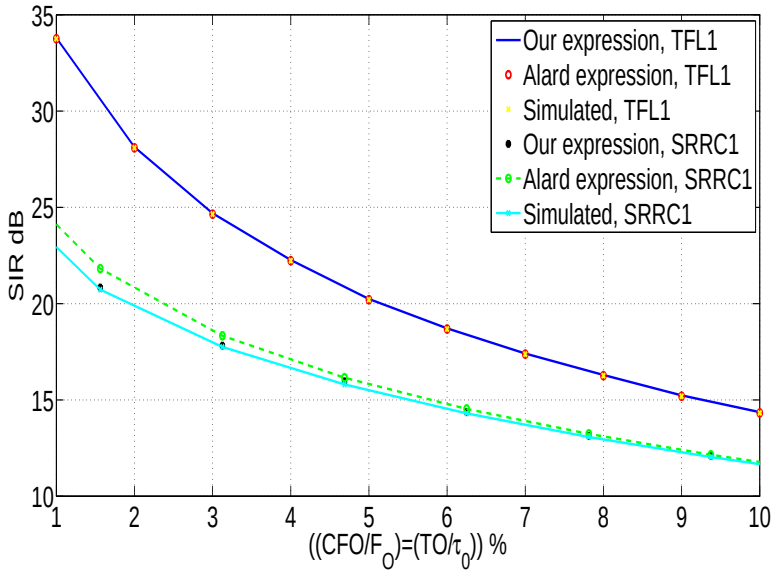

FIG. 3.5 – The theoretical SIR for TFL1 and SRRC1 Versus Alard expression as a function of equal normalized TO and CFO.

3.5.3 Simulation results

In this section, we present the numerical results that show the level of accuracy of the expression used in the previous section to arrive at the theoretical results of this analysis.

For all the results, the transmission parameters used are the same as in section 3.3.4. In our analysis, we compare the theoretical SIR derived in our analysis with the simulated SIR obtained numerically as a function of the normalized CFO and timing offsets, using 4 different prototype filters : TFL1, IOTA4, FS4 and MMB4. Figures 3.6,3.8, and 3.10 illustrate the SIR comparison between the simulation and the analytical expression (3.43) for different prototypes filters.

In Figures 3.6 and 3.7 we evaluate the performances of the 4 prototype filters against TO, we fixed CFO=5% and CFO=10%, respectively. In Figure 3.6, at the beginning, when TO=0%, we see that TFL1 has best performance, and when increasing TO, we see that IOTA4 outperforms TFL1 at TO=3.5%, FS4 and MMB4 outperform TFL1 at TO=5%, FS4 and MMB4 outperform IOTA4 for TO$\geq$ 8%, to be the best prototype filters to support TO at fixed CFO=5%. In another hand, in Figure 3.7, where CFO is increased to 10% we

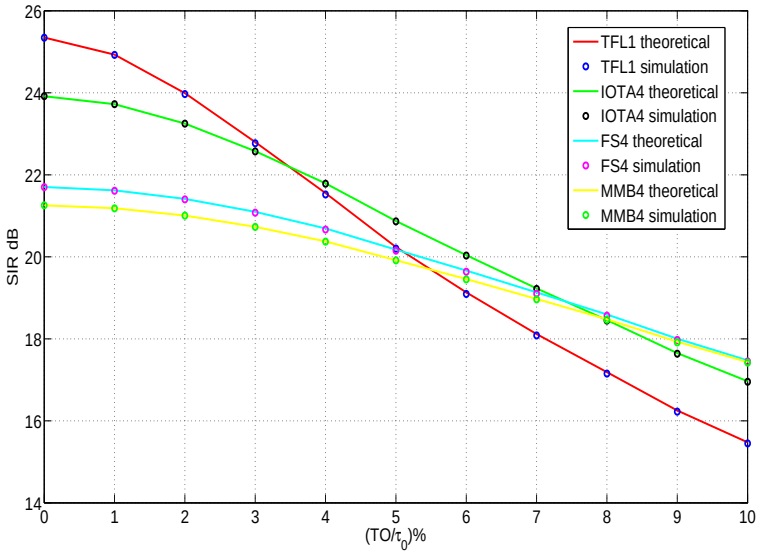

FIG. 3.6 – The theoretical and simulated SIR for TFL1, IOTA4, FS4 and MMB4 as a function of normalized TO with fixed $\frac{CFO}{F_0} = 5\%$.

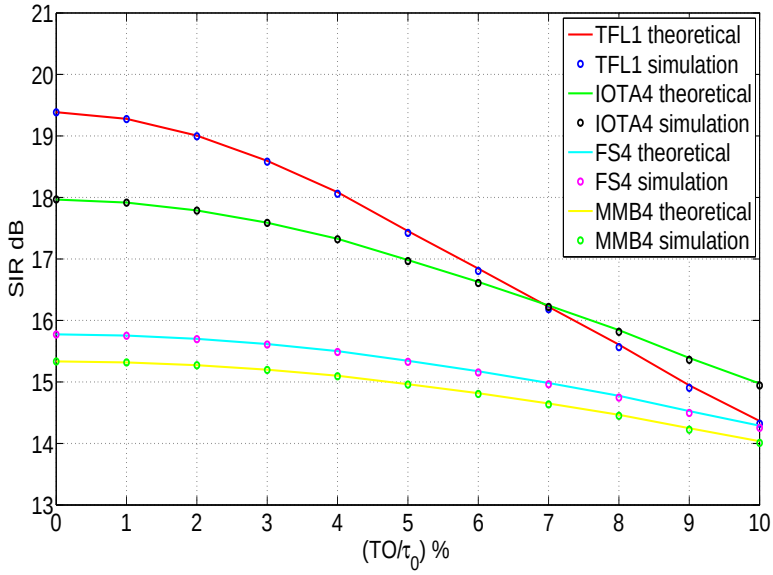

FIG. 3.7 – The theoretical and simulated SIR for TFL1, IOTA4, FS4 and MMB4 as a function of normalized TO with fixed $\frac{CFO}{F_0} = 10\%$.

remark a performance degradation of 6 dB for all the prototype filters at TO=0% and TFL1 is always better at low TO, and when increasing the TO, we see that the TFL1-

IOTA4 intersection is shifted to TO=7%. IOTA4 being the best up to TO= 10%, FS4 and MMB4 are the worst, FS4 intersects with TFL1 only at TO=10%.

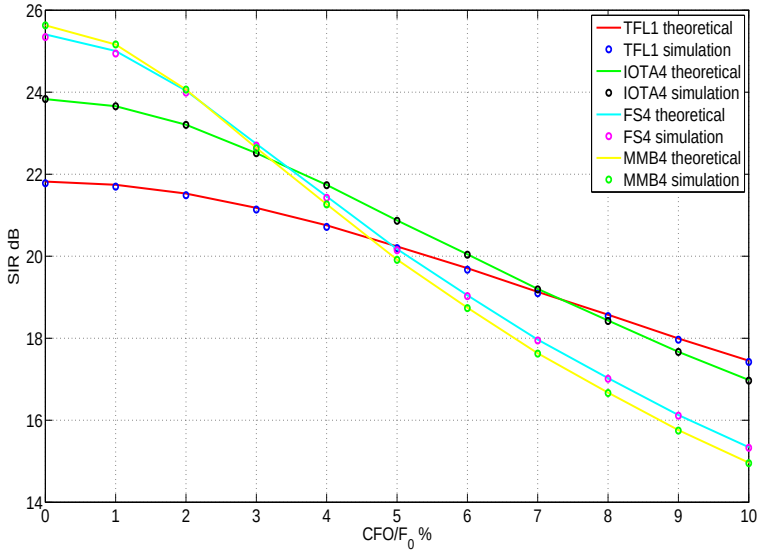

FIG. 3.8 – The theoretical and simulated SIR for TFL1, IOTA4, FS4 and MMB4 as a function of normalized CFO with fixed $\frac{TO}{\tau_0} = 5\%$.

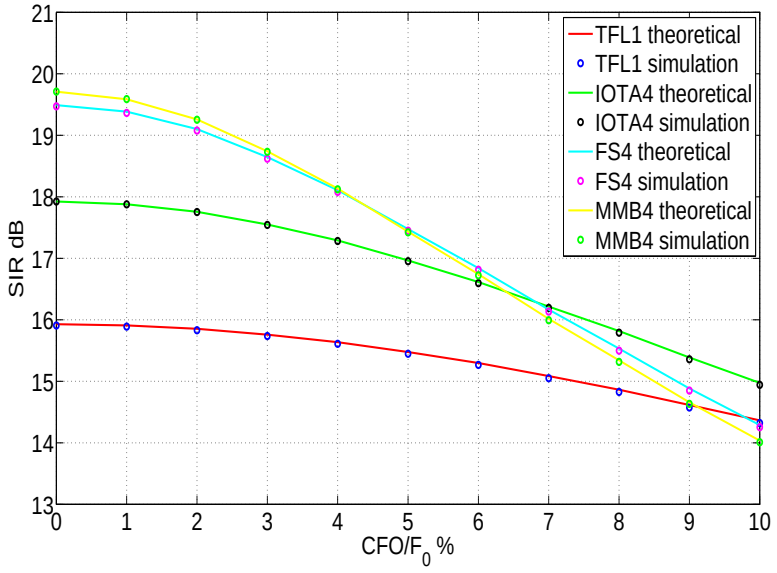

FIG. 3.9 – The theoretical and simulated SIR for TFL1, IOTA4, FS4 and MMB4 as a function of normalized CFO with fixed $\frac{TO}{\tau_0} = 10\%$.

In Figures 3.8 and 3.9 we evaluate the performances of the 4 prototype filters against CFO, we fixed TO=5% and TO=10%,respectively. In Figure 3.8 we can see at the beginning, when CFO=0%, that FS4 and MMB4 have the best performances. By increasing the CFO, we see that IOTA4 outperforms FS4 and MMB4 from CFO=3.5%, and TFL1 outperforms FS4 and MMB4 from CFO=5%, and outperforms IOTA4 from CFO=7.3%, becoming the best prototype filter to support CFO when TO=5%. In another hand, when increasing the TO=10% as depicted in Figure 3.9, we remark a performance degradation of 6 dB for all the prototype filters at CFO=0% and FS4 and MMB4 have best performances from the beginning, FS4-IOTA4 and MMB4-IOTA4 intersections are shifted to CFO=6.5%, TFL1 outperforms MMB4 at CFO=9%, TFL1 intersects with FS4 at CFO=10%, and we can see here that this time IOTA4 is the best in performance in the case of TO=10%.

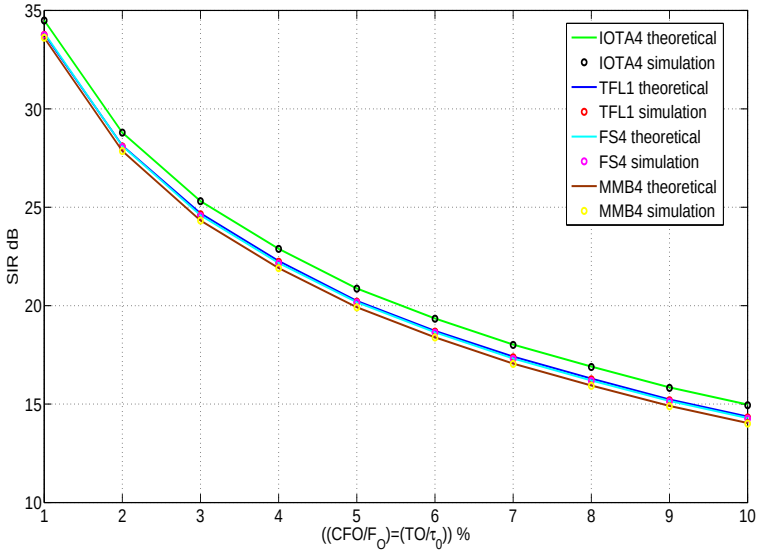

FIG. 3.10 – The theoretical and simulated SIR for TFL1, IOTA4, FS4 and MMB4 as a function of equal normalized CFO and timing offset.

In Figure 3.10 we evaluate the performances of the 4 prototype filters against equal and nonzero CFO and TO. We can see that for each $\frac{CFO}{F_0} = \frac{TO}{\tau_0} \times 100\%$, and each prototype filter, our theoretical result, based on (3.43), compared to simulation, leads to the same SIR, which proves the accuracy of our derived model. When comparing among the prototype filters, we see that TFL1, FS4 and MMB4 have nearly the same performances, and IOTA4

has the best performance by 0.5 dB.

From Figures 3.6-3.10, we can deduce that a prototype filter cannot be appropriate for any type of channel conditions but can only fit to some particular cases. Actually, we have to select the prototype filter according to given channel conditions : being well localized in frequency if the channel is time dispersive, in time if the channel is frequency dispersive and in both time and frequency if the channel is equally time-frequency dispersive.

3.6 Time-offset synchronization method for the single-user FBMC/OQAM system

Due to better performances in the frequency domain, the frequency synchronization problem is less critical for OFDM/OQAM than for OFDM. At the contrary in the time domain, differently from CP-OFDM [101], which profits from the CP, OFDM/OQAM cannot take advantage of the corresponding correlation properties. Thus, as the time synchronization may be the most critical point for this modulation, we will only focus on it on this second part of this chapter, considering the single and multiuser cases.

3.6.1 OFDM/OQAM synchronization methods

There are several methods used for time synchronization for OFDM/OQAM. Generally these methods use the correlation in the time domain of the received signal. This correlation can, for example, be created using deterministic pilots grouped in the form of preambles [34] or, alternatively, from scattered pilots based on pseudo-random sequences [50]. The synchronization used in [50] suffers from high complexity due to the use of several successive correlations. Another technique is used in [95] that performs synchronization, in the frequency domain. But then lengthy preambles are required. In this thesis, in relation with the target application described in Chapter 4, we prefer to focus on synchronization methods which are appropriate for packet transmission. As these preambles must be short, one can take [34] as a reference. According to [34], a relationship between signal samples can be obtained by a specific preamble (odd carriers are set to zero) and these relationships can be maintained after filtering using a prototype filter of odd length. A disadvantage is that the length of the preamble [34] increases with the length of the prototype filter.

More recently the thesis of Y. Dandach [22] showed the possibility to limit the preamble duration equal to one multicarrier symbol (M). In addition the choice of a deterministic preamble allows the creation of peaks at the IFFT output, which may be useful to reduce the estimator complexity.

Here we recall the basic principles of the proposed method and we will show how it can be extended to the time synchronization of multiusers.

Let us first recall that the baseband OFDM/OQAM signal in discrete time is expressed by the following equation :

$$s[k] = \sum_{m=0}^{M-1} \sum_{n=-\infty}^{+\infty} a_{m,n} g[k - nN] e^{j\frac{2\pi}{M}m(k-\frac{D}{2})} e^{j\phi_{m,n}}, \tag{3.47}$$

where $M = 2N$ is the subcarrier number. The coefficients $a_{m,n}$ are real symbols, they are noted $p_{m,n}$ when they correspond to the pilots used in the preambles. $g(k)$ is the prototype filter of length L and the delay is $D = L - 1$.

In the presence of an additive white Gaussian noise (AWGN), a time shift τ and a phase shift ϕ, the received signal can be expressed as follows :

$$r[k] = s[k - \tau] e^{j\phi} + b[k], \tag{3.48}$$

with $b[k]$ a centered complex circular Gaussian noise with a spectral density of σ_b^2.

The synchronization problem amounts to estimating the parameters τ and ϕ.

3.6.2 The proposed synchronization method

As in [34], the idea is to exploit conjugation properties that are exactly satisfied at the modulator output. Then, it is expected that after transmission through a multipath channel and an addition of noise, they will be still approximately satisfied. Then, a Least Squares (LS) measure can be used to decide which estimation leads to the best approximation.

Let us denote by $v_{k,n}$ the IFFT output of index k at time instant n of the OFDM/OQAM system depicted in Figure 2.5. Considering a prototype filter of length $L = qM$, with q an integer, it has been shown in [23] that the $v_{k,n}$'s satisfy the following relations

$$\begin{cases} v_{k,n} & = & (-1)^n v^*_{\frac{M}{2}-k-1,n} \\ v_{\frac{M}{2}+k,n} & = & (-1)^n v^*_{M-k-1,n}, \end{cases} \tag{3.49}$$

These general relations apply for any IFFT input and therefore also hold for any type of preamble, deterministic or random.

Another conjugation property appears if we select, as in [34], a preamble where one subcarrier over 2 is set to zero. Then, it can be shown [22] that in addition to (3.49), we have also

$$v_{k,n} = (-1)^n v^*_{M-k-1,n} \qquad \text{for} \qquad 0 \leq k \leq \frac{M}{2} - 1. \tag{3.50}$$

Setting $L = M$, we can use the following preamble

$$\begin{cases} p_{2m,0} = (-1)^m \frac{\sqrt{2}}{2} \\ \\ p_{2m+1,0} = 0 \end{cases} \qquad \text{for} \qquad 0 \leq m \leq \tfrac{M}{2} - 1, \tag{3.51}$$

and

$$p_{m,1} = 0, \qquad \text{for} \qquad 0 \leq m \leq M - 1. \tag{3.52}$$

The preamble duration is limited to two successive pilot symbols, here $n = 0$ and 1. The null symbol is introduced to separate pilot and data symbols.

We can note that the preamble given in (3.51) leads to 4 peaks at the IFFT output of indexes 0, $\frac{M}{2} - 1$, $\frac{M}{2}$ and $M - 1$ as shown by the example with $M = 64$ given in Figure 3.11. These peaks values are the least affected in the presence of the noise or a multipath channel. Therefore, we can make the estimators more robust and less complex by neglecting at the receiver side the calculations which do not correspond to peak values. Removing the samples and keeping only the peak values which are less affected by noise and the channel, leads to reduced estimators that have better performance.

The estimator derived in [34] is written as :

$$\hat{\tau}_{LS} = \arg\max_{\hat{\tau}} \Big| \sum_{k=0}^{\frac{M}{2}-1} r[k + \hat{\tau}] r[M - 1 - k + \hat{\tau}] \Big|. \tag{3.53}$$

Then, the estimator used in this section, and proposed in [22], can be written as follows :

$$\hat{\tau}_{LS} = \arg\max_{\hat{\tau}} |r[\hat{\tau}] r[M - 1 + \hat{\tau}] + r[\frac{M}{2} - 1 + \hat{\tau}] r[\frac{M}{2} + \hat{\tau}]|. \tag{3.54}$$

The prototype filter also impacts the performance of the estimators. Indeed, for a given prototype filter, it is better that the peak values at the output of the IFFT, not to be too

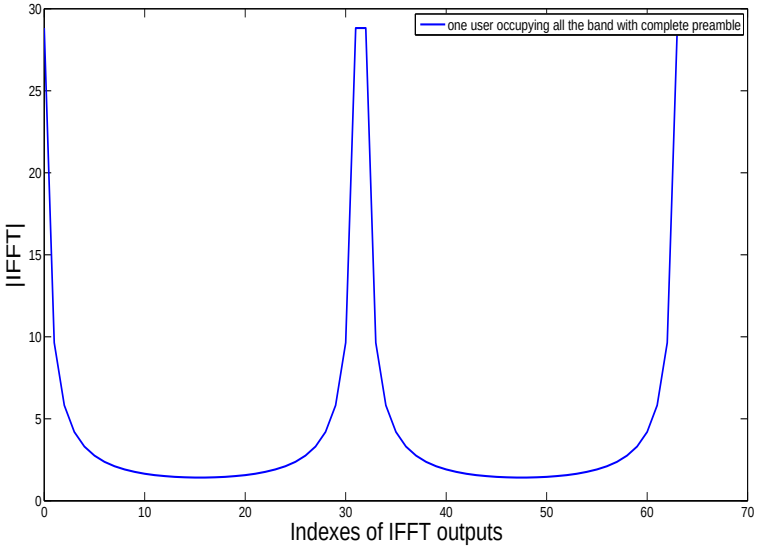

FIG. 3.11 – Magnitude value of the IFFT output for the preamble being used in single user downlink transmission system.

much attenuated. This will be the case if they are filtered by the filter coefficients of highest amplitude. The prototype filters being low-pass, their maximum amplitude coefficients are grouped around the peak value. If in addition, this filter is linear phase, case considered here, the maximum values are at the center of the filter, i.e. are distributed on the $\frac{M}{2}$ samples if the prototype filter is of length $L = M$. Then, when using the preamble presented in this section and the simplified estimator, we can benefit from one of the two couples of peaks values at positions $\{0, M-1\}$ and $\{\frac{M}{2}, \frac{M}{2}-1\}$ (after the IFFT). Here, we decided to only profit from the couple $\{\frac{M}{2}, \frac{M}{2}-1\}$, because the peaks values of index $\{0, M-1\}$ are attenuated after filtering (here we use the TFL1 prototype filter), since they are located at the filter edges. So we can use the peak values filtered by $h[qM/2-1], h[qM/2]$.

In this case, the estimator we use is reduced to :

$$\hat{\tau}_{LS} = \arg\max_{\hat{\tau}} |r[\frac{M}{2} - 1 + \hat{\tau}] r[\frac{M}{2} + \hat{\tau}]|. \tag{3.55}$$

At the receiver side, due to noise and multipath channel we partly lose the conjugation property. However, the estimator performance is good.

In addition, it is clear that the estimator in (3.55) is much less complex to implement

than the one in (3.53).

3.7 Time-offset synchronization method for the multiuser UpLink FBMC/OQAM system

Multiuser uplink (UL) synchronization is, in general, a difficult task that presents a drastically different outlook from the corresponding downlink (DL) situation [36], [35]. The main reason is that UL signals transmitted by distinct users are characterized by different timing and frequency offsets and, accordingly, the receiver has to estimate much more parameters than in the DL.

Unfortunately, the methods used in DL do not apply to an UL scenario because UL signals are affected by different synchronization errors and the correction of one user′s time and frequency offset would misalign other initially aligned users.

The better frequency localization of OFDM/OQAM compared to OFDM makes it less sensitive to CFO. This has been already illustrated in [86] for UL transmission. Therefore, in this section, we prefer to concentrate on the problem of timing estimation for multiuser OFDM/OQAM UL transmissions, which is a more critical task. For the 3GPP/LTE [98] standard, they have their own synchronization methods, although, there are still errors, so that, in our work we present a method for time synchronization which is able of correcting time desynchronizations which are within 10% of the symbol time.

In our study, we consider a multiuser UL transmission system, with a situation in which different subchannels are assigned to distinct users, even though in practice more subchannels may be allocated to a single given user depending on its requested data rate. The subcarriers are distributed among active users, they are allocated blockwise, each user has its proper adjacent carriers [70]. Assigning a group of contiguous subcarriers to each active user makes the synchronization task simple. Each of these users is suffering different timing-shifts, the multiuser system representing our simulations to evaluate the estimator of each user [70] is shown in Figure 3.12, in practice the correction is performed at transmission.

To separate the users' signals at the receiver we use a filter bank [70], which can select

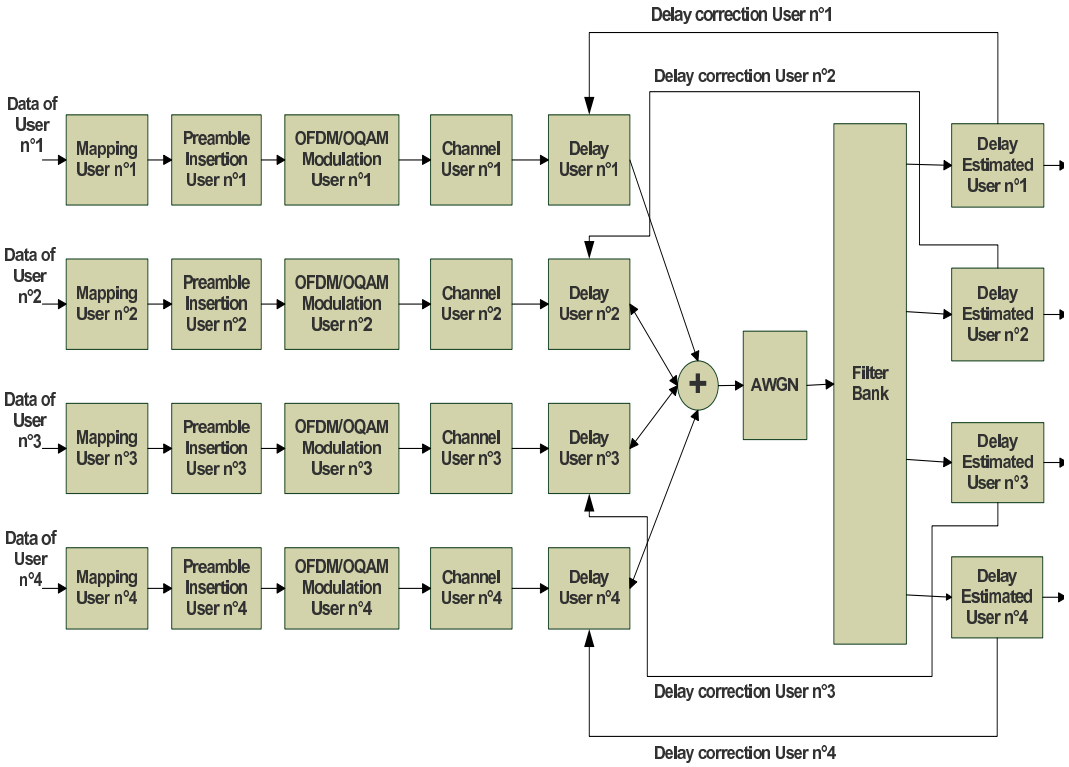

FIG. 3.12 – Multiuser uplink transmission system used in our simulations.

the appropriate users' band. This filtering operation allows the receiver to perform timing estimation independently for each active users, as we see in the following equations, where (3.56) is the filter bank input and (3.57) is the filter bank output (input of each user estimator).

$$r(t) = \sum_{u=0}^{U-1} r_u^{\tau_u}(t) = \sum_{u=0}^{U-1} r_u(t-\tau_u), \tag{3.56}$$

$$u \in \{u_0, u_1, u_2, ..., U-1\},$$

$$r_u(t-\tau_u) = r(t) \otimes P_{FB}^u(t), \tag{3.57}$$

where $\otimes$ is the convolution operation and P_{FB}^u is the filter bank used to separate the users' signals of delay τ_u.

The method in [22] was proposed to DL single user transmission, using a single preamble of FFT size as shown in Figure 3.13. To adapt the preamble for UL multiuser transmission,

Figures 3.14-3.17 show that each user has its own preamble. Then this preamble could be defined as follows

$$p^u_{2m,0} = \begin{cases} (-1)^m \frac{\sqrt{2}}{2} & \text{for} \quad m^b_u \leq m \leq m^s_u \\ 0 & \text{otherwise} \end{cases} \tag{3.58}$$

with $u = 0, 1, ..., U-1$, $\bigcup_u [m^b_u, m^s_u] = [0, M-1]$ and $\bigcap_u [m^b_u, m^s_u] = \phi$.

In our simulation setting we consider 4 users ($U = 4$) equally sharing an overall bandwidth constituted of $M = 16$ subcarriers. Then as shown in Figure 3.18, even if the IFFT output is slightly different from the one depicted in Figure 3.11 for the single user case, the four peaks are still present.

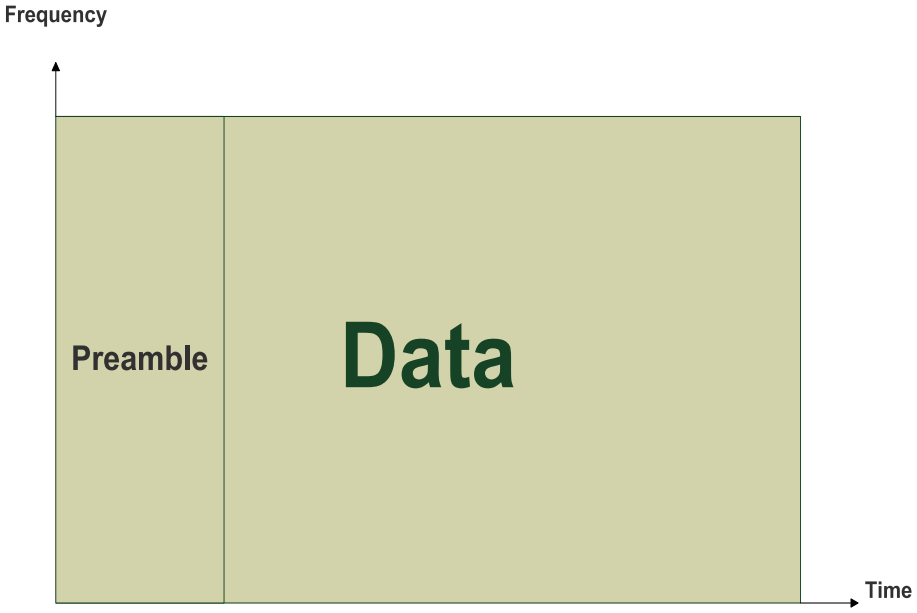

FIG. 3.13 – The preamble being used in single user downlink transmission system.

In this case, based on (3.55), the time estimator of each user would be as :

$$\hat{\tau}^u_{LS} = \arg\max_{\hat{\tau}^u} |r[\frac{M}{2} - 1 - \hat{\tau}^u] r[\frac{M}{2} - \hat{\tau}^u]|. \tag{3.59}$$

3.7.1 Simulations and results

To evaluate the performances of the new synchronization method for the UL multiuser transmission, we consider a transmission system carried out through a 30.72 MHz channel, using the simulation context of [33], i.e. QPSK modulation, $M = 64$ subcarriers, yielding to

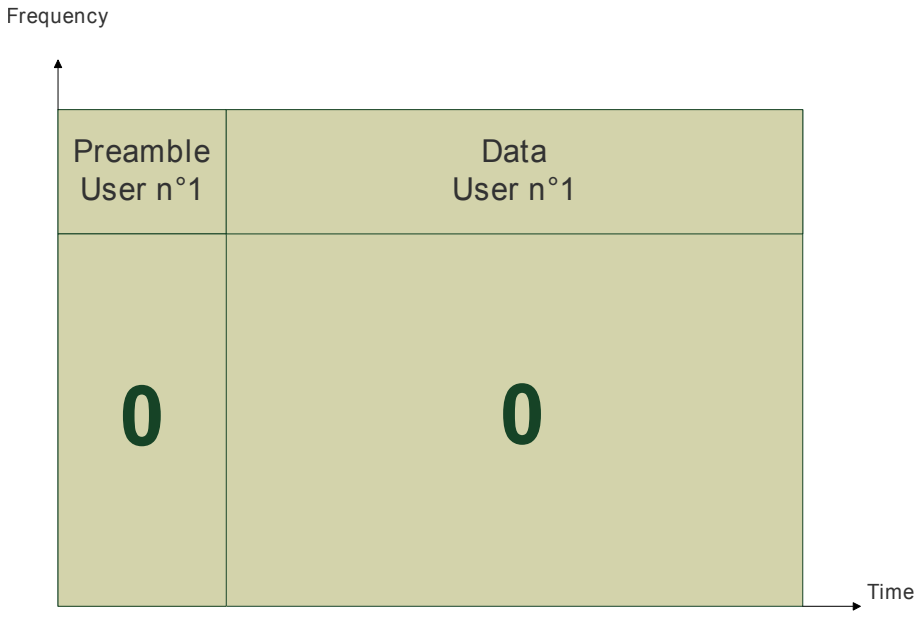

FIG. 3.14 – The modified preamble being used by user n.1 in multiuser uplink transmission system.

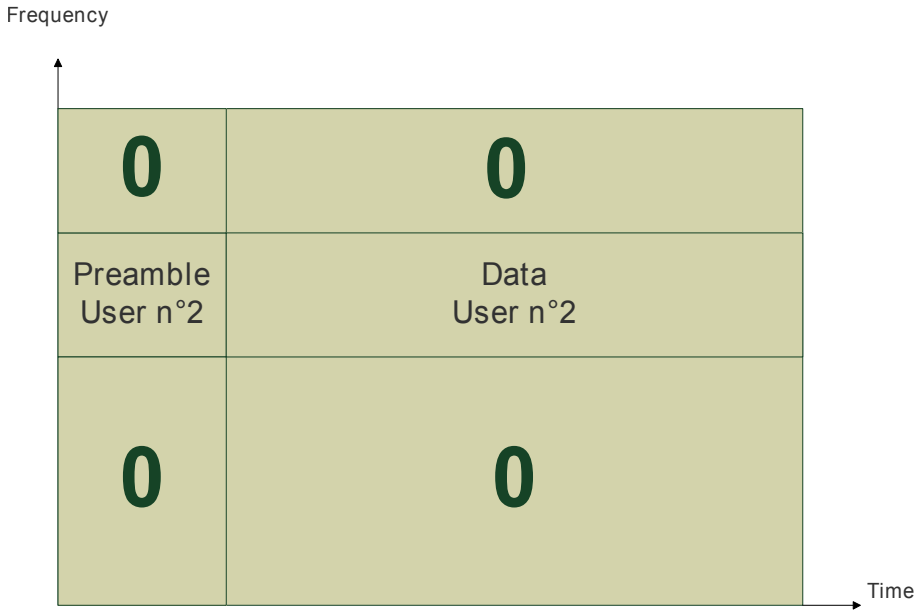

FIG. 3.15 – The modified preamble being used by user n.2 in multiuser uplink transmission system.

a subcarrier spacing of 480 kHz and a timing symbol of 2 μs. We have 4 active users, each of them is assigned a group of 16 contiguous subcarriers, the users are allocated blockwise as shown in Figures 3.14, 3.15, 3.16 and 3.17. Each users' signal is affected by a different

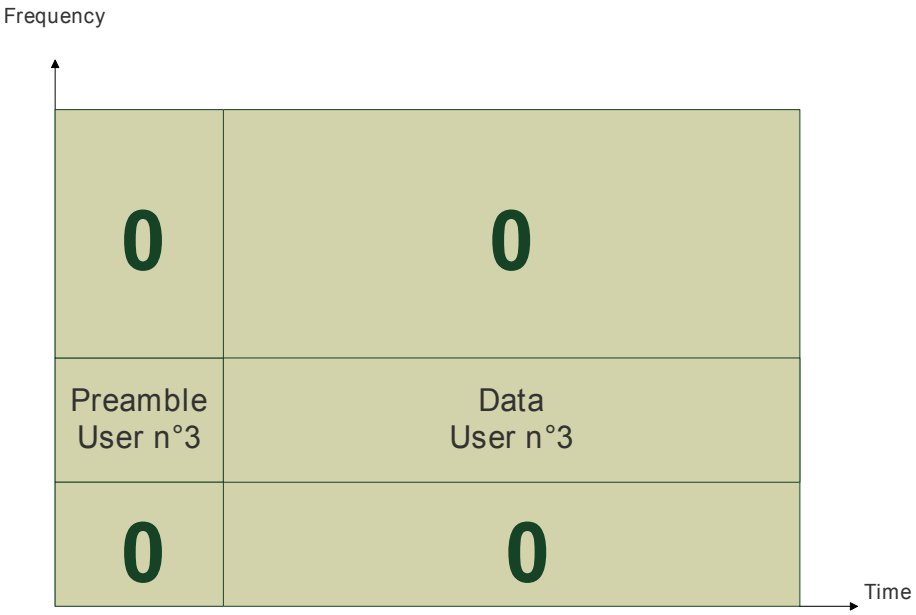

FIG. 3.16 – The modified preamble being used by user n.3 in multiuser uplink transmission system.

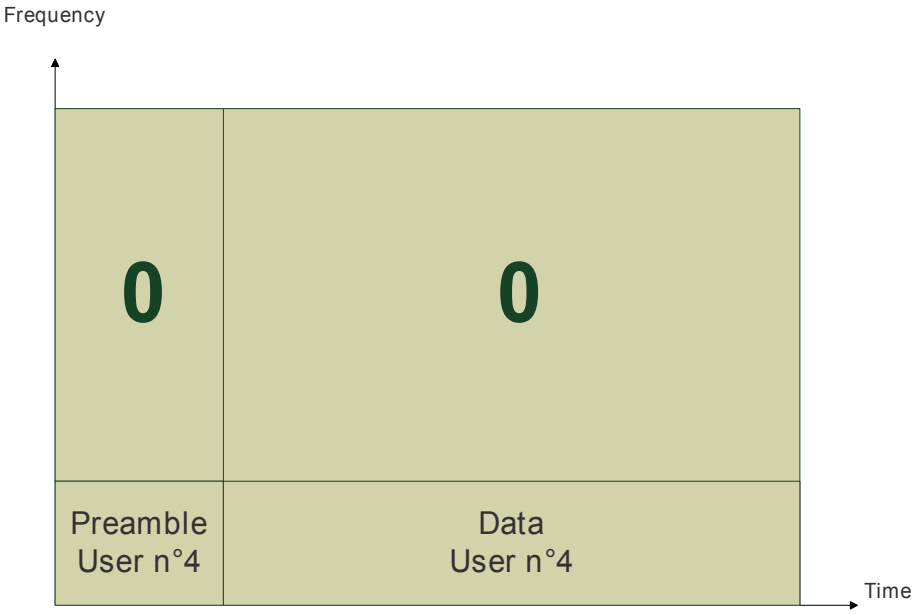

FIG. 3.17 – The modified preamble being used by user n.4 in multiuser uplink transmission system.

timing-offset. The simulations have been carried out first with an AWGN and afterwards with a 5-tap multipath channel [33] (with 5000 realizations) plus AWGN. We used TFL1 and FS4 prototype filters, and we first compared their performances in a single user scenario

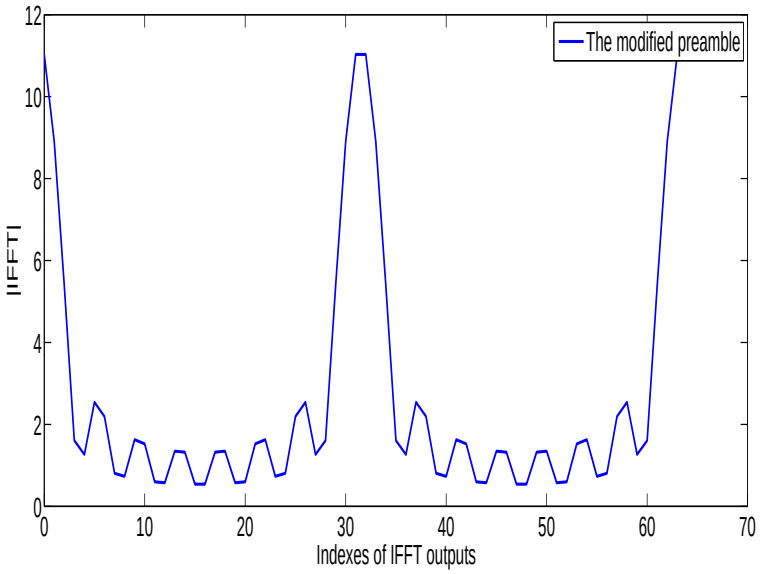

FIG. 3.18 – Magnitude value of the IFFT output for each user of the multiuser uplink transmission system.

with a 5-tap multipath channel [33] plus AWGN and with perfect synchronization, as shown in Figure 3.19. We can see that TFL1 has nearly same performance as FS4, TFL1 is a little bit worse (less frequency selectivity) for this uncoded system. By adding a powerful FEC (Forward Error Correction) code both prototypes should probably lead to similar performances. As TFL1 is more appropriate (cf. Chapter 4) for packet transmission, we retain it for the next round of simulations.

Firstly, we evaluate the performances of the estimator in the UL multiuser transmission context in the presence of AWGN. We compute the cost function of the estimator of each user at a fixed SNR= 10 dB knowing that each of them is affected by a different delay.

We can see in Figures 3.20, 3.21, 3.22 and 3.23 the good performance of the estimators being used, showing its efficiency to detect and estimate the timing-offset of each user, in our example the delays are : 10 samples for user n.1, 20 samples for user n.2, 30 samples for user n.3, and 40 samples for user n.4.

Secondly, we rerun nearly similar experiments with a multipath channel [33] plus noise. For each user the performance is evaluated in terms of a Root Mean Square Error (RMSE)

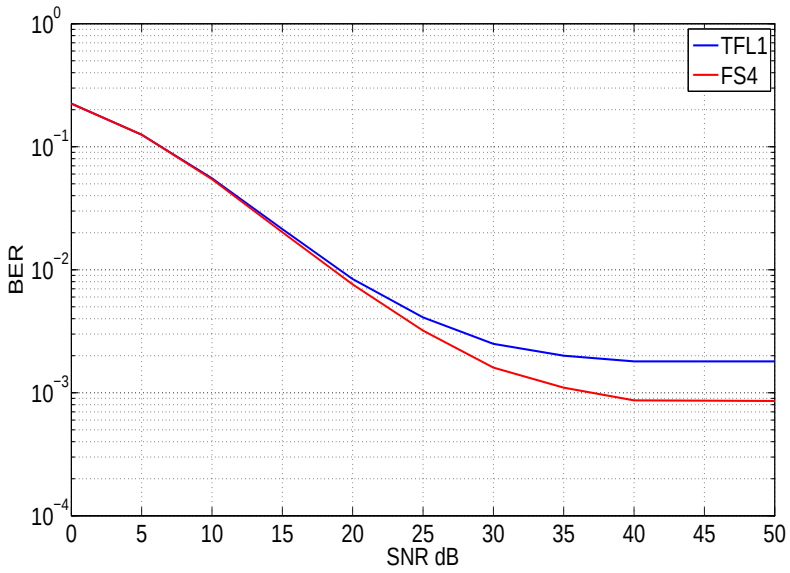

FIG. 3.19 – BER performances of TFL1 and FS4 prototype filters for single user scenario and with perfect synchronization in a multipath channel [33].

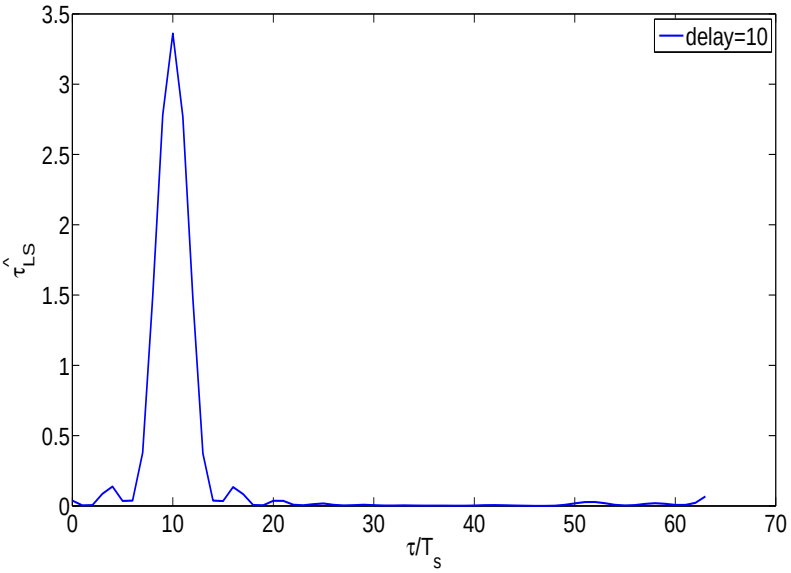

FIG. 3.20 – Cost function of the time estimator delay for the user affected with delay=10 samples when using the TFL1 prototype filter.

defined as follows

$$RMSE_u(\frac{\tau^u}{M}) = \frac{1}{M}\sqrt{\frac{1}{N_r}\sum_{i=1}^{N_r}(\tau^u - \hat{\tau_i^u})^2}, \tag{3.60}$$

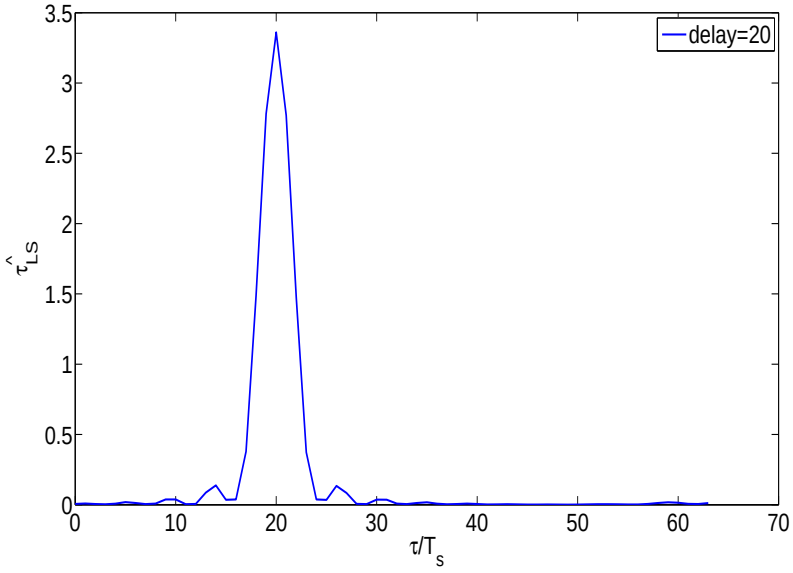

FIG. 3.21 – Cost function of the time estimator delay for the user affected with delay=20 samples when using the TFL1 prototype filter.

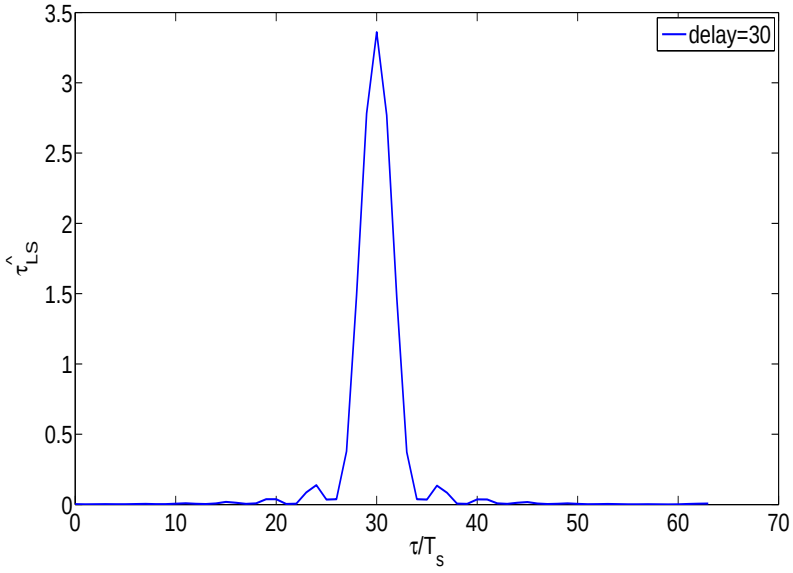

FIG. 3.22 – Cost function of the time estimator delay for the user affected with delay=30 samples when using the TFL1 prototype filter.

with N_r the number of realizations, $\hat{\tau}_i^u$ the estimation of τ_i fixed for the i^{th} realization.

In our simulations $N_r = 5000$ and $M = 64$.

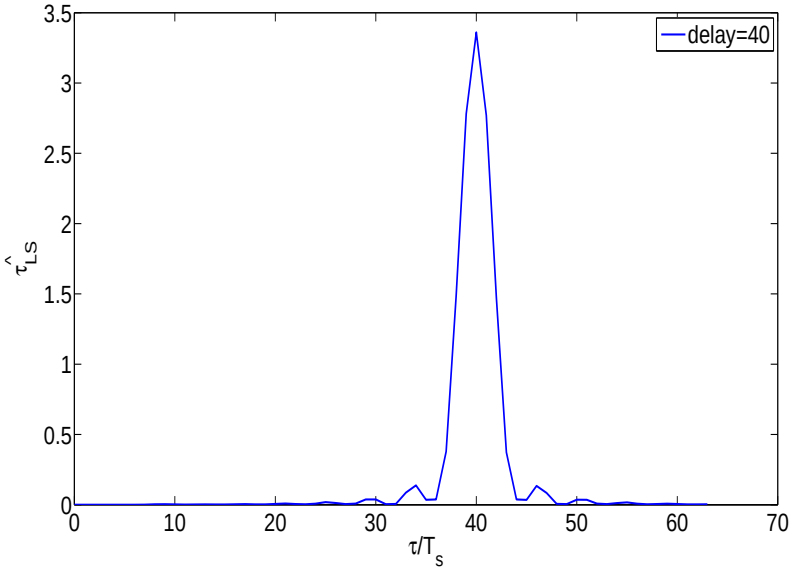

FIG. 3.23 – Cost function of the time estimator delay for the user affected with delay=40 samples when using the TFL1 prototype filter.

In a first round of evaluations we have examined each user individually with no transmission for the 3 other ones, considering 2 possible delay values : 5 or 10%.

We simulate one scenario, and we evaluate the performances from two points of view having the same simulation context. In the first point of view, we considered a user who occupies a such band (carriers from 1 :16, or 17 :32, or 33 :48 or 49 :64) and affected by different delays, in our example the delays are : 5% and 10%, we evaluated the performance of the estimator in each delay separately to see the effect of delays on the estimator, the performances are evaluated in terms of RMSE which is defined by (3.60). We repeated this scenario for all the 4 users.

We can see in Figures 3.24, 3.25, 3.26 and 3.27 the performances of the estimators used for user n.1, n.2, n.3 and n.4, respectively. We note that, by changing the delay value, the estimator performance is not affected, and this is true for all the 4 users. It shows that the delays have no impact on the estimator performance in the presence of the multipath channel, and this is true only for delays $\leq 10\%$. But we can remark that, at certain SNR, all the curves converge and have the same RMSE and become stable. For user n.1 and n.4 (the users at the edges of the band) the SNR value is 10 dB, and for user n.2 and n.3 (the

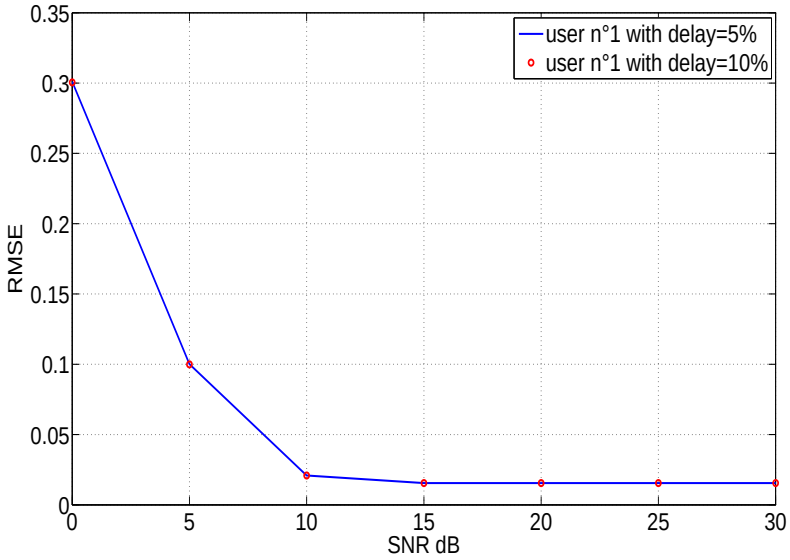

FIG. 3.24 – A comparison in performance between different delays for user ♯1 when using the TFL1 prototype filter.

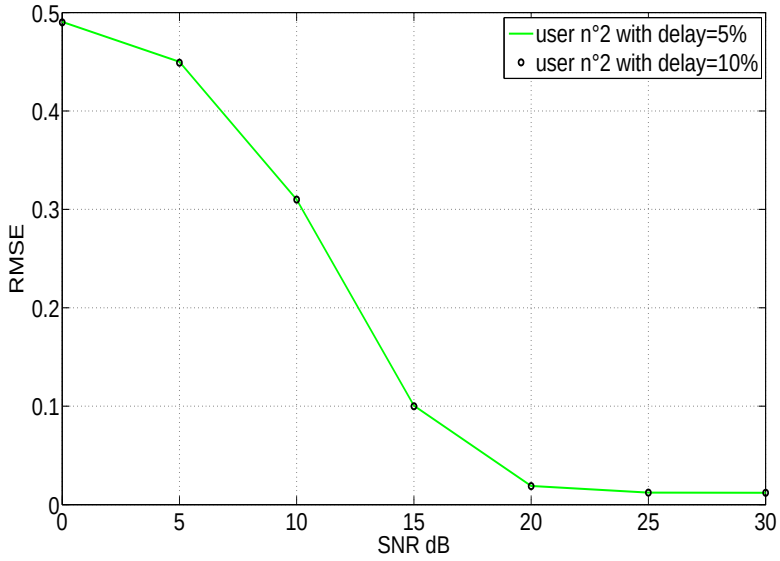

FIG. 3.25 – A comparison in performance between different delays for user ♯2 when using the TFL1 prototype filter.

users in the middle of the band) the SNR value is 20 dB.

In a second point of view, we consider all the 4 active users affected by the same delay,

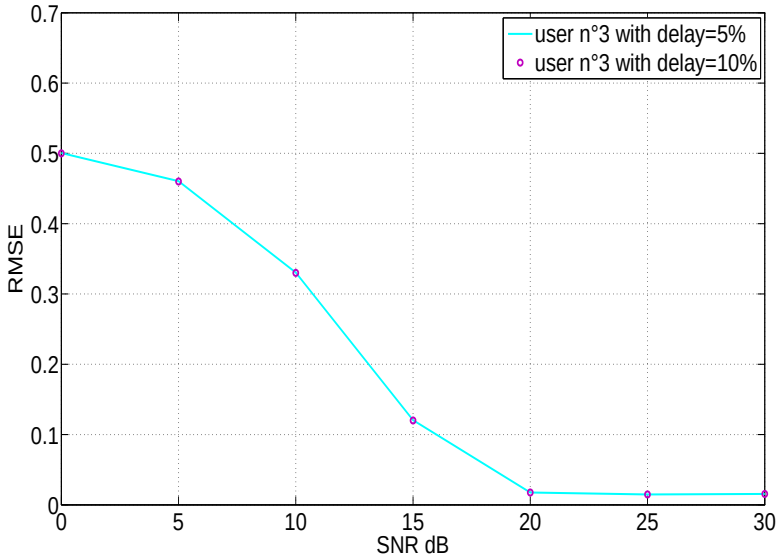

FIG. 3.26 – A comparison in performance between different delays for user ♯3 when using the TFL1 prototype filter.

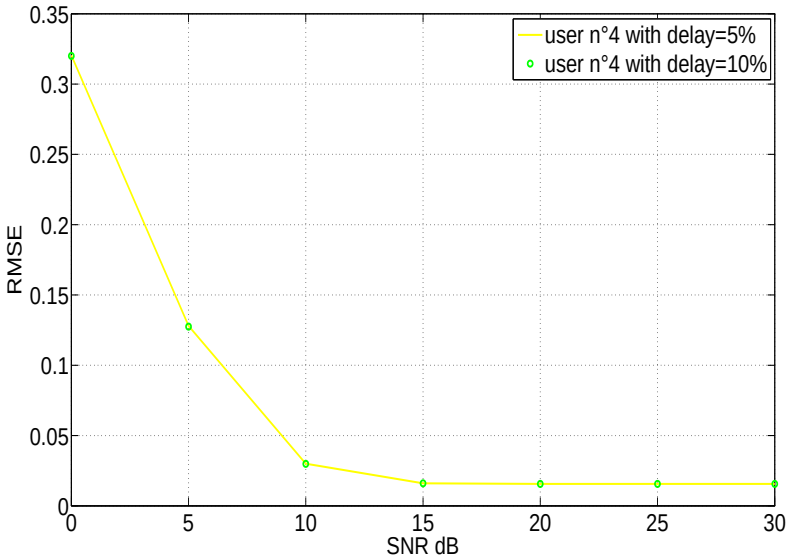

FIG. 3.27 – A comparison in performance between different delays for user ♯4 when using the TFL1 prototype filter.

we evaluate the performance of the estimator at each user separately to see the effect of the channel on the users positions in frequency. We repeated this scenario for the two delays 5% and 10%.

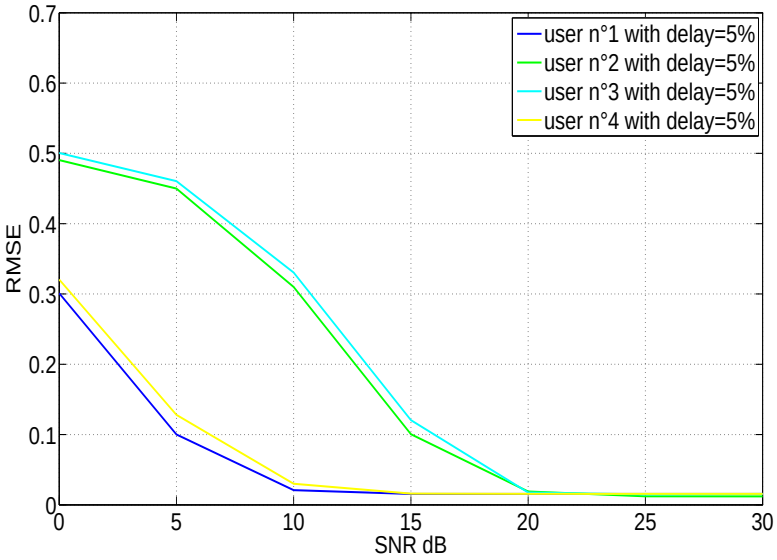

FIG. 3.28 – A comparison in performance between different users for delay=5% when using the TFL1 prototype filter.

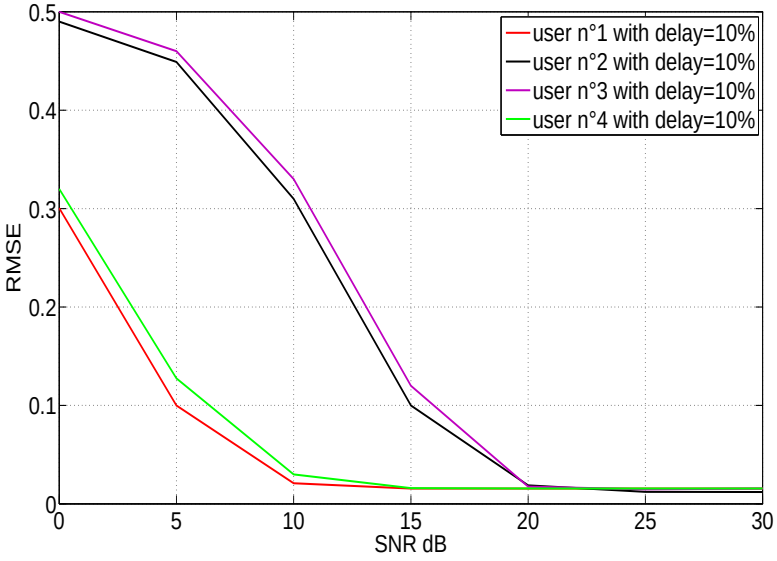

FIG. 3.29 – A comparison in performance between different users for delay=10% when using the TFL1 prototype filter.

We can see in Figures 3.28 and 3.29 the performances of the estimators used for delays 5% and 10%, respectively. It appears that, by changing the position of the user in the band (among the 4 users positions), the performance is not the same, this is also true for all the

4 delays. This proves that the estimator performance is sensitive to the users positions in the frequency band in the presence of the multipath channel[1]. And we can remark that, the users in the middle of the band have nearly the same performances, as we see for user n.2 and n.3, and for the users at the edges of the frequency band, they have also nearly the same performances, as we see for user n.1 and n.4, this is because the channel frequency response for users n.2 and n.3 is worse than for users n.1 and n.4, and this is the case for all the 4 delays. And at SNR=20 dB, all the curves converge and have the same RMSE and become stable.

Finally, we evaluate the correctness of the estimator by simulating the BER of a such user after correcting the delay estimated by the estimator, against SNR for each user and in different delays, we compare it with a perfect synchronization case. We simulate one scenario, and we evaluate the performances from two points of view having the same simulation context, the first point of view, we calculated the BER of each user (user n.1, user n.2, user n.3 and user n.4) in different delays, in our simulations the delays are 5%, 10% and 0% (which is considered as perfect synchronization).

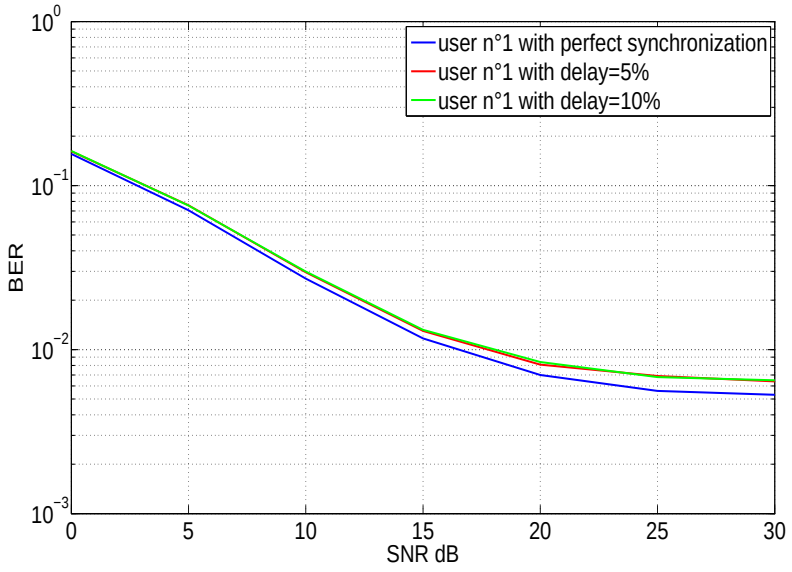

FIG. 3.30 – A comparison in performance for user n.1 between different delays using the TFL1 prototype filter and for a QPSK constellation.

[1]In this evaluation we only consider one single channel realization.

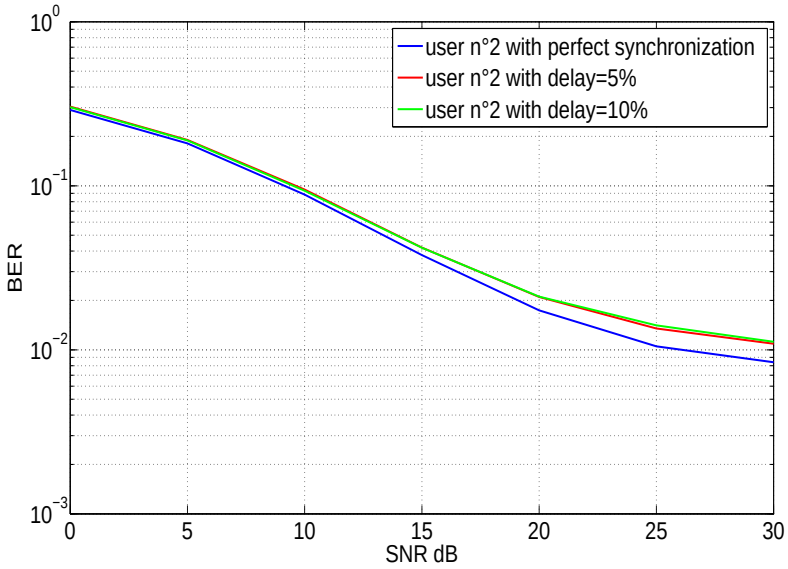

FIG. 3.31 – A comparison in performance for user n.2 between different delays using the TFL1 prototype filter and for a QPSK constellation.

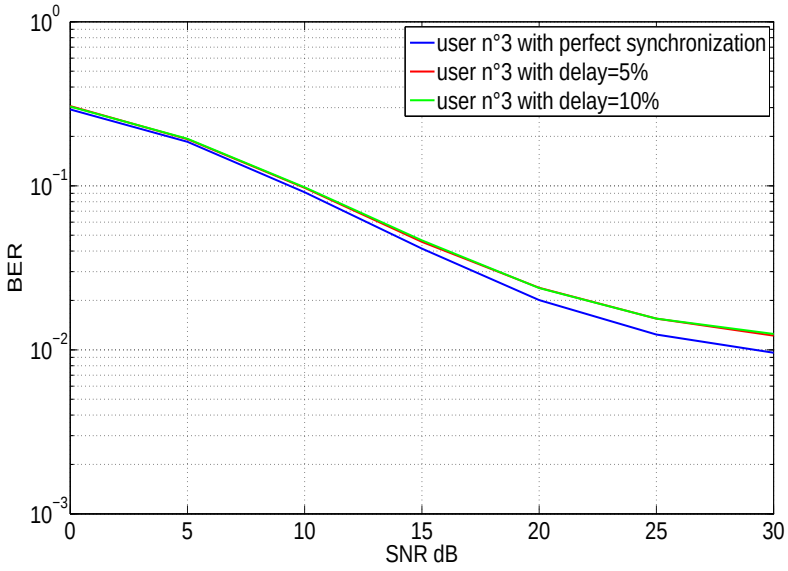

FIG. 3.32 – A comparison in performance for user n.3 between different delays using the TFL1 prototype filter and for a QPSK constellation.

From Figure 3.30, we can see that the performances of the users with the corrected delays in the two cases (5% and 10%) are the same, which proves the efficiency and stability of the estimator performance in different delays, but, with a difference of BER $\approx$ 0.001

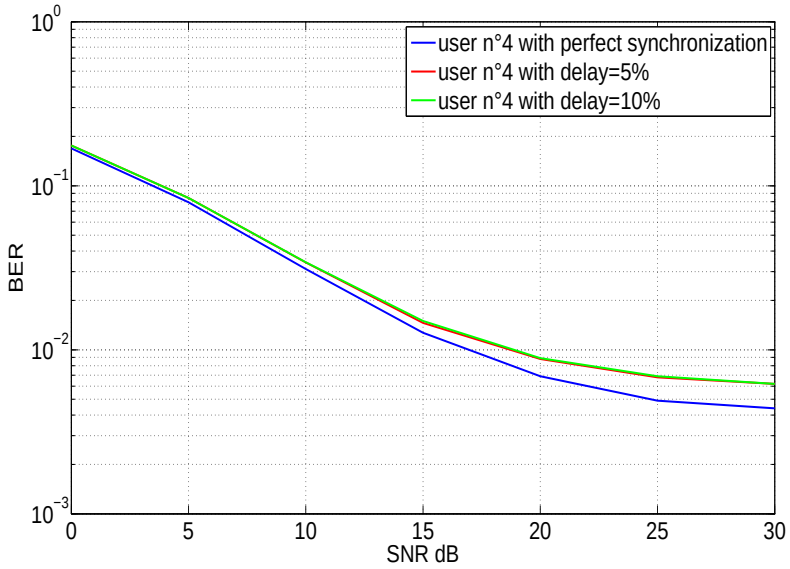

FIG. 3.33 – A comparison in performance for user n.4 between different delays using the TFL1 prototype filter and for a QPSK constellation.

compared to the perfect synchronization of 0% delay at SNR of 30 dB. And this true for the other four users, both user n.2 and user n.3 with a difference of BER more than 0.002 compared to the perfect synchronization case, and user n.4 with a BER difference ≈ 0.001, as we see in Figures 3.31, 3.32 and 3.33. We can remark here, that, in the case of the users n.1 and n.4 (at the borders of the frequency band) the difference of performances between the corrected delays and the perfect synchronization cases is lower than the cases of the users n.2 and n.3 (at the middle of the frequency band), this is because the channel frequency response for users n.2 and n.3 is worse than for users n.1 and n.4.

The second point of view, we fixed a delay to a certain value 5%, 10%, and 0% (which is considered as perfect synchronization) and then we calculated the BER of each user (user n.1, user n.2, user n.3 and user n.4).

From Figures 3.34,3.36 and 3.36, we can remark that the performances of the users are not the same, which prove that the users performances are affected by the position of the users in the frequency band with respect to the multipath channel, and it is not the estimator efficiency. And this is true for all the 4 delays.

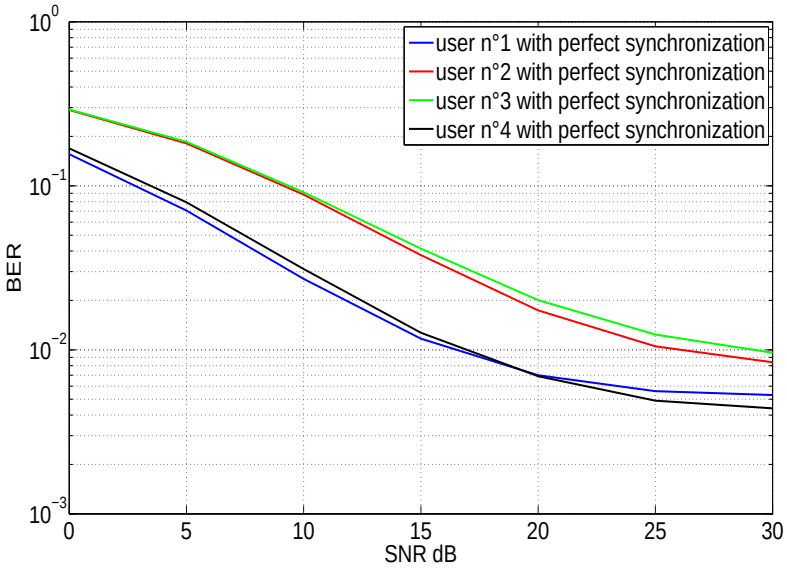

FIG. 3.34 – A comparison in performance between different users for delay=0 % using the TFL1 prototype filter and for a QPSK constellation.

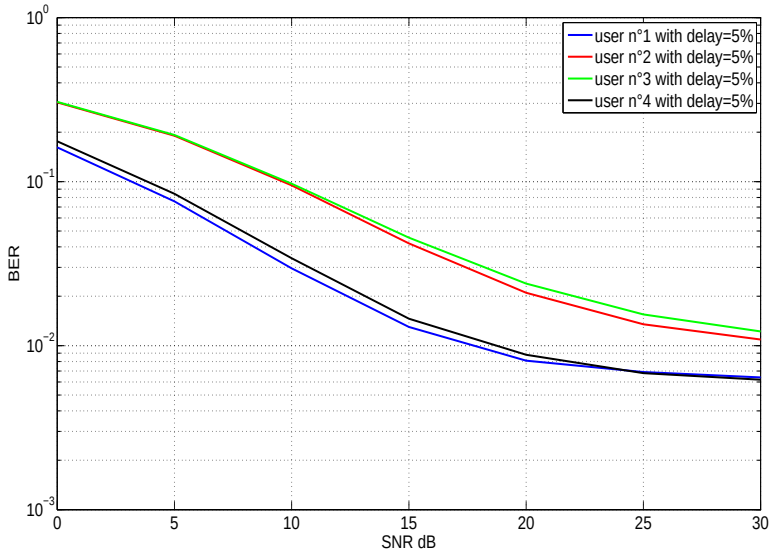

FIG. 3.35 – A comparison in performance between different users for delay=5 % using the TFL1 prototype filter and for a QPSK constellation.

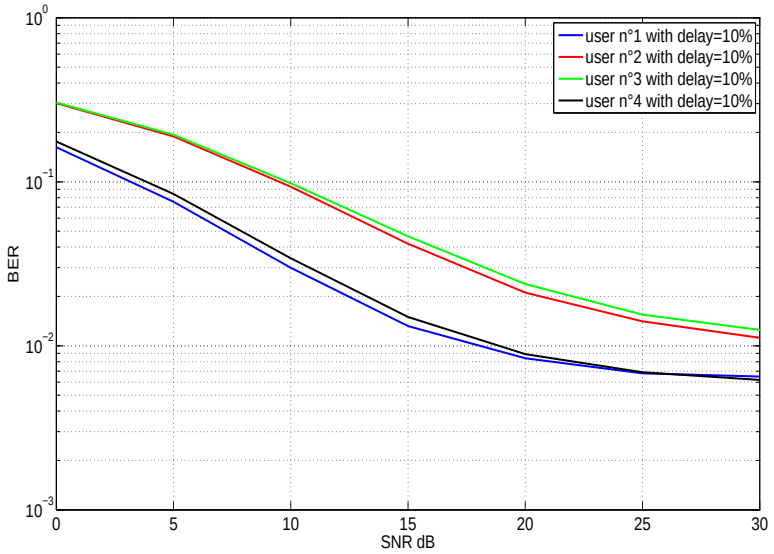

FIG. 3.36 – A comparison in performance between different users for delay=10 % using the TFL1 prototype filter and for a QPSK constellation.

3.8 Conclusion

In this chapter, our study has been concerned with the analysis of the desynchronized OFDM/OQAM system in the time and frequency domains. An analytical performance has been derived, we have derived very simple ISI and ICI expressions as well as an exact SIR expression. Then, we have illustrated the effect of the pulse shape on this interference term where we compare our exact SIR model with the simulated SIR numerically using different prototype filters. These results have been also compared with the ones obtained for OFDM showing the better performances against timing offset and frequency offset compared to OFDM without CP. In our study, through a detailed demonstration for the case of orthogonal prototype filters, we have highlighted a link between our analysis and the one in [32]. And finally, we have presented a synchronization method for UL multiuser systems which is robust in multipath channel.

Part IV

Part 4

Chapter 4

OFDM/OQAM for mobile cellular systems

Nowadays, cellular systems are in progress world wide, they have passed through tremendous developments, they are based on techniques that have not reached their limits yet. In this chapter, we refer to the latest mobile radio standard which is the 3GPP/LTE. Indeed, in 3GPP/LTE a MCM was candidate and finally retained with the Orthogonal Frequency Division Multiple Access (OFDMA) to provide a frequency access for the DL transmission. For the UL transmission the decision was in favor of the Single Carrier Frequency Division Multiple Access (SC-FDMA). However, at an earlier stage of the 3GPP debates, OFDM/OQAM was among the candidates [98] but at that time the experience around it was really limited compared to OFDM and even more with regard to OFDMA for multiple access. However, in the last few years OFDM/OQAM has become a more and more mature transmission technique and then the following question deserves to be examined : "which MCM scheme should be used in a future mobile radio multiuser standards".

Indeed, as from the transmission point of view OFDM/OQAM has some advantages w.r.t. OFDM e.g. no CP and better frequency localization. Thus, it seems natural to also explore its potential as a multiple frequency access. In this chapter, we propose to combine OFDM/OQAM with Frequency Division Multiple Access (FDMA) to get alternatives to the well-known OFDMA and to SC-FDMA techniques we name OQAMA and DFT-OQAMA for the UL transmission in the 3GPP/LTE context. On another hand, as the future mobile radio systems may be influenced by the present day technology we propose an experimental

3GPP-LTE-like setup, which in the future may evolve to cover the case of small cell wireless networks [75].

4.1 General Overview of the 3GPP Physical layer

The 3rd Generation Partnership Project Long Term Evolution (3GPP/LTE) [77], [76] is a standard for cellular communication of high-speed data. The standard is maintained as a project of the 3GPP, operating under a name trademarked by one of the associations within the partnership, the European Telecommunications Standards Institute (ETSI). The goal of LTE is to increase the capacity and speed of wireless data networks utilizing cutting-edge hardware and Digital Signal Processing (DSP) techniques that have recently been developed.

LTE is the brand name for emerging and developed technologies that comprise the existing 3G and 4G networks. The LTE specification provides downlink peak rates of at least 100 Mbps, uplink peak rates of at least 50 Mbps and Radio Access Networks (RAN) round-trip times of less than 10 ms. LTE supports scalable carrier bandwidths, from 1.25 MHz to 20 MHz and supports both frequency division duplexing (FDD) and time-division duplexing (TDD).

The main advantages with LTE are high throughput, low latency, an improved end-user experience and a simple architecture resulting in low operating costs.

Much of the standard addresses upgrading 3G UMTS (Universal Mobile Telecommunications System) to 4G mobile communications technology, which is essentially a mobile broadband system with enhanced multimedia services built on top.

The physical layer concepts are essential to improve the data rates in LTE systems. In this thesis as we focus on the modulation schemes, let us analyze more in details, the difference choices that have been done inside 3GPP.

4.2 Principles of some radio interfaces

In this section we briefly present the four different modulation and access schemes, OFDMA, SC-FDMA, OQAMA and DFT-OQAMA, considered in this chapter and reported in Fig. 4.1. In this schematic description the non-colored blocks correspond to common functionalities while the blue blocks are for OFDMA and also for SC-FDMA when adding the red blocks, finally the green blocks are for OQAMA and also DFT-OQAMA when adding the red blocks. Thus, we consider four different digital baseband processing that use common AFE (Analog Front End) functionalities (DAC, ADC, RF).

4.2.1 Multiple access with single or multiple carrier modulation

Let us first examine the two multiple options that have been retained for the 3GPP/LTE.

4.2.1.1 The OFDMA scheme

The OFDMA [29], [20], [43], [94] is a multiple access scheme based on the well known OFDM modulation technique [74].

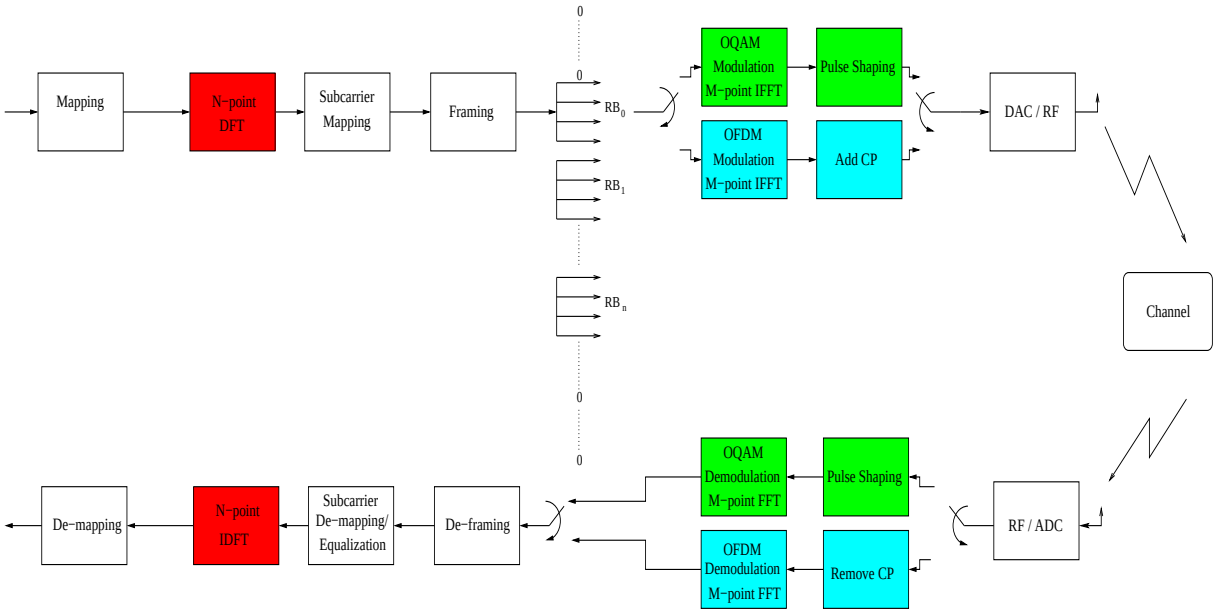

FIG. 4.1 – UL OFDMA, SC-FDMA, OQAMA and DFT-OQAMA system configurations.

At the transmitter input Fig. 4.1, a mapping block converts the binary input into a

multilevel sequence of baseband symbols leading to several possible modulation formats, including BPSK, QPSK, 16-QAM and 64-QAM. Then, the transmitter groups the modulation symbols, after being mapped to adjacent subcarriers and put in frames, into resource blocks (RBs), and being mapped on adjacent subcarriers. Before OFDM modulation and CP insertion, pilot symbols are inserted within the frame structure.

Then, based on the single user OFDM signal (2.12), we can write the transmitted baseband multiuser OFDMA signal as :

$$s[k] = \sum_{u=0}^{U-1} \sum_{n} \sum_{m=0}^{M-1} c_{m,n}^{(u)} \, \Pi_N[k - nN] e^{j\frac{2\pi}{M}mk}, \tag{4.1}$$

where $c_{m,n}^{u}$ is the complex-valued symbol transmitted on the m^{th} subcarrier at the n^{th} symbol period for user u.

The receiver transforms the received signal into the frequency domain via FFT, deframes the data subcarriers, and then performs frequency domain equalization based on one-tap Zero Forcing (ZF) [32]. Then, soft de-mapping and channel decoding (not represented in Fig. 4.1) are performed.

4.2.1.2 The SC-FDMA scheme

The SC-FDMA [20] is a multiple access scheme based on the Single-Carrier Frequency-Division Multiplexing (SC-FDM) modulation technique, sometimes also referred to as discrete Fourier transform (DFT)-Spread OFDM [19]. Its main principle is the same as for OFDM, thus the same benefits in terms of multipath mitigation and low complexity equalization are achievable [28]. The main difference is that a DFT is performed prior to the IFFT operation, which spreads the data symbols over all the subcarriers carrying information and produces a virtual single-carrier structure. As a consequence, SC-FDM presents a lower PAPR than OFDM [72]. This property makes SC-FDM attractive for the UL transmission, as the user equipment (UE) profits in terms of transmitted power efficiency. On one hand, DFT spreading allows the frequency selectivity to be exploited, since all symbols are present in several subcarriers. Therefore, if some subcarriers are in deep fade, the information can still be recovered from other subcarriers experiencing better channel condi-

tions. On the other hand, when DFT de-spreading is performed at the receiver, the noise is spread over all the subcarriers and generates a noise enhancement, which degrades the SC-FDM performance and requires the use of a more complex one-tap equalization based on a Minimum Mean Square Error (MMSE) receiver [28]. As shown recently in [108], more powerful equalization techniques could also be used.

As Fig. 4.1 shows, the SC-FDMA transceiver has much in common with OFDMA. The only, but important, difference is the presence of the N-point DFT in the SC-FDMA transmitter and the IDFT in the SC-FDMA receiver. According to Figure 4.1, the transmission processing of SC-FDMA can be mathematically illustrated as following. The mapped constellations $c_{k,n}$, which are mapped to time index n of the frame frequency-time grid, are firstly transformed by an N-point DFT process where the value of N depends on the number of RBs being allocated to user u, i.e.,

$$\widetilde{c}_{m,n} = \frac{1}{N} \sum_{n=0}^{N-1} c_{k,n} e^{\frac{-2\pi j}{N} kn}, \quad k = 0, ..., N-1, \tag{4.2}$$

Then, the $\widetilde{c}_{m,n}$ coefficients are grouped and mapped into frames, containing the complex-valued symbols transmitted on the m_{th} subcarrier and n_{th} symbol period, so that at the end the transmitted baseband multiuser SC-FDMA signal is expressed as follows :

$$s[k] = \sum_{u=0}^{U-1} \sum_{n} \sum_{m=0}^{M-1} \widetilde{c}_{m,n}^{(u)} \, \Pi_N[k - nN] e^{j\frac{2\pi}{M} mk}, \tag{4.3}$$

4.2.2 Proposed OQAMA-based multiaccess systems

4.2.2.1 The OQAMA scheme

Contrary to CP-OFDM, the OFDM/OQAM modulation does not require the use of any guard interval, which directly leads to a gain in spectral efficiency. Furthermore, the OFDM/OQAM prototype function is not restricted, as for CP-OFDM, to the rectangular window. To obtain a sufficient robustness to the channel variations, this prototype function must be well localized in both time and frequency domain. Having a good localization in time leads to the reduction of ISI while improving the localization in frequency permits

a limitation of the intercarrier interference (ICI) due for instance to Doppler effect. As depicted in Figure 4.1, compared to OFDMA, OQAMA implements a OFDM/OQAM (de) modulator with specific pulse shape. In OFDM/OQAM, each subcarrier carries a real-valued symbol $a_{m,n}$ which corresponds to either the real or the imaginary parts of a complex QAM data symbol $c_{m,n}$.

Based on the single user OFDM/OQAM signal 2.40, the transmitted baseband multiuser OQAMA signal is expressed as follows :

$$\begin{aligned} s[k] &= \sum_{u=0}^{U-1} \sum_{n} \sum_{m \in M_u} a_{m,n}^{(u)} g[k - nN] e^{j\frac{2\pi}{2N} m(k - D/2)} e^{j\phi_{m,n}} \\ &= \sum_{u=0}^{U-1} \sum_{n} \sum_{m \in M_u} a_{m,n}^{(u)} g_{m,n}[k]. \end{aligned} \tag{4.4}$$

where $a_{m,n}^{u}$ is the real-valued symbol transmitted on the m^{th} subcarrier at the n^{th} symbol period for user u.

4.2.2.2 The DFT-OQAMA scheme

The DFT-OQAMA is a multiple access scheme based on the OQAM modulation technique. Its main principle is the same as for OQAM. The main difference is that a DFT is performed prior to the OFDM/OQAM modulator, i.e. in Fig. 4.1 the red block is combined with the green blocks, which spreads the data symbols over all the subcarriers carrying information and produces a virtual single-carrier structure. As a consequence, DFT-OQAMA presents a lower PAPR [49] than OFDM/OQAM. This property makes DFT-OQAM attractive for the UL transmission, as it is also the case for the SC-FDMA scheme. Also, similarly to SC-FDMA, the equalizer can not be a single one-tap ZF but a MMSE one-tap is used instead.

The baseband multiuser DFT-OQAMA signal is expressed as follows :

$$s[k] = \sum_{u=0}^{U-1} \sum_{n} \sum_{m \in M_u} \widetilde{a}_{m,n}^{(u)} g_{m,n}[k]. \tag{4.5}$$

where $\widetilde{a}_{m,n}$ is either the real or imaginary part of the complex time domain signal $\widetilde{c}_{m,n}$ for user u.

Likely to OQAMA, a one-tap MMSE equalization is performed in the frequency domain.

4.3 Channel Estimation and Equalization for OQAM-based systems

4.3.1 General overview

At the transmission chain, it happens that a signal is disrupted by crossing the channel, because of high frequency fading, or by the presence of echoes, or by the presence of Doppler. The consequences of disturbances related to the channel can be measured in part by the BER, which indicates the amount of data bits badly transmitted on a channel considered. Thus, for difficult channels, with many different types of disturbances, it becomes necessary to compensate for the effects of the channel at the receiver. Two main classes of strategies can be envisioned. Blind techniques do not require the use of additional information for channel estimation/identification [17] or equalization [40]. Thus, they do not affect the useful bit rate. However, the required additional complexity may be too high from an implementation view point. Actually in most practical telecommunication systems, as for instance 3GPP/LTE, part of the frame is dedicated to the insertion of pilots for channel estimation (CE).

In the next section, we also focus on a preamble-based CE method that can provide an advantage to OFDM/OQAMw.r.t. CP-OFDM while keeping a low complexity implementation cost [61].

4.3.2 IAM-I Channel estimation method

To build an an appropriate CE method for OFDM/OQAM, a precise description of the transmission and channel model is required. Such a model is derived in [59].

Here, we prefer to reuse the mathematical model presented in Part 3 extending it to a multipath channel and considering the channel time-invariant for a frame duration. Then, based on (3.13) we get that, as already shown in [58], the OFDM/OQAM demodulated

signal at the time-frequency position (m_0 , n_0) writes as

$$y_{m_0,n_0} = \underbrace{\sum_{l=0}^{L_h-1} c_l A_g[-l,0] e^{-j\frac{\pi 2m_0 l}{M}}}_{\alpha_{m_0}} a_{m_0,n_0} + \sum_{(p,q)\neq(0,0)} a_{m_0+p,n_0+q} e^{j\frac{\pi}{2}(p+q+pq)} e^{j\pi p n_0} \underbrace{\sum_{l=0}^{L_h-1} c_l A_g[-qN-l,-p] e^{-j\frac{\pi(2m_0+p)l}{M}}}_{H_{m_0}^{(p,q)}}.$$

The first approximation is based on the assumption that the ambiguity function does not vary too much for $l = 0,\ldots,L_h$ - 1, i.e., $A_g[-l,0] \simeq A_g[0,0] = 1$ and $A_g[-qN-l,p] \simeq A_g[-qN,p]$. Thus, we have

$$\alpha_{m_0} \simeq \sum_{l=0}^{L_h-1} c_l e^{-j\frac{\pi 2m_0 l}{M}} = H_{m_0}^c, \tag{4.6}$$

where we denote $H_{m_0}^c$ as the channel coefficient at the m_0^{th} carrier.

The second approximation is based on the second assumption that the immediate neighboring carriers w.r.t. (m_0, n_0) position experience the same channel characteristics. And let us denote this immediate neighborhood zone as $\Omega_{\Delta m,\Delta n}$, in the vicinity of the time-frequency lattice location (m_0, n_0), defining it as $\Omega_{\Delta m,\Delta n} = \{(p,q), |p| \leq \Delta m, |q| \leq \Delta n | H_{m_0+p,n_0+q}^c \approx H_{m_0,n_0}^c\}$, means that $\Omega_{\Delta m,\Delta n}$ is an area around (m_0,n_0) where the channel is considered to be constant.

$$H_{m_0}^c \simeq \sum_{l=0}^{L_h-1} c_l e^{-j\frac{\pi(2m_0+p)l}{2M}} | p \in \Omega_{\Delta m,\Delta n}. \tag{4.7}$$

The third approximation is that when the prototype is designed to have a good localization feature in time-frequency domain, the energy is assumed to be very much concentrated inside the zone of $\Omega_{\Delta m,\Delta n}$, i.e. the interference outside of $\Omega_{\Delta m,\Delta n}$ (denoted by $\bar{\Omega}_{\Delta m,\Delta n}$) is negligible comparing to the interference inside of $\Omega_{\Delta m,\Delta n}$.

Thus, the above demodulation model can be approximated as

$$y_{m_0,n_0} \simeq H_{m_0}^c (a_{m_0,n_0} + j a_{m_0,n_0}^{(i)}), \tag{4.8}$$

where $a^{(i)}_{m_0,n_0}$ is the so-called "intrinsic" interference [53] with

$$ja^{(i)}_{m_0,n_0} = j \sum_{(p,q)\in\Omega^*_{\Delta m,\Delta n}} a_{m_0+p,n_0+q} \underbrace{e^{j\frac{\pi}{2}(p+q+pq)} e^{j\pi p n_0} A_g[-qN,-p]}_{g^{m_0+p,n_0+q}_{m_0,n_0}}. \tag{4.9}$$

with $\Omega^*_{\Delta m,\Delta n} = \Omega_{\Delta m,\Delta n} - (0,0)$.

Here, we retain the notation of $g^{m_0+p,n_0+q}_{m_0,n_0}$ given in [62] meaning the scalar product of two base functions $g_{m_0,n_0}[k]$ and $g_{m_0+p,n_0+q}[k]$. Based on (2.42), the orthogonal condition restricts the term $g^{m_0+p,n_0+q}_{m_0,n_0}$ for $(p,q) \neq (0,0)$ to be a pure real-valued. It is easy to verify that the intrinsic interference is, then, a pure imaginary-valued term.

Thus, as long as we get the information of a_{m_0,n_0} and intrinsic interference $a^{(i)}_{m_0,n_0}$, the channel coefficient at the m_0^{th} carrier straightforwardly yields

$$H^c_{m_0} = \frac{y_{m_0,n_0}}{a_{m_0,n_0} + ja^{(i)}_{m_0,n_0}}. \tag{4.10}$$

Assume that we know the denominator part of (4.10) by using a preamble sequence, say p_{m_0,n_0} (here p stands for preamble or pilot). In the presence of a noise term b_{m_0,n_0} , the stronger the pseudo-pilot is, the better the CE performs, i.e.,

$$\hat{H}^c_{m_0} = H^c_{m_0} + \frac{b_{m_0,n_0}}{\underbrace{p_{m_0,n_0} + jp^{(i)}_{m_0,n_0}}_{\tilde{p}_{m_0,n_0}}}. \tag{4.11}$$

where $\tilde{p}_{m_0,n_0}$ is the "pseudo-pilot" as named in [62].

The preamble sequence, p_{m_0,n_0}, is known by the receiver, but the knowledge of $p^{(i)}_{m_0,n_0}$ is not straightforward. Recently, Lélé et al. proposed an Interference Approximation Method (IAM) [62] to approximate this intrinsic interference with an intentionally generated preamble structure, such that the CE process (4.10) can be carried out. The basic IAM preamble structure is as follows. We insert a preamble sequence with a duration of $3\tau_0$, e.g., $p_{m,0}$, $p_{m,1}$, $p_{m,2}$, as shown in Fig. 4.2. Meaning that the interference term (4.9) is approximated by

$$a^i_{m_0,n_0} \simeq \sum_{(p,q)\in\Omega^*_{\Delta m,1}} a_{m_0,n_0} g^{m_0+p,n_0+q}_{m_0,n_0} \tag{4.12}$$

Each pilot $p_{m,n}$ for $m \in$ [0,2M-1] and $n \in [0, 2]$ can be randomly generated by taking either the real or imaginary part of a QPSK symbol, i.e., $p_{m,n} = \pm\sigma_a^2$. This leads to the proposed preamble structure called IAM2 in [62]. Then, on the receiver side, the CE is performed on the middle preamble column only, i.e.,

$$\hat{H}^c_{m_0} = H^c_{m_0} + \frac{b_{m_0,1}}{\tilde{p}_{m_0,1}}. \tag{4.13}$$

FIG. 4.2 – IAM preamble sequence.

Thus, as proved in [59], the pseudo-pilot power of this preamble structure is such that

$$\mathbf{E}[|\tilde{p}_{m_0,1}|^2] < 2\sigma_a^2 = \sigma_c^2, \tag{4.14}$$

where $\mathbf{E}[x]$ is the expectation of a random variable x, $\sigma_c^2 = 2\sigma_a^2$ is the pilot power of the OFDM system. That means the CE performance using this IAM preamble structure is worse than that of OFDM system taking into account the fact that the CP-OFDM preamble lasts $2\tau_0$, i.e. its total power is only $2M\sigma_a^2$ while for OFDM/OQAM the duration is $3\tau_0$ and the total power is $3M\sigma_a^2$ [62].

To augment the pseudo-pilot power while avoiding increasing the PAPR, in [61], the authors have proposed a particular preamble structure called IAM-I (I stands for imaginary). The IAM-I structure is such that $p_{m,0} = p_{m,2} = 0$ and for the pilots at time index $n = 1$, $p_{m,1}$, we randomly transmit a consecutive triplet such that $p_{m,1} = \pm 1$, it means that if $p_{m,1} = 1$ hence, $p_{m+1,1} = j1$ and $p_{m+2,1} = -1$, and if $p_{m,1} = -1$ hence, $p_{m+1,1} = -j1$

and $p_{m+2,1} = 1$, (see Fig. 4.3).

FIG. 4.3 – IAM-I preamble sequence.

This way, we can concentrate the preamble power on the middle column, and the pseudo-pilot power can be increased [61], as we see in (4.15), which results in a performance gain comparing with OFDM system.

$$\mathbf{E}[|\tilde{p}_{m_0,1}|^2] = 2\sigma_a^2(1 + \frac{8\beta_0^2 + 8\beta_0}{3}) > \sigma_c^2, \tag{4.15}$$

with $\beta_0 < 1$ [61].

4.3.3 The CFIR-SCE equalization

As the OFDM/OQAM signal does not contain any CP, the interference cannot be avoided. Then, either the channel is not too much harmful and/or small constellation orders are used and then a low SNR at the reception is sufficient making the interference component negligible. Or, at the contrary, we need to operate at higher SNR and then the interference cannot be neglected anymore. In the first case a one-tap ZF equalization can be appropriate while in the second one more powerful equalizers are required. As recalled in [56], various equalization methods are now available for OFDM/OQAM.

Per-carrier equalizer for OFDM/OQAM system has already been discussed long time ago by Hirosaki in his papers [45], [46]. However, this method is way of complex and it is not easy to implement [45] due to its re-alignment of QAM in-phase and quadrature compo-

nents. Later, Qin and Bellanger proposed an adaptive per-carrier equalization using double sampling and critical sampling, respectively [83]. Furthermore, Nedic *et al.*, in [73], also introduced an adaptive per-carrier equalizer for OFDM/OQAM. But its complexity still remains too high. Besides, some references (e.g. [97], [47], [106]) propose a Minimum-Mean-Square FIR per-carrier equalizer for OFDM/OQAM and the high complexity problem still exists due to the inversion of a non-diagonal channel matrix.

More recently another particularly efficient method named Equalization with Interference Cancellation (EIC) has been proposed in [57], but again depending upon the application it may appear to be too much costly. In this chapter we prefer to focus on the equalization method proposed at first in [5], [48] and adapted to OFDM/OQAM in [56].

In [5], the authors have proposed a low complexity equalizer named Adaptive Sine modulated/Cosine modulated filter bank Equalizer for Transmultiplexer (ASCET). ASCET was initially dedicated to equalization for EMFB-based transmultiplexer and renamed Complex FIR Subcarrier Equalizer (CFIR-SCE) [48]. In [56], H. Lin has proposed an adaptation of the CFIR-SCE to the OFDM/OQAM modulation.

Following the notations in [48], the 3-tap ASCET (or CFIR-SCE) equalizer at frequency index m writes $E_m^{CFIR-SCE}(z) = c_{0m}z + c_{1m} + c_{2m}z^{-1}$, where the equalizer coefficients c_{im} are calculated by evaluating the transfer function, which is set to the target response, at chosen frequency points, wherein half of the chosen frequencies are nothing else than the central carrier frequencies and the rest half can be chosen from the transition band, e.g. the simplest ones could be the middle frequency points between two consecutive subcarrier frequencies. Therefore, the ICI on the chosen frequencies can be perfectly compensated by this method. Knowing the principle, modified coefficients c_{im} for OFDM/OQAM has been found and presented in [56].

The modification is that OFDM/OQAM corresponds to an even-stacked filter bank system, i.e. the 0^{th} subcarrier centers at frequency 0. Therefore, the three frequencies are chosen to be, as shown in Fig. 4.4, $\omega = \{-\frac{\pi}{M}, 0, \frac{\pi}{M}\}$ for the 0^{th} subcarrier, and $\omega = \{\frac{\pi}{M}, \frac{2\pi}{M}, \frac{3\pi}{M}\}$ for the 1-st subcarrier, which corresponds to the normalized frequencies $\omega_{nom} = \{-\frac{\pi}{2}, 0, \frac{\pi}{2}\}$ for even subcarrier and $\omega_{nom} = \{\frac{\pi}{2}, \frac{2\pi}{2}, \frac{3\pi}{2}\}$ for odd subcarrier. Straightforwardly, the target

responses should also be shifted to be even-stacked as $\eta_{im} = \frac{1}{H(e^{(2m+i)\frac{\pi}{M}})}$ with $(i = -1, 0, 1)$. This basic principle to apply CFIR-SCE to OFDM/OQAM is illustrated in Fig. 4.4.

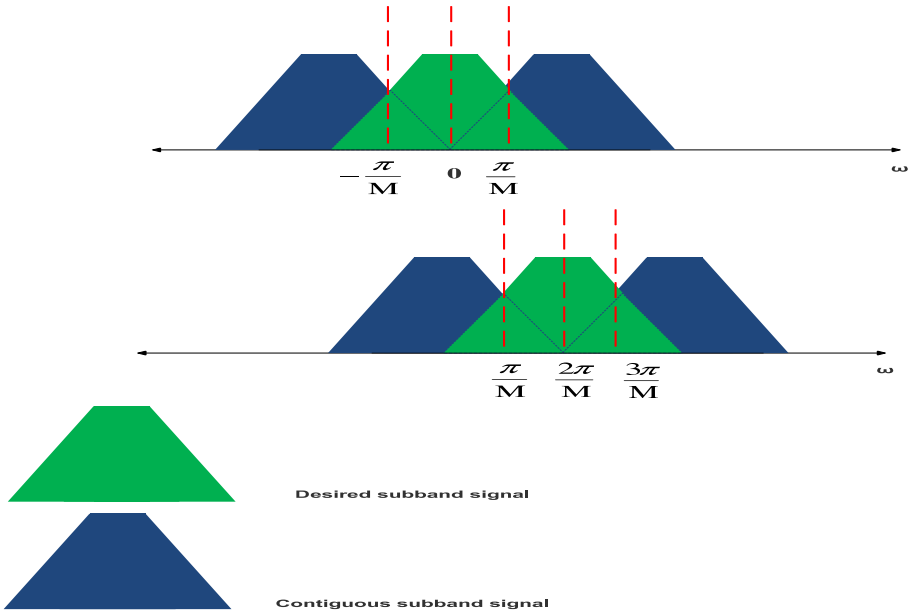

FIG. 4.4 – Subbands signal for OFDM/OQAM.

In addition to this alternance rule the adaptation to OFDM/OQAM has also to take into account the phase term $\phi_{m,n}$ used to generate the transmitted signal (2.36). Setting it to $\phi_{m,n} = \frac{\pi}{2}(m+n)$, as in (2.36), leads to CFIR-SCE equalizer coefficients given in the ZF case by [56, (7.3)]

$$c_{0m} = -\frac{1}{2}\left(\frac{\eta_{-1m}^{ZF} - \eta_{1m}^{ZF}}{2} - j\left(\eta_{0m}^{ZF} - \frac{\eta_{-1m}^{ZF} + \eta_{1m}^{ZF}}{2}\right)\right)$$

$$c_{1m} = \frac{\eta_{-1m}^{ZF} + \eta_{1m}^{ZF}}{2}$$

$$c_{2m} = -\frac{1}{2}\left(\frac{\eta_{-1m}^{ZF} - \eta_{1m}^{ZF}}{2} + j\left(\eta_{0m}^{ZF} - \frac{\eta_{-1m}^{ZF} + \eta_{1m}^{ZF}}{2}\right)\right) \tag{4.16}$$

with $\eta_{im}^{ZF} = \frac{1}{H(e^{(2m+i)\frac{\pi}{M}})}$ the channel distortion compensation at a chosen frequency.

If instead, we choose to compute the CFIR-SCE coefficients using the MMSE criterion, there expression is given by

$$c_{0m} = -\frac{1}{2}\left(\frac{\eta_{-1m}^{MMSE} - \eta_{1m}^{MMSE}}{2} - j\left(\eta_{0m}^{MMSE} - \frac{\eta_{-1m}^{MMSE} + \eta_{1m}^{MMSE}}{2}\right)\right)$$

$$c_{1m} = \frac{\eta_{-1m}^{MMSE} + \eta_{1m}^{MMSE}}{2}$$

$$c_{2m} = -\frac{1}{2}\left(\frac{\eta_{-1m}^{MMSE} - \eta_{1m}^{MMSE}}{2} + j\left(\eta_{0m}^{MMSE} - \frac{\eta_{-1m}^{MMSE} + \eta_{1m}^{MMSE}}{2}\right)\right) \tag{4.17}$$

with $\eta_{im}^{MMSE} = \frac{H^*(e^{(2m+i)\frac{\pi}{M}})}{|H(e^{(2m+i)\frac{\pi}{M}})|^2+\sigma_n^2}$

Using a 3-tap ZF or MMSE equalizer may naturally be beneficial compared to any 1-tap configuration, with which useful symbols can be totally lost in a multipath transmission when a deep fade occurs at a given frequency.

In Figure 4.5, we can see that for DFT-OQAMA CFIR-SCE equalizer outperforms MMSE by 0.22 dB at a fixe BER of 10^{-4}.

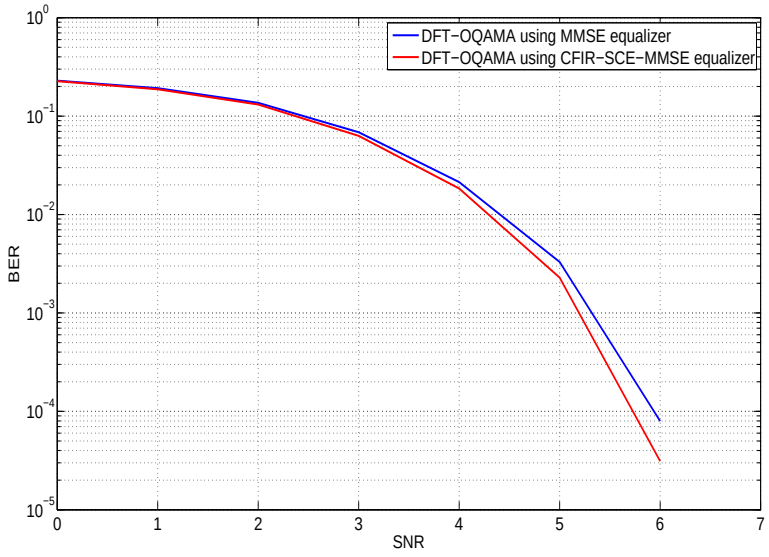

FIG. 4.5 – DFT-OQAMA using 3-tap CFIR-SCE and one-tap MMSE equalizers.

Another illustration of the 3-tap CFIR-SCE efficiency is provided in section 4.5 in the case of DFT-OQAMA scheme.

4.3.4 Application to the LTE context

In the next section, we will see how the IAM-I preamble can be interpreted in a 3GPP/LTE frame signal based on OQAMA and DFT-OQAMA. In another hand, we have presented a synchronization method in chapter 3 (subsection 3.7), which also uses preamble-based pilots but are different from the IAM-I ones. Based on the results we have got in chapter 3, here we consider that the synchronization is not problematic for OQAMA-based systems in the 3GPP/LTE context and, thus we assume perfect time and frequency synchronization. That is not a practical problem, w.r.t. 3GPP. Indeed, as it can be seen in [2], contrary to CE which requires a preamble in each slot, for synchronization the preambles are less frequent, i.e. a single one for each 20 slots, and are not constrained to be built the same way.

4.4 Environment and system parameters

4.4.1 The OFDM/OQAM within Multiple Access

We have simulated the OFDM/OQAM modulation within multiple access (OQAMA) to see the impact of possible intrinsic interference provided by adjacent users. In this chapter, as in [61], we used a prototype filter optimized for the time frequency localization (TFL). As its length is only one time the symbol period we name it TFL1. Thus, compared to CP-OFDM, there is no extra latency and the extra complexity is reduced.

As shown in [56], for a static multipath channel, the Signal to Interference plus Noise Ratio (SINR) can be explicitly derived for any subcarrier. As this interference follows a Gaussian distribution, for a Gray coded $K-QAM$ coded modulation, assuming a one-tap ZF equalization and real part extraction, the BER for the m_{th} subcarrier can be expressed as [37] :

$$P_b(m_0) \cong \frac{\sqrt{K}-1}{\sqrt{K}\log_2(\sqrt{K})}\text{erfc}(\sqrt{\frac{3}{2}.\frac{SINR_{m_0}}{K-1}}) + \frac{\sqrt{K}-1}{\sqrt{K}\log_2(\sqrt{K})}\text{erfc}(3\sqrt{\frac{3}{2}.\frac{SINR_{m_0}}{K-1}}). \quad (4.18)$$

Applying this result to multicarrier OQAMA allows us to derive the BER for a user

transmitting in consecutive subcarriers going from index l_u to u_u by :

$$P_b = \frac{1}{u_u - l_u + 1} \sum_{m_0=l_u}^{u_u} P_b(m_0). \tag{4.19}$$

Let us assume that this user, say the second one ($user_2$), is surrounded by two other users transmitting in the frequencies between l_u and u_u, with $u = 1$ and 3 as shown in Fig. 4.6, each user employing 12 subcarriers with different modulation orders, denoted $m_{o_{upper}}$ and $m_{o_{lower}}$, respectively. In each simulation, we change the modulation format of the neighboring users (keeping the allocated power the same for all), for the purpose of analyzing the effect of changing the modulation on the target user (the user in the middle). This scenario has been tested for the following experimental set up : sampling frequency F_s =30.72 MHz, a 2-tap static channel, power profile (in dB)= 0 and -3, delay profile (μs)=0 and 5, with perfect CE, no channel coding and $M = 2048$.

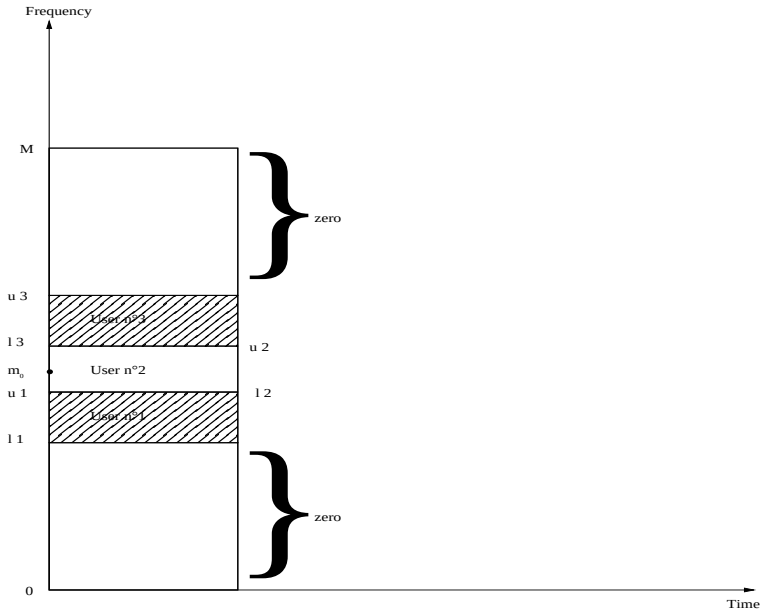

FIG. 4.6 – Users positions.

Firstly, we allocate the second user a QPSK modulation, and then we compute its BER. We have simulated 5 cases, and in each case we have changed the modulation of the first and third users as reported in Table 4.1 :

We then repeated the simulations, by changing the modulation of the second user to the 16-QAM one then to 64-QAM, each time with the 5 different cases reported in Table

TAB. 4.1 – Ambiguity function for TFL1 delay=0

case \ user	user n.1	user n.2	user n.3
case n.1	$QPSK$	$QPSK$	$QPSK$
case n.2	$16-QAM$	$QPSK$	$QPSK$
case n.3	$16-QAM$	$QPSK$	$16-QAM$
case n.4	$64-QAM$	$QPSK$	$16-QAM$
case n.5	$64-QAM$	$QPSK$	$64-QAM$

4.1.

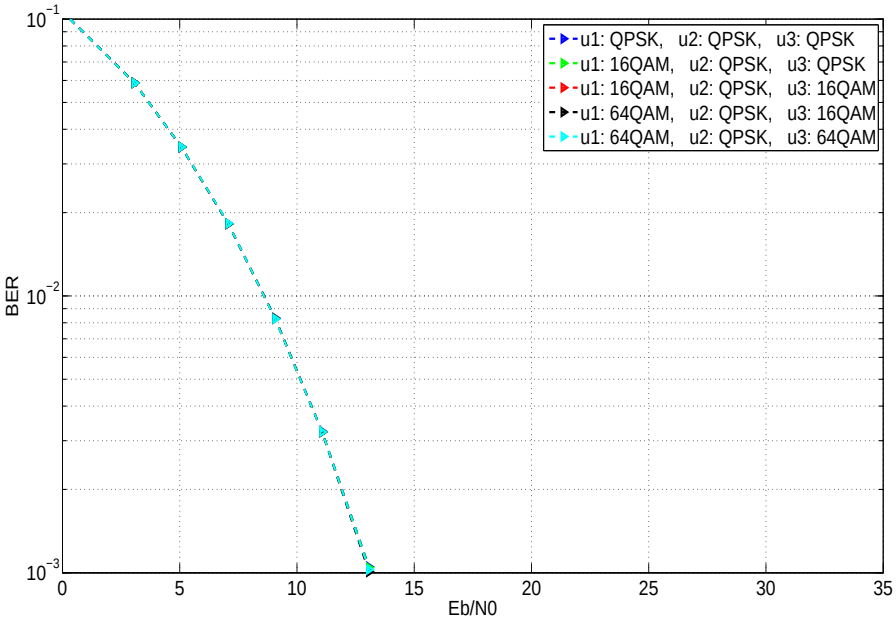

FIG. 4.7 – Second user fixed by QPSK modulation.

As shown in Figures 4.7, 4.8 and 4.9, the performance for the targeted user only depends upon the channel and prototype function being used and not of the modulation orders $m_{o_{upper}}$ and $m_{o_{lower}}$ used by its neighbors, as it is clear from (4.18)-(4.19) where the modulation orders coefficients of the neighbors do not appear in the BER equation. In these figures it can be also noted that when the SNR (here expressed as the energy per bit over the monolateral noise density, i.e. $\frac{E_b}{N_0}$) increases the risk of an error floor also increases. Indeed, an error floor occurs for the 16-QAM 64-QAM constellations, see Fig. 4.8 and 4.9, respectively.

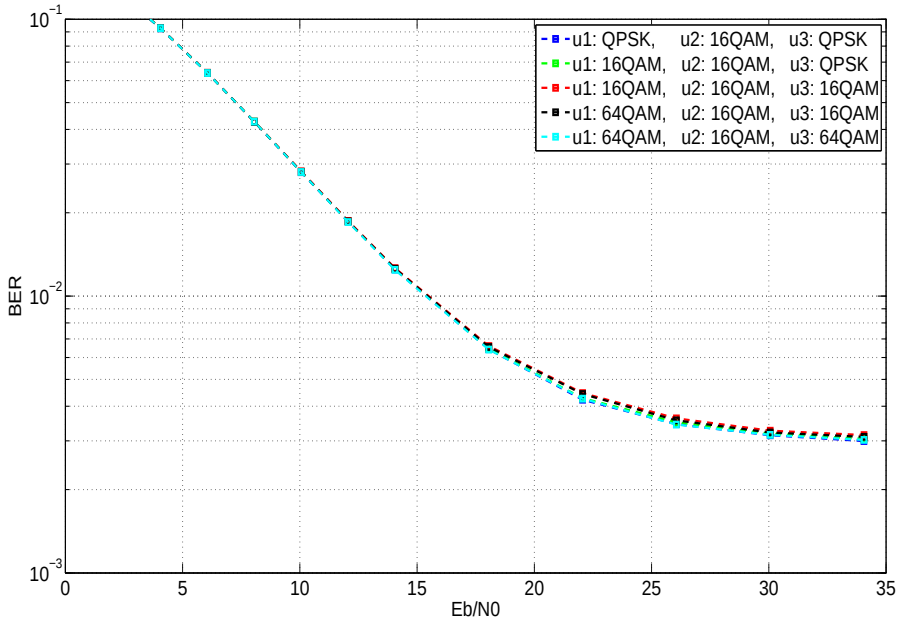

FIG. 4.8 – Second user fixed by 16-QAM modulation.

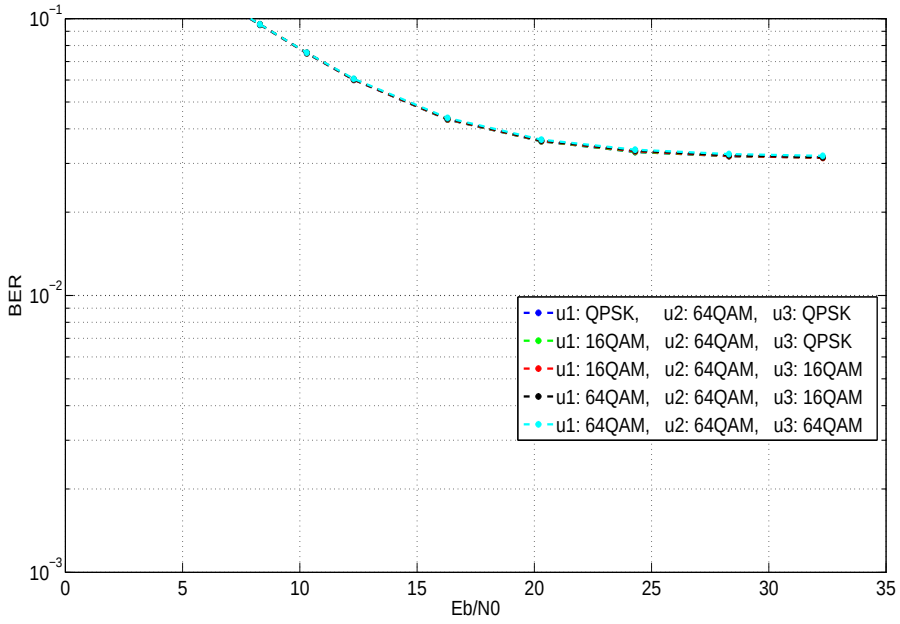

FIG. 4.9 – Second user fixed by 64-QAM modulation.

4.4.2 The OFDM/OQAM within the 3GPP/LTE framework

The OFDMA and SC-FDMA being introduced within the DL and UL 3GPP/LTE standards [2], respectively, come the questions : "*How can we integrate the OFDM/OQAM in the LTE ? How to adapt the OFDM/OQAM within the LTE ?*"

For this purpose, since OFDM/OQAM does not require CP, we need to change some parameters to map the LTE system frame structure.

To introduce the OFDM/OQAM within the 3GPP/LTE framework, we start from the OFDMA 3GPP/LTE system parameters in short CP configuration, shown in Fig 4.10, considered for the 20 MHz FDD mode [2]. In this transmission mode, one frame is composed of 10 subframes (or Resource Block (RB)) at most, as we see in Fig. 4.11. The subframe is composed of 2 slots, and a slot duration equals to 0.5 ms, 7 complex OFDM symbols are transmitted corresponding to 12 subcarriers, i.e. forming a slot as shown in Fig. 4.12. The minimum transmission time duration being of 1 ms, at least, 14 OFDM symbols are transmitted per frame, i.e. 168 complex data symbols, pilots included, are transmitted.

Several RBs can be allocated per each user. As for symbol transmission each user performs one 2048-point FFT, subcarriers not modulated are off. We have also considered that users transmit on adjacent subcarriers. When considering the 20 MHz bandwidth, up to 1200 subcarriers can be modulated leading to a maximum of 100 RBs. Then, up to 100 users can transmit simultaneously in the UL.

By adding the 7 CP durations, we obtain $\frac{T_0}{2}$ as excess in time duration, allowing us to put 15 OFDM/OQAM symbols within one slot as shown in Fig. 4.12, and formulated as : $K \times (\frac{M}{F_s}) = 0.5$ ms, where K is the number of OQAM symbols. For $F_s = 30.72$ MHz and M= 2048, we have $K = \frac{15}{2}$.

So, one OFDM/OQAM slot, as shown in Fig. 4.12, is composed of 15 real-valued symbols, the 15^{th} symbol is an additional information with regard to the CP-OFDM slot, this yields higher rates for OFDM/OQAM than for CP-OFDM. For our application, we propose to use this additional OFDM/OQAM symbol for pilot CE symbol definition. The 3GPP/LTE transmission parameters for the OFDM/OQAM in FDD mode (it requires two distinct channels for transmitting DL subframe and UL subframe at the same time slot,

Bandwidth		1.25 Mhz	2.5 Mhz	5 Mhz	10 Mhz	15 Mhz	20 Mhz
Slot duration		0.5 ms					
Intercarrier spacing		15 Khz					
Sampling frequency		1.92 Mhz	3.84 Mhz	7.68 Mhz	15.36 Mhz	23.04 Mhz	30.72 Mhz
FFT size		128	256	512	1024	1536	2048
Number of occupied subcarriers		76	151	301	601	901	1201
Number of OFDM symbols per subframe (Short/Long CP)		7/6					
CP duration (µs/samples)	Short	(4.69/9)*6 (5.21/10)*1	(4.69/18)*6 (5.21/20)*1	(4.69/36)*6 (5.21/40)*1	(4.69/72)*6 (5.21/80)*1	(4.69/108)*6 (5.21/120)*1	(4.69/144)*6 (5.21/160)*1
	Long	(16.67/32)	(16.67/64)	(16.67/128)	(16.67/256)	(16.67/384)	(16.67/512)

FIG. 4.10 – 3GPP/LTE transmission parameters for the CP-OFDM in FDD mode.

compared to TDD which is another duplexing scheme that requires only one channel for transmitting downlink and uplink subframes at two distinct time slots, TDD therefore has higher spectral efficiency than FDD) are presented in Fig. 4.13.

In 3GPP/LTE, in each subframe, the 4^{th} and 11^{th} SC-FDMA symbols are used for the UL reference signals transmission, especially for CE. The reference signals based on Zadoff Chu sequences [2] are transmitted as preamble on the RBs used for the user payload.

The principle of preamble-based CE together with a simple one-tap ZF equalization also works for OFDM/OQAM, if the prototype filter g is well localized in time and frequency.

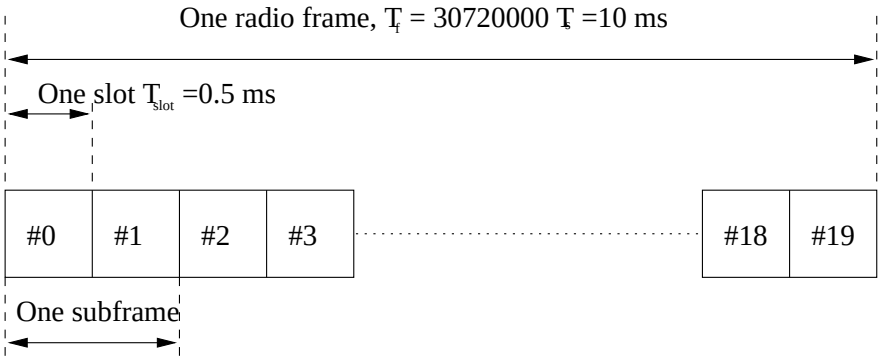

FIG. 4.11 – The structure of CP-OFDM and OQAM generic frame.

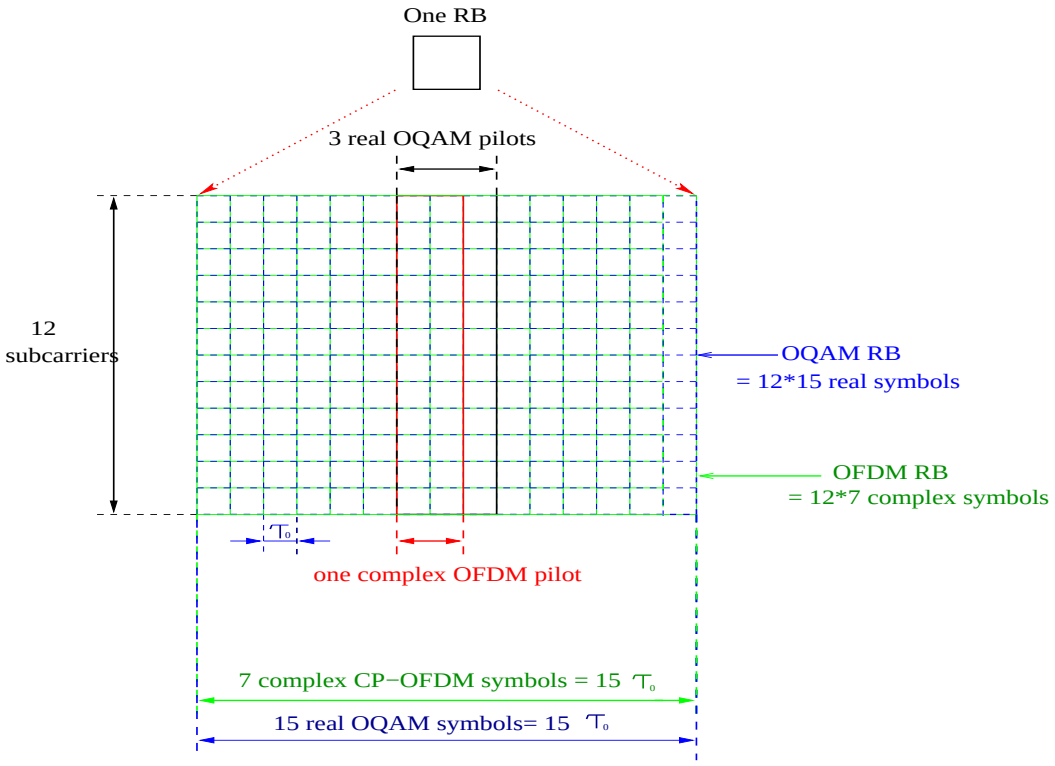

FIG. 4.12 – The structure of CP-OFDM and OQAM slot.

Indeed, in spite of the fact that OFDM/OQAM only exhibits a real orthogonality property, efficient CE techniques are available [60], [61] to yield complex-valued estimates of the channel. In this chapter, we consider the IAM-I technique for real CE, that was proposed and evaluated in [61], and whose principle is recalled in subsection 4.3.2.

As depicted in Fig. 4.12, we insert the IAM-I preamble pilots in the OFDM/OQAM

Bandwidth	1.25 Mhz	2.5 Mhz	5 Mhz	10 Mhz	15 Mhz	20 Mhz
Slot duration	0.5 ms					
Intercarrier spacing	15 Khz					
Sampling frequency	1.92 Mhz	3.84 Mhz	7.68 Mhz	15.36 Mhz	23.04 Mhz	30.72 Mhz
FFT size	128	256	512	1024	1536	2048
Number of occupied subcarriers	76	151	301	601	901	1201
Number of OQAM symbols per slot	15					
CP duration	0					

FIG. 4.13 – 3GPP/LTE transmission parameters for the OQAM in FDD mode.

slots. Their time occupancy is equal to $3\tau_0$. The OFDM/OQAM slots being composed of 15 real-valued symbols ($= 15\tau_0$), the pilots are inserted in positions ♯7, ♯8 and ♯9, the rest are the data symbols from ♯1 to ♯6 and from ♯10 to ♯15. Also, as OFDM/OQAM produces a spreading in time proportional to the prototype filter length, for TFL1 a guard interval of duration τ_0 is inserted between two pairs of frames. This results in a spectral efficiency that is only $\frac{30}{31}$ the one of OFDMA and SC-FDMA, i.e. in terms of Signal to Noise Ratio (SNR) the loss is equal to 0.14 dB.

4.5 Performances evaluations

Our simulations have been carried out with a TU6 (Typical Urban with 6 taps) channel model [3] and modulation parameters that are borrowed from the 3GPP/LTE standard. The channel profile and the main parameters of the system used are : sampling frequency F_s = 30.72 MHz, number of paths=6, power profile (in dB)= -3, 0, -2, -6, -8 and -10, delay profile (μs)= 0, 0.2, 0.5, 1.6, 2.3 and 5, binary turbo coding scheme of one half rate [1], QPSK modulation and $M = 2048$, the transmission scheme used in our simulations is

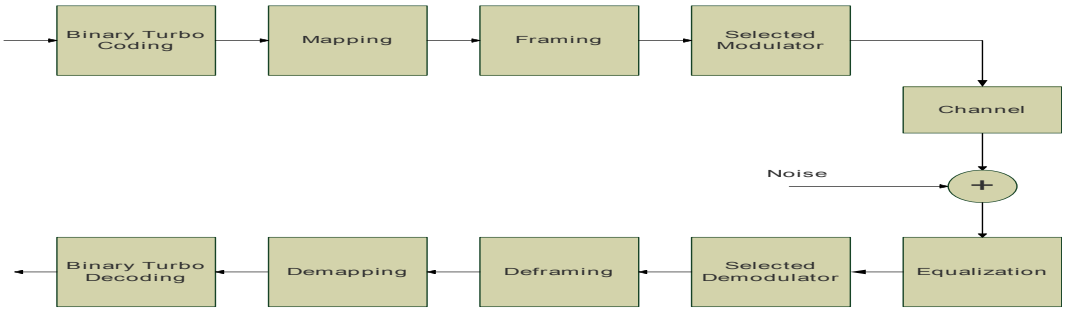

FIG. 4.14 – UL OFDMA, SC-FDMA, OQAMA and DFT-OQAMA system configurations for our simulations.

illustrated in Fig. 4.14. The TFL1 prototype filter is used, it is preferred among the other prototype filters, it maps the frames, it has no extra latency, and has a reduced complexity thanks to its one time symbol period length. Furthermore, as explained more in details in section 4.6, due to its short length an appropriate packet transmission technique can be used to prevent the potential loss due do its spreading in time.

In our work, we have compared OQAMA [37] and DFT-OQAMA [39] to the well-known OFDMA and SC-FDMA techniques, in the UL 3GPP/LTE context, within perfect time and frequency synchronizations and regardless to PAPR.

Here, the first solution to adapt the OFDM/OQAM to the 3GPP/LTE frame, in order to avoid the interference between successive frames, simply consists in the addition of a τ_0 duration guard interval between two pairs of frames.

Using this solution, we simulated users occupying either 20 RBs or 1 RB at velocities of 3 Km/h and 120 Km/h, with real CE. For OFDMA and SC-FDMA, we used the Zadoff Chu complex pilots sequence [2], and for OQAMA and DFT-OQAMA we used the IAM-I method for real CE.

Figures 4.15 and 4.16 show the performances, BER versus the SNR at the transmitter (SNR_{TX}), obtained for 20 RBs at 3 Km/h and 120 Km/h respectively, with real CE. In Figure 4.15 we can see that OQAMA outperforms OFDMA by 0.7 dB at BER= 10^{-3}, and DFT-OQAMA is better than SC-FDMA by 0.7 dB thanks to the boost of the pilots symbols produced by the IAM-I CE method. In Figure 4.16, OQAMA outperforms OFDMA by 0.9 dB and DFT-OQAMA has a gain of 0.6 dB compared to SC-FDMA thanks the use of

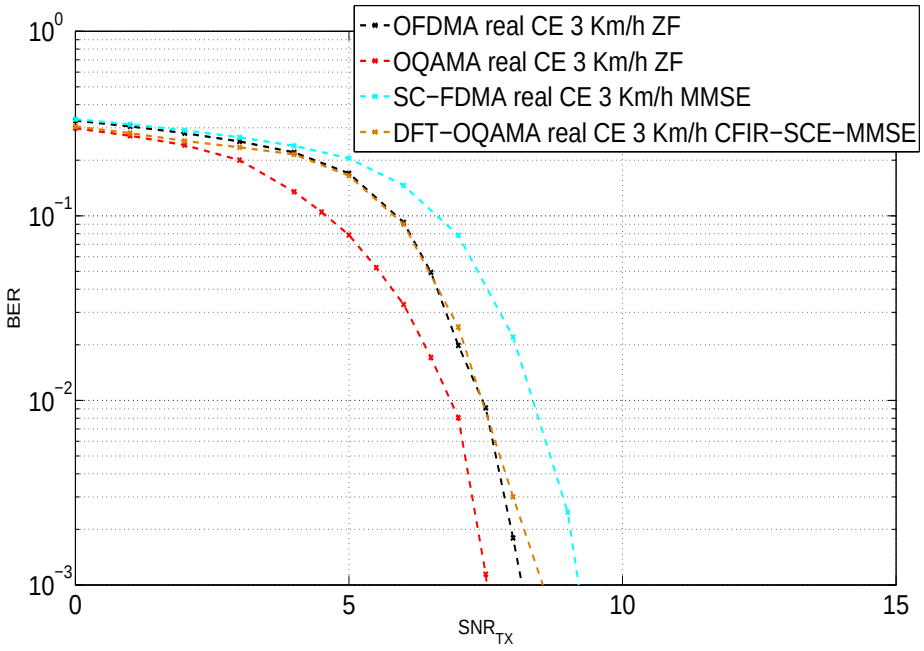

FIG. 4.15 – One user occupying 20 RBs simulated at 3 Km/h, BER versus SNR_{TX}.

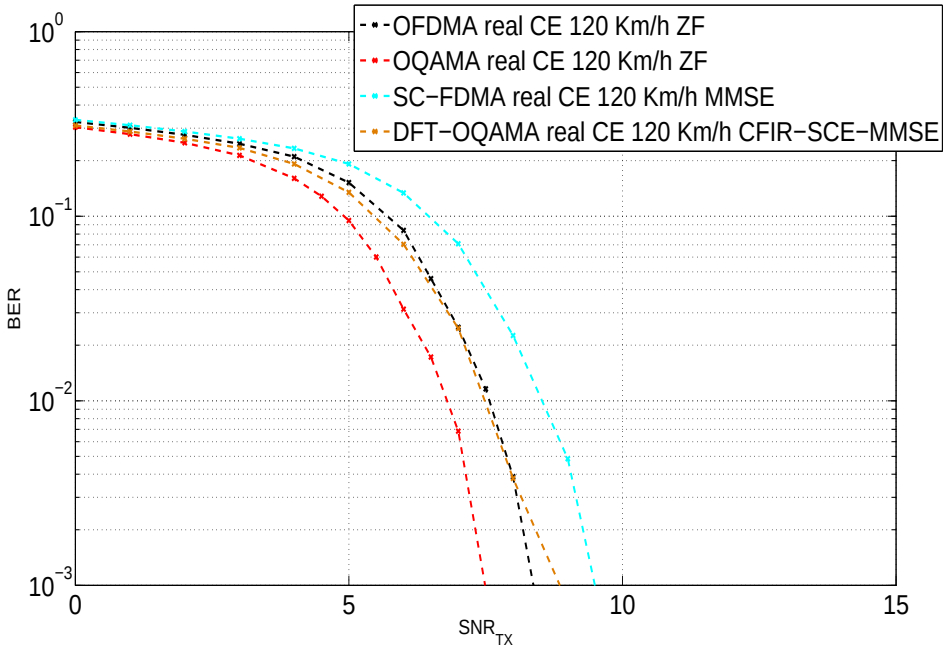

FIG. 4.16 – One user occupying 20 RBs simulated at 120 Km/h, BER versus SNR_{TX}.

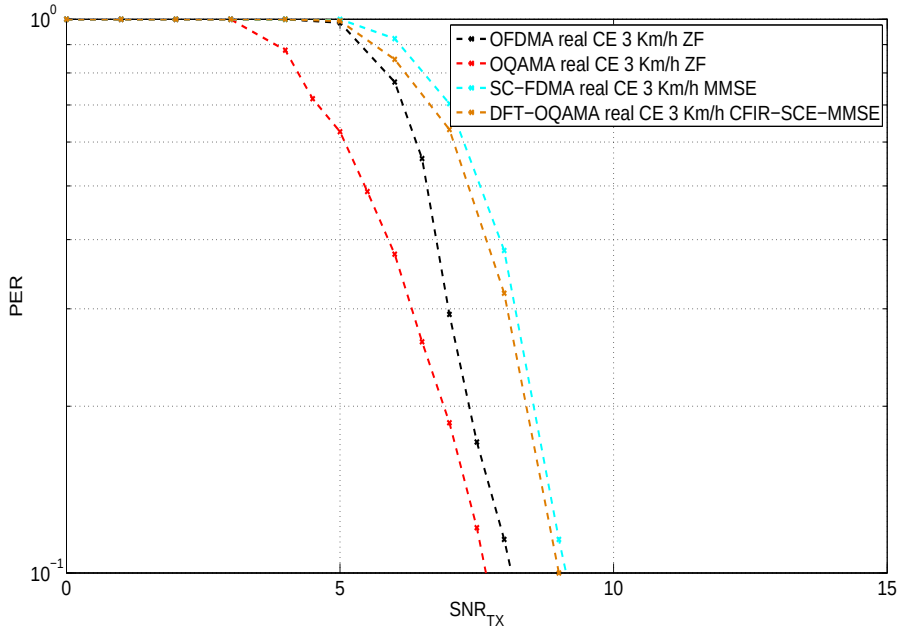

FIG. 4.17 – One user occupying 20 RBs simulated at 3 Km/h, PER versus SNR_{TX}.

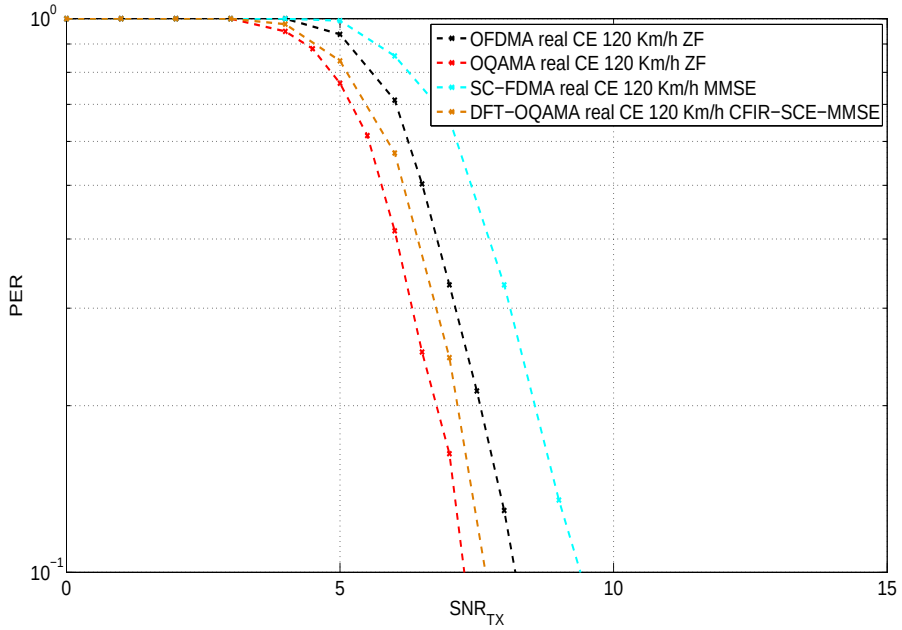

FIG. 4.18 – One user occupying 20 RBs simulated at 120 Km/h, PER versus SNR_{TX}.

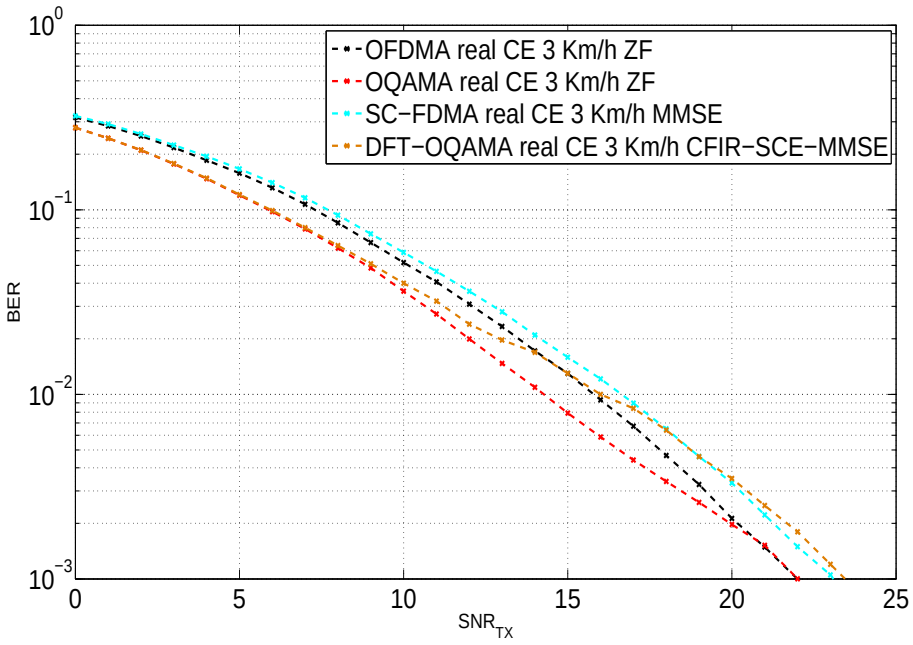

FIG. 4.19 – 1 user occupying 1 RB simulated at 3 Km/h, BER versus SNR_{TX}.

IAM-I CE method.

Figures 4.17 and 4.18 show the performances, PER (Packet Error Rate) versus the SNR at the transmitter (SNR_{TX}), obtained for 20 RBs at 3 Km/h and 120 Km/h respectively, with real CE. In Figure 4.17, we can see that OQAMA outperforms OFDMA by 0.6 dB at PER= 10^{-1}, and DFT-OQAMA has the same performance as SC-FDMA but with a slight gain thanks to the use of IAM-I CE method. In Figure 4.18, OQAMA outperforms OFDMA by 0.9 dB and DFT-OQAMA has a gain of 1.7 dB compared to SC-FDMA thanks to the use of IAM-I CE method.

Figures 4.19 and 4.20 show the BER performances obtained for 1 RB, located at the beginning of the frame, at 3 Km/h and 120 Km/h with real CE. Figure 4.19 shows that at SNR higher than 20 dB OQAMA and OFDMA have the same performances and DFT-OQAMA has better performances than SC-FDMA for SNR lower than 17 dB but when increasing the SNR SC-FDMA becomes slightly better than DFT-OQAMA. In Figure 4.20, OQAMA performs better than OFDMA with a 1.25 dB gain at BER=10^{-3}, for SC-FDMA and DFT-OQAMA, we remark an error floor that occurs in the high SNR region (higher

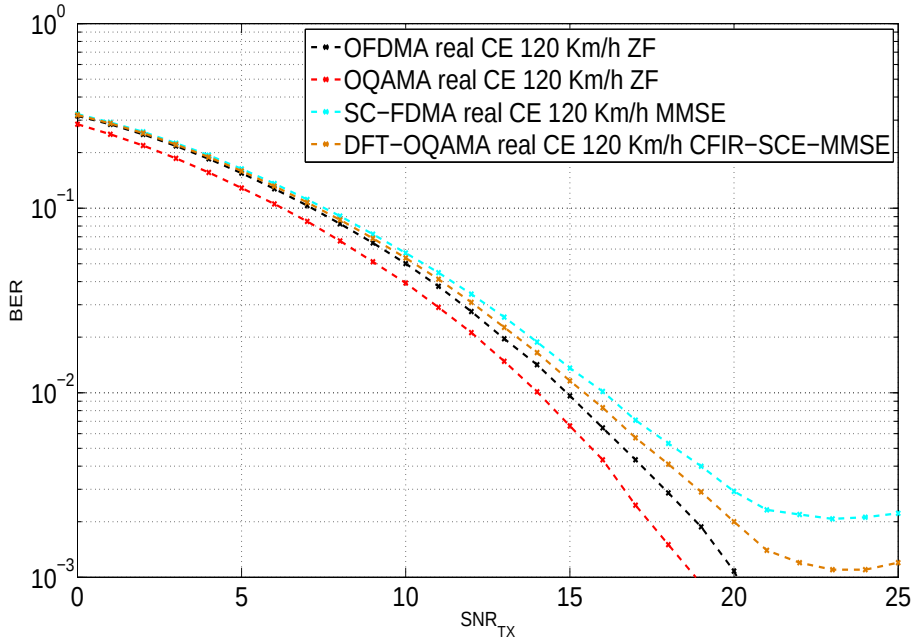

FIG. 4.20 – 1 user occupying 1 RB simulated at 120 Km/h, BER versus SNR_{TX}.

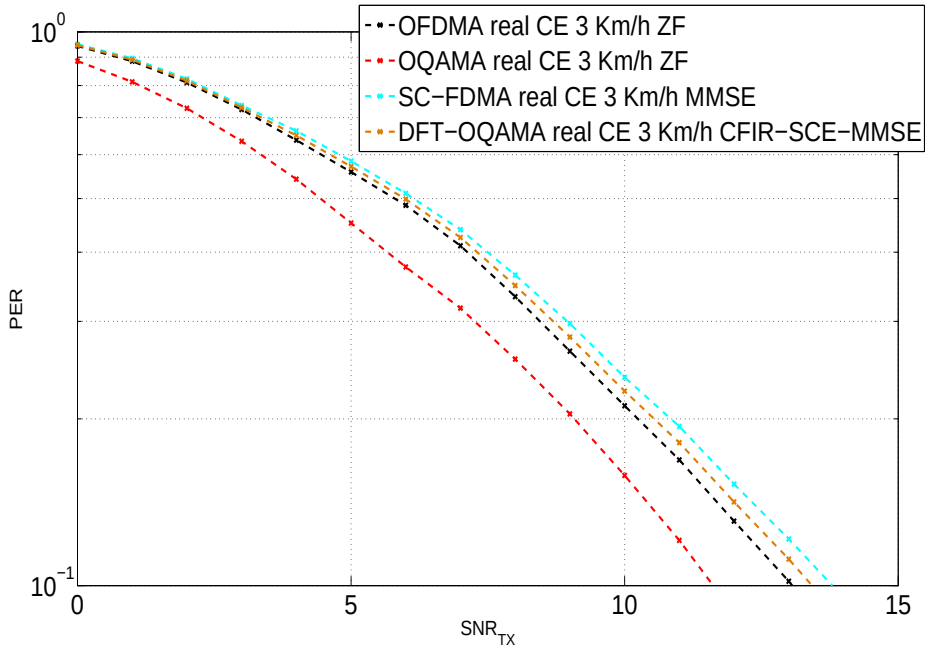

FIG. 4.21 – 1 user occupying 1 RB simulated at 3 Km/h, PER versus SNR_{TX}.

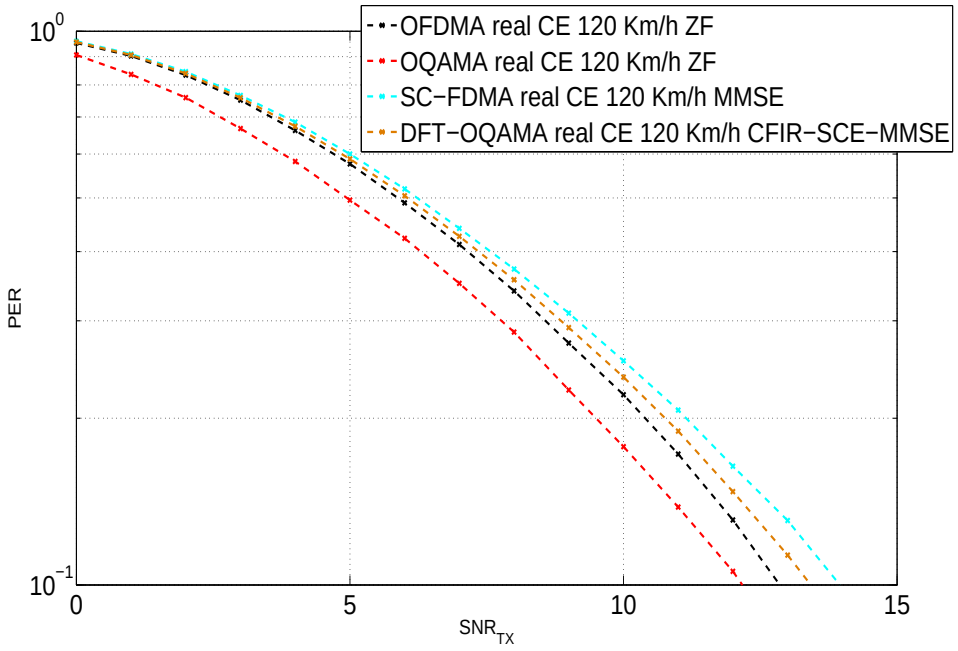

FIG. 4.22 – 1 user occupying 1 RB simulated at 120 Km/h, PER versus SNR_{TX}.

than 20 dB), due to the interference that becomes more significant than noise. So higher is the velocity, bigger is the difference. We note that when transmitting with 1 RB, we have less frequency diversity on the channel, yielding to higher SNR than with 20 RBs.

Figures 4.21 and 4.22 show the PER performances obtained for 1 RB, located at the beginning of the frame, at 3 Km/h and 120 Km/h with real CE. In Figure 4.21 OQAMA has better performance than OFDMA with a gain of 1.4 dB at PER=10^{-1} and DFT-OQAMA is better than SC-FDMA, thanks to the use of IAM-I CE method. In Figure 4.22, OQAMA outperforms OFDMA by 0.7 dB and DFT-OQAMA is better by 0.5 dB thanks to the use of IAM-I CE method.

As a result we see that for the same targeted BER and PER for real CE, in most of the cases, OQAMA has a SNR gain greater than 0.14 dB over OFDMA and SC-FDMA and therefore outperforms these both transmission schemes, and that is also true for DFT-OQAMA compared to SC-FDMA. Indeed, thanks to the boost of the pilots symbols produced by the IAM-I method, which yields to a pseudo virtual pilot power that is superior to the CP-OFDM instantaneous pilots power, we have a better CE. So the use of preamble pilot

symbols in the 3GPP/LTE framework is in favor of OQAMA and DFT-OQAMA compared to OFDMA and SC-FDMA showing that OQAMA and DFT-OQAMA are robust for the UL 3GPP/LTE transmission.

4.6 Impact of the packet transmission for OQAMA

Up to now we have considered that at the modulation side the only distortions were due to channel distortion and to the additive noise. This is true for the OFDMA and SC-FDMA schemes that do not introduce any overlap between the successive symbols. On the contrary, with OFDM/OQAM the successive multicarrier symbols overlap and consequently the duration to transmit a sequence of data symbols has to be extended in proportion of the length of the prototype filter. A previous work has analyzed this problem, in [10], where the authors try to reduce the border effects by the introduction of a weighting function. If the method is usable for long prototype filters, it nevertheless does not permit, as [24], a perfect recovery of the truncated symbols even in ideal situations. This problem is illustrated in Fig. 4.23 borrowed from [22], which shows that to transmit a packet of K data symbols a duration of $KT + \frac{T}{2}$, with K an integer, is required, if the prototype filter is only of length $L = T = M$.

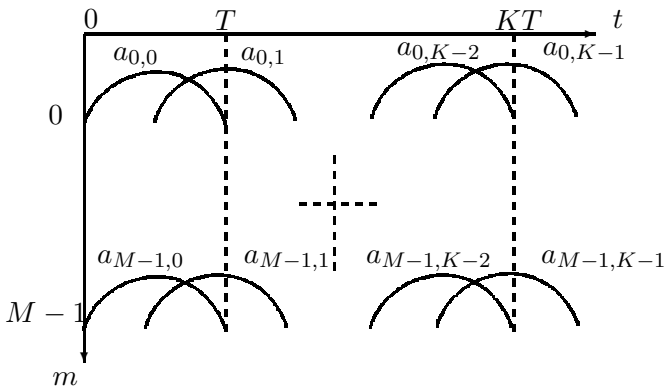

FIG. 4.23 – Truncation effect for the OFDM/OQAM signal at the end border.

Indeed, assuming a distortionless channel and no noise, the transmitted $a_{m,n}$ symbols

can be recovered, using the conventional OFDM/OQAM demodulation equation.

$$\hat{a}_{m,n} = \Re\{< g_{m,n}, s >\} = \Re\{\int_0^{T_E} g^*_{m,n}(t)s(t)dt\}, \tag{4.20}$$

where T_E is adjusted according to the packet duration and the prototype filter length. For instance, in the case of a prototype filter length $L = M = T$ and a packet of K complex data symbols $T_E = KT + \frac{K}{2}$ and (4.20) allows us to recover all the real valued symbols $a_{m,n}$ for $m \in 0, ..., M-1$ and $n \in 0, ..., K-2$.

But, in this particular and interesting case where $L = M$, it has also been proved in [24] that setting $T_E = KT$ we could also exactly recover the whole set of transmitted symbols by (4.20), including the symbols of index $n = -1$ and $n = K-1$. However, the condition to get this result is, for $n = K-1$, and equivalently for $n = -1$, to transmit data symbols only on subcarriers with even or odd indexes.

Applying this technique [22], [24] at each side of the transmitted packet, it can be seen that we can get a spectral efficiency being equivalent to the OFDM one. Indeed, let us take as an example the case of a packet of length $L = M = T$. Then, the two truncated multicarrier symbols at the two borders transmit $2 \times \frac{M}{2}$ OQAM symbols while the non truncated one carries M OQAM symbols. This corresponds to the transmission of M complex data symbols for one multicarrier symbol, i.e. as for OFDM without CP.

In [22], [24], the packet mode transmission is only analyzed in a theoretical setup : no channel, no noise. In this section we investigate the effect of two preamble transmission strategies to build the 3GPP/LTE frame and we evaluate them in realistic transmission conditions.

In the previous section we presented the results we already obtained in [37] where, in order to avoid the overlap between successive subframes, i.e. between users, we introduced a guard interval of length τ_0, cf. Fig. 4.24. Then, in the next subsection,we compare the two options for the OFDM/OQAM 3GPP/LTE framing.

In this comparison we consider the most critical case w.r.t. the interference between users in the OQAMA setting, where the frame is reduced to two slots, i.e. a subframe.

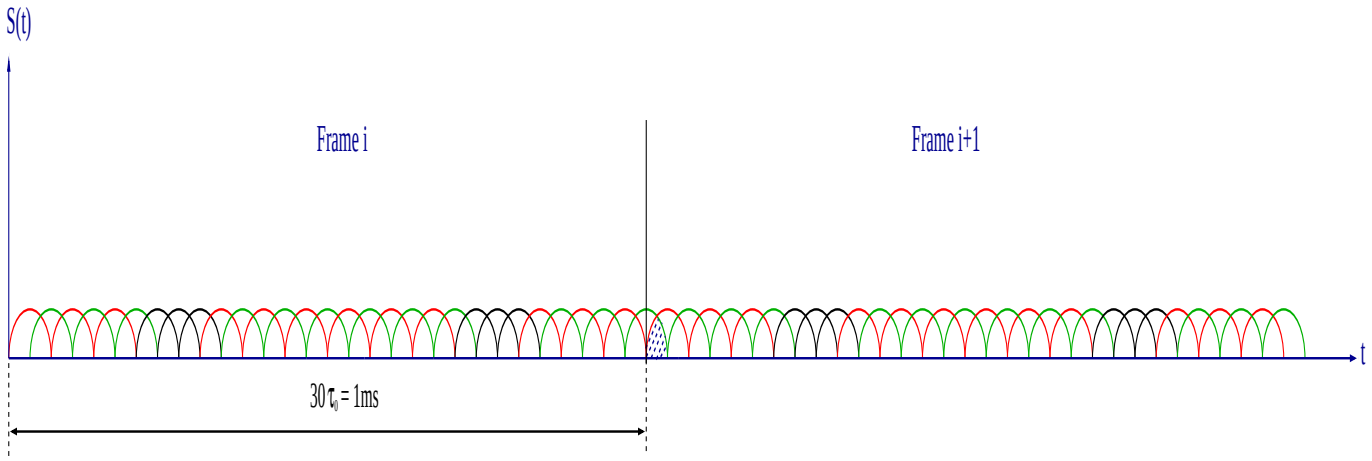

FIG. 4.24 – Symbol overlapping at the subframes frontier.

4.6.1 Simulation results

Using the first solution, in section 4.5, we could avoid the interference, but it resulted in a loss of spectral efficiency, which is $\frac{30}{31}$ (or 0.14 dB).

To avoid this loss we have applied, in the 3GPP/LTE context for the UL transmission, the method recalled in section 4.6. Using it we can recover a complete symbol while only transmitting a truncated version of its associated waveform.

The purpose is to recover the last real symbol of each frame when the guard interval between two pairs of frames is removed. For that, we split the last real symbol of the frame into 2 real half-symbols, one containing even subcarriers data and the other containing odd subcarriers data. One of these 2 half-symbols is put at the beginning of the frame and the other one at the end. By the way, for each frame we transmit 31 real symbols instead of 30. Then, in order to satisfy the 1 ms duration per frame, we truncate the first and last multicarrier symbols of the frame. So that, as depicted in Fig. 4.25, only one-half of the 1st and 31st waveforms are transmitted at the beginning and end of each frame.

At the receiver, after OFDM/OQAM demodulation, ZF equalization and real-part-taken operation, based on (4.20), the first and last complete half-symbols of the frame can be recovered. Then, we can reconstruct the estimate of the last complete data symbol of the frame using these 2 half-symbols.

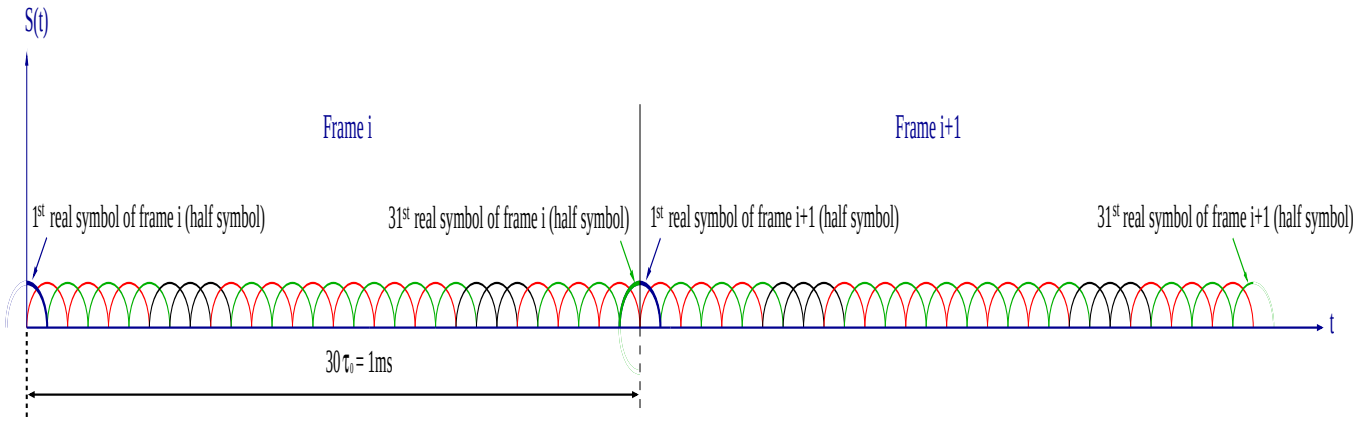

FIG. 4.25 – Applying the new method of transmission.

Using this method, we were able to send 31 real data symbols instead of 30, and we can get the same performances as the one presented in [37] avoiding the loss of 0.14 dB due to the τ_0 guard interval.

To check this more precisely, we have evaluated the performances of the OFDM/OQAM packet mode and we have compared with the ones of the OFDM/OQAM system simulated in [37], for the single user case using 20 RBs and assuming perfect CE. The simulations have been carried out with the same parameter values as in [37] using the same 6-tap and a one-tap mobile channels.

Figs. 4.26 and 4.27, show the BER performances of the new OQAMA packet transmission using 6-tap and one-tap channel, respectively, compared to the ones of OQAMA with a zero guard band added between the frames. In Fig. 4.26 for the 6-tap channel, we can see that at 3 Km/h and 120 Km/h the performances of the new OQAMA packet transmission are the same as the ones in [37]. While, when using a one-tap channel, as shown in Fig. 4.27, there is only a slight loss of 0.05 dB for a BER of 10^{-4}.

From these figures, we can see that the curves of the OQAMA packet transmission nearly lead to the same results as the ones of OQAMA with a zero guard band added between the frames. This proves the efficiency of this method of packet transmission in the UL 3GPP/LTE context.

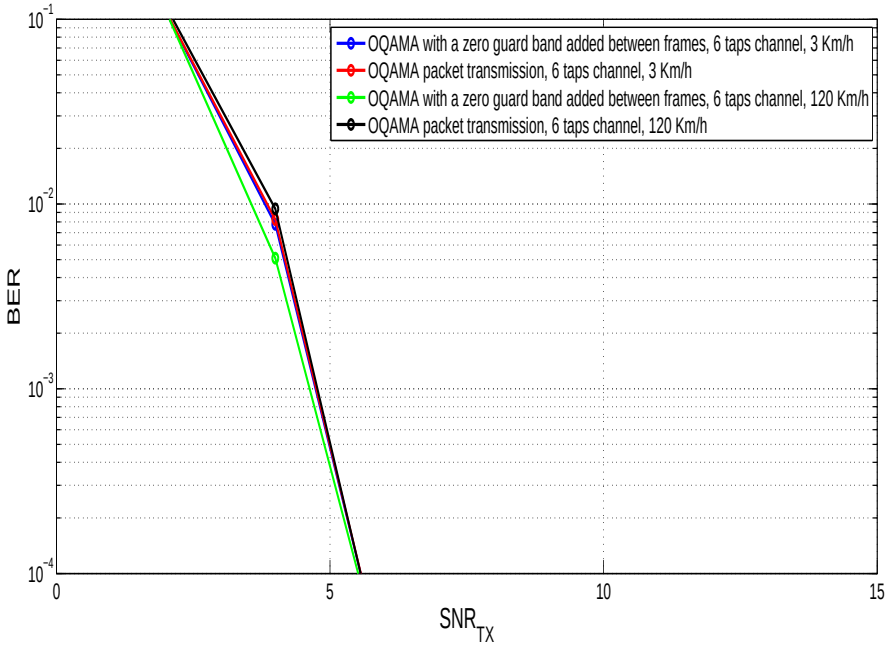

FIG. 4.26 – OQAMA packet transmission BER performances in a 6-tap channel.

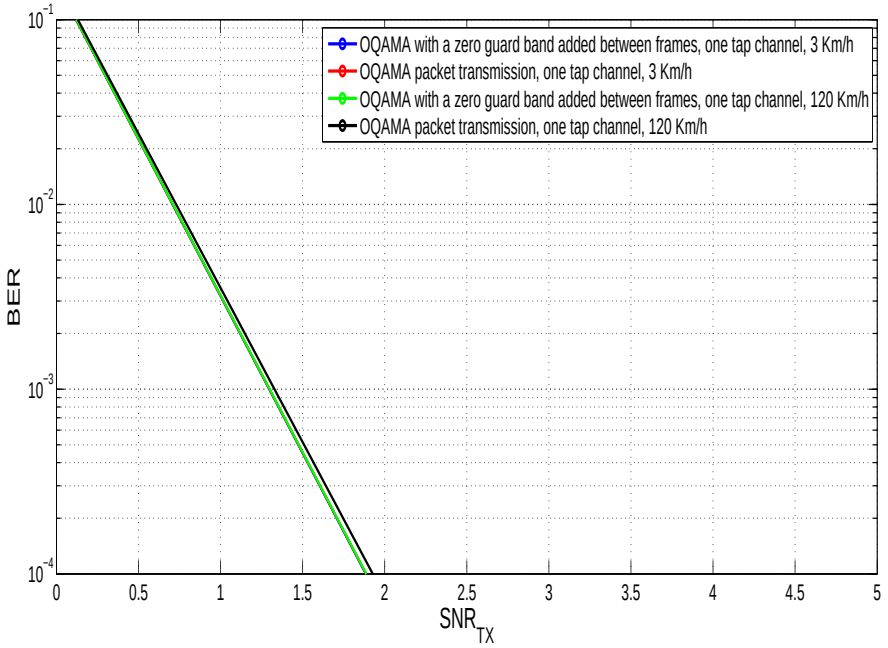

FIG. 4.27 – OQAMA packet transmission BER performances in a one tap channel.

4.7 Conclusion

In this chapter, we have proposed alternative multiple access schemes based on OFDM/OQAM to the well-known OFDMA and SC-FDMA techniques for the UL transmission in 3GPP/LTE context. The OFDM/OQAM has been analyzed and combined with multiple access demonstrating its suitability and efficiency. The OFDM/OQAM frame structure has been adapted to map the 3GPP/LTE framework. The OQAMA has been theoretically evaluated and tested within different configurations. It has been shown that the use of the IAM-I method for CE, improves the OQAMA and DFT-OQAMA performances. Indeed the performances obtained for OQAMA, without PAPR consideration, are better compared to OFDMA and SC-FDMA, and also DFT-OQAMA outperforms SC-FDMA. We have also introduced and evaluated a new method of packet transmission for OFDM/OQAM, which proved its efficiency in the 3GPP/LTE context. All this shows that even if OQAMA and DFT-OQAMA have not been introduced within 3GPP/LTE standard, they remain strong candidates for the future radio networks. Indeed they have the advantage of a better spectrum efficiency, which is an essential feature we need to the scarceness of frequency band.

Conclusion

This thesis mainly focused on OFDM/OQAM modulation to build an alternative multiple access scheme to OFDMA and SC-FDMA.

Our first chapter is a French extended summary of the thesis. In the second chapter, we have presented the main framework of the OFDM and OFDM/OQAM systems. Nowadays, the main multi-carrier modulation is CP-OFDM. The large popularity of CP-OFDM, which is now present at the physical layer of many transmission standards and specifications, mainly comes from its two most attractive features. Firstly, OFDM corresponds to a modulated transform that can be easily implemented using fast algorithms. Secondly, the equalization problem is simply solved with OFDM thanks to the addition of the CP. However, CP-OFDM has also some drawbacks including a loss of spectral efficiency due to the CP and the use of a sinc shaped frequency response makes the transmission spectrum very poorly localized in frequency. These weaknesses have shifted researchers to other multicarrier systems. To cope with these shortcomings, a possible alternative is the modulation OFDM/OQAM [32]. This modulation has the same spectral efficiency than the OFDM without CP while having the possibility of using pulse shapes other than the rectangular one. For this, the data transmission scheme is changed in order to transmit real data symbols only. The orthogonality is not verified in the complex field as in OFDM, but in the real field. Since the OFDM/OQAM modulation does not require the use of a CP during the transmission, it inherently exhibits a higher spectral efficiency compared to CP-OFDM. In addition, we have seen that different sorts of prototype filters can be used in OFDM/OQAM. Moreover, we can physically suppose that the different presented filters will impact differently the system regarding to their time and/or frequency localization(s) measures towards the propagation channel characteristics (timing offset, carrier frequency offest...). These both aspects seem to be advantageous when implementing OFDM/OQAM instead of CP-OFDM.

In the third chapter, our study has been concerned with the analysis of the desynchronized OFDM/OQAM system in the time and frequency domains. The OFDM/OQAM, also named FBMC/OQAM, has its own shortcomings. As it can not take advantage of a CP, its sensitivity to time offset remains questionable. This makes interference analysis [87] due to desynchronization be a very important topic in the physical layer design. The

results presented in [32] are interesting but they are not fully analyzed. On another hand, the more detailed analysis provided in [87] only leads to approximations of the SIR. In this chapter, we focused on the interference caused by timing and carrier frequency offsets for FBMC/OQAM. Reusing the analysis provided in [58] concerning the transmission of an FBMC/OQAM signal through a multipath channel, we derived very simple ISI and ICI expressions as well as an exact SIR expression. Then, we illustrated the effect of the pulse shape on this interference term where we compared our exact SIR model with the simulated SIR numerically using different prototype filters. These results were also compared with the ones obtained for OFDM showing the better performances against timing offset and frequency offset compared to OFDM without CP. In our study, through a detailed demonstration for the case of orthogonal prototype filters, we highlighted a link between our analysis and the one in [32]. And finally, we have presented a synchronization method for UL multiuser systems which is robust in multipath channels.

In the fourth chapter, we have proposed alternative multiple access schemes based on OFDM/OQAM to the well-known OFDMA and SC-FDMA techniques in 3GPP/LTE context. For the downlink, 3GPP/LTE standard has unanimously considered OFDMA as the most appropriate technique for achieving high spectral efficiency. For the UL, 3GPP/LTE has selected the SC-FDMA [2] instead of OFDMA, since it leads to lower PAPR. SC-FDMA can be viewed as a new hybrid modulation scheme that provides quasi-similar PAPR as single-carrier systems. On one hand, SC-FDMA has already proved its ability to fight against frequency selective channels, thanks to the use of the CP-OFDM modulation and its flexibility in multiple access, thanks to the FDMA component. The OFDMA and SC-FDMA, being both based on the OFDM modulation with cyclic prefix, give rise to 2 drawbacks, loss of spectral efficiency and sensitivity to frequency dispersion, e.g. Doppler spread. Both of them can be counteracted using OFDM/OQAM. In this chapter, we discussed the suitability of using OQAMA and DFT-OQAMA instead of OFDMA and SC-FDMA for the UL 3GPP/LTE scenario, regardless to the PAPR and considering perfect time and frequency synchronizations. The OFDM/OQAM has been analyzed and combined with multiple access demonstrating its suitability and efficiency. The OFDM/OQAM frame structure has been adapted to map the 3GPP/LTE frame-

work. The OQAMA has been theoretically evaluated and tested within different configurations. It has been shown that the use of the IAM-I method for channel estimation, improves the OQAMA and DFT-OQAMA performances. Indeed the performances obtained for OQAMA, without PAPR consideration, are better compared to OFDMA and SC-FDMA, and also DFT-OQAMA outperforms SC-FDMA. We ave also introduced and evaluated a new method of packet transmission for OFDM/OQAM, which proved its efficiency in the 3GPP/LTE context. All this shows that even if OQAMA and DFT-OQAMA have not been introduced within 3GPP/LTE standard, they remain strong candidates for the future radio networks.

Our perspectives, are to analyze the OFDM/OQAM modulation scheme within asynchronous multi-cellular networks including the impact of intra-cell and inter-cell interferences [66] and to compare it with CP-OFDM, to find a simple interference expression for desynchronized multipath channel, to analyze synchronization for interleaved allocated multiusers, and to analyze and study a synchronization method to frequency desynchronization for the UL multiuser OFDM/OQAM system [8].

Contributions

- M. Gharba, R. Legouable and P. Siohan, "An alternative Multiple Access Scheme for the uplink 3GPP/LTE based on OFDM/OQAM", ISWCS2010, York, UK, 19-22 September 2010.
- M. Gharba, H. Lin and P. Siohan, "Time offsetted FBMC/OQAM transmission system : A theoretical analysis", MIC-CSC2011, Larnaca, Cyprus, 7-9 October 2011.
- M. Gharba, H. Lin, P. Siohan and F. Labeau, "DFT-OQAMA : An Alternative Multiple Access for Future Mobile Networks", VTC2012, Quebec, Canada, September 2012.
- M. Gharba, H. Lin and P. Siohan, "Comparative analysis of OFDM and OFDM/OQAM in presence of time and frequency offsets", Journal paper in preparation.

Appendices

Appendix A

Appendix

A.1 Proof that $P_{l_d} = 2$

Let us show firstly that $P_{l_d} = 2$ when l_d=0. Setting $L = aM$ with $a \in \mathbb{N}^*$, for an orthogonal filter g, P_0 can be written as

$$\begin{aligned} P_0 &= \sum_{p,q} A_g^2[-qN, -p] = \sum_{p,q} (e^{-j\frac{\pi pl}{M}} \sum_k g[k]g[k+l]e^{-j\frac{2\pi pk}{M}})^2 \\ &= \sum_{p=-m_0}^{M-1-m_0} \sum_{q=-a}^{a} \sum_{k=0}^{aM-1} \sum_{l=0}^{aM-1} g[k]g[l]g[k-qN]g[l-qN]e^{j\frac{2\pi p}{M}(l-k)} \\ &= A_{k.l} \sum_{q=-a}^{a} \sum_{k=0}^{aM-1} \sum_{l=0}^{aM-1} g[k]g[l]g[k-qN]g[l-qN], \end{aligned} \tag{A.1}$$

where

$$\begin{aligned} A_{k.l} &= \sum_{p=-m_0}^{M-1-m_0} e^{j\frac{2\pi p}{M}(l-k)} \\ &= e^{j\frac{2\pi}{M}(l-k)m_0} \times \frac{1 - e^{j2\pi(l-k)}}{1 - e^{j\frac{2\pi(l-k)}{M}}}. \end{aligned} \tag{A.2}$$

When $l - k = \alpha M$, with $\alpha \in]1-a, a-1[$

$$A_{k.l} = M, \tag{A.3}$$

and,when $l - k \neq \alpha M$

$$A_{k.l} = 0, \tag{A.4}$$

hence

$$P_0 = M \sum_{\alpha=1-a}^{a-1} \sum_{q=-a}^{a} \sum_{k=0}^{aM-1} g[k]g[k+\alpha M]g[k-qN]g[k-qN+\alpha M]. \tag{A.5}$$

In the case of orthogonal filter (see A.2), we have

$$\sum_{q=-a}^{a} g[k-qN]g[k-qN+\alpha M] = \begin{cases} 0, \alpha \neq 0 \\ \\ \frac{1}{N}, \alpha = 0, \forall k \end{cases}. \tag{A.6}$$

Then, we have

$$P_0 = \frac{M}{N} \underbrace{\sum_{k=0}^{aM-1} |g[k]|^2}_{=1} = 2 \tag{A.7}$$

It is valid for $l_d = 0$ and it also holds for $l_d \neq 0$, where we also have

$$\sum_{q=-a}^{a} g[k-qN-l_d]g[k-qN-l_d+\alpha M] = \begin{cases} 0, \alpha \neq 0 \\ \\ \frac{1}{N}, \alpha = 0, \forall k \end{cases}, \tag{A.8}$$

then

$$P_{l_d} = \frac{M}{N} \underbrace{\sum_{k=0}^{aM-1} |g[k]|^2}_{=1} = 2 \tag{A.9}$$

A.2 Orthogonality features

The polyphase decomposition for a prototype filter g of order $M = 2N$

$$G(z) = \sum_{k=0}^{2N-1} z^{-k} P_k(z^{2N}), \tag{A.10}$$

with $P_k(z) = \sum_n g[k+2N]z^{-n}$

The orthogonality conditions of the FBMC/OQAM system are [79] for $k \in [0, ..., N-1]$

$$P_k(z)P_k(z^{-1}) + P_{k+N}(z)P_{k+N}(z^{-1}) = \frac{1}{N}. \tag{A.11}$$

Leading to

$$\sum_n \sum_m [g[k+2nN]g[k+2mN] + g[k+(2n+1)N]g[k+(2m+1)N]]$$

$$\times z^{n-m} = \frac{1}{N}. \tag{A.12}$$

When $m = n$

$$\sum_n [g^2[k+2nN] + g^2[k+N+2nN]] = \sum_n g^2[k+n] = \frac{1}{N}, \tag{A.13}$$

and, when $m = n + 2a$ with $a \neq 0$

$$\sum_n [g[k+2nN]g[k+2(n+2a)N] + g[k+2nN+N]g[k+2(n+2a)N+N]]$$
$$= \sum_n g[k+nN]g[k+(n+2a)N] = 0. \tag{A.14}$$

A.3 Proof that $P_{\frac{1}{r}} = 2$

Let us show firstly that $P_{\frac{1}{r}} = 2$ when $\frac{1}{r}$=0. Setting $L = aM$ with $a \in \mathbb{N}^*$, for an orthogonal filter g, P_0 can be written as

$$\begin{aligned} P_0 &= \sum_{p,q} A_g^2[-qN,-p] = \sum_{p,q} (e^{-j\frac{\pi pl}{M}} \sum_k g[k]g[k+l]e^{-j\frac{2\pi pk}{M}})^2 \\ &= \sum_{p=-m_0}^{M-1-m_0} \sum_{q=-a}^{a} \sum_{k=0}^{aM-1} \sum_{l=0}^{aM-1} g[k]g[l]g[k-qN]g[l-qN]e^{j\frac{2\pi p}{M}(l-k)} \\ &= A_{k.l} \sum_{q=-a}^{a} \sum_{k=0}^{aM-1} \sum_{l=0}^{aM-1} g[k]g[l]g[k-qN]g[l-qN], \end{aligned} \tag{A.15}$$

where

$$\begin{aligned} A_{k.l} &= \sum_{p=-m_0}^{M-1-m_0} e^{j\frac{2\pi p}{M}(l-k)} \\ &= e^{j\frac{2\pi}{M}(l-k)m_0} \times \frac{1-e^{j2\pi(l-k)}}{1-e^{j\frac{2\pi(l-k)}{M}}}. \end{aligned} \tag{A.16}$$

When $l - k = \alpha M$, with $\alpha \in]1-a, a-1[$

$$A_{k.l} = M, \tag{A.17}$$

and,when $l - k \neq \alpha M$

$$A_{k.l} = 0, \tag{A.18}$$

It is valid for $\frac{1}{r} = 0$ and it also holds for $\frac{1}{r} \neq 0$, where we also have

$$\begin{aligned} A_{k.l} &= \sum_{p=-m_0}^{M-1-m_0} e^{j\frac{2\pi(p+\frac{1}{r})}{M}(l-k)} \\ &= e^{j\frac{2\pi}{M}(l-k)(m_0+\frac{1}{r})} \times \frac{1-e^{j2\pi(l-k)}}{1-e^{j\frac{2\pi(l-k)}{M}}}. \end{aligned} \tag{A.19}$$

When $l-k = \alpha M$, with $\alpha \in]1-a, a-1[$

$$A_{k.l} = M, \tag{A.20}$$

and,when $l-k \neq \alpha M$

$$A_{k.l} = 0, \tag{A.21}$$

hence

$$P_{\frac{1}{r}} = M \sum_{\alpha=1-a}^{a-1} \sum_{q=-a}^{a} \sum_{k=0}^{aM-1} g[k]g[k+\alpha M]g[k-qN]g[k-qN+\alpha M]. \tag{A.22}$$

In the case of orthogonal filter (see A.2), we have

$$\sum_{q=-a}^{a} g[k-qN]g[k-qN+\alpha M] = \begin{cases} 0, \alpha \neq 0 \\ \\ \frac{1}{N}, \alpha = 0, \forall k \end{cases}. \tag{A.23}$$

Then, we have

$$P_{\frac{1}{r}} = \frac{M}{N} \underbrace{\sum_{k=0}^{aM-1} |g[k]|^2}_{=1} = 2 \tag{A.24}$$

A.4 Proof that $P_{l_d,\frac{1}{r}} = 2$

Previously, we have seen that $P_{l_d} = 2$ and $P_{\frac{1}{r}} = 2$. Now, we want to prove that $P_{l_d,\frac{1}{r}} = 2$ based on A.1-A.3.

For an orthogonal filter g, $P_{l_d,\frac{1}{r}}$ can be written as

$$\begin{aligned} P_{l_d,\frac{1}{r}} &= \sum_{p,q} A_g^2[-qN - l_d, -(p+\frac{1}{r})] \\ &= \sum_{p=-m_0}^{M-1-m_0} \sum_{q=-a}^{a} \sum_{k=0}^{aM-1} \sum_{l=0}^{aM-1} g[k]g[l]g[k-qN-l_d]g[l-qN-l_d] e^{j\frac{2\pi(p+\frac{1}{r})}{M}(l-k)} \\ &= A_{k.l} \sum_{q=-a}^{a} \sum_{k=0}^{aM-1} \sum_{l=0}^{aM-1} g[k]g[l]g[k-qN-l_d]g[l-qN-l_d], \end{aligned} \tag{A.25}$$

based on A.20, where

$$\begin{aligned} A_{k.l} &= \sum_{p=-m_0}^{M-1-m_0} e^{j\frac{2\pi(p+\frac{1}{r})}{M}(l-k)} \\ &= e^{j\frac{2\pi}{M}(l-k)(m_0+\frac{1}{r})} \times \frac{1-e^{j2\pi(l-k)}}{1-e^{j\frac{2\pi(l-k)}{M}}} \\ &= M, \end{aligned} \tag{A.26}$$

and based on A.23 we have

$$\sum_{q=-a}^{a} \sum_{k=0}^{aM-1} \sum_{l=0}^{aM-1} g[k]g[l]g[k-qN-l_d]g[l-qN-l_d] = \frac{1}{N}. \tag{A.27}$$

Hence, we obtain

$$\begin{aligned} P_{l_d,\frac{1}{r}} &= \frac{M}{N} \\ &= 2. \end{aligned} \tag{A.28}$$

A.5 Computation of the interference for OFDM with time-offset

Substituting (3.24) and (3.25) into (3.26) and after some operations, the demodulated signal writes

$$y_{m_0} = \alpha_{m_0} c_{m_0,n} + I_{m_0}^{(n-1)} + I_{m_0}^{(n)}, \tag{A.29}$$

with

$$\alpha_{m_0} = \frac{M-l_d}{M} e^{-j\frac{2\pi m_0 l_d}{M}}; \tag{A.30}$$

$$I_{m_0}^{(n-1)} = \frac{1}{M}\sum_{m=0}^{M-1} c_{m_0,n-1} e^{-j\frac{2\pi m l_d}{M}} \underbrace{\sum_{k=0}^{l_d-1} e^{-j\frac{2\pi k(m-m_0)}{M}}}_{T_{m,m_0}^{(n-1)}}; \tag{A.31}$$

$$I_{m_0}^{(n)} = \frac{1}{M}\sum_{\substack{m'=0 \\ m'\neq m_0}}^{M-1} c_{m',n} e^{-j\frac{2\pi m' l_d}{M}} \underbrace{\sum_{k=0}^{l_d-1} e^{-j\frac{2\pi k(m'-m_0)}{M}}}_{T_{m',m_0}^{(n)}}; \tag{A.32}$$

where α_n stands for the fading coefficient ; $I_{m_0}^{(n-1)}$ and $I_{m_0}^{(n)}$ represent the interference from the previous OFDM symbol ($(n-1)$) and current OFDM symbol (n), respectively.

After ZF equalization, the estimated symbol yields

$$\hat{c}_{m_0,n} = \frac{y_{m_0}}{\alpha_{m_0}} = c_{m_0,n-1} + J_{m_0}^{(n-1)} + J_{m_0}^{(n)}, \tag{A.33}$$

with

$$J_{m_0}^{(n-1)} = \frac{1}{M}\sum_{m=0}^{M-1} c_{m_0,n-1} e^{-j\frac{2\pi l_d(m-m_0)}{M}} T_{m,m_0}^{(n-1)}; \tag{A.34}$$

and

$$J_{m_0}^{(n)} = \frac{1}{M}\sum_{\substack{m'=0 \\ m'\neq m_0}}^{M-1} a_{m'}^1 e^{-j\frac{2\pi l_d(m'-m_0)}{M}} T_{m',m_0}^{(n)}; \tag{A.35}$$

Then, the interference power can be straightforwardly derived as

$$P_{m_0}^{J^{(n-1)}} = \frac{\sigma_c^2}{(M-l_d)^2}\sum_{m=0}^{M-1}\left|T_{m,m_0}^{(n-1)}\right|^2 \tag{A.36}$$

and

$$P_{m_0}^{J^n} = \frac{\sigma_c^2}{(M-l_d)^2}\sum_{\substack{m'=0 \\ m'\neq m_0}}^{M-1}\left|T_{m',m_0}^{(n)}\right|^2. \tag{A.37}$$

Aggregating the interference power, i.e. $P_{m_0}^I = P_{m_0}^{J^{(n-1)}} + P_{m_0}^{J^n}$, yields

$$P_{m_0}^I = \sigma_c^2\frac{l_d^2}{(M-l_d)^2} + \frac{2\sigma_c^2}{(M-l_d)^2}\underbrace{\sum_{\substack{m=0 \\ m\neq m_0}}^{M-1}\left|\sum_{k=0}^{l_d-1} e^{-j\frac{2\pi k(m-m_0)}{M}}\right|^2}_{Q}. \tag{A.38}$$

In what follows, we prove that the Q term does not depend on the carrier index m_0 and (A.38) can have a compact expression. Let us first denote $q = m - m_0$; $\xi = e^{j\frac{2\pi}{M}}$; $a = l_d$.

Then the Q term in (A.38) can be alternatively written as

$$Q = \sum_{q=1}^{M-1} \left| \sum_{k=0}^{a-1} \xi^{kq} \right|^2 = \sum_{q=1}^{M-1} \left| \frac{\xi^{aq}-1}{\xi^q-1} \right|^2. \tag{A.39}$$

Next, we layout the following identity

$$\left| \frac{\xi^{aq}-1}{\xi^q-1} \right|^2 = \left| \xi^{\frac{-(a-1)q}{2}} \frac{\xi^{aq}-1}{\xi^q-1} \right|^2 = \xi^{-(a-1)q} \left(\frac{\xi^{aq}-1}{\xi^q-1} \right)^2 \tag{A.40}$$

The first equality is obvious since ξ is on the unit circle. The proof of the second equality is as following

$$\xi^{\frac{-(a-1)q}{2}} \frac{\xi^{aq}-1}{\xi^q-1} = \frac{\xi^{\frac{-aq}{2}}(\xi^{aq}-1)}{\xi^{\frac{-q}{2}}(\xi^q-1)} = \frac{\xi^{\frac{aq}{2}}-\xi^{\frac{-aq}{2}}}{\xi^{\frac{q}{2}}-\xi^{\frac{-q}{2}}} = \frac{\sin\left(\frac{\pi aq}{M}\right)}{\sin\left(\frac{\pi q}{M}\right)} \in \mathcal{R}. \tag{A.41}$$

Then, we substitute (A.40) into (A.39) and also take advantage of the following identity

$$\xi^{aq}-1 = (\xi^q-1)(\xi^{q(a-1)} + \xi^{q(a-2)} + \xi^{q(a-3)} + \cdots + 1).$$

we can rewrite (A.39) as

$$\begin{aligned} Q &= \sum_{q=1}^{M-1} \xi^{-q(a-1)} \left(\xi^{q(a-1)} + \xi^{q(a-2)} + \xi^{q(a-3)} + \cdots + 1 \right)^2 \\ &= \sum_{q=1}^{M-1} \sum_{t=-(a-1)}^{(a-1)} c_t \xi^{tq}, \text{for } c_t \in \mathcal{N}. \end{aligned} \tag{A.42}$$

In this expression c_t represents the coefficient of the cross-products, i.e. $c_0 = a$.

Then, permuting the summations we have

$$Q = \sum_{t=-(a-1)}^{(a-1)} \sum_{q=1}^{M-1} c_t \xi^{tq} = \sum_{t=-(a-1)}^{(a-1)} \underbrace{\sum_{q=0}^{M-1} c_t \xi^{tq}}_{\gamma} - \underbrace{a^2}_{Q|_{(q=0)}}. \tag{A.43}$$

It is easy to compute (A.43) because γ is a comb function, i.e. $\gamma = 0$ for $t \neq 0$. Then we have

$$Q = c_0 M - a^2 = aM - a^2. \tag{A.44}$$

Finally, we have a compact expression of (A.38), which is independent of the carrier index m_0, given by

$$P^I = \sigma_c^2 \frac{l_d(2M - l_d)}{(M - l_d)^2}. \tag{A.45}$$

Bibliography

[1] 3GPP TS 36.212 V8.2.0 (2008-03). 3rd generation partnership project ; technical specification group radio access network ; evolved universal terrestrial radio access (E-UTRA) ; multiplexing and channel coding (release 8). 166

[2] 3GPP TS 36.201V 8.1.0. LTE physical layer - general description (release 8). *Nov. 2007.* 24, 26, 32, 51, 53, 108, 159, 163, 164, 167, 182

[3] DVB-T2 Document A133. Implementation guidelines for a second generation digital terrestrial television broadcasting system (DVB-T2) (draft TR 102 831 V1.1.1). 166

[4] M. Alard. Construction of a multicarrier signal. *Patent WO 96/35278, 1996.* 38, 77, 99, 106, 112, 116

[5] J. Alhava and M. Renfors. Adaptive sine-modulated/cosine-modulated filter bank equalizer for transmultiplexers. *ECCTD'01 - European Conference on Circuit Theory and Design, Espoo Finland, August 28-31, 2001.* 156

[6] J. Alhava and M. Renfors. Complex lapped transforms and modulated filter banks. *Proc. Int. TICSP Workshop Spectral Methods and Multirate Signal Processing, Toulouse, France, pp. 87-94, 2002.* 78

[7] J. Alhava and M. Renfors. Exponentially-modulated filter bank-based transmultiplexer. *Proc. IEEE Int. Symp. Circuits and Systems, Bangkok, Thailand, Vol. 4, pp. 233-236, May 2003.* 78

[8] B. Aziz, I. Fijalkow, and M. Ariaudo. Intercarrier interference in uplink ofdma systems with carrier frequency offset. *IEEE 21st International Symposium on Personal*

Indoor and Mobile Radio Communications (PIMRC), 2010 Istanbul, Turkey, September 2010. 183

[9] M. Bellanger and J. L. Daguet. TDM-FDM transmultiplexer : Digital polyphase and FFT. *IEEE Transactions on Communications, Vol. 22, pp. 1199-1205, September 1974.* 77

[10] M. Bellanger, M. Renfors, T. Ihalainen, and C.A.F da Rocha. OFDM and FBMC transmission techniques : a compatible high performance proposal for broadband power line communications. *IEEE International Symposium on Power Line Communications and Its Applications (ISPLC), 2010.* 54, 173

[11] M.G. Bellanger. Specification and design of a prototype filter for filter bank based multicarrier transmission. *ICASSP, Salt Lake City, UT, USA, May 2001.* 39, 80, 108

[12] D. Bhatoolaul. An investigation into the implementation and performance of spectrally shaped orthogonal frequency division multiplex. *Ph.D. Thesis University of Plymouth, 1999.* 67

[13] H. Bölcskei. Advances in Gabor Analysis. *Birkhäuser, 2003, chapter Orthogonal frequency division multiplexing based on offset QAM, pages 321-352.* 71

[14] G. Cariolaro and F. Vagliani. An OFDM scheme with a half complexity. *IEEE Journal on Selected Areas in Communications, pp.1586-1599, 1995.* 73

[15] R. W. Chang. Synthesis of band-limited orthogonal signals for multi-channel data transmission. *Bell. Syst. Tech. Journal, volume 45, pages 1775-1796, December 1966.* 24, 33, 59, 67

[16] G. Cherubini, E. Eleftheriou, and S. Olcer. Filtered multitone modulation for VDSL. *Global Telecommunications Conference GLOBECOM'99, volume : 2, 1999.* 35, 66

[17] P. Ciblat, A. Chevreuil, and P. Loubaton. Repetition/modulation and blind second order equalization. *IEEE Transactions on Signal Processing, vol. 48 , no. 11, pp. 3153-3161, November 2000.* 151

[18] L. J. Cimini. Analysis and simulations of a digital mobile channel using orthogonal frequency division multiplexing. *IEEE Trans. on Communications, volume COM-33, number 7, pages 665-675, July 1985.* 60

[19] C. Ciochina, D. Mottier, and H. Sari. An analysis of OFDMA, precoded OFDMA and SC-FDMA for the uplink in cellular system. *Lecture Notes in Electrical Engineering, Volume 1, pp.25-36, 2007.* 148

[20] C. Ciochina and H. Sari. A review of OFDMA and single-carrier FDMA and some recent results. *Advances in Electronics and Telecommunications, VOL. 1, NO. 1, April 2010.* 147, 148

[21] T. Cooklev. Wireless communication standards. *IEEE standards wireless networks, New York : IEEE Press, 2004.* 24, 32, 60

[22] Y. Dandach. Etude de nouvelles méthodes de design, d'implémentation, de synchronisation et d'égalisation pour le système de modulation FBMC/OQAM. *Ph.D. Thesis, University of Rennes 1, France, January 2011.* 43, 44, 45, 47, 54, 67, 122, 123, 126, 173, 174

[23] Y. Dandach and P. Siohan. FBMC/OQAM modulators with half complexity. *Globecom 2011, Houston, USA.* 44, 73, 122

[24] Y. Dandach and P. Siohan. Packet transmission for overlapped offset QAM. *International Conference on Wireless Communications and Signal Processing (IC-WCSP), Suzhou, China, October 2010.* 54, 173, 174

[25] I. Daubechies. The wavelet transform, time-frequency localization and signal analysis. *IEEE Trans. on Information Theory, volume 36, number 5, pages 961-1005, September 1990.* 65

[26] M. Doelz, E. Heald, and D. Martin. Binary data transmission techniques for linear systems. *Proceedings of IRE, volume 45, pages 656-661, May 1957.* 59

[27] M. I. Doroslovacki. Product of second moments in time and frequency for discrete-

time signals and the uncertainty limit. *Signal Processing, Vol. 67 (1), pp. 59-76 May 1998.* 39, 84

[28] D. Falconer, S.L. Ariyavisitakul, A. Benyamin-Seeyar, and B. Eidson. Frequency domain equalization for single-carrier broadband wireless systems. *IEEE Commun. Mag., vol.40, no.4, Apr. 2002, pp.58-66.* 148, 149

[29] K. Fazel and S. Kaiser. Multi-carrier and spread spectrum systems : From OFDM and MC-CDMA to LTE and WiMAX. *2nd Edition, John Wiley and Sons, 2008.* 147

[30] H. G. Feichtinger and T. Strohmer. *Gabor Analysis and Algorithms.* Birkhäuser, 1998. 34, 64, 65, 66

[31] N. J. Fliege. Orthogonal multiple carrier data transmission. *European Transactions on Telecommunications, Vol. 3 (3), pp. 255-264, May-June 1992.* 25, 33, 67

[32] B. Le Floch, M. Alard, and C. Berrou. Coded orthogonal frequency division multiplex. *Proceedings of the IEEE, vol. 83, no. 6, jun. 1995.* 24, 25, 26, 32, 33, 38, 40, 42, 43, 51, 64, 67, 71, 75, 77, 85, 99, 104, 106, 108, 112, 116, 141, 148, 181, 182

[33] T. Fusco, A. Petrella, and M. Tanda. Data-aided symbol timing and CFO synchronization for filter bank multicarrier systems. *Wireless Communications, IEEE Transactions, volume 8, number 5, pages 2705-2715, May 2009.* 127, 129, 130, 131

[34] T. Fusco, A. Petrella, and M. Tanda. A data-aided symbol timing estimation algorithm for OFDM/OQAM systems. *Proc. Intern. Conf. on Communications (ICC), Dresden, Germany, 2009, pp. 1-5.* 43, 44, 45, 121, 122, 123

[35] T. Fusco, A. Petrella, and M. Tanda. Joint symbol timing and CFO estimation in multiuser OFDM/OQAM systems. *Signal Processing Advances in Wireless Communications, 2009, SPAWC '09.* 46, 125

[36] T. Fusco, A. Petrella, and M. Tanda. Sensitivity of multi-user filter-bank multicarrier systems to synchronization errors. *3rd International Symposium on Communications Control and Signal Processing (ISCCSP), March 2008.* 46, 125

[37] M. Gharba, R. Legouable, and Pierre Siohan. An alternative multiple access scheme for the uplink 3GPP/LTE based on OFDM/OQAM. *ISWCS2010, York, UK, 2010.* 54, 55, 159, 167, 174, 176

[38] M. Gharba, H. Lin, and P. Siohan. Time offsetted FBMC/OQAM transmission system : A theoretical analysis. *MIC-CSC2011, Larnaca, Cyprus, 7-9 October 2011.* 103, 108

[39] M. Gharba, H. Lin, P. Siohan, and F. Labeau. DFT-OQAMA : An alternative multiple access for future mobile networks. *VTC2012, Québec City, Canada , 3-6 September 2012.* 167

[40] A. Goupil and J. Palicot. New algorithms for blind equalization : the constant norm algorithm. *IEEE Transactions on Signal Processing, vol. 55, N. 4, pp1436 - 1444, april 2007.* 151

[41] R. Haas. Application des transmissions à porteuses multiples aux communications radio mobiles. *Ph.D. Thesis ENST Paris, ISSN 0751-1353, 1996.* 38, 67, 79

[42] R. Haas and J.-C. Belfiore. A time-frequency well-localized pulse for multiple carrier transmission. *Wireless Personal Communications, 18(1) :1-18, Jul. 1997.* 38, 79, 85

[43] L. Hanzo, M. Münster, B.J. Choi, and T Keller. OFDM and MC-CDMA for broadband multi-user communications, WLAN and broad-casting. *Wiley/IEEE Press, 2003.* 147

[44] W. Henkel, G. Taubock, P. Odling, P. O. Borjesson, and N. Petersson. The cyclic prefix of OFDM/DMT - an analysis. *International Zurich Seminar on Broadband Communications Access-Transmission-Networking, Zurich, Switzerland, Feb. 2002.* 107

[45] B. Hirosaki. An analysis of automatic equalizers for orthogonally multiplexed QAM systems. *IEEE Transactions on Communications, volume 28, number 1, pages 73-83, January 1980.* 25, 33, 155

[46] B. Hirosaki. An orthogonally multiplexed QAM system using the discrete fourier transform. *IEEE Trans. on Communications, volume 29, number 7, pp. 982-989, July 1981.* 24, 33, 67, 155

[47] R. Hleiss. Conception et égalisation de nouvelles structures de modulations multi-porteuses. *Ph.D. Thesis ENST, 2000.* 67, 156

[48] T. Ihalainen, T. H. Stitz, M. Rinne, and M. Renfors. Channel equalization in filter bank based multicarrier modulation for wireless communications. *EURASIP Journal on Advances in Signal Processing, 2007(ID 49389), Aug. 2007.* 156

[49] T. Ihalainen, A. Viholainen, T. H. Stitz, M. Renfors, and M. Bellanger. Filter bank based multi-mode multiple access scheme for wireless uplink. *17th European Signal Processing Conference (EUSIPCO 2009), Glasgow, Scotland, August 2009.* 150

[50] B. Jahan, M. Lanoiselée, G. Degoulet, and R. Rabineau. Full synchronization method for OFDM/OQAM and OFDM/QAM modulations. *in Proc. International Symposium on Spread Spectrum Techniques and Applications (ISSSTA'08), Bologna, Italy, Aug. 2008, pp. 344-348.* 43, 121

[51] T. Karp and N. J. Fliege. Modified DFT filter banks with perfect reconstruction. *IEEE Transactions on Circuits and Systems, Vol. 46 (11), pp. 1404-1414, November 1999.* 77

[52] W. Keasler. Reliable data communications over the voice bandwidth telephone channel using orthogonal frequency division multiplexing. *Ph.D.Thesis, University of Illinois, USA, 1982.* 60

[53] D. Lacroix and J.-P. Javaudin. A new channel estimation method for OFDM/OQAM. *Proceeding 7th International OFDM Workshop, Hamburg, Germany, Sept. 2002.* 153

[54] Y. Li and G. Stuber. *Orthogonal Frequency Division Multiplexing for Wireless Communications.* Springer, 2006. 24, 32

[55] G. Lin. On the design and optimization of OFDM systems. *Ph.D. Thesis University of Science and Technology, NTNU, 2006.* 67

[56] H. Lin. Analysis and design of multi-carrier systems for power line communications. *Ph.D. Thesis, TELECOM ParisTech, 2009.* 53, 67, 83, 101, 102, 155, 156, 157, 159

[57] H. Lin, C. Lélé, and P. Siohan. Equalization with interference cancellation for hermitian symmetric OFDM/OQAM systems. *ISPLC'08, Jeju Island, South Korea, Apr. 2008.* 156

[58] Hao Lin and Pierre Siohan. Capacity analysis for indoor PLC using different multicarrier modulation schemes. *IEEE Transactions on Power Delivery, Vol.25, Iss.1, pp.113, 2010, ISSN : 08858977.* 26, 40, 101, 102, 151, 182

[59] C. Lélé. OFDM/OQAM modulation : Channel estimation methods, and applications to multicarrier CDMA and multi-antenna transmission. *PhD thesis, Conservatoire National des Arts et Métiers, Paris, France, Nov. 2008.* 67, 151, 154

[60] C. Lélé, J.-P. Javaudin, R. Legouable, A. Skrzypczak, and P. Siohan. Channel estimation methods for preamble-based OFDM/OQAM modulations. *European Wireless'07, Paris, France, April 2007.* 165

[61] C. Lélé, P. Siohan, and R. Legouable. 2 dB better than CP-OFDM with OFDM/OQAM for preamble-based channel estimation. *ICC'08, pp.1302-1306, May 2008.* 151, 154, 155, 159, 165

[62] C. Lélé, P. Siohan, R. Legouable, and J.-P. Javaudin. Preamble-based channel estimation techniques for OFDM/OQAM over the powerline. *IEEE International Symposium on Power Line Communications and its Applications, pages 59-64, Pisa, Italy, Mar. 2007.* 53, 153, 154

[63] H. S. Malvar. Fast algorithm for modulated lapped transform. *Electronics Letters, volume 27, number 9, pages 775 - 776, April 1991.* 79

[64] H. S. Malvar. Modulated QMF filter banks with perfect reconstruction. *Electronics Letters, volume 26, number 13, pages 906 - 907, June 1990.* 79

[65] K. Martin. Small side-lobe filter design for multi-tone data communication applica-

tions. *IEEE Transactions on Circuits and Systems, Vol. 45, No. 8, Aug. 1998.* 39, 80

[66] Y. Medjahdi, M. Terre, D. Le Ruyet, D. Roviras, and A.Dziri. Performance analysis in the downlink of asynchronous OFDM/FBMC based multi-cellular networks. *IEEE Trans. on Wireless Communications, vol. 10, no. 8, August 2011.* 183

[67] S. Mirabbasi and K. Martin. Overlapped complex-modulated transmultiplexer filters with simplified design and superior stopbands. *IEEE Trans. on Circuits and Systems II : Analog and Digital Signal Processing, 50(8) :456-469, Aug. 2003.* 39, 80, 108

[68] B. Mongol, T. Yamazato, H. Okada, and M. Katayama. On the second-order statistics of the channel parameters for BFDM/OQAM systems. *ISWCS'05, Siena, Italy, September 2005, pages 534-538.* 71

[69] P.H. Moose. A technique for orthogonal frequency-division multiplexing frequency offset correction. *IEEE Trans.Commun. 42(10) (1994) 2908-2914.* 112, 114

[70] M. Morelli, C.-C. Jay Kuo, and Man-On Pun. Synchronization techniques for orthogonal frequency division multiple access (OFDMA) : A tutorial review. *Proceedings of the IEEE, vol. 95, July 2007.* 46, 63, 125

[71] R. Mosier. A data transmission system using pulse phase modulation. *IRE Convention record of First Nation Convention on Military Electronics, pages 233-238, June 1957.* 59

[72] Hyung G. Myung, Junsung Lim, and David J. Goodmand. Single carrier FDMA for uplink wireless transmission. *Tech. Mag., Vol.1, Sept. 2006, pp. 30-38.* 148

[73] S. Nedic and N. Popovic. Per-bin DFE for advanced OQAM-based multi-carrier wireless data transmission systems. *International Zurich Seminar on BroadBand Communications Access-Transmission-Networking, ETH Zurich, February 2002.* 156

[74] R. Van Nee and R. Prasad. OFDM for wireless multimedia communications. *2000.* 147

[75] IEEE ICC2012 Workshop on Small Cell Wireless Networks. http ://www.ieee-icc.org/workshops. 146

[76] Long Term Evolution (LTE) : A Technical Overview. Motorola. 146

[77] LTE Overview. http ://www.3gpp.org/lte. 146

[78] A. Peled and A. Ruiz. Frequency domain data transmission using reduced computational complexity algorithms. *ICASSP'80, volume 3, Denver, USA, April 1980, pages 964-967.* 24, 32, 62

[79] D. Pinchon, P. Siohan, and C. Siclet. Design techniques for orthogonal modulated filterbanks based on a compact representation. *IEEE Trans. on signal processing, 52(6) :1682-1692, June 2004.* 39, 82, 84, 106, 108, 190

[80] D. Pinchon, P. Siohan, and C. Siclet. A fast design method for orthogonal modulated filter banks. *ICASSP'02, Orlando, USA, May 2002.* 39, 82

[81] PHYDYAS Project. http ://www.ict-phydyas.org. 23, 32

[82] L. Qin. Perfectionnement aux techniques de transmission à porteuses multiples. *Ph.D. Thesis Conservatoire National des Arts et Métiers, 1998.* 67

[83] L. Qin and M. G. Bellanger. Adaptive sub-channel equalizatiion in multicarrier transmission. *IEEE International Conference on Acoustics, Speech, and Signal Processing, vol.3, pp.2321-2324, Munich, Germany, April 1997.* 156

[84] P. K. Remvik and Nils Holte. Carrier frequency offset robustness for OFDM systems with different pulse shaping filters. *IEEE Global Communications Conference GLOBECOM'97, vol. 1, pages 11-15, Phoenix, USA, november 1997.* 114

[85] M. Rossi, Z. Jin-Yun, and W. Steenaart. Iterative constrained least squares design of near perfect reconstruction pseudo QMF banks. *Canadian Conference on Electrical and Computer Engineering, volume :2, 1996.* 83

[86] H. Saeedi-Sourck, Y. Wu, J. W. M. Bergmans, S. Sadri, and B. Farhang-Boroujeny. Complexity and performance comparison of filter bank multicarrier and OFDM in

uplink of multicarrier multiple access networks. *IEEE Transactions on Signal Processing, vol. 59, no. 4, April 2011.* 125

[87] H. Saeedi-Sourck, Y. Wu, J. W.M. Bergmans, S. Sadri, and B. Farhang-Boroujeny. Sensitivity analysis of offset QAM multicarrier systems to residual carrier frequency and timing offsets. *Signal Processing, Volume 91, Issue 7, July 2011, Pages 1604-1612.* 25, 26, 33, 40, 108, 114, 181, 182

[88] B. R. Saltzberg. Performance of an efficient parallel data transmission system. *IEEE Transactions on Communications Technology, Vol. 15,no. 6, pp. 805-811, 1967.* 24, 33, 59, 67

[89] C. Siclet. Application de la théorie des bancs de filtres à l'analyse et à la conception de modulations multiporteuses orthogonales et biorthogonales. *Ph.D. Thesis, University of Rennes 1, 2002.* 36, 65, 67, 71, 73, 77, 114

[90] C. Siclet and P. Siohan. Design of BFDM/OQAM systems based on biorthogonal modulated filter banks. *Globecom, November 2000.* 67, 71

[91] P. Siohan and C. Roche. Derivation of extended gaussian functions based on the Zak transform. *IEEE Signal Processing Letters, Vol. 11 (3), pp. 401-403, March 2004.* 77

[92] P. Siohan, C. Siclet, and N. Lacaille. Analysis and design of OFDM/OQAM systems based on filterbank theory. *IEEE Transactions on Signal Processing, Vol. 50(5), pp. 1170-1183, May 2002.* 25, 33, 36, 39, 41, 67, 71, 72, 73, 77, 82, 84, 100, 106

[93] A. Skrzypczak. Contribution à l'étude des modulations multiporteuses OFDM/OQAM et OFDM suréchantillonnées. *Ph.D. Thesis, University of Rennes 1, 2007.* 35, 66, 67

[94] S. Srikanth, V. Kumaran, C. Manikandan, and Murugesapandian. Orthogonal frequency division multiple access : is it the multiple access system of the future ? *AU-KBC Research Center, Anna University, India.* 147

[95] T. Stitz, T. Ihalainen, and M. Renfors. Practical issues in frequency domain synchronization for filter bank based multicarrier transmission. *3rd International Symposium on Communications, Control and Signal Processing(ISCCSP)march 2008, pp. 411-416.* 43, 121

[96] T. Strohmer and S. Beaver. Optimal OFDM design for time-frequency dispersive channels. *IEEE transactions on Communications, volume : 5, Issue : 7, pages : 1111-1122, 2003.* 64

[97] J. C. Tu. Optimum MMSE equalization for staggered modulation. *Conference Record of The Twenty-Seventh Asilomar Conference on Signals, Systems and Computers, pp.1401-1406 vol.2, Pacific Grove, CA, Nov 1993.* 156

[98] 3GPP TR 25.892 V2.0.0. 3rd generation partnership project ; technical specification group radio access network ; feasibility study for OFDM for UTRAN enhancement ; (release 6). *June 2004.* 125, 145

[99] A. Vahlin and N. Holte. Optimal finite duration pulses for OFDM. *Globecom'94, San Francisco, USA, November 1994, pages 258-262.* 25, 33, 38, 79

[100] P. P. Vaidyanathan. Multirate systems and filter banks. *Englewood Cliffs, New-York, New Jersey : Prentice Hall, 1993.* 82

[101] J. J. van de Beek, P. O. Börjesson, M. L. Boucheret, D. Landström, J. M. Arenas, P. Ödling, M. Wahlqvist, M. Wahlqvist, and S. K. Wilson. A time and frequency synchronization scheme for multiuser OFDM. *IEEE Journal on Selected areas in Communications, vol. 17, no. 11, November 1999.* 121

[102] L. Vangelista and N. Laurenti. Efficient implementations and alternative architectures for OFDM-OQAM systems. *IEEE Trans. on Communications, volume 49, numéro 4, pages 664-675, Avril 2001.* 73

[103] M. Vetterli. Perfect transmultiplexers. *ICASSP 1986, vol. 11, pp. 2567-2570 May 1986.* 77

[104] A. Viholainen. Modulated filter bank design for communications signal processing. *Thesis for the degree of Doctor of Technology, Tampere University of Technology, Finland, 2004.* 78

[105] A. Viholainen, M. Bellanger, and M. Huchard. PHYDYAS d5.1. *PHYDYAS Report, Prototype filter and filter bank structure, Deliverable n. D5.1, January 2009.* 80

[106] D. S. Waldhauser and J. A. Nossek. Mmse equalization for bandwidth-efficient multicarrier systems. *International Symposium on Circuits and Systems (ISCAS 2006), Island of Kos, Greece, May 2006.* 156

[107] S. Weinstein. History of OFDM. *IEEE Communications magazine, vol. 47, pp. 26-35, November 2009.* 60

[108] Y. S. Yameogo. Etudes de nouvelles techniques d'estimation et d'égalisation de canal adaptées au système SC-FDMA. *PhD thesis, University of Rennes 1, Rennes, France, September 2011.* 149

Acronyms

- $3GPP$: 3rd Generation Partnership Project
- $ADSL$: Asymmetric Digital Subscriber Line
- AFB : Analysis Filter Bank
- $ASCET$: Adaptive Sine modulated/Cosine modulated filter bank Equalize
- $AWGN$: Additive White Gaussian Noise
- BER : Bit Error Rate
- $BPSK$: Binary Phase Shift Keying
- CE : Channel Estimation
- CFO : Carrier Frequency Offset
- $CMFB$: Cosine Modulated Filter Bank
- CP : Cyclic Prefix
- $CP-OFDM$: OFDM with Cyclic Prefix.

- DAB : Digital Audio Broadcasting
- DFT : Discrete Fourier Transform
- $DFT-OQAMA$: DFT-Offset Quadrature Amplitude Modulation Access
- DL : Down Link
- DSP : Digital Signal Processing
- $DVB-T$: Digital Video Broadcasting-Terrestrial
- $EDGE$: Enhanced Data rates for GSM Evolution
- EGF : Extended Gaussian Function
- $EMFB$: Exponentially Modulated Filter Banks
- $ETSI$: European Telecommunications Standards Institute
- $FBMC$: Filter Bank Multi Carrier
- FDD : Frequency Division Duplexing
- FDM : Frequency Division Multiplexing
- $FDMA$: Frequency Division Multiple Access
- FFT : Fast Fourier Transform

- FIR : Finite Impulse Response
- FMT : Filtered Multi Tone
- FS : Frequency Selective
- GSM : Global System for Mobile Communications
- $HSDPA$: High Speed Down Link Packet Access
- $HSPA$: High Speed Packet Access
- $HSUPA$: High Speed Up Link Packet Access
- IAM : Interference Approximation Method
- $IAM - I$: Interference Approximation Method for Imaginary
- IBI : Inter-Block Interference
- ICI : Inter-Carrier Interference
- $IDFT$: Inverse Discrete Fourier Transform
- $IEEE$: Institute of Electrical and Electronics Engineers
- $IFFT$: Inverse Fast Fourier Transform
- IFT : Inverse Fourier Transform

- $IOTA$: Isotropic Orthogonal Transform Algorithm
- ISI : Inter-Symbol Interference
- LE : Linear Equalizer
- LS : Least Square
- LTE : Long Term Evolution
- MCM : Multi Carrier Modulation
- $MDFT$: Modified Discrete Fourier Transform
- $MIMO$: Multiple Input Multiple Output
- MMB : Martin-Mirabbasi-Bellanger
- $MMSE$: Minimum Mean Square Error
- NPR : Nearly Perfect Reconstruction
- $OFDM$: Orthogonal Frequency Division Multiplexing
- $OFDMA$: Orthogonal Frequency Division Multiple Access
- $OFDP$: Optimal Finite Duration Pulse
- OMC : Orthogonal Multiple Carrier

- $OQAM$: Offset QAM
- $OQAMA$: OQAM Access
- PAM : Pulse Amplitude Modulation
- $PAPR$: Peak to Average Power Ratio
- $PHYDYAS$: PHYsical layer for DYnamic AccesS and cognitive radio
- PR : Perfect Reconstruction
- P/S : Parallel-to-Serial
- PSK : Phase Shift Keying
- QAM : Quadrature Amplitude Modulation
- $QPSK$: Quadrature Phase Shift Keying
- RAN : Radio Access Networks
- RB : Resource Block
- $RMSE$: Root Mean Square Error
- $SC-FDMA$: Single Carrier Frequency Division Multiple Access
- SFB : Synthesis Filter Bank

- $SINR$: Signal to Interference plus Noise Ratio
- SIR : Signal to Interference Ratio
- SNR : Signal to Noise Ratio
- SNR_{TX} : Signal to Noise Ratio at transmitted side.
- S/P : Serial-to-Parallel
- $SRRC$: Square Root Raised Cosine
- TDD : Time Division Duplexing
- TO : Timing Offset
- TFL : Time Frequency Localization
- UE : User Equipment
- UL : Up Link
- $UMTS$: Universal Mobile Telecommunications System
- ZF : Zero Forcing